



Global Cardiac Phosphoproteome Analysis In Nitric Oxide-Induced Heart Failure

Inaugural-Dissertation

to obtain the scientific degree
Dr. rer. nat. of the
Department of Mathematics and Natural Sciences
of the Heinrich-Heine-University Düsseldorf

submitted by

Annamária Simon

from Keszthely (Hungary)

Düsseldorf, June 2009

From the Institute of Cardiovascular Physiology
of the Heinrich-Heine-University Düsseldorf

Printed with the authorization of the
Department of Mathematics and Natural Sciences of the
Heinrich-Heine-University Düsseldorf

First Supervisor: Prof. MD Jürgen Schrader
Second Supervisor: Prof. Dr. Rainer Weinkauff

Day of the oral examination: 16. July 2009

This work is dedicated to my family

ACKNOWLEDGEMENTS

First and foremost I would like to thank Prof. Dr. med. Jürgen Schrader for giving me the opportunity to work at his laboratory. I am deeply grateful for his excellent supervision at every stage of this work.

Furthermore, I would like to thank Prof. Dr. Rainer Weinkauf for the fast preparation of the expert opinion.

I would also like to thank the Graduate College 1089 “Protein interactions and modifications in the heart” for the interesting courses and for the financial support.

Additionally I would like to thank Prof. Dr. Albert Sickmann for giving me some practical tips and tricks in proteomics.

I am grateful to have the possibility of performing some test measurements on LTQ Orbitrap XL at Thermo Scientific in Bremen.

Furthermore, I would like to thank Dr. Michael Reinartz and Dr. Ulrich Flögel for performing the heart perfusion experiments, additional thanks to Dr. Michael Reinartz also for mentoring me during my PhD thesis and for the critical reading of this manuscript.

I would also like to thank Dr. Christoph Jacobi for helping me in computer problems and for programming MSanalysis.

Hereby I would like to thank Dr. Peter Schneider for taking care of the MASCOT server cluster and introducing me into the basics of intranet to reach analyzed results and used databases.

Additionally, I would like to thank Dr. Peter Mortensen for providing dimethyl labeling compatible version of MSQuant and Dr. Bas van Breukelen for some bioinformatics programs enabling easier and quantitative analysis of measured data.

I am especially grateful for Jan Heye Buß for helping me in the MATLAB program based proteomic data management.

Furthermore, I would like to thank all my colleagues and PhD students from the Institute of Cardiovascular Physiology and from the Graduate School 1089 for fruitful scientific discussions and for a nice atmosphere at the laboratory.

At last but not at least I thank my family and all my friends, who supported and motivated me during the last years.

TABLE OF CONTENTS

ABSTRACT.....	8
ABSTRAKT (IN GERMAN).....	9
ABBREVIATIONS.....	10
I. INTRODUCTION.....	17
PHYSICAL AND CHEMICAL PROPERTIES OF NO	17
NITRIC OXIDE AS REGULATOR MOLECULE IN THE HEART	18
NO SYNTHESIS – THE NOSs	18
NO DEPENDENT SIGNALING PATHWAYS	20
HEART FAILURE AND NO	22
HEART FAILURE MODEL (iNOS+/MYO-/-) MICE	23
MASS SPECTROMETRY IN PROTEOMICS	25
PRINCIPLE	25
ION SOURCES	25
MASS ANALYZER	26
ANALYSIS OF PROTEIN PHOSPHORYLATION USING MASS SPECTROMETRY	28
OVERVIEW OF MS BASED QUANTIFICATION STRATEGIES.....	29
II. AIM OF THE STUDY.....	32
III. MATERIALS AND METHODS	33
USED MATERIALS	33
CHEMICALS AND MATERIALS	33
MS STANDARDS.....	34
ANIMALS	34
PRIMARY AND SECONDARY ANTIBODIES	34
LABORATORY INSTRUMENTS.....	35
SOFTWARE.....	36
LANGENDORFF-PERFUSION OF ISOLATED MOUSE HEARTS	37
BIOANALYTICAL METHODS.....	37
PROTEIN ASSAY USING BICINCHONINIC ACID (BCA)	37
TWO DIMENSIONAL GEL ELECTROPHORESIS (2-D PAGE)	38
ISOELECTRICAL FOCUSING (1. DIMENSION).....	38
GRADIENT SDS-PAGE (2. DIMENSION)	39
PROQ DIAMOND PHOSPHOPROTEIN STAIN	40
MS COMPATIBLE SILVER STAIN	40
COLLOIDAL COOMASSIE STAIN	40
WESTERN BLOT.....	41
IN GEL DIGESTION WITH TRYPSIN	42
PREPARATION OF HEART SAMPLES FOR COMPARATIVE PHOSPHOPROTEOME ANALYSIS USING STABLE ISOTOPE DIMETHYL LABELING	42
PROTEIN EXTRACTION AND FRACTIONATION FOR IN SOLUTION DIGEST.....	42
INTERNAL STANDARD – A REFERENCE FOR RELATIVE QUANTITATIVE ANALYSIS	42
REDUCTION AND ALKYLATION OF CYSTEINE RESIDUES.....	43
METHANOL-CHLOROFORM PRECIPITATION OF PROTEINS.....	43

ETHANOL PRECIPITATION	43
PROTEIN DIGESTION	43
STABLE ISOTOPE DIMETHYL LABELING	43
SAMPLE CLEAN UP USING SOLID PHASE EXTRACTION	44
PHOSHOPEPTIDE ENRICHMENT USING TITANIUM DIOXIDE MICRO PARTICLES FILLED TOP TIP	44
PHOSHOPEPTIDE ENRICHMENT USING CALCIUM PHOSPHATE PRECIPITATION	45
SAMPLE FRACTIONATION USING SCX FILLED TOP TIP	45
SAMPLE FRACTIONATION USING ACE MIXED BED FILLED TOP TIP	45
NANOLC-ESI-MS ANALYSIS	45
PREPARATION OF A REVERSE PHASE NANO HPLC COLUMN WITH ESI TIP INTERFACE	45
GLASS FIBER SOL GEL FRIT	46
NANO ETTAN HPLC SETUP FOR REVERSE PHASE CHROMATOGRAPHY	46
ULTIMATE 3000 HPLC SETUP FOR OFF LINE 2D CHROMATOGRAPHY	47
MS DATA PROCESSING	51
CALIBRATION AND TUNING OF THE MASS SPECTROMETER	51
LTQ SETUP TO ANALYZE PHOSPHORYLATED PEPTIDES	52
LTQ ORBITRAP	53
DATABASE SEARCHING	55
RELATIVE QUANTITATION USING QUALBROWSER	55
MSQUANT SETTINGS FOR AUTOMATED QUANTITATION OF PHOSHOPEPTIDES	56
IV. RESULTS	57
PRELIMINARY EXPERIMENTS	57
TESTS TO CLARIFY THE INITIAL CONDITIONS OF THE DIFFERENTIAL PHOSHOPEPTIDE ANALYSIS USING	
PHARMACOLOGICAL INHIBITION / ACTIVATION OF NO FORMATION	57
1D-PAGE BASED EXPERIMENTS	57
2D-PAGE BASED EXPERIMENTS	58
COMPARATIVE PHOSHOPEPTIDE ANALYSIS OF WILD TYPE VERSUS iNOS+/MYO-/- HEARTS	59
PERFUSION PROTOCOL FOR FURTHER EXPERIMENTS	60
SWITCHING FROM GEL BASED TO GEL FREE ANALYSIS	61
OPTIMIZATION OF METHODS REQUIRED FOR GEL FREE RELATIVE QUANTIFICATION	
OF PHOSHOPEPTIDES	61
STABLE ISOTOPE DIMETHYL LABELING OF PRIMARY AMINO GROUPS	62
OPTIMIZATION OF REACTION CONDITIONS	63
CALIBRATION FOR RELATIVE QUANTIFICATION	64
PHOSHOPEPTIDE ENRICHMENT	65
IMMOBILIZED METAL AFFINITY CHROMATOGRAPHY (IMAC)	65
TITANIUM DIOXIDE	66
CALCIUM PHOSPHATE PRECIPITATION	66
SCX FRACTIONATION	67
MULTIDIMENSIONAL PROTEIN IDENTIFICATION TECHNOLOGY (MUDPIT)	67
MANUAL SCX FRACTIONATION USING TOP TIP	68
OFFLINE SCX FRACTIONATION USING MICRO FLOW HPLC	69
NANO FLOW REVERSE PHASE CHROMATOGRAPHY	70
ETTAN NANO LC	70
ULTIMATE 3000	70
QUANTITATIVE ANALYSIS OF iNOS DERIVED NO INDUCED CHANGES IN THE HEART	
PHOSHOPEPTIDE	72
REPEATED ANALYSIS FOR STATISTICAL VALIDATION - EXPERIMENTAL SETUP	72
COMPARISON OF PROTEIN EXPRESSION PROFILES OF iNOS+/MYO-/- MICE	74
IDENTIFIED CARDIAC PHOSHOPEPTIDE USING LTQ	75
DIFFERENTIALLY REGULATED PHOSHOPEPTIDES UPON ENHANCED NO FORMATION	78
IDENTIFIED PHOSHOPEPTIDES WHICH ARE NOT REGULATED BY NO	84

NOT QUANTIFIABLE PHOSHOPEPTIDES.....	108
IDENTIFIED CARDIAC PHOSPHOPROTEOME USING LTQ ORBITRAP XL	112
IDENTIFIED NOVEL AND KNOWN PHOSPHORYLATION SITES - NOT REGULATED BY NO	113
PROTEINS WITH DECREASED PHOSPHORYLATION UPON ENHANCED NO FORMATION	115
PROTEINS SHOWING INCREASED PHOSPHORYLATION UPON ENHANCED NO FORMATION.....	116
V. DISCUSSION	121
GEL BASED PRELIMINARY STUDIES	121
NEWLY ESTABLISHED METHODS FOR IMPROVED PHOSPHOPROTEOME ANALYSIS	122
STUDY MODEL: NO-INDUCED HEART FAILURE IN MICE.....	122
OVERVIEW OF RESULTS	123
NOVEL VS. KNOWN TARGETS OF iNOS-DERIVED NO SIGNALING	123
NO-INDUCED VASCULAR SMOOTH MUSCLE RELAXATION.....	124
NO-TARGETED CONTRACTILE PROTEINS	133
MITOCHONDRIAL RESPIRATION	139
GLYCOLYSIS AND PYRUVATE METABOLISM	142
APOPTOSIS AND NO	149
BEYOND NO INDUCED PHOSPHORYLATION - KINASES AND PHOSPHATASES	149
SUMMARY	155
VI. OUTLOOK	158
VII. REFERENCES.....	159
CURRICULUM VITAE.....	178

ABSTRACT

Myoglobin, the major oxygen binding and transporting heme protein of the heart can act as a nitric oxide (NO) scavenger, compartmentalizing the physiological and pathophysiological effects of produced NO. The inducible isoform of nitric oxide synthase (iNOS) is only expressed during pathophysiological conditions in the myocardium including diseases such as ischemia-reperfusion, septicemia and heart failure. End-targets and signaling pathways of iNOS-derived NO in the modulation of cardiac function are not fully understood.

To perform a global gel-free phosphoproteome analysis in a model of NO-induced heart failure, isolated perfused hearts of transgenic mice with cardiac specific iNOS overexpression on a myoglobin deficient background (iNOS⁺/myo^{-/-}) were co-perfused either with the NOS substrate L-arginine (200μM) or with saline buffer. After 1 minute L-arginine exposure the contractile force was decreased by 30% to a new steady state, at which point hearts were freeze clamped.

For mass spectrometry based quantitative analysis, stable isotope dimethyl labeling of digested peptides was applied which introduced a 4Da mass difference per labelled primary amino group of peptide N-terminus and lysine residues. To reduce sample complexity peptides were fractionated on a strong cation exchange column, followed by phosphopeptide enrichment on titanium dioxide particles. Fractions were further separated and analyzed by nano flow reverse phase liquid chromatography online coupled with a tandem mass spectrometer (nanoRP-LC-MS/MS). In order to obtain reliable results, two biological and two technical replicates were measured of each membrane and cytosolic fraction (n=8).

Elaborated technology enabled the identification of 826 phosphorylation sites (246 novel) corresponding to 772 peptides which relate to 475 proteins. Phosphorylation site distribution was 81.2% serine, 18.2% threonine and 0.6% tyrosine. In this model of iNOS-induced heart failure 50 phosphorylation sites were downregulated (31 novel) and 69 were upregulated (16 novel) in proteins involved in calcium homeostasis (e.g. L-type calcium channel, phospholamban, ryanodine receptor, sarcalumenin), cardiac contractility (e.g. myosin-6, myosin binding protein C), energetics (e.g. pyruvate dehydrogenase, ATP citrate lyase) mitochondrial respiration (e.g. NADH dehydrogenase I alpha subcomplex subunit 7, ATP synthase subunit alpha) and transcription (e.g. histone deacetylase 4, isoform 2 of glucocorticoid receptor). Additionally, kinases and phosphatases (e.g. protein kinase C alpha, MAP kinase kinase 4, protein phosphatase 2A B56 delta subunit) were also regulated upon iNOS derived NO release.

In summary, this study provides the first global account of the cardiac phosphoproteome in NO-induced heart failure. Many novel phosphorylation sites were discovered which can be linked to depressed contractility, cardiac energetics and remodeling and are likely to have important novel regulatory functions.

ABSTRAKT (IN GERMAN)

Myoglobin ist das wichtigste sauerstoffbindende Hämoprotein des Herzens. Es fungiert als NO-Scavanger und sorgt für eine räumliche Begrenzung der physiologischen und pathophysiologischen Effekte des im Herzen gebildeten NO. Die induzierte Isoform der Stickstoffmonoxidsynthase (iNOS) wird nur unter pathophysiologischen Bedingungen im Myokard exprimiert, wie z.B. bei Ischämie-Reperfusion, Sepsis und bei einer Herzinsuffizienz. Die Zielproteine und Signalwege von NO und deren Rolle bei der Regulation der Herzfunktion sind bislang noch nicht vollständig aufgeklärt.

In dieser Arbeit wurde eine gelfreie Phosphoproteomanalyse etabliert und damit ein NO-induziertes Herzinsuffizienzmodell der Maus analysiert. Zu diesem Zweck wurden transgene Mäuse mit herzspezifischer iNOS Überexpression bei gleichzeitigem Mangel von Myoglobin (iNOS⁺/myo^{-/-}) verwendet. Die Herzen dieser Tiere wurden isoliert und mit einem salinen Medium perfundiert, welches das NOS-Substrat L-Arginin (200µM) enthielt. Nach Arginin Zugabe nahm die Kontraktionskraft des Herzens um 30% ab und erreichte bereits nach einer Minute stabile hämodynamische Werte. Danach wurden die Herzen schockgefroren und anschließend eine stabile Isotopen Dimethyl-Markierung der verdauten Peptide durchgeführt, welche eine 4 Da große Massendifferenz pro markierter primärer Aminogruppe der Peptid N-Termini und der Lysinreste bewirkt. Diese Massendifferenz war dann die Grundlage für eine quantitative Analyse des Phosphoproteoms mittels Massenspektrometrie. Hierzu wurden die Peptide zunächst über eine starke Kationenaustauschersäule fraktioniert und anschließend erfolgte die Anreicherung der Phosphopeptide über Titaniumdioxidpartikel. Danach wurden die Einzelfraktionen durch nanofluß Umkehrphasen Flüssigkeitschromatographie getrennt und mit Hilfe eines daran gekoppelten Tandem Massenspektrometers analysiert (nanoRP-LC-MS/MS). Insgesamt wurden zwei biologische und zwei technische Replikate gemessen, wobei jeweils die Membran- und die cytosolische Fraktion analysiert wurde (n=8).

Mit Hilfe der neu etablierten und validierten analytischen Methoden war es möglich 826 Phosphorylierungsstellen (246 neue Stellen) zu identifizieren, welche sich auf 772 Peptide bzw. auf 475 Proteine verteilen. Die Verteilung der Phosphorylierungsstellen im Einzelnen war: 81.2% Serin, 18.2 Threonin und 0.6% Tyrosin.

Bei dem iNOS induzierten Herzinsuffizienzmodell wurden 50 Phosphorylierungsstellen gefunden, die herunterreguliert (31 neue) bzw. 69 die hochreguliert waren (16 neue). Hierbei fanden sich wesentliche Proteine der Kalzium-Homöostase (z. B. L-Typ Kalziumkanal, Phospholamban, Ryanodinrezeptor, Sarcalumenin), kardialen Kontraktilität (z.B. Myosin-6, Myosin bindendes Protein C), Energetik (z.B. Pyruvatdehydrogenase, ATP Citrat-Lyase), mitochondrialer Atmung (z.B. NADH Dehydrogenase I alpha Unterkomplex Untereinheit 7, ATP Synthase Untereinheit alpha) und der Transkription (z.B. Histon Deacetylase 4, Isoform 2 des Glucocorticoid Rezeptors). Interessanterweise wurde auch der Phosphorylierungsgrad verschiedener Kinasen und Phosphatasen (z.B. Proteinkinase C alpha, MAP Kinase Kinase 4, Protein Phosphatase 2A B56 delta Untereinheit) durch NO direkt beeinflusst.

Zusammengefasst lässt sich feststellen, dass es sich bei dieser Studie um die erste Erfassung des globalen kardialen Phosphoproteoms in einem NO-induzierten Herzinsuffizienzmodell handelt. Die Vielzahl der neu entdeckten Phosphorylierungsstellen machen eine wichtige regulatorische Funktion bei der NO-induzierten Herzinsuffizienz wahrscheinlich. Jedoch muss die Funktionalität dieser neuen Phosphorylierungsstellen in weiterführenden Studien geklärt werden.

ABBREVIATIONS

ABLIM1	actin binding LIM protein
ACE	angiotensin-converting enzyme, somatic isoform precursor
Acly	ATP cytrate lyase
Acyp2	acylphosphatase
ADP	adenosine diphosphate
Akt or PKB	v-Akt murine thymoma viral oncogene or protein kinase B
ALDOA	fructose-bisphosphate aldolase A
AMP	adenosine monophosphate
AMPK- β 2	5'-AMP-activated protein kinase subunit beta-2
AngII	angiotensin II
ANT	adenosine nucleotide translocator
ATP	adenosine-5'-triphosphate
Atp5a1	ATP synthase subunit alpha, mitochondrial
AQUA	absolute quantification of proteins
β -AR	beta-1-adrenergic receptor
BH ₄	tetrahydrobiopterin
BP	base peak
bpm	beats per minute
°C	degree Celsius
Ca ²⁺	calcium
Cacna1c	L-type calcium channel α -1C subunit
Cacnb2	L-type calcium channel β -2 subunit
cADPR	cyclic ADP ribose
CaM, or CAL	calmodulin
cAMP	adenosine 3'-5'-cyclic-monophosphate
Ca _v 1.2 or LTCC	L-type calcium channel
CaMKII	Ca ²⁺ /calmodulin-dependent protein kinase II
Ca ₃ (PO ₄) ₂	calcium phosphate
CARLA	current assay for real time liquid baseline analysis
Cbx3	chromobox protein homolog 3

cGMP	guanosine 3'-5'-cyclic-monophosphate
CID	collision-induced dissociation
CK I	casein kinase I
CKII	casein kinase II
cNOS	constitutive nitric oxide synthase
COX5B	cytochrome c oxidase subunit Vb
CRM	charged residue model
CSRP3 or MLP	cysteine and glycine-rich protein 3
Cx43	connexin-43
Cyt c	cytochrome c
D	deuterium
2D	two dimensional
DAVID	Database for Annotation, Visualization and Integrated Discovery
DCDO	d2-formaldehyde
DCM	dilated cardiomyopathy,
DHB	2,5-dihydroxybenzoic acid
DNA	deoxyribonucleic acid
1D-PAGE or SDS-PAGE	one dimensional or SDS polyacrylamide gel electrophoresis
2D-PAGE	two-dimensional polyacrylamide gel electrophoresis
DT	double transgenic
DTT	1,4-dithiothreitol
EDRF	endothelial-derived relaxing factor
EDTA	ethylene diamine tetraacetic acid
eNOS	endothelial nitric oxide synthase
ESI	electrospray ionization
ETF	electron transfer flavoprotein subunit alpha, mitochondrial precursor
ETU	2-ethyl-2-thiopseudourea
FA	formic acid
FAD	flavin adenine dinucleotide
FADH ₂	flavin-adenine dinucleotide (reduced)
FMN	flavin mononucleotide
FTMS	Fourier-transformed mass spectrum

G3BP1	Ras GTPase-activating protein-binding protein 1
GSK3 β	glycogen synthase kinase 3 β
GC	guanylate cyclase
GLUT3	glucose transporter, type 3
GMP	guanosine-5'-monophosphate
GTP	guanosine-5'-triphosphate
H	hydrogen
Hb	hemoglobin
HCD	higher energy collision dissociation
HCHO	formaldehyde
HCM	hypertrophic cardiomyopathy,
HDAC4	histone deacetylase 4
Hdgfrp2	hepatoma-derived growth factor-related protein 2, isoform 1
HFBA	heptafluorobutyric acid
H ₂ O ₂	hydrogen peroxide
HPLC	high pressure liquid chromatography
HRC	histidine rich calcium binding protein
IAA	iodoacetamide
ICAT	isotope coded affinity-tag
ID	inner diameter
IEM	ion evaporation model
IMAC	immobilized metal affinity chromatography
iNOS	inducible nitric oxide synthase
iNOS ^{+/myo} ^{-/-}	double transgenic mice with cardiac specific inducible nitric oxide synthase overexpression on a myoglobin deficient background
iTRAQ	isobaric tag for relative and absolute quantitation
L-arg	L-arginine
LDHD	lactate dehydrogenase D
Lmo7	LIM domain only 7 protein
L-NMMA	NG-monomethyl-L-arginine
Lys or K	lysine
μ M	micromolar

MALDI	matrix-assisted laser desorption/ionization
MAP4	microtubule associated protein 4
MAPK	mitogen activated protein kinase
Myo or Mb	myoglobin
Mb(Fe ²⁺)	ferrous myoglobin
Mb(Fe ³⁺)	ferric myoglobin
Mb(Fe ⁴⁺)	ferryl myoglobin
MbO ₂	oxygenated myoglobin
MEKK3	mitogen activated protein kinase kinase kinase 3
MeCOOH	acetic acid
MeOH	methanol
MeCN	acetonitrile
metMb	metmyoglobin
MH ²⁺	doubly-protonated peptide ion
MHC	myosin heavy chain
α-MHC	myosin-6
min	minute
ms	millisecond
nl	nanoliter
MA	integrated peak area
MH	peak height
MLCK	myosin light chain kinase
MRLC2	myosin regulatory light chain 2-B, smooth muscle isoform
MS	mass spectrometry
MS/MS	tandem mass spectrometry
mtNOS	mitochondrial nitric oxide synthase
MyI7	myosin regulatory light chain 2, atrial isoform
Myo or Mb	myoglobin
MYPC3	myosin binding protein-c
m/z	mass per charge
N ₂	molecular nitrogen

NADH	nicotinamide-adenine dinucleotide (reduced)
NADPH	nicotinamide-adenine dinucleotide phosphate (reduced)
NaF	sodium fluoride
NaH ₄ CN	cyanoborohydride
NaH ₂ PO ₄	sodium dihydrogen phosphate
nanoRP-LC-MS/MS	nano flow reverse phase chromatography online coupled with a tandem mass spectrometer
NCX	sodium/calcium exchanger
Ndr _g 2	protein NDRG2, isoform I
Nd _u fa7	NADH dehydrogenase I alpha subcomplex subunit 7
nNOS	neuronal nitric oxide synthase
NO	nitric oxide
NO [•]	nitroxyl
NO ₃ ⁻	nitrate
NO _x	mono nitrogen oxides
NOS	nitric oxide synthase
Nr3c1	glucocorticoid receptor isoform 2
NUCSKS	nuclear ubiquitous casein and cyclin-dependent kinases substrate
O ₂	molecular oxygen
O ₂ ⁻	superoxide
p34cdc2	cyclin B kinase
pCr	phosphocreatine
PDH	pyruvate dehydrogenase
Pdha1	mitochondrial pyruvate dehydrogenase alpha subunit, E1 component
PKD1	phosphoinositol-dependent protein kinase-1
PFK2	6-phosphofructo-2-kinase/fructose-2,6-bisphosphate
PGM1	phosphoglucomutase-1
phos. site	phosphorylation site
Pi	free phosphate
Pi4kb	phosphatidylinositol 4-kinase beta
PIP ₃	phosphoinositol-1,4,5-trisphosphate
PLB	phospholamban

PKA	protein kinase A or cAMP-dependent protein kinase
PKA I α	cAMP-dependent protein kinase I- α regulatory subunit
PKC	protein kinase C
PKG	protein kinase G or cGMP-dependent protein kinase
PPI	protein phosphatase I
PP2A	protein phosphatase 2A
pPLB	phosphorylated phospholamban (at Ser-16)
pS	phosphoserine
pT	phosphothreonine
ppm	parts per million
PTM	post-translational modification
PTP	mitochondrial permeability transition pore
pY	phosphotyrosine
Q	ubiquinone
QqTOF	quadrupole-quadrupole-TOF
ROS	reactive oxygen species
rpm	rotation per minute
RS \bullet	sulfenyl radical
RS-NO	nitrosothiol
RT	room temperature
RyR2	ryanodine receptor
s or sec	second
SCX	strong cation exchange
S.D.	standard deviation
Ser	serine
SILAC	stable isotope labeling with amino acids in cell culture
SEK1	dual specificity mitogen-activated protein kinase kinase 4
SERCA2A	cardiac isoform of sarco/endoplasmic reticulum Ca ²⁺ -ATPase
SNAP	\pm S-nitroso-N-penicillamine
SOD	superoxide dismutases
SOD I	superoxide dismutase [Zn-Cn]

SR	sarcoplasmic reticulum
Src	Src kinase
SRL	sarcalumenin
OD	outer diameter
ONNO ⁻	peroxynitrite
TCA cycle	Szent-Györgyi-Krebs cycle or citric acid cycle
TIC	total ion count
TiO ₂	titanium dioxide
TFA	trifluoroacetic acid
Thr	threonine
TOF	time-of-flight
Tyr	tyrosine
V	voltage
VDAC	voltage-dependent anion channel
VHP	Villin headpiece domain
VSMC	vascular smooth muscle cell
WT	wild type
XIC _H	extracted ion chromatogram of heavy labeled peptide
XIC _L	extracted ion chromatogram of light labeled peptide

I INTRODUCTION

Nitric oxide (NO) is an omnipresent intracellular messenger molecule in all vertebrates, modulating blood flow, coagulation, neural activity, bone mineralization and many other processes. (for review see: Rastaldo et al., 2007; D'Atri et al., 2009). Endogenous NO release is also important for nonspecific host defense by macrophages against bacterial and parasitic infections. Due to its blood vessel relaxant effect, NO is used to treat persistent pulmonary hypertension in newborns by inhalation of low concentrations of gaseous NO.

For a century, nitroglycerin and other nitrovasodilators have been used clinically to decrease systematic vascular resistance and blood pressure without understanding their mechanism of action. Murad's group found that sodium nitroprussid, nitroglycerin, NO and other oxidants were able to activate guanylate cyclase (GC) (Katsuki et al., 1977; Braughler et al., 1979; Murad et al., 1979) and thereby stimulate intracellular cyclic GMP (cGMP) accumulation (DeRubertis et al., 1976; Arnold et al., 1977). Interestingly, although the vasorelaxant properties of NO was shown already in 1979 (Gruetter et al., 1979), nobody thought that NO, a major air pollutant, could be synthesized in mammals. The major candidates for in vivo GC activation were considered to be nitrosothiols at that time.

Furchgott and Zawadzki showed in 1980 that acetylcholine-induced relaxation of blood vessels was dependent on the endothelium. The released diffusible factor termed endothelial-derived relaxing factor (EDRF) was quickly inactivated by oxyhemoglobin and superoxide dismutases (SOD). EDRF was proposed to be a protective factor by scavenging superoxide. In 1986, Furchgott proposed and in 1987 Ignarro identified EDRF as NO by spectrophotometric analysis (Ignarro et al., 1987).

The important discovery of NO as a signaling molecule in the cardiovascular system was awarded with the Nobel Prize in Physiology and Medicine in 1998 to the three scientists R.L. Furchgott, L.J. Ignarro and F. Murad.

Following the discovery that EDRF is NO the focus of cardiovascular research concentrated on the analysis of the physiological and pathophysiological roles of endogenous NO and cGMP in the regulation of systemic blood pressure, organ blood flow, hemostasis and cardiac contractility. Further studies established role of NO for example in inflammation, tumor progression, apoptosis, neuronal aging, gastroprotection, renal tissue fibrosis and erectile dysfunction (for review see: Galkina et al., 2009; Sonveaux et al., 2009; Afanas'ev 2009; Rettori et al., 2009 and Sandner et al., 2009).

I.1 PHYSICAL AND CHEMICAL PROPERTIES OF NO

Nitric oxide is a two atomic free radical gas with odd number of electrons in the molecule. From a chemical point of view, NO as free radical is quite unreactive. NO does not participate in hydrogen abstraction reactions, only yields addition reactions with other chemical centers or molecules that also have unpaired electrons such as heme iron, O_2^- and O_2 . The reason of this relative unreactivity is in the structure of NO, which is an intermediate between molecular oxygen (O_2) and nitrogen (N_2). All three gases have low solubility and can readily diffuse through membranes and cytoplasm.

Molecular oxygen is a biradical with two unpaired electrons in separate orbitals, which shows a limited kinetic reactivity, and prevents its direct interaction with most biological molecules. On the other hand oxygen ($\bullet\text{OO}\bullet$) binds strongly to metals such iron in hemoglobin or cytochrome-c oxidase, and reacts quickly with an unpaired electron on other free radicals, leaving the second unpaired electron free for further reactions. Accordingly, molecular oxygen supports free radical damage and has a central role in oxidative stress.



Nitrogen gas is one of the most inert molecules, with two electron pairs, three bonds and quite small distance separating the nuclei. $\text{NO}\bullet$ with just one unpaired electron is a hybrid between $\bullet\text{OO}\bullet$ and NN , thus NO it is generally less reactive than O_2 . NO like O_2 binds strongly to metals such iron in hemoglobin or cytochrome-c oxidase moreover reacts with free radicals quickly in a chain terminating reaction, like sulfenyl ($\text{RS}\bullet$) radical conversion into nitrosothiols:



Via such chain terminating reactions NO can convert free radicals into less damaging transient intermediate products, which can then be repaired by antioxidants like ascorbate, tocopherol or glutathione resulting the original compound. Therefore nitrosative stress can also be seen as antioxidant activity.

1.2 NITRIC OXIDE AS REGULATOR MOLECULE IN THE HEART

Nitric oxide regulates many different functions in the cardiovascular system. Illustrating its pleiotropic effects, NO controls cardiac contractility and heart rate, limits the deleterious effects of cardiac remodeling after myocardial infarction, and contributes to the protective effect of ischemic pre- and postconditioning. NO furthermore modulates oxygen consumption, substrate utilization, sensitivity to apoptosis, hypertrophy and regenerative potential.

1.2.1 NO SYNTHESIS – THE NOSS

NO is formed by NO synthases (NOS) - a family of proteins which catalyses the five-electron oxidation of the guanidino nitrogen group of L-arginine to L-citrulline and NO . NOS s require essential cofactors for their activity like tetrahydrobiopterin (BH_4), haem, flavin mononucleotide (FMN), flavin adenine dinucleotide (FAD) and calmodulin (CAL) (Fig. 1.1). Oxidation of L-Arg to L-citrulline occurs via two successive monooxygenation reactions producing N-hydroxy-L-arginine as an intermediate. In this reaction for production of each mol of NO 2 mol of O_2 and 1.5 mol of NADPH are consumed as co-substrates.

So far four different NOS isoforms: neuronal (nNOS ; type I), inducible (iNOS , type II), endothelial (eNOS , type III) and mitochondrial (mtNOS , splice variant α of nNOS) have been described and named according to the cell type and conditions in which they first have been found. Nowadays it is well known that different isoforms can be even co-expressed within the same cell type, but depending on their sub-cellular localization's isoforms target different downstream functions. For example, nNOS colocalizes with the ryanodine receptor (RyR) in the sarcoplasmic reticulum

(SR) in cardiac myocytes and its activation increases cardiac contractility (positive inotrope). In contrast, eNOS binds to the β_3 adrenergic receptor in caveolae in endothelial cells and in cardiac myocytes, thereby inhibits L-type Ca^{+2} channels, and thus inhibits β -AR-mediated increases in myocardial contractility (negative inotrope).

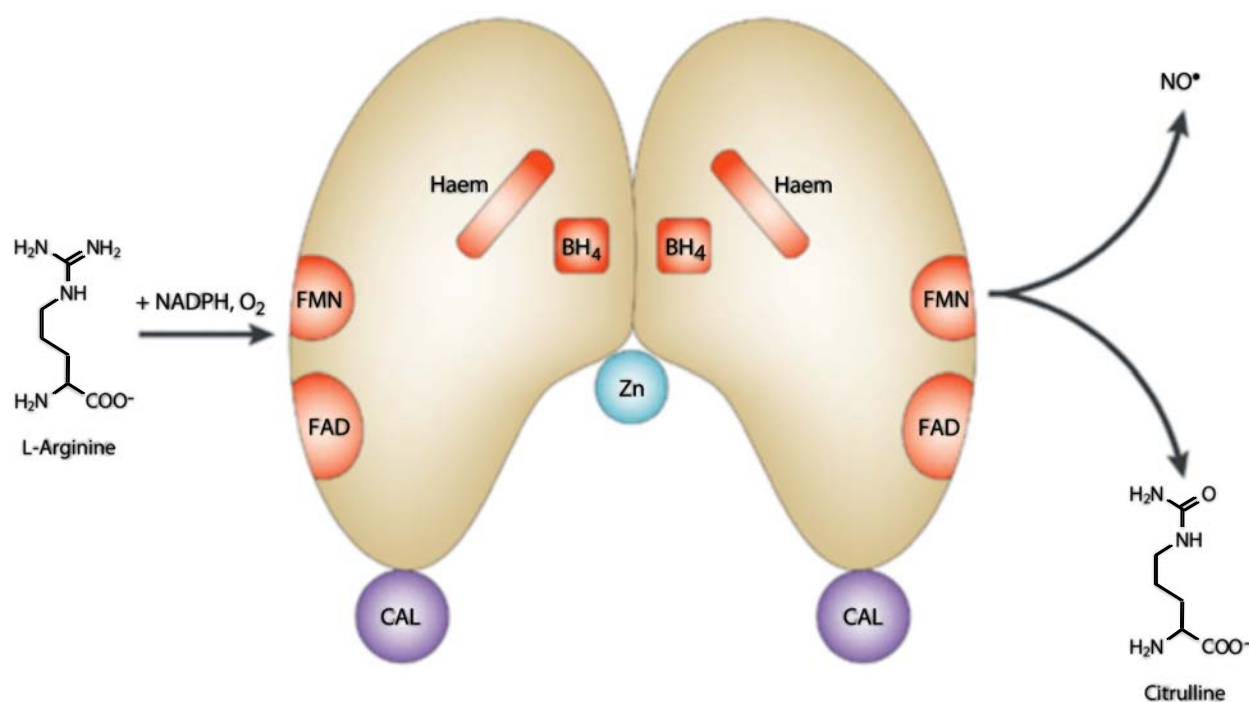


Figure I.1. NO synthesis by NOSs. Active NOS enzymes are dimerized, thereby coordinating a single zinc (Zn) atom. NOSs bind the essential cofactors tetrahydrobiopterin (BH₄), haem, flavin mononucleotide (FMN) and flavin adenine dinucleotide (FAD). Upon binding calmodulin (CAL) NOS catalyze the oxidation of L-arginine to citrulline and NO using thereby O₂ and NADPH as cosubstrate (Figure was taken from Vallance et al., 2002).

iNOS is a cytosolic protein, which is normally not expressed in the heart, but its expression is induced by inflammatory cytokines, endotoxin, hypoxia and oxidative stress after ischemia/reperfusion. Induced iNOS produce high, sustained levels of NO, which can inhibit mitochondrial respiration, oxidize myoglobin hence decrease oxygen supply to the mitochondria.

mtNOS is structurally attached to both complex I (NADH ubiquinone reductase) and IV (cytochrome oxidase) of the mitochondrial respiratory chain in different tissues including heart. mtNOS released NO regulates mitochondrial respiration by the reversible and O₂-competitive inhibition of cytochrome oxidase. mtNOS is regulated by important physiological effectors, such as mitochondrial inner membrane potential, electron transfer through NADH-dehydrogenase, environmental oxygen, autonomic regulation, angiotensin, thyroxine and insulin (Navarro et al, 2008). Interestingly, mtNOS is a key mediator of oxidative damage in ischemia/reperfusion (Ignarro, 2007).

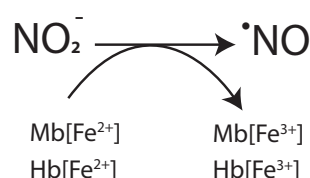
Calmodulin binding enhances the rate of electron transfer through the reductase domain to the oxygenase domain and thereby is important for NOS enzyme activity. In iNOS, calmodulin is bound tightly to the enzyme, whereas in eNOS, nNOS and mtNOS calmodulin binding and therefore

enzyme activity is calcium dependent. eNOS and nNOS are also called constitutive NOS (cNOS) because they are constitutively expressed. However, cNOS shows also important changes in their activity caused by post-translational modifications (PTM) and by protein-protein interactions. For example eNOS activity can be stimulated by oxidative phosphorylation at Ser-617, Ser-635 and Ser-1179 and inhibited by interaction with caveolin-1 or with Thr 497 phosphorylation (Fleming et al., 1999; Fulton et al., 1999).

Furthermore, hyperthermia increases the activity of NO synthases (eNOS is activated by heat-shock protein 90 (HSP90)), resulting in increased NO release and blood flow, thereby decreasing the initial activating factor, the temperature. Furthermore, NO blocks the major source of heat production, by inhibiting cytochrome oxidase c, the last enzyme of the respiratory electron transport chain in the mitochondria. Thus, NO may be an important part of the feedback loop to prevent excessive heating and heat damage of tissues during exercise or fever.

One should not forget about the importance of the bioavailability of NOS substrates, such as O_2 , L-arginine and NADPH. Regarding nNOS and iNOS, O_2 can be a synthesis limiting substrate because of the high K_M values being 130 and 350 μM O_2 , respectively. Furthermore, inhibition of arginase and arginase II, enzymes, which degrade and remove the NOS substrate L-arginine, increases nNOS and mtNOS activity resulting in an inhibition of contractility (Steppan et al., 2006).

A further source of NO can be the vascular endocrine nitrite reservoir, which can be converted into nitric oxide under ischemic conditions (Gladwin et al., 2006). This reaction can be catalyzed by hemoglobin and myoglobin, which change their NO scavenging properties under normoxia to NO-producing nitrite reductase activity under hypoxic/ischemic conditions.



Therefore myoglobin may act as an oxygen sensor in the heart, which forms NO to relax vessels, increase blood flow and improve myocardial oxygenation upon falling pO_2 (Rassaf et al., 2007).

1.2.2 NO DEPENDENT SIGNALING PATHWAYS

The effects of NO depends on its concentration and localization within the cell, therefore, NO deriving from different NOS isoforms have contradictory physiological role. For example, low NO concentrations induce small amounts of cGMP and inhibits phosphodiesterase 3, thereby preventing cAMP hydrolysis. The downstream activation of protein kinase A (PKA) opens the sarcolemmal voltage-operated and sarcoplasmic ryanodine receptor Ca^{2+} channels by phosphorylation (Fig. 1.2), and leads to increased myocardial contractility (positive inotrope).

At higher NO concentrations there is activation of the cGMP-dependent protein kinase (PKG) and its downstream signaling (Ogut et al., 2008; Bryan et al., 2009; Walter and Gambaryan, 2009) which leads to vasodilatation and decreased myocardial contractility (negative inotrope). Furthermore,

the NO-cGMP-PKG signaling pathway can induce inhibition of platelet aggregation, antiremodeling, anti-inflammatory and anti-apoptotic tissue protective effects (Fig. I.3).

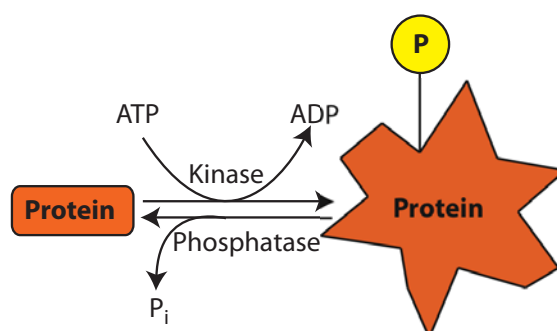


Figure I.2: Activated protein kinase can transfer phosphoryl group from ATP to various proteins thereby leading to protein phosphorylation of serine, threonine or tyrosine residues located in a particular kinase sequence motif, while removal of phosphate groups is catalyzed by protein phosphatases. NO activates various kinases and phosphatases like PKA, PKG and myosin light chain kinase phosphatase thereby leading to phosphorylation/dephosphorylation of their downstream targets.

On the other hand, if superoxide is present NO can form peroxynitrite (ONOO^-), a more powerful oxidant, what reacts with electron-rich groups, such as sulfhydryls, iron-sulfur centers, zinc-thiolates and active site sulfhydryl in tyrosine phosphatases. It can also react with transition metals centers, and thus modifies proteins containing a heme prosthetic group, such as hemoglobin, myoglobin and cytochrome c. Furthermore, it can oxidize cysteine residues, form nitrotyrosine, nitrotryptophan and nitrated lipids leading to tissue injury effects.

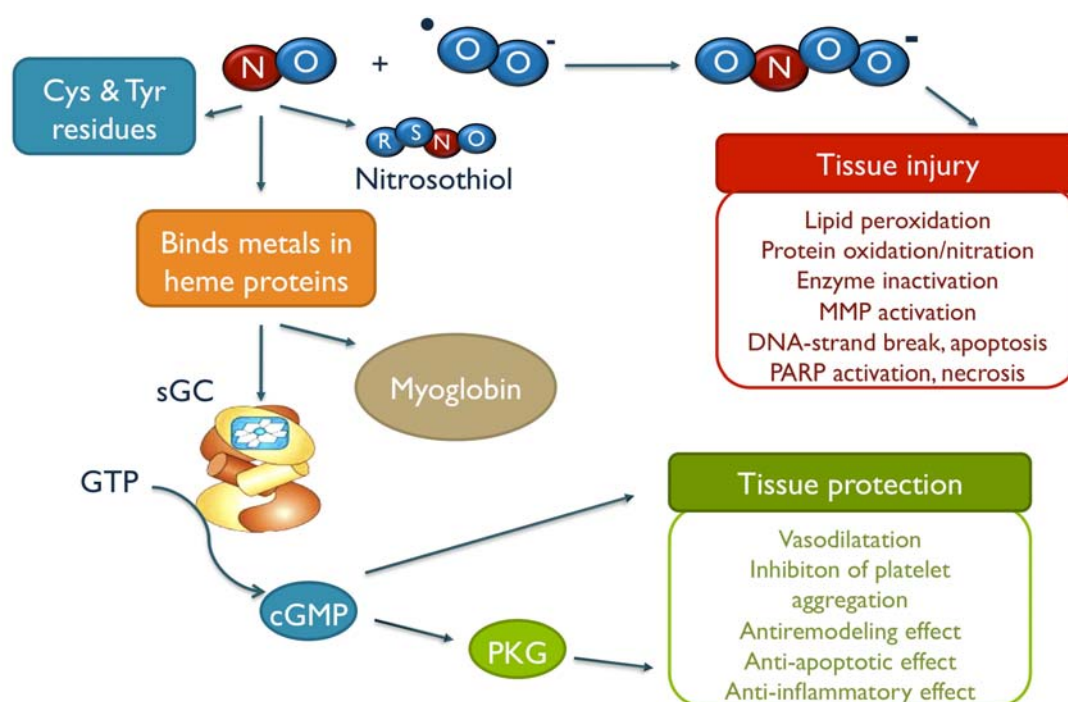


Figure I.3: Dual mechanisms of nitric oxide (NO) action leading to tissue injury effects over peroxynitrite (ONOO^-) formation or to tissue protective effects mediated by soluble guanylyl cyclase (sGC), cyclic guanosine monophosphate (cGMP) and protein kinase G (PKG). O_2^- : superoxide, GTP: guanosine-5'-triphosphate (Figure was modified from Evgenov et al., 2006).

There are efficient means minimizing NO accumulation in the body. NO is rapidly removed by its fast diffusion through tissues into red blood cells (Butler et al., 1998; Joshi et al., 2002) where due to its reaction with oxyhemoglobin it will be rapidly converted to nitrate. This limits biological half-life of NO in vivo to less than a second.

I.2.3 HEART FAILURE AND NO

Human heart failure is characterized by myocardial dysfunction causing insufficient blood supply to meet the body's demands. Typically the disease is triggered by hypertension, ischemic changes, atherosclerosis, valvular insufficiency, viral myocarditis or even mutations of genes encoding sarcomeric proteins. On the molecular level, development of human heart failure involves for example the activation of the neurohormones, neurotransmitters and the local renin-angiotensin system, downregulation of the β -adrenergic signal transduction cascade, induction of growth factors and proinflammatory cytokines. This leads to downstream activation of cell surface receptors and protein kinases including calcium/calmodulin-dependent kinase II (CaMKII), Akt, glycogen synthase kinase 3 β (GSK3 β), mitogen-activated protein kinases (MAPKs) and cyclic GMP-dependent protein kinase (PKG) (Mudd et al., 2008). These pathways are involved in pathophysiological responses resulting in a failing heart with an increased muscle-wall mass, a sign of cardiac hypertrophy. This occurs together with either wall thickening and preserved contraction (hypertrophic cardiomyopathy, HCM) or chamber enlargement and weakened contraction (dilated cardiomyopathy, DCM). The resulting changes can lead to severe fatigue, breathlessness and ultimately, death. Chronic heart failure is estimated to affect about 1-2% of the population in Europe and the US, with 550.000 new diagnosed cases annually alone in the US.

There is mounting evidence that an acute inflammatory response accompanies the decrement in left ventricular systolic function associated with heart failure and cardiogenic shock and that this response may affect survival outcomes. Therefore, much attendance was given to myocardial iNOS expression induced by proinflammatory cytokines during heart failure and cardiogenic shock. So far, iNOS derived levels of NO are known to inhibit the mitochondrial respiratory chain (Kelm et al., 1997), induce apoptosis in cardiac myocytes (Taimor et al., 2001), cause catecholamine resistant vasodilatation and reduced myocardial inotropy, resulting in hypotension and a fall in cardiac output (Kojda et al., 1996). In the failing heart superoxide production is also increased, leading to an exponential amount of peroxynitrite formation, which is directly toxic to the cells via modification of proteins and DNA. In addition, NO produced by iNOS is mainly responsible for the cardiodepression in septic shock (Rastaldo et al., 2007).

Recently, animal studies and clinical trials have been made to investigate if the inhibition of NOS by L-NMMA (NG-monomethyl-L-arginine,) might have clinical utility in septic shock treatment. Early studies were encouraging but the large randomized TRIUMPH trial had to be terminated because of a lack of efficacy, even increased mortality (Bailey et al., 2007). This failure may have been due to the little selectivity of tested iNOS inhibitor compound L-NMMA, which may have blocked other NOS isoforms essential for cardiac function. Therefore further studies have to prove the efficacy of iNOS inhibition using more selective molecules.

Dilated and ischemic cardiomyopathies were also characterized by a 50% reduced myocardial myoglobin content (O'Brien et al, 1992) and have been associated by compromised energy supply.

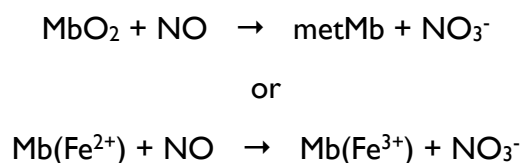
I.2.4 HEART FAILURE MODEL (iNOS⁺/MYO^{-/-}) MICE

Myoglobin (Mb) and hemoglobin (Hb) belong to an ancient superfamily of haem-associated globin proteins. A tetrapyrrole ring structure of the haem group provides four nitrogen ligands to the central iron atom which is essential for the protein function. If this iron is in the ferrous (Fe²⁺) redox state, it can reversibly bind gaseous ligands such oxygen. Therefore, Hb was described as oxygen transporting, whereas Mb as oxygen storing hemoprotein, to augment oxygen diffusion in the cytoplasm of high oxygen consuming and mitochondria rich muscles like the heart. Interestingly, animal models with dilated and ischemic cardiomyopathies were characterized with decreased myocardial Mb content (O'Brian et al., 1995), but myoglobin levels patient's blood were failed as biomarker for detection of myocardial infarction.

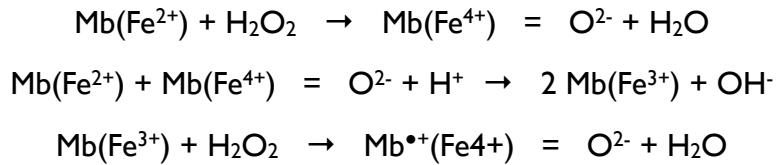
To study the role of myoglobin in cardiac function, myoglobin knock out mice were generated in our institute by deleting the functionally essential heme binding site encoding exon 2 region of the myoglobin gene (Gödecke et al., 1999). Surprisingly, the Myo^{-/-} mice were viable, fertile and didn't show any obvious sign of functional limitations. This unchanged viability could be attributed to the activation of multiple compensatory mechanisms, like elevated hemoglobin (molecular relative to myoglobin), capillary density, coronary flow and coronary reserve. Taken together, these changes reduced the diffusion path length for O₂ between capillary and mitochondria, to steepen the pO₂ gradient to the mitochondria. These results suggested an important role of myoglobin in oxygen transport processes.

As a consequence of limited oxygen bioavailability, myoglobin free hearts switch from fatty acid to O₂-sparing glucose utilization, by downregulation of key enzymes of the β-oxidation pathway (Flögel et al., 2004). Interestingly, similar changes in cardiac substrate selection were already described in patients with ischemic cardiomyopathy, heart failure, hypertrophy and dilated cardiomyopathy (Sambandam et al., 2002).

A further study explored the role of myoglobin in cardiac NO homeostasis by using isolated hearts of Myo^{-/-} and WT mice to measure the conversion of oxygenated myoglobin (MbO₂) to metmyoglobin (metMb) by reaction with NO (Flögel et al., 2001). Infusion of NO solutions or bradykinin (to induce endogenous NO production) resulted in dose dependent metMb formation in WT hearts. Additionally, NO or bradykinin coperfusion in Myo^{-/-} mice resulted in a more pronounced vasodilatation and cardiodepressant reaction, which suggested that myoglobin effectively degrades NO to NO₃⁻ thereby reducing the cytosolic NO concentration.



A century ago, Koberg has already shown that Mb and Hb can react with peroxides, by oxidizing the ferrous ($\text{Mb(Fe}^{2+})$) protein generating a ferryl ($\text{Mb(Fe}^{4+})$) state and in the case of the ferric ($\text{Mb(Fe}^{3+})$) protein, a protein based cation radical ($\text{Mb}^{\bullet+}$; Kelso-King et al. 1967) as follows:



However, this enzymatic activity was believed to have no relevance in vivo. Although, during the last 20 years it has become apparent that the redox chemistry of Mb and Hb has a real biological importance, typically under pathological conditions following ischaemia/reperfusion injury. But it still remained unclear whether these redox reactions result in a breakdown or even in an increased radical formation by the strong oxidizing ferryl derivative of Mb.

To clarify the role of Mb during oxidative stress wild type and $\text{Myo}^{-/-}$ mice were perfused with H_2O_2 or endogenously generated superoxide ($\text{O}_2^{\bullet-}$) (Flögel et al., 2004). Here, cardiac contractility of $\text{Myo}^{-/-}$ hearts showed a greater depression compared with WT controls. Moreover, after ischemia/reperfusion a delayed recovery and an enhanced release of reactive oxygen species (ROS) was observed in $\text{Myo}^{-/-}$ mice. All in all, myoglobin seems to be an important factor in redox signaling to protect the heart from oxidative damage.

Transgenic mice overexpressing iNOS under the cardiospecific α -myosin heavy chain promoter (iNOS^+) were generated in our institute (Heger et al., 2002). These mice were viable and appeared normal, although the hearts showed an about 260 to 400 fold increased iNOS activity in vitro. The index of in vivo NOS activity, the NO_x levels were increased 40-fold in the heart and 2.5-fold in the blood over the normal WT control. Interestingly, ventricular mass/body ratio did not differ and heart rate, cardiac output and mean arterial pressure were decreased just by 10%. Furthermore, cardiac hemodynamics, ATP and phosphocreatine levels were unaltered. As a consequence of higher iNOS activity, cardiac L-arginine (NOS substrate) levels were 6.7-fold reduced, whereas L-citrulline (NOS product) was 20-fold elevated compared with the WT. This suggested a possible limiting substrate availability. All in all, that results seemed to demonstrate that the heart in the presence of myoglobin can tolerate high levels of iNOS activity without leading to severe cardiac dysfunction.

To study the in vivo effects of myoglobin under nitrosative stress, a double transgenic cardiac specific iNOS-overexpression and concomitant myoglobin-deficiency mice was generated in our institute (Gödecke et al., 2003). Interestingly, crossing the iNOS^+ mice (no phenotype) with $\text{myo}^{-/-}$ mice (no phenotype) gave a pathological phenotype. As a consequence of the enormously increased iNOS mediated nitrosative stress, signs of heart failure with cardiac hypertrophy, ventricular dilatation and intestinal fibrosis were observed. Furthermore, functional cardiac depression, like reduced contractility, cardiac output, ejection fraction and cardiac energetics were found.

Phosphorylation sites and the downstream targets of NO-induced cell biological processes leading to the described pathophysiological phenotype have not been explored previously.

There is now considerable evidence that novel functions of myoglobin include: scavenging of nitric oxide, superoxide and reactive oxygen species thereby contributing to NO compartmentalization and constituting an important barrier against NO-induced heart failure by nitrosative stress.

I.3 MASS SPECTROMETRY IN PROTEOMICS

Since the present study utilized mass spectrometry (MS) to measure the NO-induced changes in the phosphorylation of cardiac proteins, due to its high throughput, speed, accuracy and potential to identify site specifically novel and known phosphorylation sites, a short introduction of MS based techniques shall be given here. During the last ten years, mass spectrometry developed into a powerful tool for analyzing complex biological samples and generating large data sets. (Aebersold and Mann, 2003; Köcher and Superti-Furga, 2007 and Chen et al., 2009).

I.3.1 PRINCIPLE

Mass spectrometric measurements are carried out in the gas phase on ionized analytes. Each mass spectrometer consists of an ion source, a mass analyzer and a detector (Fig. I.4), which ionize the analytes, measures the mass to charge ratio (m/z) of the ionized analytes and registers the number of ions at each m/z value, respectively.



Figure I.4: Principle of mass spectrometers used in proteome research.

I.3.2 ION SOURCES

Two ‘soft’ ionization techniques are commonly used for ionizing nonvolatile biological macromolecules intact (Fig. I.5): **electrospray ionization (ESI)** (Fenn et al., 1989) involves high voltage to charge the liquid containing the analyte, which forces the liquid to form an aerosol mist of charged droplets (Fig. I.5.A). There are two models to explain the mechanism of this process: the ion evaporation model (IEM) (Iribarne et al., 1976) and the charged residue model (CRM) (Dole et al., 1968). The IEM suggests that if the droplet reaches a certain radius (10^{-6} cm) by solvent evaporation, electrical field strength at the surface of the droplet becomes large enough to the field desorption of solvated ions. According to the CRM theory, droplets undergo evaporation and fission cycles leading to progeny droplets that contain on average one analyte ion. Thereafter, the solvent evaporates, resulting in multiply charged molecular ions that move to the mass spectrometer (MS) for detection. ESI can be easily coupled with front-end fractionation methods like high pressure liquid chromatography (HPLC) thus it is the most widely used ionization technique in proteomic studies. John Fenn was honored with part of the 2002 Nobel prize in chemistry for his development of ESI for the ionization of proteins.

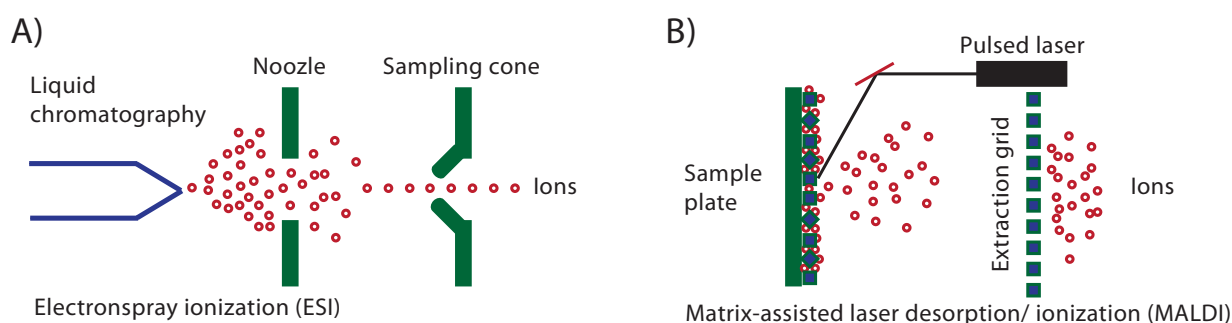


Figure I.5: A) Ionization and sample introduction process in electrospray ionization (ESI) and B) in matrix-assisted laser desorption/ionization (MALDI).

The other ‘soft’ ionization technique is **MALDI, or matrix-assisted laser desorption/ionization**, which uses a matrix (often a weak organic acid) to fix proteins or peptides on a special plate (Fig. I.5.B). Deposited spots are pulsed with a laser which heats the mixture resulting in fast expansion and ionization of the analyte which is transferred thereby into the gas phase. Unlike ESI, MALDI can not be easily coupled to HPLC, eluting drops have to be first mixed with a matrix and spotted to a MALDI plate. Koichi Tanaka showed for the first time how proteins can be ionized by MALDI without its disruption (Tanaka et al., 1988) and this was honored with part of the 2002 Nobel prize in chemistry.

I.3.3 MASS ANALYZER

There are several mass analyzer techniques on the market: **time-of-flight (TOF)** instruments (Fig. I.6.A) are the simplest and least expensive mass analyzer, in which ions are accelerated to a uniform kinetic energy and are introduced to a field-free tube. The velocity of the ions depends on its m/z value, it is proportional to the reciprocal square root of m/z . Thus, the ion traveling time to the detector (time-of-flight) can be used to determine m/z ratio. In the tandem mode (TOF/TOF instrument, Fig. I.6.B), ions of one m/z are selected by the first TOF section, fragmented in the collision cell and fragments are separated by the second TOF section. TOF is a fast but a less sensitive mass analyzer than ion trap instruments which cover a very wide m/z range.

Quadrupole mass analyzers use four parallel rods with fixed direct current and alternating radio-frequency potentials which permit stable trajectory only for ions of a particular desired m/z . Triple quadrupole (Fig. I.6.C) or quadrupole-quadrupole-TOF (QqTOF) (Fig. I.6.D) instruments are well suited for MS/MS experiments because efficient ion selection by the quadrupole, fragmentation in the collision cell and fragment ion detection by quadrupole or TOF (better mass accuracy) is available.

Ion trap mass analyzers (Fig. I.6.E) isolate ions within a three-dimensional or rectangular storage cell surrounded by electrodes of opposite polarity. Here, radio-frequency and direct-current potentials are varied to eject ions with different m/z from the storage cell to the detector, allowing mass detection as well as ion selection and fragmentation to be carried out by the same cell.

Sensitivity of detection can be enhanced by longer filling time periods. Ion fragmentation in an ion trap is very efficient, but ion trapping is suboptimal for low mass ions (under 200 m/z).

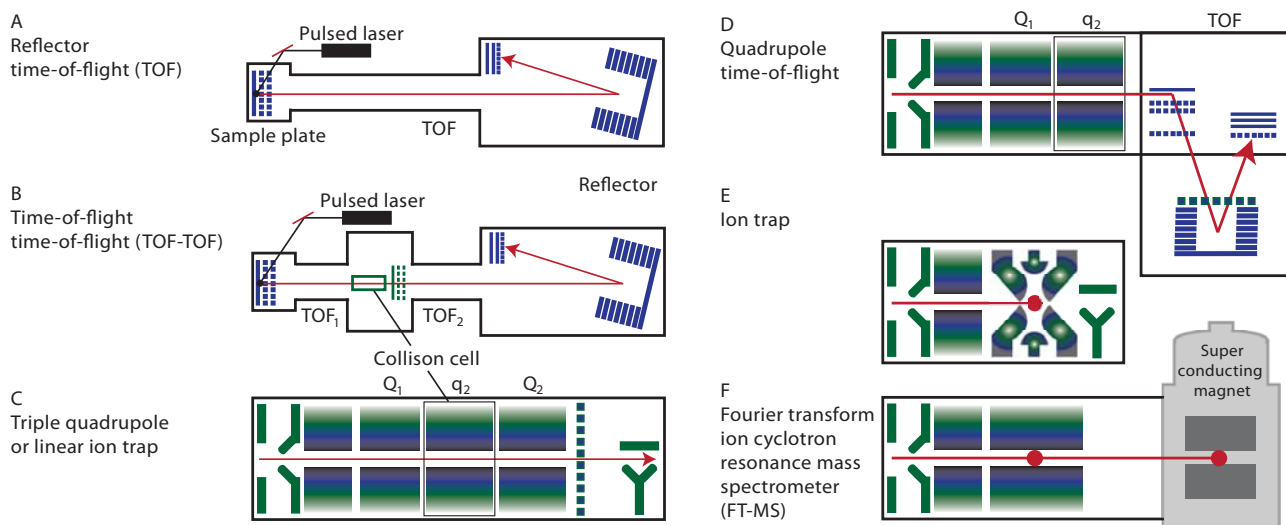


Figure I.6: Different instrumental configurations with their typical ion source.

Fourier-transform ion cyclotron resonance mass spectrometry (FT-MS) moves ions in circles within a static and strong magnetic field. Ion masses are determined by detecting their cyclotron frequencies within the image current, this ion cycling frequency is irreversibly proportional to m/z ratio. FT-MS technique provides a very high mass resolution, but lower sensitivity as that of ion trap instruments. Combination of FT-MS with the linear ion trap for efficient isolation, fragmentation and fragment detection in the FT-MS section is shown at Fig. I.6.F.

Orbitrap is a new, high-resolution, high mass accuracy and high sensitivity mass analyzer, which electrostatically maintains ions in an orbit around a central electrode (Fig. I.7). Orbitrap has also high dynamic range detection capabilities, and thus can be considered to be presently the most sensitive and versatile MS available.

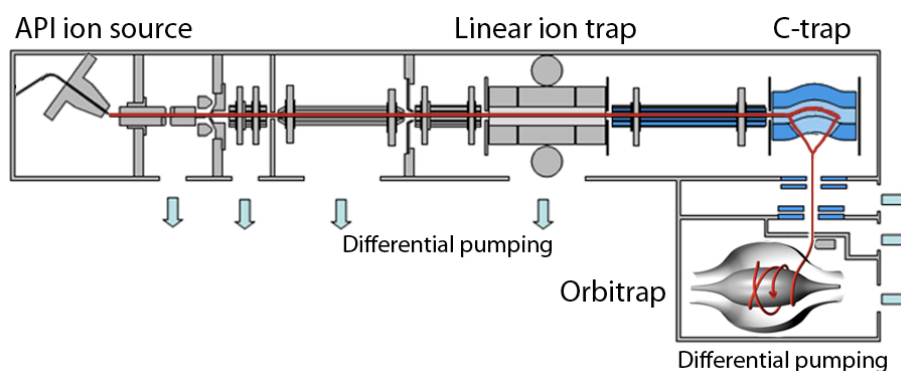


Figure I.7: Schematic view of an LTQ Orbitrap XL mass spectrometer.

Because of its advantages, in the present work LTQ (linear ion trap) and LTQ Orbitrap XL (linear ion trap with an orbitrap) mass spectrometers were used in combination with nano flow reverse phase liquid chromatography (nano-RP-LC) and electrospray ionization.

I.3.4 ANALYSIS OF PROTEIN PHOSPHORYLATION USING MASS SPECTROMETRY

During the last ten years, mass spectrometry based phosphoproteome analysis improved from identifying several phosphorylation sites from 2D-PAGE separated proteins (Alms et al., 1999) up to analyzing more than then thousand phosphorylation sites using gel free multi dimensional fractionation including HPLC followed by peptide identification on a high sensitivity mass spectrometer in one study (Hilger et al., 2009).

A few example from the field of phosphoproteome analysis:

One of the best proteomics research groups, the Mann group at the MPI in Munich, published the first global quantitative phosphoproteome on epidermal growth factor (EGF) stimulated HeLa cells (Olsen et al, 2006). They managed to detect 6600 phosphorylation sites on 2244 proteins by LTQ-FT high mass accuracy mass spectrometer and quantified them at five different time points to study phosphorylation dynamics. Another novel study of this group found in dissected melanoma by analysis of 2 mg of lysate with titanosphere chromatography and 8 mg with strong cation exchange together 5600 phosphorylation sites on 2250 proteins (Zanivan et al., 2008).

On the other hand, only 78 phosphorylation sites in 103 unique phosphopeptides from 78 proteins were found in bacterium *Bacillus subtilis* by the same group (Macek et al., 2007).

Very recently, analysis of the cytosolic protein fractions of the bloodstream form of trypanosoma brucei, the causative agent of African sleeping sickness, resulted in the identification of 491 phosphoproteins based on the identification of 852 unique phosphopeptides and 1204 phosphorylation sites (Nett et al., 2009).

Thus, the result of any phosphoproteome analysis strongly depends on analyzed species, cell type, treatment, amount of starting material and methods of analysis like fractionation, phosphopeptide enrichment and used MS fragmentation method.

Studies on the cardiac phosphoproteome usually identified phosphorylation sites of purified proteins or organelles only, mostly from mitochondria (Palmisano et al., 2007; Lu et al., 2008; Aponte et al., 2009). For example, phosphoproteome analysis of isoflurane-protected heart mitochondria using 2D-PAGE resulted in identification of 26 potential phosphorylation sites from which only one phosphorylation site was unknown (Feng et al., 2008).

Taken together, the global cardiac phosphoproteome is still quite unknown. Up to date, only two global phosphoproteomic studies were published with relatively limited results: 2-D gel electrophoresis in combination with ^{32}P autoradiography enabled the identification of nine phosphoproteins to study cardiac β -adrenergic signaling (Chu et al., 2004). Applying gel free methods resulted only in identification of 47 human cardiac phosphopeptides (Ruse et al., 2004). This non-quantitative study used immobilized metal affinity chromatography (IMAC) for phosphopeptide enrichment and worked without biological and technical replicates (n=1).

I.3.5 OVERVIEW OF MS BASED QUANTIFICATION STRATEGIES

As already introduced, compared to the 2D-PAGE based techniques gel-free separation methods enable the downstream identification of a higher number of protein and phosphorylation sites. On the other hand, the following MS based peptide identification is not quantitative, therefore comparison of different biological samples is not possible. To overcome this problem, different strategies were developed for relative or absolute protein/peptide quantification (Aebersold & Mann, 2003; Bantscheff et al., 2007). Table 5.1 shows a summary of this methods.

Metabolic labeling introduces a stable isotope signature into proteins at the earliest possible point of time by using ^{15}N (Oda et al., 1992) or $^{13}\text{C}_6$ -arginine and $^{13}\text{C}_6$ -lysine (SILAC; Ong et al., 2002) enriched cell culture medium.

Table 5.1: Comparison of different mass spectrometry based quantification methods.

	Metabolic labeling		Postmetabolic labeling				Label free
	^{15}N -labeling	SILAC	Enzymatic ^{18}O	ICAT	iTRAQ	Stable isotope dimethyl labeling	AQUA
Labeling chemicals	95% ^{15}N in medium	$^{13}\text{C}_6$ -arginine, $^{13}\text{N}_6$ -lysine in cell culture medium or food	H_2^{18}O after protease mediated cleavage	protein reactive group, mass-encoded linker and affinity tag	balancing group and reporter group, isobaric	d0 and d2 formalde-hyde and sodium cyanoboro-hydride	heavy isotope labeled peptides as internal standards
Labeled group	^{15}N in all amino acids	Lys, Arg	C-terminal oxygen atoms	Cys	N-term, Lys	N-term, Lys	-
Efficiency	Complete, but theoretically calculated and expected ratios differ	Excess of 90% achieved by 6-8 passages in labeled medium or after the 3. mouse generation	Slow, incomplete for acidic peptides, back exchange of ^{18}O to ^{16}O	Need to be optimized	Need to be optimized	Complete, fast	-
Labels	Cells, fruit fly, rat, etc.	Cells, mice, etc.	Peptides	Peptides	Proteins, peptides	Peptides	-
Spacing H-L	Not fixed	Fixed	Fixed, 4Da	8 Da pro Cys	No spacing, equal mass	Not fixed, 4 Da pro labeling	-
Disadvantages	Retention time spacing in HPLC	Metabolic conversion of Arg to Pro	Limiting the choice of protease, only Glu-C and Trypsin	Labels only peptides with Cys residue	Limited choice of mass spectrometer	Minimal retention time spacing in HPLC	Applicable only if preprocessing steps can be carried out highly reproducible
Multiplex	2	up to 5	2	2	up to 8	up to 4	2
Costs	+++	+++++	++	++++	++++	+	+++
Published	Oda et al, 1992	Ong et al., 2002	Heller et al., 2003	Gygi et al., 1999	Ross et al., 2004	Hsu et al., 2003	Gerber et al., 2003

Recently, a mice completely labeled with a diet containing either the natural or the $^{13}\text{C}_6$ -substituted version of lysine was introduced as SILAC-mouse (Krüger et al., 2008). Protein identification is based on fragmentation spectra of at least one of the co-eluting “heavy” and “light” labeled peptides and relative quantitation is performed by comparing the intensities or the peak area of the heavy and light labeled peptides.

Advantage of SILAC compared with ^{15}N -labeling is, that the number of incorporated label in SILAC is not dependent on the peptide sequence, therefore enabling easier data analysis. The main advantage of metabolic labeling strategies is that differentially treated samples can be combined already at the level of intact cells or isolated tissues, excluding all other sources of quantification errors.

Postmetabolic labeling of proteins or peptides is performed by chemical or enzymatic derivatization *in vitro*. ^{18}O incorporation by trypsin or Glu-C introduces a mass shift of 4 Da during or after protein digestion, allowing for relative quantification (Heller et al., 2003). One drawback of the method is the back-exchange of ^{18}O to ^{16}O with a concomitant loss of the isotope label at extreme pH values. Furthermore, acidic peptides are resistant against ^{18}O incorporation leading to different labeling ratios in different peptides, further complicating data analysis.

Isotope coded affinity-tag (ICAT) specifically derivatizes cysteine residues with a reagent containing zero or eight deuterium atoms as well as a biotin group for affinity purification of the labeled peptides (Gygi et al., 1999). As cysteine is a rare amino acid, ICAT reduces sample complexity of the peptide mixture to cysteine containing peptides. Thus, ICAT is not suitable for quantifying proteins with no or only few cysteine residues. It is therefore of limited use for the analysis of post translational modifications and splice isoforms. Labeling the peptide N-terminus and the epsilon-amino group of lysine residues via the N-hydroxysuccinimide (NHS) chemistry or other active esters and acid anhydrides has been used in various labeling procedures. The most often used isotope tags is iTRAQ, which can be used for relative and absolute quantification (Ross et al., 2004). In this technique the isotopomers of heavy and light labeled peptides can be distinguished only upon peptide fragmentation by the mass spectrometer allowing for quantitation due to different tags ($m/z=113$ -121). Thus, mass spectrometers with low mass cut off are disadvantageous for detection.

Label free quantitation using isotope-labeled synthetic standard peptides added in known quantity to the digested protein mixture is able to perform absolute quantification of proteins (AQUA; Gerber et al., 2003). This method focuses usually on a few particular proteins of interest, unlike in metabolic and postmetabolic labeling where relative quantification is performed for a huge number of peptides present in the mixture. A more specific method called multiple reaction monitoring (MRM; Kirkpatrick et al., 2005) combines retention time, peptide mass and masses of one or more specific fragment ion, eliminating interference of isobaric peptides and extends quantification range to 4-5 orders of magnitude. However, sample manipulation prior adding synthetic standards may mask true protein expression levels in a cell.

Stable isotope dimethyl labeling (Hsu et al., 2003) of lysine residues and peptide N-terminus via Schiff base formation by normal (D0) or deuterized (D2)-formaldehyde and subsequent reduction by cyanoborohydride is a fast, specific reaction, which labels all peptides. It is

also comparatively cost effective and therefore altogether an optimal choice for a phosphoproteome study. Furthermore, labeling leads to better peptide identification scores due to enhanced $\alpha(1)$ and $\gamma(n-1)$ fragment ion intensity. A drawback of the method is that physiochemical differences of deuterium and hydrogen results in small, but significant differences in retention time after reverse phase HPLC separation of heavy and light labeled peptide pairs. Therefore, in contrast to other methods where one MS spectrum can be enough to relatively quantify heavy and light labeled peptides, stable isotope dimethyl labeling requires integration of peak area (based on minimum 5 MS spectra) of eluting peptides for accurate quantitation.

Due to its advantages, being fast, specific and cost effective, the complete labeling of all possible peptides by stable isotope dimethyl labeling is an optimal choice to perform a quantitative phosphoproteome study.

2 AIM OF THE STUDY

The aim of the study was to investigate the global cardiac phosphoproteome and evaluate the NO-induced changes as related to cardiac contractile force. This study was made possible by the availability of an interesting NO-induced heart failure model in mice generated in our institute. In this model the inducible nitric oxide synthase was overexpressed on a myoglobin (NO scavenger) lacking background (*iNOS⁺/myo^{-/-}*) in which large amounts of NO result in heart hypertrophy, reduced contractility, cardiac output, ejection fraction and cardiac energetics.

NO is known to activate kinases and phosphatases leading to changed protein activity due to protein phosphorylation and dephosphorylation. The NO-induced cardiac signaling is not fully understood and many of the NO-induced phosphorylation sites are most likely unknown. In addition, mass spectrometry based phosphoproteome analysis has grown to be a powerful tool during the last few years.

To be able to measure changes in the global cardiac phosphoproteome, various state of the art proteomic methods were introduced and individually validated. They include:

- 1) stable isotope dimethyl labeling of peptide N-terminus and lysine residues which introduces a 4 Da mass difference per labeled primary amino group to be able to perform quantitative mass spectrometry based measurements
- 2) sample fractionation on a strong cation exchange column using micro flow HPLC to reduce sample complexity
- 3) phosphopeptide enrichment to remove non-phosphorylated peptides which would preclude phosphopeptide identification due to its better ionization and its excess amount
- 4) nano flow reverse phase chromatography (nano-RP-LC) to further separate peptides and concentrate them to a specific point of time to elute into the online coupled mass spectrometer which improve sensitivity of measurements
- 5) diverse fragmentation methods for tandem mass spectrometry based phosphopeptide identification and quantification, to optimize speed, sensitivity, number of identified peptides and data quality for quantitative measurements
- 6) integration of bioinformatic tools for automatic extraction of quantitative data from original in .raw format measured mass spectrometry files

In summary, the improvement of methodology should enable to obtain a first insight into the cardiac global phosphoproteome as influenced by endogenously formed nitric oxide.

3 MATERIALS AND METHODS

3.1 USED MATERIALS

3.1.1 CHEMICALS AND MATERIALS

Chemicals and Materials	Chemicals and Materials
Acrylamide-bis 30 %	Serva
Immobiline DrySrtip pH 4-7, 18 cm	Amersham Biosciences
Immobiline DryStrip pH 3-11, 18 cm	Amersham Biosciences
PlusOne DryStrip Cover Fluid	Pharmacia Biotech AB, Uppsala, Sweden
Formic acid	Merck
Acetic acid	Merck
o-Phosphoric acid	Merck
Ammonia solution	Merck
Chloroform	Merck
Methanol	Riedel-de Häen
Isopropanol	Riedel-de Häen
Acetonitrile	Riedel-de Häen
Heptafluorobutyric acid	Promega
Sequencing grade modified trypsin	Promega
Formaldehyde-d2 98%	Isotec
BCA Protein Assay Kit	Pierce
Endoproteinase Glu-C sequencing grade	Roche
Complete mini protease inhibitor cocktail tablets	Roche
PhosStop	Roche
Phosphatase inhibitor cocktail set II	Calbiochem
Protran nitrocellulose transfer membrane	Whatman
Western lightning chemiluminescence reagent plus	Perkin Elmer
BioMax XAR film	Kodak
Rapigest SF	Waters
ZipTip U C18	Millipore
TopTip C18	Glygen Corp.
TopTip Titandioxid	Glygen Corp.
TopTip Polysulfoethyl A	Glygen Corp.
TopTip WAX	Glygen Corp.
SPEC PT C18	Varian
SPEC C18AR 3ML (15 mg, 30 mg)	Varian
PicoTip EMITTER	NewObjective
C18 PepMap100, 3 µm 100A	Dionex
Polysulfoethyl-Asp 5 µm 300A	Dionex
Nucleodur Gravity C18 3 µm	Macherey-Nagel
Partisphere SCX 5 µm	Whatman
Fused silica capillary (10, 20, 25, 75, 100, 200 µm ID, 360 µm OD)	Polymicro
Double distilled water (max. 18.2mOhmcm)	Millipore

Table 3.1 List of used chemicals and materials

All other chemicals were purchased from Fluka. All materials were used highest purity available.

3.1.2 MS STANDARDS

Calibrating agents	Peptide sequence	Monoisotopic mass [MH ⁺]	Manufacturer
Caffeine solution	-	195.09	Sigma
MRFA	MRFA	524.26	Research Plus, Inc., Manasquan, NJ
Ultramark 1621	-	1022.01, 1122.00, 1221.99, 1321.99, 1421.98, 1521.97, 1621.96, 1721.95, 1821.95, 1921.94	Lancaster Synthesis, Inc., Pelham, NH

Table 3.2 Agents for ESI-MS mass calibration

Peptides	Peptide sequence	Monoisotopic mass [MH ⁺]	Manufacturer
Angiotensin I	DRVYIHPFHL	1296.68	Sigma Aldrich
Angiotensin II	DRVYIHPF	1046.54	Sigma Aldrich
Neurotensin	pELYENKPRRPYIL	1673.92	Sigma Aldrich
Substance P	RPKPQQFFGLM	1348.63	Sigma Aldrich
Bradykinin	RPPGFSPFR	1060.57	Sigma Aldrich
Bradykinin Fragment 1-5	RPPGF	573.31	Sigma Aldrich
Synthetic phosphopeptide (pS)	GTYSPPSAQEYCNPR	1652.67	BMFZ, University of Düsseldorf

Table 3.3 List of used standard peptides

Proteins	Molecular mass	Manufacturer
β-Casein, bovine	25,107 Da	Sigma Aldrich

Table 3.4 Used standard protein

3.1.3 ANIMALS

Mice were bred at the Tierversuchsanlage of the Heinrich-Heine-Universität, fed with a standard chow diet and received tap water ad libitum. Animal experiments were performed in accordance with the national guidelines on animal care and approved by the Bezirksregierung Düsseldorf.

3.1.4 PRIMARY AND SECONDARY ANTIBODIES

Antibody	Manufacturer
Anti-iNOS	Transduction Lab., Lexington, KY
Anti-Myoglobin	Dunn Labortechnik GmbH, Asbach
Anti-Phosphotyrosine-RC20:HRPO	BD Biosciences, San Jose, CA
Anti-Phospholamban	Calbiochem, Darmstadt

Anti-Phospholamban, Phospho-Specific (Ser ¹⁶)	Calbiochem, Darmstadt
Anti-VASP	Alexis Corp., Lausen, Schweiz
Anti-VASP, Phospho-Specific (Ser ²³⁹)	Alexis Corp., Lausen, Schweiz
Peroxidase-conjugated AffiniPure Goat Anti-Mouse IgG (H+L) (minimal cross-reaction to Human, Bovine, Horse Rabbit and Swine Serum Proteins)	Jackson ImmunoResearch Lab. Inc., Wes Grove, PA
Peroxidase-conjugated AffiniPure Goat Anti-Rabbit IgG (H+L) (minimal cross-reaction to Human, Bovine, Horse Rabbit and Swine Serum Proteins)	Jackson ImmunoResearch Lab. Inc., Wes Grove, PA

Table 3.5 List of primary and secondary antibodies

3.1.5 LABORATORY INSTRUMENTS

Instrument	Manufacturer
Milli Q Plus	Millipore Corporation, Billerica, MA
Sorvall Ultracentrifuge OTD55B	DuPont, Wilmington, DE
Precidor	Infors AG, Basel
Potter S	B.Braun Melsungen AG, Melsungen
Ultra Turrax T18 basic	IKA Works do Brasil Ltaquara, RJ
Spectra Count BS1000I	Packard Inst. Comp. Inc., Warrenville, IL
Centrifuge 5418	Eppendorf AG, Hamburg
Thermomixer Comfort	Eppendorf AG, Hamburg
pH Meter, pH 526	Wissenschaftlich – Technische Werkstätten, Weilheim
InLab423 pH combination electrode	Mettler Toledo International Inc., Columbus, OH
REAX 2000	Heidolph Instruments GmbH, Schwabach
IPGphor	Amersham Pharmacia Biotech, San Francisco, CA
Ettan DALT II System	Amersham Pharmacia Biotech, San Francisco, CA
Triphoon 8600	Amersham Pharmacia Biotech, San Francisco, CA
Powerlook III Scanner	Amersham Pharmacia Biotech, San Francisco, CA
Julabo 20BVC	Julabo Labortechnik GmbH, Seelbach
Mini-PROTEAN 3 Cell	Bio-Rad, Hercules, CA
Fastblot B33	Whatman Biometra, Göttingen
Power Pack P25	Whatman Biometra, Göttingen
Multitemp II Thermostatic Circulator	LKB Producta AB, Bromma, Sweden
CURIX 60	AGFA
KL-2 Swip	Edmund Bühler GmbH, Tübingen
Lyovac GT 2	Leybold-Heraeus GmbH, K“oln
SpeedVac Concentrator	Bachofer GmbH, Weilheim/Teck
A-905 Autosampler	Amersham Pharmacia Biotech, San Francisco, CA
Ettan microLC	Amersham Pharmacia Biotech, San Francisco, CA
Model P-2000	Sutter Instrument Co., Novato, CA
FinniganLTQ	Thermo Scientific, San Jose, CA
LTQ Orbitrap XL	Thermo Scientific, San Jose, CA
Ultimate 3000	Dionex Corporation, Sunnyvale, CA

Table 3.6 List of instruments

Instrument	Manufacturer
Pump DGP-3600MB	Dionex Corporation, Sunnyvale, CA
Solvent Rack SRD-3600	Dionex Corporation, Sunnyvale, CA
Flow Manager FLM-3100B, NANO	Dionex Corporation, Sunnyvale, CA
Well Plate Sampler WPS-3000TB	Dionex Corporation, Sunnyvale, CA
VWD-3100	Dionex Corporation, Sunnyvale, CA
UZ-View flow cell VWD 3 nL	Dionex Corporation, Sunnyvale, CA
UZ-View flow cell VWD 180 nL	Dionex Corporation, Sunnyvale, CA
Automated off-line 2D-LC	Dionex Corporation, Sunnyvale, CA

Table 3.7 Parts of the Ultimate 3000 nanoHPLC System with fraction collection

3.1.6 SOFTWARE

Software	Manufacturer
Chart 4	AD Instruments Pty Ltd, Castle Hill, Australia
PlateReader	Packard Inst. Comp. Inc., Warrenville, IL
I-Smart	Packard Inst. Comp. Inc., Warrenville, IL
Software	Manufacturer
Unicorn 5.01	Amersham Pharmacia Biotech, San Francisco, CA
Chromeleon	Dionex Corporation, Sunnyvale, CA
LTQ 2.4	Thermo Scientific, San Jose, CA
XCalibur 2.07	Thermo Scientific, San Jose, CA
Bioworks 3.3	Thermo Scientific, San Jose, CA
DTASupercharge (version 1.19)	www.msquant.sourceforge.net
MASCOT (version 2.2)	Martix Sci. Ltd, London, UK
MSQuant (version for N-term modifications kindly provided by Dr. Lennart Martens)	www.msquant.sourceforge.net

Table 3.8 Used software

3.2 LANGENDORFF-PERFUSION OF ISOLATED MOUSE HEARTS

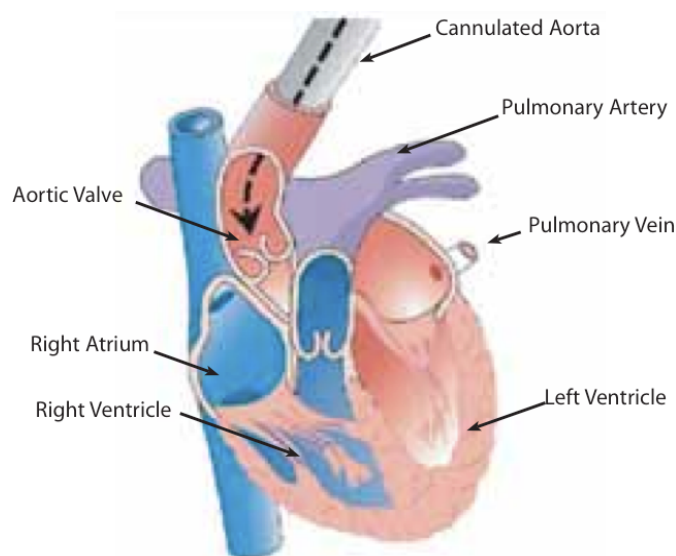


Figure 3.1. Cannulated aorta

Chemicals	Concentration
KCl	4.63 mmol/l
MgSO ₄	1.1 mmol/l
NaHCO ₃	24.9 mmol/l
NaCl	116 mmol/l
KH ₂ PO ₄	1.18 mmol/l
Glucose	8.32 mmol/l
Pyruvate	2.0 mmol/l
EDTA	0.5 mmol/l
Add Millipore water to 2 l and mix	
Equilibrated with carbogen (95% O ₂ /5% CO ₂) for 15 min, pH 7.4	
Add CaCl ₂	2.52 mmol/l
Filtrate (20µm filter)	

Table 3.9. Modified Krebs-Henseleit buffer (KHB)

Mice were anesthetized by IP injection of urethane (1.5 g/kg body weight) and heparinized with 500 U IP. Hearts were rapidly excised and placed in ice-cold KHB (see table 3.9) for preparation of the aortic arch. Heart perfusion was done at constant coronary pressure (95 mm Hg) with KHB (37°C) equilibrated with carbogen (95% O₂ / 5% CO₂) in non-recirculating mode. Perfusion pressure and coronary flow were recorded with the Chart 4 (AD Instruments) software. After stabilization of the coronary flow cardiac pacing (500 bpm) was initiated and continued throughout. Fifteen minutes after the beginning of cardiac pacing and perfusion with KHB the coronary perfusion was switched to constant flow at the flow rate at which the hearts were stabilized. Afterwards 20 mmol/l L-arginine (L-arg) was coperfused (dilution 1:100) into the KHB buffer with a final concentration of 200 µmol/l (corresponds to in vivo L-arg concentration). After one min of L-arg coperfusion the heart was snap frozen with a clamp precooled in liquid nitrogen and the sample was stored at -80°C.

3.3 BIOANALYTICAL METHODS

3.3.1 PROTEIN ASSAY USING BICINCHONIC ACID (BCA)

The BCA protein assay was performed using the microplate protocol according to the manufacturers instructions. The samples were measured with a Spectra Count BS10001 Microplate Reader (Packard Inst. Comp. Inc., Warrenville, IL) at 540 nm and data were analyzed using I-Smart Software.

3.3.2 TWO DIMENSIONAL GEL ELECTROPHORESIS (2-D PAGE)

3.3.2.1 Isoelectrical focusing (1. Dimension)

Heart samples were lysed in 5 ml phosphatase inhibitor cocktail containing lysis buffer using an ice cooled Sartorius glass homogenizer and centrifuged for 10 minutes at 12500 g. The supernatant was aliquoted and stored at -20°C.

Chemicals	Amount
Urea	9.5M
CHAPS	2%
Tris	40 mM
NaF	10 mM
Na ₂ VO ₃	2 mM
Na ₂ H ₂ P ₂ O ₇	10 mM
β-glycerophosphate	60 mM
DTT	1%

Table 3.10 Lysis buffer composition for isoelectric focusing

Protein concentrations were determined using the Bradford protein assay. Equal amounts of sample (300 µg/gel) were taken and proteins were precipitated by chloroform-methanol extraction to remove salts. Sediments were resolved in 420 µl sample buffer. After centrifugation (10 min, 14000 g) the sample was loaded into a 18 cm-Stip-Holder, an IPG strip was placed on top (without air bubbles) and covered with DryStrip Cover Fluid (mineral oil) to prevent desiccation during focusing.

Chemicals	Amount
Urea	8M
CHAPS	1%
Bromphenol blue	a few grains
Pharmalyte (according to pH of used strips)	0.5%
DTT	0.33%

Table 3.11 Sample buffer composition

First dimensional isoelectric focusing was performed on a IPGPhor (Amersham Pharmacia Biotech) instrument. The protocol shown in table 3.12 was applied with 50µA/strip electric current.

After focusing the strips were incubated under reducing (1% DTT, 15 min, RT, 100rpm, 7.5 ml/strip) and alkylating conditions (2.5% IAA, 15 min, RT, 100rpm, 7.5ml/strip) in an SDS containing equilibration buffer (see table 3.13). For the second dimensional separation strips were placed onto a gradient SDS-PAGE and hold in place by covering with agarose sealing solution.

pH range	Step	Volt (V)	Time (h:min)	Volthours (kVh)
3-11, 4-7	Rehydration			
	Step & Hold	500	1:00	0.5
	Gradient I	1000	8:00	6.0
	Gradient II	8000	3:00	13.5
	Step & Hold	8000	2:00	16.7
	Step & Hold	500	5:00	2.5

Table 3.12 Steps of first dimensional isoelectric focusing

Chemicals	Amount
4xRB	16,75 ml
Urea	6 M
Glycerol (87%)	33.3%
SDS	2%

Table 3.13 Composition of equilibration buffer

Chemicals	Amount
Tris	1.5 M
Adjust pH to 8.8 using HCl	

Table 3.14 Composition of 4x resolving buffer (4xRB)

Chemicals	Amount
1xEB	250 g
Low gelling agarose	2.5 g
Bromphenolblue	a few grains

Table 3.15 Agarose sealing solution

Chemicals	Amount
Tris	25 mM
Glycine	192 mM
SDS	0.1%
Add 2 l double distilled water	

Table 3.16 10x electrophoresis buffer (10xEB)

3.3.2.2 Gradient SDS-PAGE (2. Dimension)

Gradient gels were prepared from 4% and 16% acrylamide containing separating gel solutions using a mixing chamber. Table 3.17 shows the composition of the gel solutions.

Samples for 1D electrophoresis were desalted and delipidated by methanol-chloroform extraction, resolved in 1x sample buffer with DTT and reduced at 37°C for 30 minutes.

Chemical	4% gel	16% gel
Acrylamide / Bis (30%)	1,3 ml	5,3 ml
Tris-HCl 1,5M (pH 8.8)	2,5 ml	2,5 ml
Water	6,1 ml	-
Glycerol (86%)	-	2,1 ml (18,3%)
SDS (10%)	100 µl	100 µl
APS (10%)	100 µl	100 µl
TEMED	5 µl	5 µl

Table 3.17 Composition of the 4% and 16% acrylamide containing gel solutions for gradient SDS-PAGE

Chemical	Amount
Tris-HCl 0.5M (pH 6.8)	2.5 ml
SDS (10%)	4.0 ml
Glycerol (86%)	2.3 ml
Water	1.2 ml
Bromphenol blue	a few grains
DTT	7.7 mg/0.5ml added freshly

Table 3.18: 2x sample buffer composition for 1D electrophoresis

3.3.3 PROQ DIAMOND PHOSPHOPROTEIN STAIN

The gel separated phosphoproteins were stained using ProQ Diamond according to the manufacturers instruction (fast protocol). Removing the interfering salts and lipids via methanol/chloroform extraction prior to gel electrophoresis was an important step to achieve optimal staining results. Phosphoproteins were detected with a Typhoon 8600 scanner (Amersham Pharmacia Biotech) by applying the following parameters: 200 µm pixel, fluorescence, 532 nm excitation source, 560 nm high pass emissions filter, 480 V PMT.

3.3.4 MS COMPATIBLE SILVER STAIN

MS compatible silver stain (sensitivity up to 0.1 ng) was performed as described by Shevchenko et al. (1996). Gels were developed for one minute and digitized using an Amersham Pharmacia Biotech Powerlook III Scanner.

3.3.5 COLLOIDAL COOMASSIE STAIN

SDS-PAGE separated proteins were visualized using colloidal Coomassie stain according to Kang et al. (2002). This stain shows an enhanced sensitivity (up to 1 ng) compared to the common Coomassie protocol (up to 50 ng) with lower background staining and reaches a signal intensity up to 80% after two hours. Table 3.19 shows the components of the staining and destaining solutions.

Chemicals	Staining solution		Destaining solution	
	amount	[%]	amount	[%]
CBB-G250	0,4 g	2%	-	-
Aluminiumsulfat-18-Hydrat	100 g	5%	-	-
Ethanol (96%)	200 ml	10%	200 ml	10%
o-Phosphoric acid	40 ml	2%	40 ml	2%
Water	Up to 2000 ml		Up to 2000 ml	

Table 3.19 Composition of staining and destaining solution of the colloidal Coomassie stain

3.3.6 WESTERN BLOT

Semi dry western blot using anti-phosphotyrosine-RC20 antibody was carried out according to Maile et al. (2002). Phospholamban detection was performed as described by Mayer et al. (2000). Since phospholamban is a membrane protein it was important to reduce the sample with DTT at 37°C for 30 minutes and not at 98°C for 10 minutes to avoid its precipitation. Detection of myoglobin and iNOS was performed according to the standard semi dry blot protocol.

Chemicals	Amount	Concentration
Glycine	5,86 g	39 mM
Tris (pH 8.5)	11,62 g	48 mM
SDS	0,75 g	375%
Methanol	400 ml	20%
Water	Fill up to 2000 ml	

Table 3.20 Components of the standard semi dry western blot transfer buffer

Briefly, according to the standard protocol gels with the separated samples were washed in semi dry blot transfer buffer for 10 minutes and blotted with 2 mA/cm², 10°C, 2h to a nitrocellulose membrane. The membrane was washed in semi dry blot wash buffer for 10 minutes and blocked with wash buffer containing 5% milk powder at 37°C for 30 minutes.

Chemicals	Amount	Concentration
Tris (pH 8.3)	6,065 g	25 mM
NaCl	17,532 g	150 mM
Tween-20	4ml	2%
Water	Fill up to 2000 ml	

Table 3.21 Components of the standard semi dry western blot wash buffer

Incubation with the primary antibodies was done over night (1:2000, 4°C, 200 rpm). Afterwards the membrane was washed three times and incubated with a horseradish peroxidase (HRPO) conjugated secondary antibody (1:10000, 4h, 20°C, 200 rpm). After three washing steps blots were developed with Western Lightning Chemiluminescence Reagent Plus (Perkin Elmer) and BioMax

XAR Film (Kodak). The film exposure time was varied to optimize signal intensity. For development a CURIX 60 (AGFA) instrument was used.

3.3.7 IN GEL DIGESTION WITH TRYPSIN

In gel digestion of protein spots from 2-D gels was performed according to the modified protocol of the EMBL Bioanalytical Research Group. Following the normal EMBL protocol the colloidal Coomassie stained spots could not be destained. Using the destain solution of the colloidal Coomassie staining protocol (Table 3.19) solved this problem.

3.3.8 PREPARATION OF HEART SAMPLES FOR COMPARATIVE PHOSPHOPROTEOME ANALYSIS USING STABLE ISOTOPE DIMETHYL LABELING

3.3.8.1 Protein extraction and fractionation for in solution digest

Hearts were homogenized with an ice cooled Sartorius glass homogenizer in 5 ml homogenization buffer (Table 3.22) and centrifuged for 15 minutes at 7500 g and 4 °C to remove cell debris and nuclei. The supernatant was further centrifuged for 2 hours at 4 °C, 100,000 g to separate cytosolic (supernatant) and membrane fraction (pellet). Supernatant was aliquoted and stored at -80 °C until further use.

Chemicals	Amount
Tris HCl pH 8.0	20 mM
EDTA pH 8.0	2 mM
NaCl	150 mM
NaF	10 mM
Na ₂ H ₂ P ₂ O ₇	10 mM
Na ₂ VO ₃	2 mM
β-glycerophosphate	60 mM
Phosphatase inhibitor cocktail II (Calbiochem)	100 x diluted
Add freshly PMSF (500 mM stock in DMSO)	5 mM

Table 3.22 Components of the homogenization buffer

Nuclear and membrane pellets were resolved in a mass spectrometry compatible anionic detergent 1% Rapigest SF (Waters) containing homogenization buffer, centrifuged for 15 minutes at 7500 g and 4 °C, aliquoted and stored at -80 °C until further use.

3.3.8.2 Internal standard – a reference for relative quantitative analysis

Before reduction, alkylation and digestion 10 µg beta casein was added as internal standard to all samples to control the entire work flow. Furthermore, homogenization buffer, protein concentration and sample volume of sample pairs was adjusted to the same values to achieve

comparability. In addition the sample pairs were always handled in parallel in the same way. During the entire process low bind tips and tubes were used to minimize sample loss.

3.3.8.3 Reduction and alkylation of cysteine residues

To reduce sample complexity it is necessary to reduce and alkylate the cysteine residues, which might form disulfide bridges or become modified by glutathiolation and oxidation. The reduction was performed using 1,4-dithiothreitol (10 mM DTT, 37°C, 1h) followed by alkylation with iodoacetamide (50 mM IAA, 25°C, 2h, dark). Iodoacetamide was quenched with L-cysteine (50 mM, 25°C, 2h, dark).

3.3.8.4 Methanol-chloroform precipitation of proteins

To concentrate the sample, remove salts, detergents and lipids, methanol-chloroform precipitation, a quantitative protein precipitation method was performed according to Wessel et al. (1984). Briefly, to each 0.1 ml of sample solution 0.4 ml of methanol was added and mixed well by vortexing. Next 0.1 ml of chloroform was added and mixed vigorously. Afterwards 0.1 ml of water was added, mixed well and centrifuged at 16000 g for 10 min. The upper phase was removed and 0.3 ml of methanol was added. The sample was mixed well and centrifuged for 10 minutes at 16000 g. After discarding the supernatant the pellet was dried under the fume hood. The desalted and delipidated pellet was resolved in digestion buffer for in solution digest.

3.3.8.5 Ethanol precipitation

To each 0.2 ml protein sample 1.8 ml ethanol was added and mixed well by vortexing. The sample was incubated at -40°C for 4 h and centrifuged for 10 minutes at 20.000 g (4°C). The supernatant was removed and the pellet was dried under the fume hood. Finally, the pellet was resolved in digestion buffer for in solution digest.

3.3.8.6 Protein digestion

The pH of the alkylated sample was adjusted to 7.8 using 500 mM ammonium bicarbonate. Additionally, the trypsin cofactor calcium (5 mM CaCl_2) was added. The digestion with trypsin was performed at an enzyme to protein ratio of 1:20 (over night, 37°C, 600 rpm). Proteolysis was stopped by adjusting the pH to 2-3 with formic acid (FA). Digestion was controlled on a coomassie stained SDS-PAGE using 5 µg digested sample.

3.3.8.7 Stable isotope dimethyl labeling

Stable isotope dimethyl labeling of digested peptide samples was performed according to Hsu et al. (2003) with minor modifications. Briefly, digested and desalted peptide samples were resolved in 100 mM NaCH_3COOH (pH 5.4) to a final peptide concentration of 0.5 mg/ml. After peptide solubilization the pH was measured again and adjusted if necessary. Freshly prepared 4% d0-

formaldehyde (HCHO) or d2-formaldehyde (DCDO) and 600 mM sodium cyanoborohydride (NaH_4CN) was added (5 μl per 100 μl) and mixed well. The labeling reaction was performed in a Thermomixer comfort (30°C, 600 rpm, 1h) and quenched by adding a solution of 7% NH_4OH (5 μl per 100 μl). The labeling procedure had to be performed under the safe hood because of the high toxicity of formaldehyde and cyanoborohydride. Furthermore, it was necessary to prevent the presence of acids because the reaction of cyanoborohydride and acids forms the highly toxic cyan.

3.3.8.8 Sample clean up using solid phase extraction

The LC-MS procedure interfering substances were removed using solid phase extraction (SPE) of digested peptides. After adjusting the pH to 2-3 the sample was loaded to a preconditioned C18 microcolumn. To prevent sample loss the column size was varied according to the sample amount. The C18 column was preconditioned using methanol and washed three times with wash buffer. Afterwards the sample was loaded onto the column and the flow through was reloaded two additional times to prevent sample loss. Salts, detergents and other chemicals were washed away using wash buffer five times. Peptides were eluted by applying stepwise increasing acetonitrile in the elution buffer which decreased the hydrophobic interactions between the column material and the sample. The collected eluate was dried in a speed vacuum concentrator and stored at -80°C until further use.

Solution	Buffer composition
Column preconditioning	MeOH followed by washing
Loading buffer	0.1% TFA, 0,012% HFBA (pH 2-3)
Wash buffer	0.1% TFA, 0,012% HFBA
Elution buffer I	0.1% FA, 20% MeCN
Elution buffer II	0.1% FA, 40% MeCN
Elution buffer III	0.1% FA, 60% MeCN

Table 3.23 Buffer compositions for peptide solid phase extraction

3.3.8.9 Phosphopeptide enrichment using titanium dioxide micro particles filled TopTip

Enrichment of phosphopeptides was carried out according to Larsen et al. (2005) with minor modifications. Briefly, the previously digested, labeled, desalted and in loading buffer resolved peptide mixture was loaded onto the TiO_2 micro particles filled TopTip. Gentle centrifugal force was applied to press the solutions through the filled tip. To enhance sample binding the collected flow through was loaded again two additional times. The column was washed three times using wash buffer I and six times with wash buffer II to remove non phosphorylated peptides from the column. Bound peptides were eluted using elution buffer with increasing pH. The pH of the eluted peptide solution was immediately adjusted to 2-3 with 100% formic acid.

Name	Buffer composition
Loading buffer	20 mg/ml DHB, 30% MeCN, 2% FA
Wash buffer I	20 mg/ml DHB, 30% MeCN, 2% FA
Wash buffer II	80% MeCN, 4% FA
Elution buffer I	250 mM NH_4HCO_3 , pH 9
Elution buffer II	Elution buffer II: 500mM NH_4OH , pH 10
Elution buffer III	5mM NH_4OH , pH 10.5

Table 3.24 Buffer compositions for phosphopeptide enrichment on TiO_2

3.3.8.10 Phosphopeptide enrichment using calcium phosphate precipitation

Phosphopeptide enrichment using calcium phosphate precipitation was performed according to Zhang et al. (2007) with minor modifications. The digested, labeled and desalted peptide sample was resolved in 50 mM ammonium bicarbonate (NH_4HCO_3) and 0,5 M Na_2HPO_4 was added at a ratio of 1:26. The sample was mixed vigorously and the pH was adjusted to 10.5 using 5 mM NH_4OH . 2M CaCl_2 was added at a ratio of 1:26 and mixed well. The sample was centrifuged (20.000g, 10 min, RT) and washed with 80 mM CaCl_2 . Finally, the sample was centrifuged again and the pellet was resolved in 5% FA and desalted on a C18 column.

3.3.8.11 Sample fractionation using SCX filled TopTip

Translating the MudPit protocol of Washburn et al. (2001) to manual fractionation using SCX chromatography material filled TopTip offers the opportunity to handle higher sample amounts and easily reduce sample complexity by salt step fractionation.

3.3.8.12 Sample fractionation using ACE mixed bed filled TopTip

Following the idea of Motoyama et al. (2007) to enhance chromatography separation of enriched phosphopeptide fractions, anion and cation mixed-bed ion exchange chromatography was performed. Chromatography material of two WAX and one Polyaspartamid A TopTip column was removed, mixed and filled back into one of the empty TopTips. Afterwards the newly prepared ACE TopTip was used for fractionation of stable isotope labeled and desalted complex peptide mixtures. Fractionation was performed the same way as mentioned for the SCX filled TopTip.

3.3.9 NANOLC-ESI-MS ANALYSIS

3.3.9.1 Preparation of a reverse phase nanoHPLC column with ESI tip interface

The polyimide coating of a 50 cm long fused silica capillary (75 μm ID x 360 μm OD) was burned away in the middle of the capillary at a length of 3 cm. The surface was cleaned using an ethanol wetted dust free wipe and the capillary with the prepared window in the polyimide coating was placed into a Model P-2000 (Sutter Instrument Co., Novato, CA) laser pulling instrument. The fused silica capillary was pulled according to the steps described in table 3.25.

	Heat	Fil	Vel	Del	Pul
Step 1	290	-	25	128	-
Step 2	280	-	20	128	-
Step 3	260	-	20	128	-
Step 4	250	-	20	128	-

Table 3.25 Pulling steps of the fused silica capillary

Thereby two 25 cm long fused silica capillaries were generated with 1 μm ID pulled tips, which is a prerequisite for a good ESI ionization and functions as a frit also. The pulled capillaries were loaded in a high pressure bomb with C18 PepMap100 3 μm particle (taken out from a 1 mm ID x 15 cm Micro C18 PepMap100 3 μm 100Å Dionex column) suspended in 30% isopropanol (iPrOH) and 70% methanol (MeOH) mixture. Packing was continued until the fused silica capillary was filled up to 20 cm with the particles. The prepared column was dried under high pressure nitrogen flow and stored at room temperature in a dust free and dry environment.

3.3.9.2 Glass fiber sol gel frit

To minimize precolumn dead volume, to place the column in the column oven (not as an ESI interface) and to control peptide separation using UV detection (214 nm) there is a need to prepare nanoHPLC columns with a pressure stable frit. A glass fiber sol gel frit matches this requirements and was prepared according to the protocol described by Maiolica et al. (2005). Briefly, a glass microfibre filter (GC/C Whatman) was wetted with a 2 μl mixture of 100 μl Kasil (gift of PQ Europe) and 50 μl 25% formamide solution. The glass fiber frit was prepared by pushing the capillary on the wetted glass microfibre filter and heated overnight at 85°C. The filter containing capillary was washed with MeOH and packed as described above. Precolumns were filled up to 2 cm, separating columns up to 20 cm bed volume with the corresponding material.

3.3.9.3 nanoEttan HPLC setup for reverse phase chromatography

The μEttan HPLC system (Amersham Pharmacia Biotech) was modified to produce a nano flow rate of 200 nl/min using suitable fused silica capillaries, a flow splitter and a nano valve. The sample was loaded in microliter pick up mode with an A-905 autosampler and injected to a C18 PepMap precolumn. The sample bound to the precolumn was online desalted by extensive washing with buffer A for 20 minutes with a flow rate of 20 $\mu\text{l}/\text{min}$.

Buffer	Buffer composition
Buffer A	2.5% MeCOOH, 0.012% HFBA
Buffer B	84% MeCN, 2.5% MeCOOH, 0.012% HFBA

Table 3.26 Buffers used in reverse phase chromatography with Ettan nanoLC.

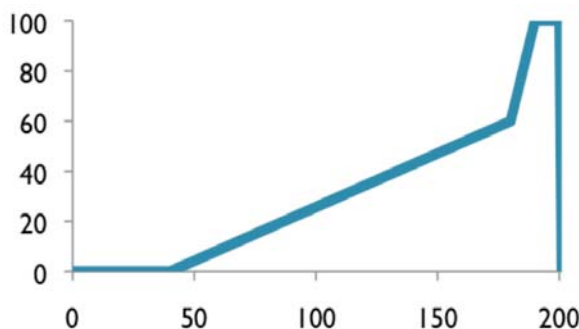


Figure 3.3. MeCN gradient used to separate in gel digested peptides on a RP column

After this period the precolumn was automatically switched in line with the separating column and a 80 minutes long acetonitrile (MeCN) gradient (see figure 3. 3) with a nano flow rate of 200 nL/min to separate the peptides on the reverse phase column was started. The column was coupled to an ESI-MS/MS tandem mass spectrometer (LTQ, Thermo Scientific) for online identification of the eluting peptides.

3.3.9.4 Ultimate 3000 HPLC setup for off line 2D chromatography

The Ultimate 3000 HPLC (see figure 3.4) with fraction collection offers the possibility to perform off-line 2D chromatography. Compared with 1D chromatography and lab in a tip fractionations, 2D chromatography provides a better reduction of sample complexity, which is essential for relative quantification using LC-MS.

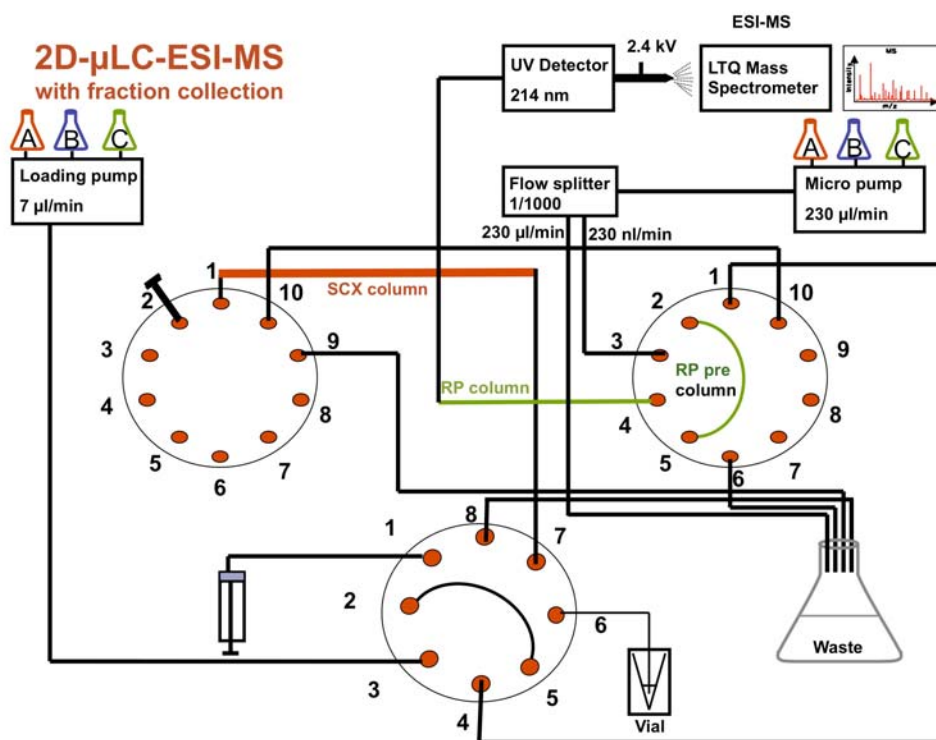


Figure 3.4 Ultimate 3000 set up for off line 2D chromatography

Solvent	Flow rate	Buffer Composition
Loading pump buffer A	7 μ l/min	0.1% TFA
Loading pump buffer B	50 μ l/min	5 mM NaH ₂ PO ₄ (pH 2.7)
Loading pump buffer C	50 μ l/min	500 mM NaCl, 15% MeCN, 5 mM NaH ₂ PO ₄ (pH 2.7)
Micro pump buffer A	230 nl/min	0.1% FA
Micro pump buffer B	230 nl/min	84% MeCN, 0.1% FA

Table 3.27 Buffer composition and flow rate for off-line 2D Chromatography

The Ultimate 3000 system software program Chromeleon was programmed to perform the following washing, separation and fractionation steps as shown in Fig. 3.5-3.11. Before starting the experiment, loading pump buffers were prepared freshly and the system was washed overnight to remove remaining TFA. The presence of TFA would preclude sample binding to the Polysulfoethyl-Aspartamid SCX column (300 μ m ID, 15 cm). Initially, a standard run with a peptide mixture of eight trypsin digested proteins was performed to test system performance. Afterwards, the labeled, phosphopeptide enriched and desalted heart peptide mixture was dissolved in 5 mM NaH₂PO₄ (pH 2.7) and injected onto the preparative SCX column by switching the autosampler valve from load into inject position (Fig. 3.5).

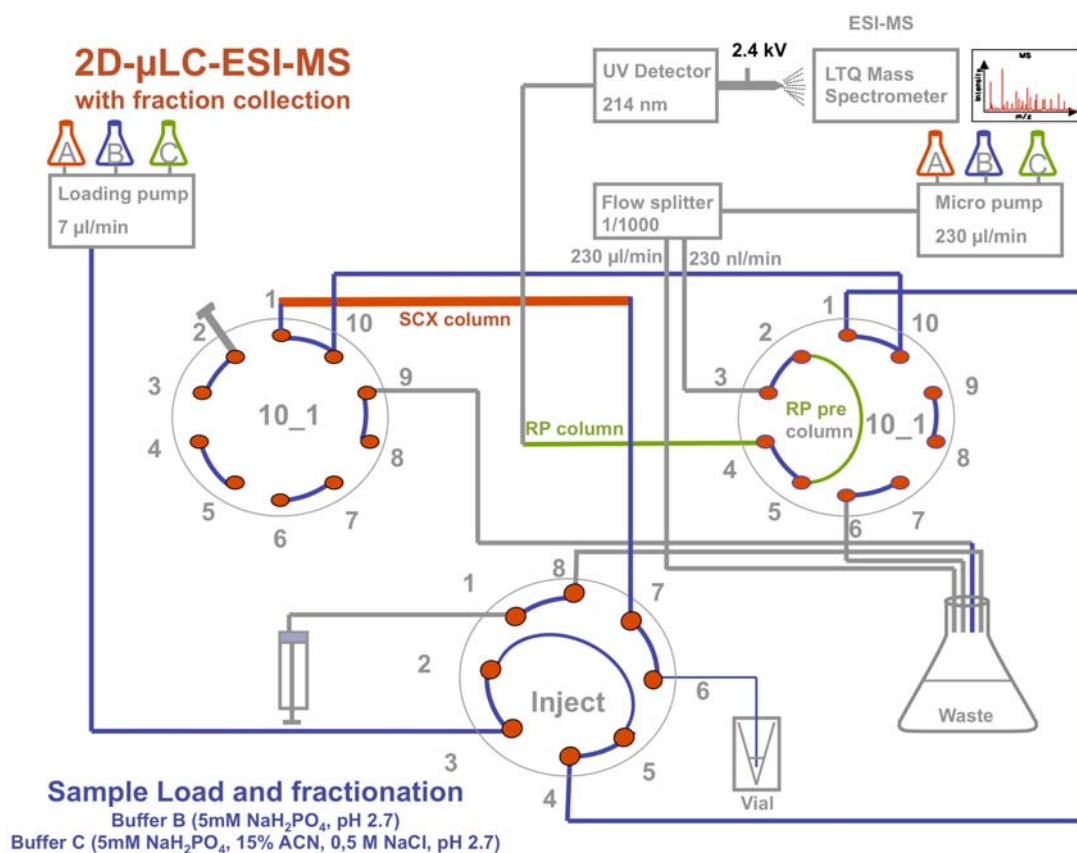


Figure 3.5 Ultimate3000 set up for first dimensional off-line SCX separation and fraction collection (blue marked capillaries indicate solvent flow).

An optimized binary salt gradient (Fig. 3.6) was applied to elute peptides from the column. Using the Ultimate 3000 fraction collection option, the eluate was collected into small glass vials (100 μ l volume) with a frequency of one minute per vial. The collected eluate was dried in a SpeedVac concentrator and stored at -80 °C until further use. Before second dimension separation was started, 40% acetonitrile was added to the loading pump buffer A and B, mixed and the system was washed for one hour to remove salt and prevent microbial growth. Next, the left valve was switched into position I_2.

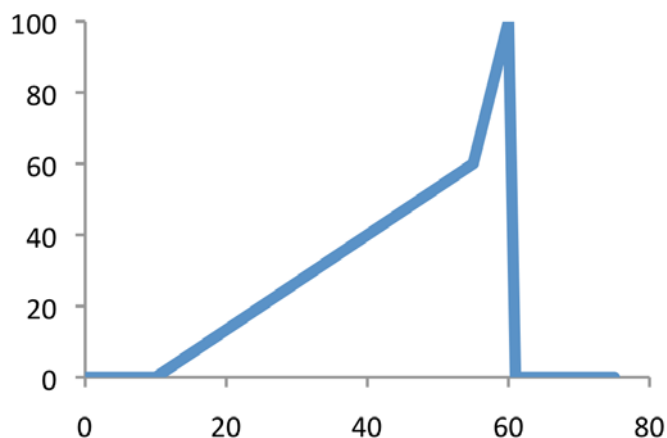


Fig 3.6 Optimized binary salt gradient for SCX fractionation

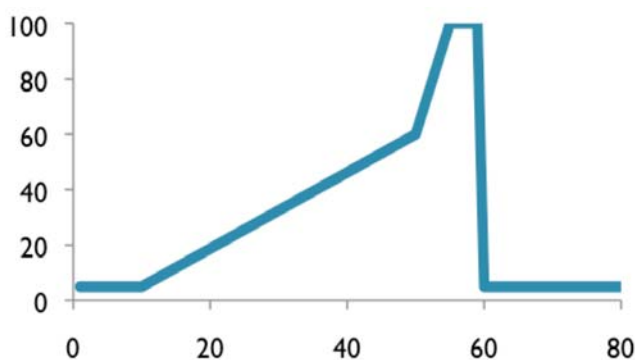


Figure 3.7. Acetonitrile gradient used for system check with peptide standard

Before starting second dimensional separation on the reverse phase column, capillaries were washed over night with 0.1% TFA solution. To test HPLC and MS performance 1 pmol synthetic peptide mixture was injected onto the reverse phase precolumn (7 μ l/min) and eluted by a binary acetonitrile gradient (see Fig. 3.6) with a flow rate of 200 nl/min. The HPLC was online coupled to the LTQ mass spectrometer by a coated PicoTip emitter (FS360-20-10-D-20, Coating: IP-4P, Tip: 10 \pm 1 μ m, New Objective) providing a nanoLC-ESI-MS/MS interface.

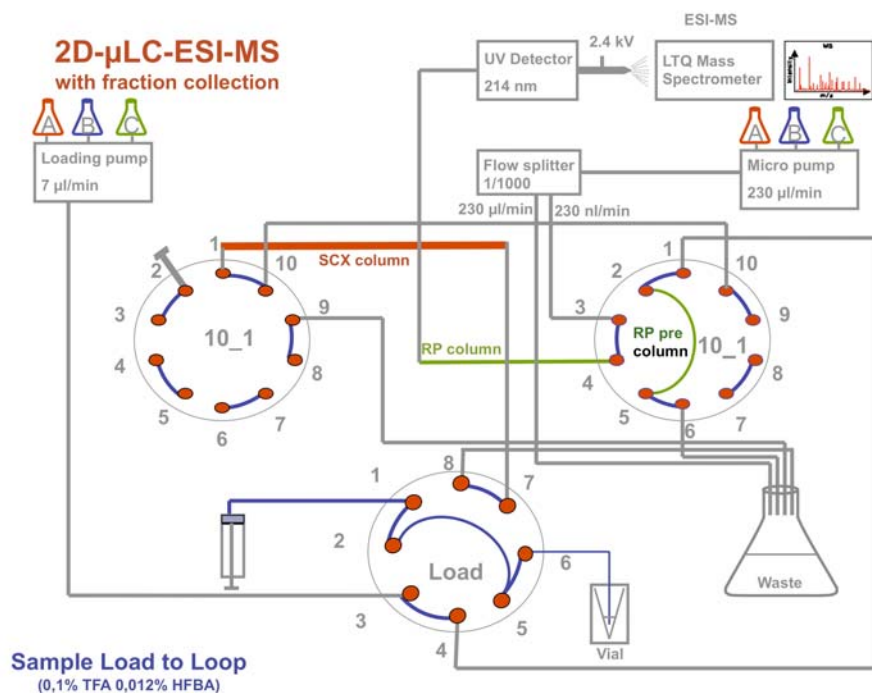


Figure 3.8 Sample load from vial into the sample loop (blue marked capillaries indicate solvent flow).

After successfully testing the system performance, sample fractions (resolved in 0.1% TFA) from the first dimensional SCX separation were injected one by one following the order of increasing salt concentrations. Peptides were online desalted by washing with 0.1% TFA for 40 minutes at a flow rate of 7 μl/min.

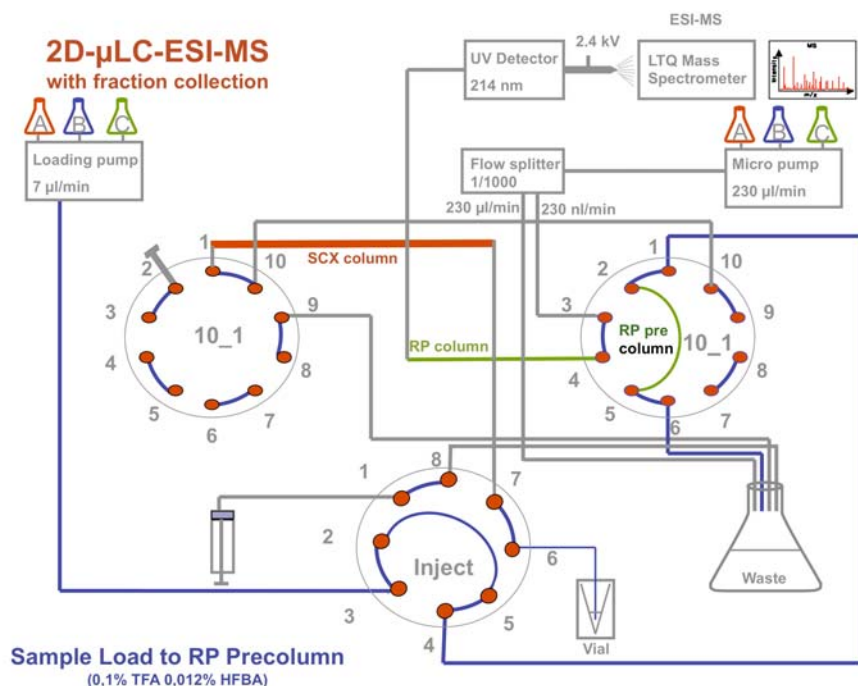


Figure 3.9 Sample load from sample loop onto the reverse phase (RP) precolumn (blue marked capillaries indicate solvent flow).

Finally, the precolumn was switched in line with the separating column and peptides were eluted by an increasing acetonitrile gradient (see Fig. 3 9).

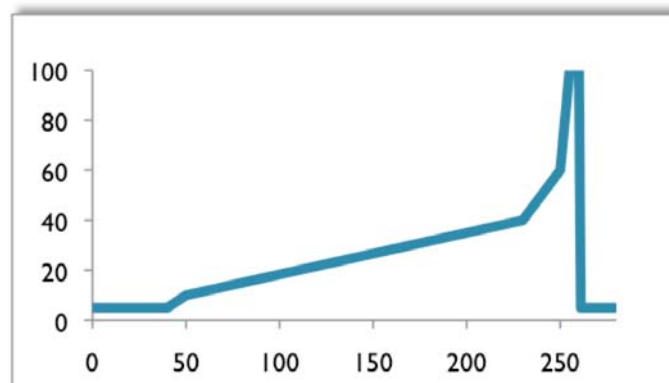


Figure 3.10 Binary acetonitrile gradient for online desalting and peptide separation.

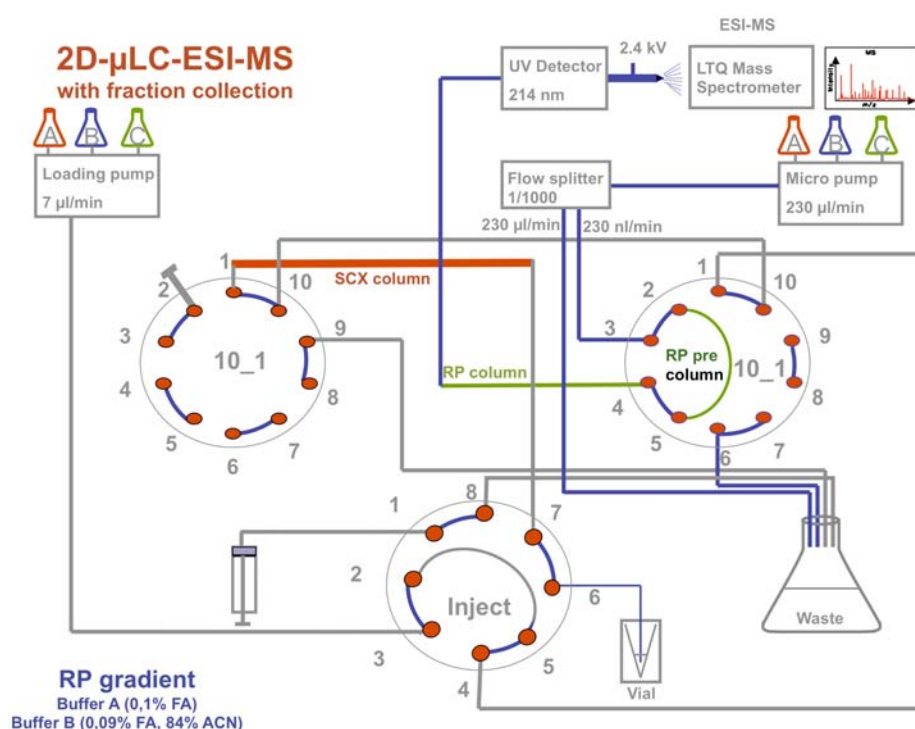


Figure 3.11 Ultimate 3000 switches to perform reverse phase separation (second dimension) of on-line desalted sample. Blue marked capillaries indicate solvent flow.

3.3.10 MS DATA PROCESSING

3.3.10.1 Calibration and tuning of the mass spectrometer

The LTQ mass spectrometer was calibrated using the standard ESI calibration solution for normal mass range (caffeine, MRFA, Ultramark) from 50 to 2000 m/z as suggested by the manufacturer.

Capillary voltage and tube lens parameters were optimized manually to achieve the highest TIC signal intensity for the $[MH^{2+}]$ ion signal of Angiotensin I under mimic of standard LC-MS conditions (30% buffer B, 200 nl/min flow rate). Additionally, LTQ lens parameters were tuned automatically for the $[MH^{2+}]$ ion signal of angiotensin I (648.86 m/z) in enhanced MS scan mode to maximize signal intensity and signal to noise ratio. Data dependent MS/MS acquisition was performed using parameters described in table 3.28.

MS Parameter	Value
Spray voltage	2.4 kV
Capillary temperature	100 °C
Capillary voltage	38 V
Tube lens	245 V
Microscans	1

Table 3.28 Optimized parameters of the LTQ ion source.

3.3.10.2 LTQ setup to analyze phosphorylated peptides

Multistage activation experiments were performed using enhanced MS full scan rate for higher mass accuracy and better charge state screening in a scan range of 400 – 2000 m/z. The mass spectrometer was operated in positive polarity and signals were measured in the centroid data mode. MS/MS data dependent scans were performed with wideband activation on the first, second and third highest MS peak with a minimum signal threshold of 1000, 500 and 250 counts, respectively. To increase numbers of discovered peptides dynamic exclusion was enabled using the following parameters:

Dynamic exclusion parameters	Value
Repeat count	2
Repeat duration	180 s
Exclusion list size	500
Exclusion duration	60 s
Exclusion mass width by mass low and high	1.5

Table 3.29 LTQ parameters for dynamic exclusion.

MS/MS parameter	Value
Activation type	CID
Default charge state	2+
Isolation width	2 m/z
Normalized collision energy	30.0
Exclusion mass width by mass low and high	1.5 m/z

Table 3.30: LTQ parameters for MS/MS activation using collision induced dissociation (CID).

LTQ parameters for MS/MS activation are described in table 3.30. Charge state screening with charge state rejection for 1+, 4+ and higher charged ions was enabled. If neutral loss of 32.66, 48.9 or 97.97 within top 10 MS/MS peaks occurred, further peak fragmentation was performed automatically (pseudo MS³). Resulting spectra of this multistage activation experiments contain both neutral loss (MS/MS/MS on the neutral loss peak) and phosphorylated peptide fragment (MS/MS). Thus, information is more suitable for phosphopeptide identification and phosphorylation site determination in comparison to the single spectra. By application of the described set up, one MS measurement cycle with one enhanced full MS scan followed by three MS/MS multistage activation experiments on the first three most intense ions took only 1.8s. Therefore the method enables to record eleven full MS scan during a usual peak elution profile with a peak width of 20s.

3.3.10.3 LTQ Orbitrap

The LTQ Orbitrap high mass resolution mass spectrometer was calibrated and tuned as described for the LTQ. To increase phosphopeptide identification, peptides were fragmented by Higher Energy Collision Dissociation (HCD) or by multistage activation using Collision Induced Dissociation (CID). Using Higher Energy Collision Dissociation (HCD) full MS scans were performed with a mass resolution of 15000 in a scan range of 400-1700. Additionally, MS/MS scan were measured with a mass resolution of 7500. The mass spectrometer was operated in positive polarity and data were measured in the profile mode. MS/MS data dependent scans were performed with wideband activation on the first, second and third highest MS peak with a minimum signal threshold of 500. Charge state screening with charge state rejection for unassigned and 1+ ions was enabled. HCD activation parameters are listed in table 3.31.

Parameter	Value
FT MS resolution	15000
MS MS resolution	7500
Activation type	HCD
Minimum signal required	500
Isolation width	3.00
Normalised collision energy	65.0
Default charge state	2
Activation Q	0.140
Activation time	30.000 ms
Nuber of scan events	4
Neutral loss mass list	97.97
Neutral loss in top	3
Most intense if no parent mass found	Not enabled
Charge state screening	Enabled
Charge state rejection for unassigned and 1+	Enabled
Neutral loss candidates processed by	Decreasing intensity

Table 3.31 LTQ Orbitrap parameters for MS/MS activation using Higher Energy Collision Dissociation (HCD).

In multistage activation mode MS full scans were performed with a mass resolution of 60000 in a scan range of 400-1700. The mass spectrometer was used in positive polarity mode and profile data type was measured. MS/MS data dependent scans were performed with wideband activation on the first, second, third and fourth highest MS peak with a minimum signal threshold of 500. Charge state screening with charge state rejection for unassigned and 1+ ions was enabled.

If neutral loss of 24.49, 32.66, 48.99 or 97.97 within top 10 MS/MS peaks occurred, further peak fragmentation was performed automatically (pseudo MS³). CID measurement parameters are listed in table 3.32.

Parameter	Value
FT MS resolution	60000
MS scan range	400-1700
Activation type	CID
Minimum signal required	500
Isolation width	2.00
Normalised collision energy	35.0
Default charge state	2
Activation Q	0.250
Activation time	30.000 ms
Nuber of scan events	5
Multistage activation	Enabled
Neutral loss mass list	24.49, 32.66, 48.99, 97.97
Neutral loss in top	10
Most intense if no parent mass found	Not enabled
Add/substract mass	Not enabled
FT master scan preview mode	Enabled
Charge state screening	Enabled
Monoisotopic precursor selection	Enabled
Non-peptide monoisotopic recognition	Not enabled
Charge state rejection for unassigned and 1+	Enabled
Correlation	Disabled

Table 3.32 LTQ Orbitrap parameters for MS/MS multistage activation using Collision Induced Dissociation (CID).

To increase the number of discovered peptides dynamic exclusion was enabled in both measurement modes using the following parameters:

Dynamic exclusion	Value
Repeat count	1
Repeat duration	30 sec
Exclusion list size	500
Exclusion duration	60 sec
Exclusion mass width relative to	Mass, ± 5 ppm
Expiration	Disabled

Table 3.33 LTQ Orbitrap parameters for dynamic exclusion.

3.3.11 DATABASE SEARCHING

Raw data from the LTQ instrument were processed using the program DTASuperCharge (version 1.19, SourceForge) and converted into Mascot generic format (mgf) files according to the protocol. Peak reduction of MS/MS peaks was performed using the software default settings.

Database searching was performed with the mgf files using the Mascot database search program (version 2.2). The searched database was the International Protein Index IPI_mouse_20080129 (5878816 sequences; 2026657434 residues). The database searches were performed with the fixed modifications carbamidomethyl (Cys) and dimethylation (Lys and peptide N-term) and variable modifications oxidation (Met), phosphorylation (Ser, Thr, Tyr) and dimethylation:2H (Lys and peptide N-term). Enzyme specificity was selected to trypsin/P with a maximum of two allowed missed cleavage sites. For the data obtained using the LTQ Orbitrap XL instrument a mass accuracy of ± 5 ppm was used for the parent ion, and ± 0.5 Da was used for the fragment ions. For data obtained with the LTQ instrument a mass accuracy of ± 0.5 Da was used for the parent ion, and ± 0.5 Da was used for the fragment ions. The charge state was set to +2 and +3 for LTQ data and additionally +4 was allowed for data measured with the LTQ Orbitrap. One ^{13}C isotope per peptide was allowed.

The minimum peptide identification score in MASCOT was set to 49 and the significance threshold expect value had to be <0.05 . Using these criteria the false positive discovery rate varied below 1 % based on target decoy database search.

Phosphorylation site determination was further evaluated using the PTM localization probability score function of MSQuant, which was described by Olsen et al (2006).

All identified phosphorylated peptides were manually evaluated according to the following criteria: peptide fragmentation spectra had to include a minimum of three y ions, had to show some y ions with neutral losses of -97.9769 Da (loss of H_3PO_4) to ensure phosphorylation (79.969331 Da, - HPO_3) over sulfation (79.956815 Da, - SO_3). Additionally, the MASCOT identification score of the top peptide match had to be $>15\%$ higher than the next possible match.

Annotated spectra from each identified peptide have been included in the supplemental data. Spectra were taken from the MSQuant program (www.sourceforge.net) including Y- and B-ion masses that have been assigned to the peptide.

3.3.12 RELATIVE QUANTITATION USING QUALBROWSER

Integrated peak areas of identified peptide peaks were calculated manually using the QualBrowser software (part of the XCalibur 2.07 software). Peak masses ± 0.5 Da (for LTQ data) or ± 5 ppm (for LTQ Orbitrap data) were extracted from the MS base peak chromatograms and integrated using the Genesis peak detection mode. Only peaks eluting at the time of peptide identification ± 0.5 minutes were accepted. To calculate the relative differences in peptide amounts the peak areas of heavy and light peptides were divided by each other. The obtained ratios had to be multiplied by

$$\text{H/D} = (99.99\% + 2\%) / (0.01\% + 98\%) = 1.0406$$

to correct for the isotopic ratios of the natural sources (0.01% D / 99.99% H) and of the formaldehyde labeling solution (98% D / 2% H).

3.3.13 MSQUANT SETTINGS FOR AUTOMATED QUANTITATION OF PHOSPHOPEPTIDES

Automated relative quantitation of stable isotope dimethyl labeled peptides was performed using MSQuant version 1.4.3 allowing for the identification of differential N-terminal modifications. MASCOT 2.2 results were saved as .xml files displayed in peptide summary report using Internet explorer 5.0 and parsed with the original .raw file in MSQuant. For each identified peptide pair, MSQuant calculated the two extracted ion chromatogram (XIC) values, and the assignments used for quantitation were visually displayed and validated. Used MSQuant parameters are listed in table 3.34.

Parameter	Value
Misc Options	
Mass window for XIC LTQ	1.0
Mass for mass window LTQ	-1000
Mass window function LTQ	Constant mass
Quantitations modes	
StabDimLab for MASCOT 2.2	+28.03130 Da or +32.056407 Da for K and peptide N-term

3.34 MSQuant parameters for relative quantification of LTQ data. All other parameters were used as given in the default settings.

The regulated peptides ($XIC_H/XIC_L > 1.3$ or < 0.7) were manually validated using QualBrowser. This evaluation step is very important in the case of LTQ measured low mass accuracy MS data to disqualify the false positive peptide hits deriving from peptide base peak overlapping. MSQuant results were exported to tab delimited text file and merged using a MATLAB based home made program. Localization and function of the resulted proteins was determined by online analysis of the official gene symbol list of the resulted proteins using the Database for Annotation, Visualization and Integrated Discovery (DAVID) 2008 (Dennis et al., 2003).

4 RESULTS

4.1 PRELIMINARY EXPERIMENTS

4.1.1 TESTS TO CLARIFY THE INITIAL CONDITIONS OF THE DIFFERENTIAL PHOSPHOPROTEOME ANALYSIS USING PHARMACOLOGICAL INHIBITION / ACTIVATION OF NO FORMATION

4.1.1.1 ID-PAGE based experiments

To investigate the effect of rapidly released nitric oxide (NO) on changes in the phosphorylation status of proteins involved in NO signaling, hearts of wild type (WT) and myoglobin deficient ($Myo^{-/-}$) mice were treated with the NO donor SNAP or the NOS inhibitor ETU in a Langendorff apparatus. NO induced phosphorylation was detected with phosphorylation site specific antibodies and with phosphoprotein stain (Fig. 4.1).

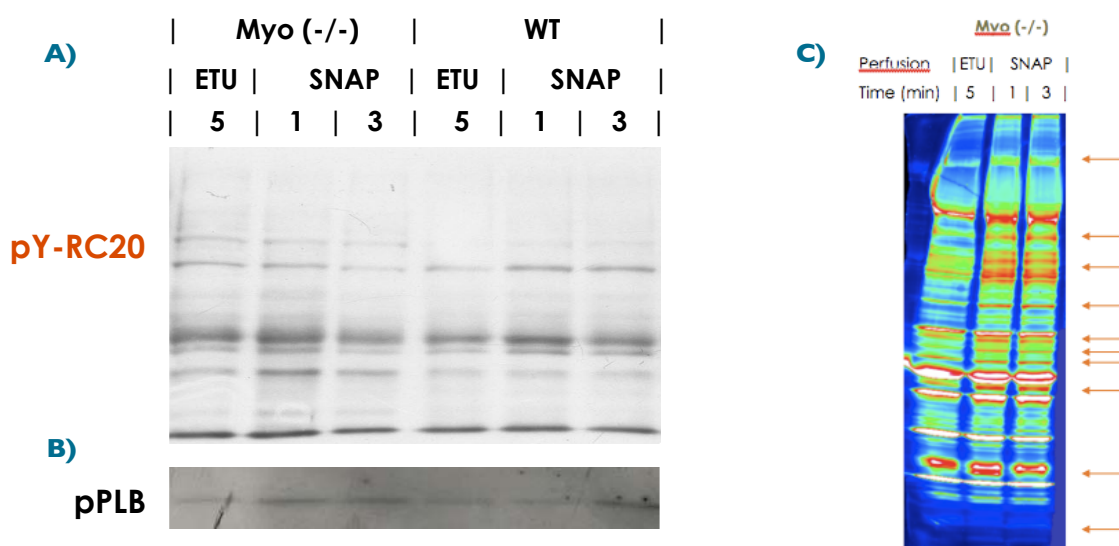


Figure 4.1. A) $Myo^{-/-}$ and WT hearts show an enhanced tyrosine phosphorylation (pY) after one minute of +/-S-nitroso-N-penicillamine (SNAP, NO donor, 100 μ M) treatment in comparison to 2-ethyl-2-thiopseudourea (ETU, NOS inhibitor, 100 μ M) treated hearts. Tyrosine phosphorylation decreases after prolonged SNAP activation (three minutes). pY-RC20 antibody was used for specific pY detection. B) Western blot analysis shows that SNAP treatment enhanced phosphorylation of phospholamban at Ser-16 (pPLB) already after one minute in myoglobin deficient hearts, while wild type hearts needed three minutes treatment to obtain the same effect. C) ProQ Diamond staining shows an enhanced total phosphoprotein (pSTY) level in $myo^{-/-}$ hearts after SNAP activation.

Staining with a specific anti-phosphotyrosine antibody pY-RC20 showed enhanced phosphorylation (Fig 4.1.A) already after one minute of SNAP perfusion for both WT and $myo^{-/-}$ hearts. Interestingly, this enhanced signal intensity decreases again almost back to the original level after three minutes of SNAP activation.

In contrast to tyrosine phosphorylation kinetics, ProQ Diamond, which globally stains phosphoproteins (binds to phosphorylated serine, threonine and tyrosine, pSTY), shows an enhanced phosphorylation level after SNAP activation for both point of time (Fig. 4.1.C).

Phosphorylation of phospholamban (PLB), a well known target of the NO/cGMP/PKG pathway was also analyzed. PLB is a small, plasma membrane-associated phosphoprotein found in the sarcoendoplasmic-reticulum (SER) of cardiac, smooth and slow-twitch muscle. PLB regulates cardiac contractility and inhibits Ca^{2+} re-uptake by SER Ca^{2+} ATPase (SERCA2a). Upon phosphorylation, PLB dissociates from SERCA2a and subsequently increases Ca^{2+} reuptake into the SER. Immunoblot analysis of hearts shows that addition of the NO donor SNAP resulted in an enhanced phospholamban phosphorylation at the NO/cGMP/PKG target site serine-16 when compared to inhibition of NOS by ETU (Fig. 4.1.B). WT hearts showed this signal transduction effect after 3 minutes, while in myoglobin lacking hearts phosphorylation of phospholamban occurred already after one minute of SNAP perfusion. Faster kinetics of NO signaling in myoglobin lacking hearts is likely due to the NO scavenger activity of myoglobin in WT hearts.

4.1.1.2 2D-PAGE based experiments

To identify which phosphoproteins are modified due to the SNAP treatment, two dimensional gel electrophoresis (2D-PAGE) was performed. Since the position of protein spots in 2D-PAGE is determined by protein charge (1st dimension - horizontal) and size (2nd dimension - vertical), alterations in protein phosphorylation can be detected by a spot shift in the horizontal and vertical position. The introduction of a strongly negatively charged phosphate group on serine, threonine or tyrosine residues shifts the protein spot position by about 0.3 pH units to the acidic site. Furthermore, the molecular mass is increased by 80 Da with each additional phosphate group. Therefore, each additional phosphate group shifts protein spot positions slightly to the left and up while each lost phosphorylation does the opposite.

First, 2D-PAGE separation technique was optimized: before loading, samples were desalted by protein precipitation which reduced streaking. In addition, gradient gels (4-16%) were carefully prepared one by one manually with a mixing chamber (instead of using the Ettan DALT II System, Amersham Pharmacia Biotech) to obtain improved gel polymerization and better spot resolution in the vertical range. Sensitive and mass spectrometry compatible silver (Shevchenko, 1996) and Coomassie (Kang, 2003) staining methods were also tested. In contrast to silver, Coomassie stain gave quantitative, and easy reproducible results with comparable spot intensities in each gel. Hence, this staining was used in the following experiments.

Extracted heart proteins were first separated on a 16 cm x 16 cm gel from pH 3-11 in the horizontal and from 10 to 200 Da molecular mass in the vertical direction. These gels showed that most of the protein spots were located in the acidic range of the gel. Consequently, this range was chosen for the further analysis where spot alterations could more likely be observed.

To enhance spot resolution in the horizontal direction, zoom strips ranging from pH 4 to pH 7 were applied for the first dimensional separation. The resulting zoom 2D gels showed that cytochrome c oxidase subunit Vb (COX5B) became dephosphorylated upon NO donor SNAP perfusion (1 min) in myoglobin deficient hearts (Fig. 4.2).

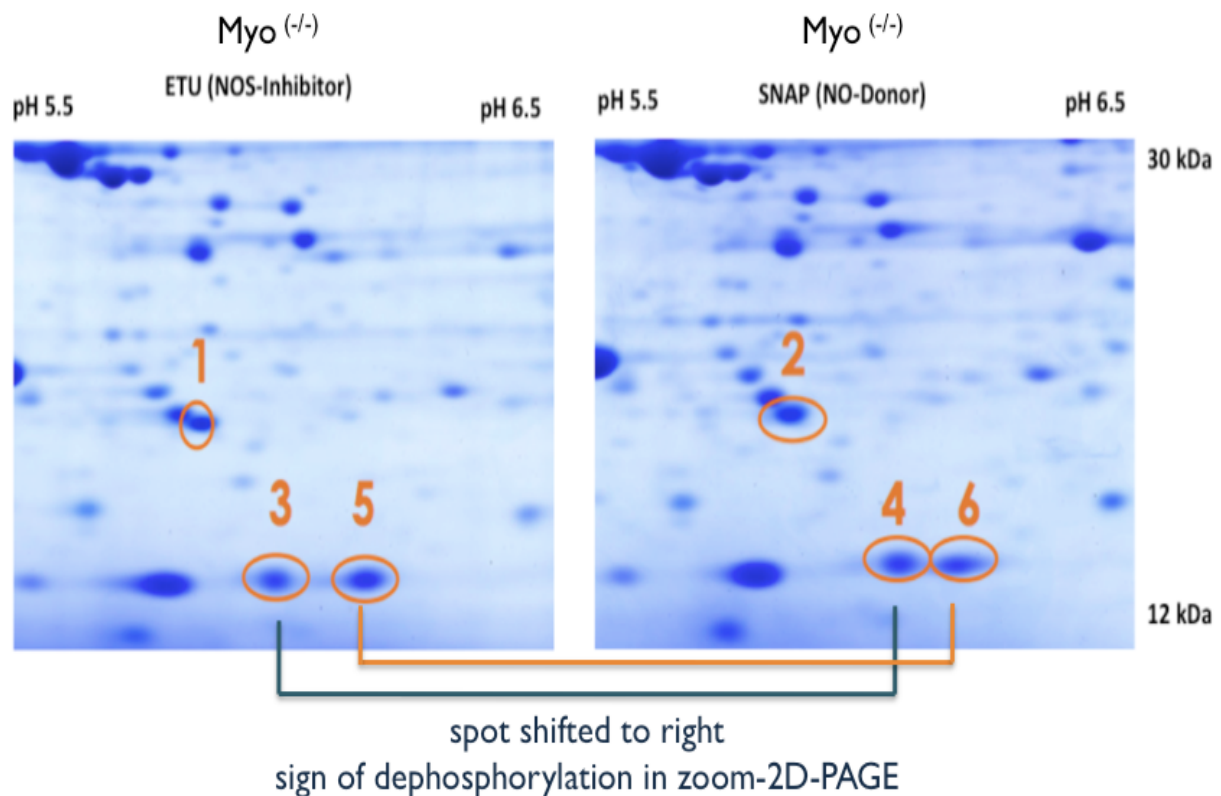


Figure 4.2: Detail of zoom-2D-PAGE separated proteins of *myo*^{-/-} hearts treated with the NO donor SNAP or the NOS inhibitor ETU. The shift in spot position (3 and 4) represents Cytochrome c oxidase subunit Vb (COX5B) dephosphorylation upon pharmacological NO activation. (Spot 1, 2: ATP synthase, H⁺ transporting, mitochondrial FO complex, subunit D; spot 3, 4: COX5B; spot 5, 6: fatty acid binding protein, muscle and heart)

4.1.2 COMPARATIVE PHOSPHOPROTEOME ANALYSIS OF WILD TYPE VERSUS *iNOS*^{+/+}/*MYO*^{-/-} HEARTS

To identify phosphoproteins of the NO signaling cascade on a proteomic scale, a physiologically more relevant heart failure model with a cardiac specific overexpression of iNOS on a myoglobin deficient background (*iNOS*^{+/+}/*myo*^{-/-}, published by Gödecke et al., 2003) was used. These mice show an about 300 fold increased cardiac NO production. In addition, the lack of myoglobin leads to an elevated cardiac NO level, as proved by increased tissue levels of nitrate.

As a consequence, the mice develop heart failure together with cardiac hypertrophy and left ventricular dilatation. When perfused in a Langendorff setup, coperfusion of the NOS substrate L-arginine (L-arg) results in strongly increased NO production by iNOS, which leads to vessel relaxation (coronary perfusion pressure decreases from 104.26 ± 5.89 mmHg to 65.73 ± 8.56 mmHg by -37% (n=6) (Fig. 4.3.A)) and to a drop in cardiac contractile force (LVDP) by $29.11 \pm \gamma\%$ (n=6).

2D gel electrophoresis followed by ProQ Diamond phosphoprotein staining shows an enhanced protein phosphorylation level of this double transgenic mouse mutant as compared to the WT (Fig. 4.3.B), which indicates that protein phosphorylation plays an important role in the transduction of NO signaling.

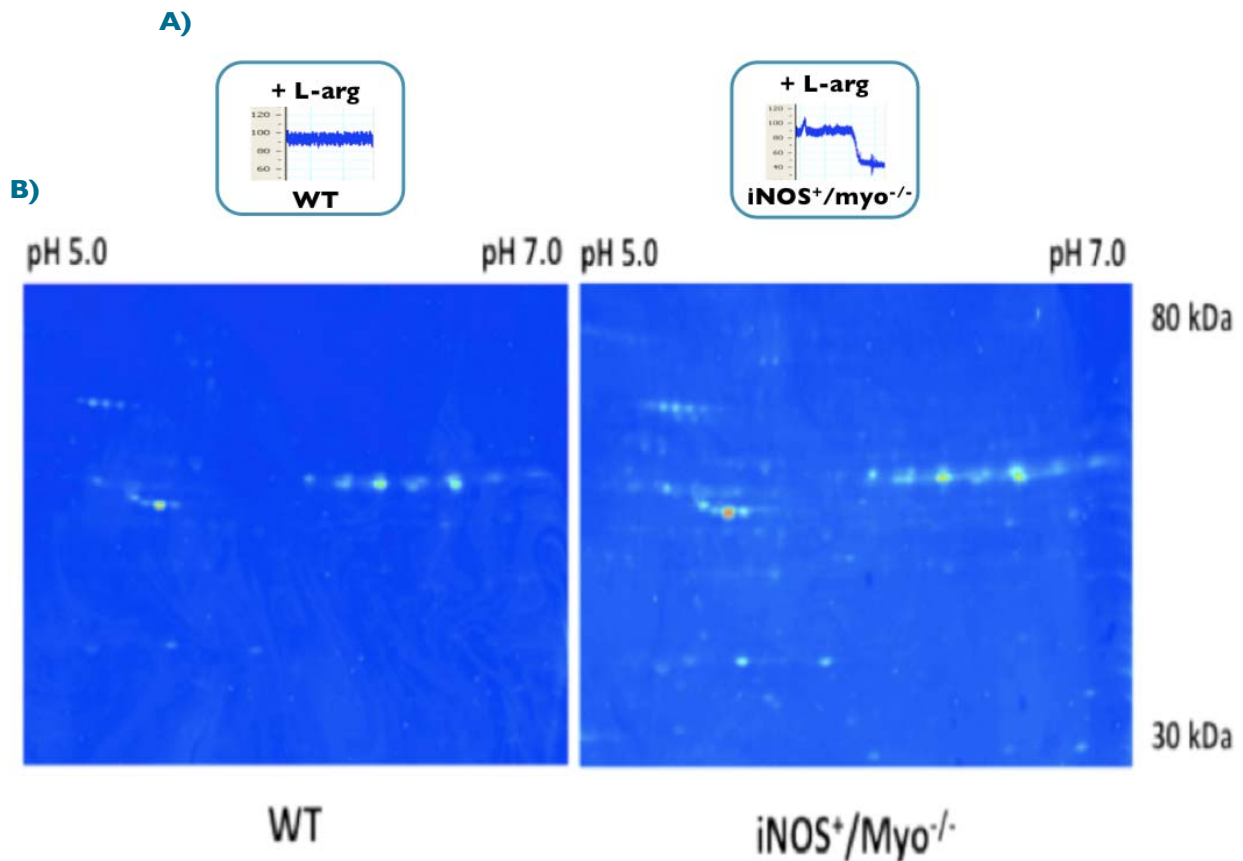


Fig. 4.3: Coronary perfusion pressure (A) and cardiac phosphoproteins (B) of wild type (WT) and *iNOS⁺/myo^{-/-}* double transgenic (DT) mice after one minute L-arg (NOS substrate) coperfusion. DT hearts respond with stronger vasodilatation and show much higher protein phosphorylation levels. A) Perfusion pressure during 1 minute L-arg coperfusion in Langendorff-perfused WT and double transgenic hearts. WT hearts are unaffected, while perfusion pressure drops fast (-37% (n=6)) in DT hearts during 1 minute L-arg treatment. B) *iNOS⁺/myo^{-/-}* hearts show enhanced protein phosphorylation after 1 min L-arg perfusion in comparison to the wild type.

4.1.3 PERFUSION PROTOCOL FOR FURTHER EXPERIMENTS

Based on the preliminary results of the previous section, the following experimental setup for a differential phosphoproteome analysis was chosen: in order to achieve always the same protein expression level as a basis for comparative phosphoproteome analysis, the cardiac phosphoproteome of mice with cardiac specific overexpression of iNOS in a myoglobin deficient background (*iNOS⁺/myo^{-/-}*) perfused with or without L-arginine will be compared (Fig. 4.4). Hence, in one case the long initial saline perfusion step leads to a substrate limited iNOS activity (nearly inactive), while in the other case L-arginine serves as NOS substrate and high concentrations of NO are rapidly synthesized.

To minimize secondary effects of iNOS derived NO release, L-arginine coperfusion will be applied only for one minute (Fig. 4.4). This treatment time was chosen, since already after one minute functional parameters (coronary resistance, contractile force) archived a new steady state (Fig 4.3.A) in addition the signal was transduced to the protein phosphorylation level (Fig. 4.3.B). In addition, pharmacological experiments showed that phospholamban phosphorylation (a well known target of the NO/cGMP/PKG signaling cascade) was already increased after one minute perfusion with the NO donor SNAP (Fig. 4.1.B).

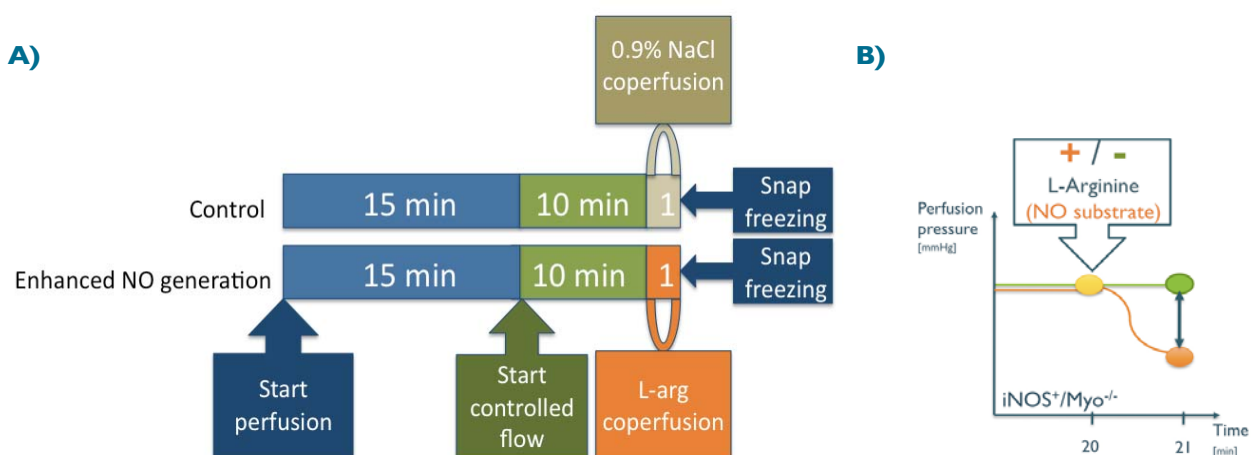


Figure 4.4. A) Final protocol for Langendorff-perfusion to study NOS induced phosphoproteome. In both cases, $iNOS^{+}/myo^{-/-}$ hearts were perfused. Enhanced NO generation originates from additional L-arg (NOS substrate) perfusion for one minute. B) Perfusion pressure of 0.9% NaCl (constant perfusion pressure and contractile force, green) or L-arginine (drop in perfusion pressure and contractile force, orange) coperfused mouse hearts.

4.1.4 SWITCHING FROM GEL BASED TO GEL FREE ANALYSIS

To identify NO induced changes in the cardiac phosphoproteome, classical gel based methods were used during the preliminary studies. These techniques have several disadvantages, like inadequate resolution, sensitivity and inconvenient handling.

The increasing number of available phosphorylation site specific antibodies offers the possibility of immunoblot based analysis. But this method is still rather time consuming, expensive and only applicable to already known phosphorylation sites.

In order to enhance specificity, sensitivity and overcome limitations of 1D and 2D-PAGE based methods, modern and highly efficient methods for LC-MS phosphoproteomic analysis were established and implemented.

4.2 OPTIMIZATION OF METHODS REQUIRED FOR GEL FREE RELATIVE QUANTIFICATION OF PHOSHOPEPTIDES

In the following, numerous methods were tested and optimized to enable gel free relative quantification of phosphorylated peptides. Methods of choice (Fig. 4.5) were stable isotope dimethyl labeling, phosphopeptide enrichment, strong cation exchange chromatography and nano flow reverse phase HPLC separation online coupled with an electrospray to a tandem mass spectrometer (nano-RP-HPLC-ESI-MS/MS).

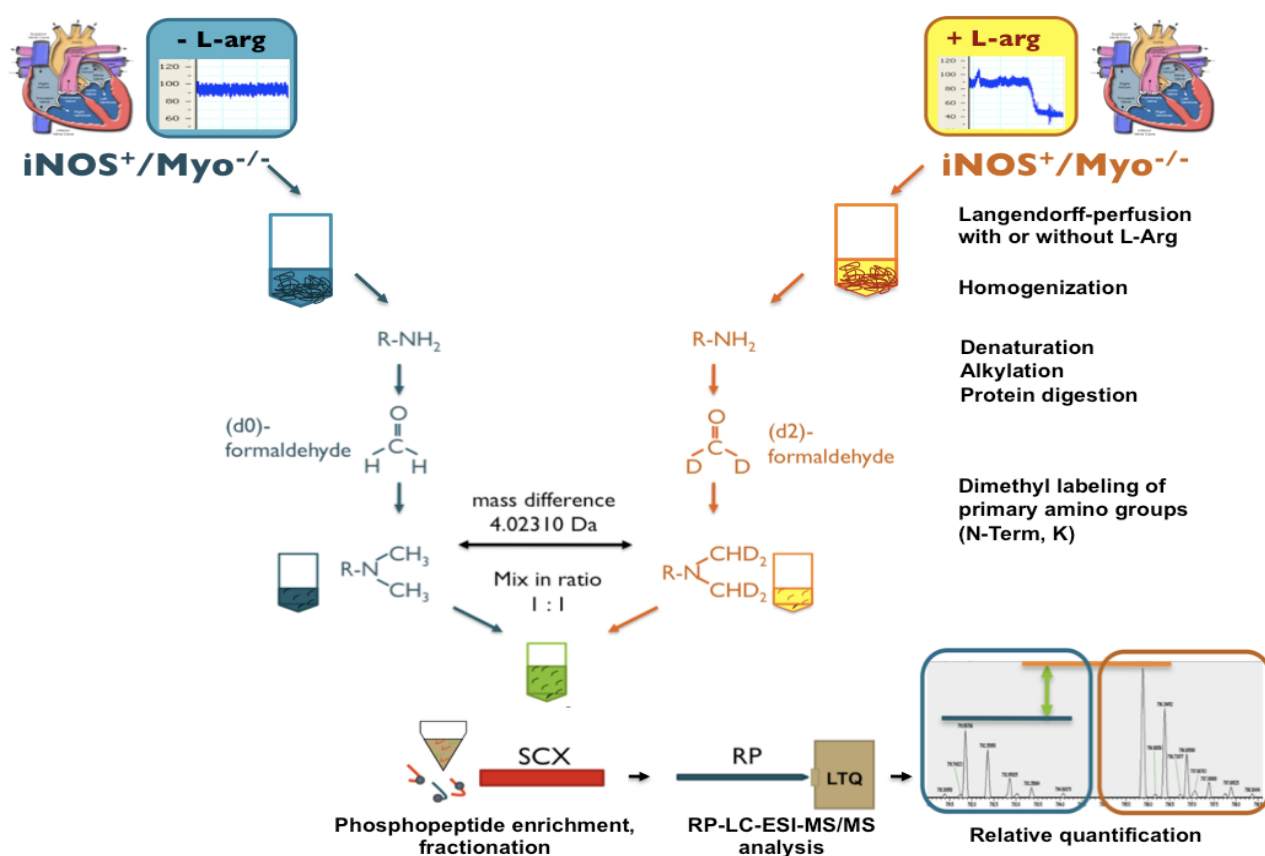


Figure 4.5. Flow chart of methods for gel free relative quantification of protein phosphorylation. Stable isotope dimethyl labeling with heavy (d2)- and light (d0)-formaldehyde gives a mass difference of 4.02310 Da per labeled primary amino group (N-terminal peptides and lysine) which allows for relative quantification of labeled peptide pairs using LTQ mass spectrometry (MS). Application of phosphopeptide enrichment, strong cation exchange (SCX) and reverse phase (RP) chromatography reduce sample complexity and improve sensitivity of MS analysis.

4.2.1 STABLE ISOTOPE DIMETHYL LABELING OF PRIMARY AMINO GROUPS

Hsu et al. (2003) introduced a stable isotope labeling strategy for quantitative proteomics which labels the N-terminus and epsilon amino group of lysine (Lys or K) through reductive amination. Labeling with heavy (d2) and light (d0) formaldehyde introduces a mass difference of 28 or 32 mass units for each derivatized site relative to its original counterpart. Consequently, each derivatized isotopic pair differs by 4 mass units enabling relative quantification using MS (Fig. 4.5).

The reaction is simple, fast, cost efficient and complete without any detectable byproduct. In addition, a_1 and y_{n-1} ion intensities were reported to be enhanced in MS/MS spectra of labeled peptides. I could observe enhanced y_{n-1} ion intensities, while according to the low mass cut of property of LTQ mass spectrometer a_1 ions are not measurable in the used CID fragmentation mode (Fig. 4.6).

Good correlation between the experimental and theoretical peptide ratio with small standard deviation were also reported and could be reproduced in our laboratory (Fig. 4.8).

By these advantages, stable isotope dimethyl labeling method combined with multidimensional liquid chromatography provides an optimal alternative to 2D-PAGE based quantitative proteomics.

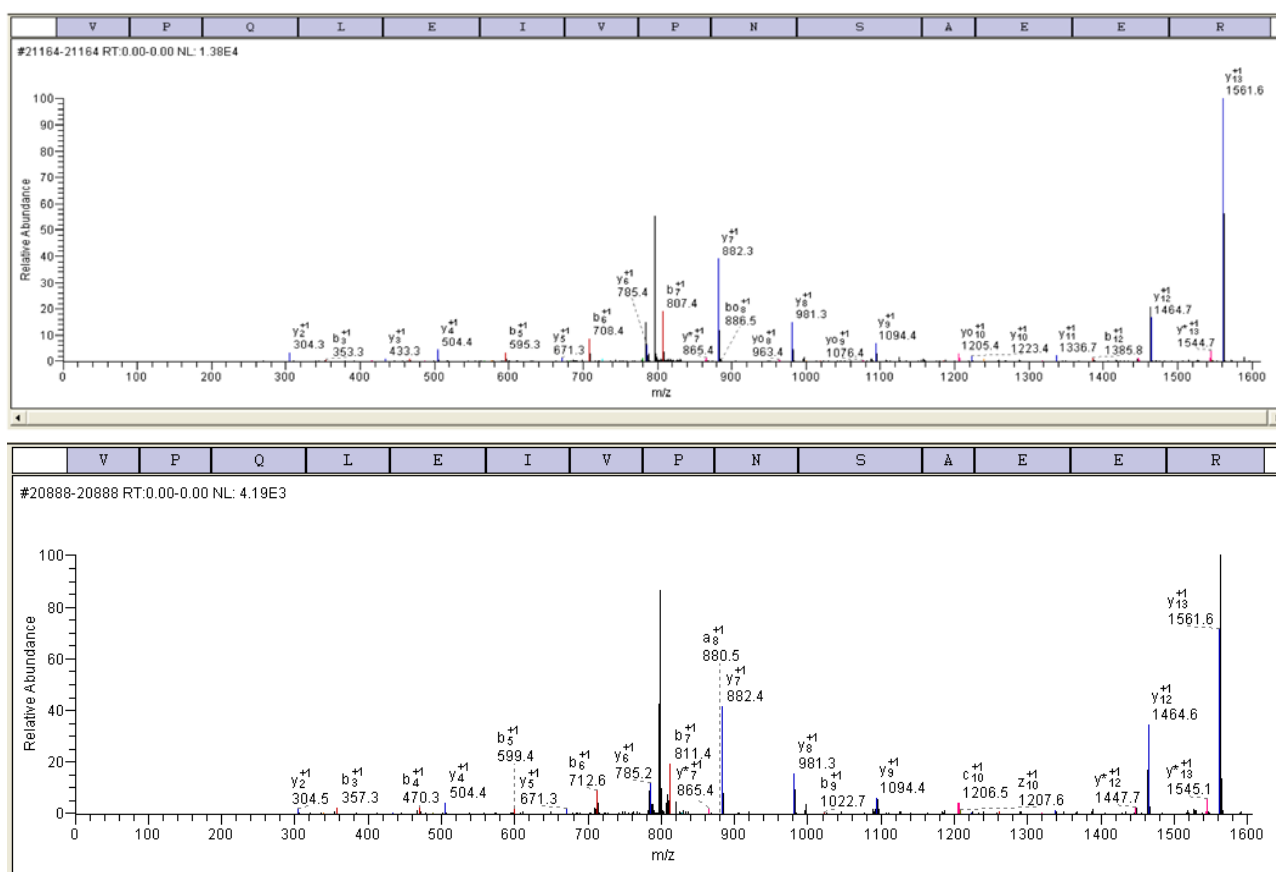


Figure 4.6: MS/MS spectra of light (upper panel) and heavy (lower panel) dimethyl isotope labeled trypsin digested casein phosphopeptide (sequence: *VPQLEIVPNpSAEER, * shows dimethyl labeling of N-terminal amino acid) analyzed by the SEQUEST algorithm. N-terminal 'b' ion masses show the typical 4 mass unit difference between heavy and light labeled peptides derived from mass differences between deuterated and normal formaldehyde reagent. Masses of C-terminal 'y' ions are the same in both MS/MS spectra. Typically enhanced y_{n-1} (here: y_{13}^{+1}) ion fragment intensities of dimethyl labeled peptides are also observable.

4.2.1.1 Optimization of reaction conditions

Following the published protocol, the labeling efficiency of standard peptides derived from the phosphoprotein casein was tested. Usage of the SEQUEST algorithm enabled an automated peptide and protein identification, by setting the following parameters: K +28 Da, N-term +28 Da for the first search and K +32 Da, N-term +32 Da for the second search. Hits were combined in order to see how many heavy, light and not labeled peptides were identified. In this way, close to 100% labeling efficiency was obtained for both N-terminal and lysine amino acids.

Applying the same labeling conditions to a trypsin digested protein mixture extracted from a wild type mouse heart, about 98% N-terminal labeling, but only around 49% lysine labeling was found. Increasing the pH from 5.4 to 5.8 led to an almost complete labeling of the peptide N-termini, while none of the lysine residues were labeled. Doubling the reaction time to one hour decreasing the pH to 5.5 and increasing the temperature from 25 to 30°C resulted in an excellent labeling efficiency for both lysine and N-terminal primary amino groups without any detectable non-derivatized counterpart. These conditions were used for stable isotope dimethyl labeling of tryptic peptides throughout the subsequently performed experiments.

4.2.1.2 Calibration for relative quantification

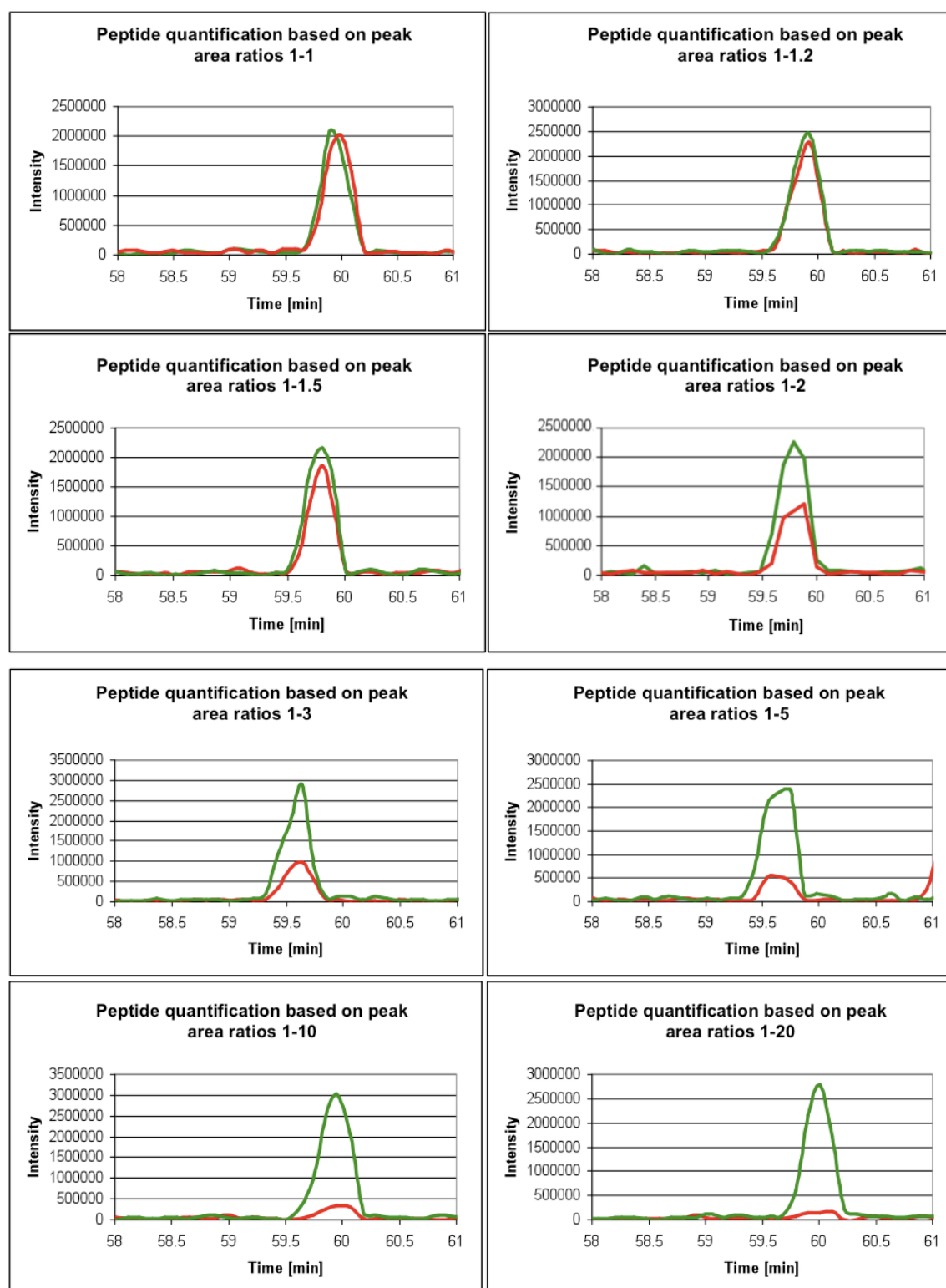


Figure 4.7. Excellent correlation between experimental and theoretical peptide ratio measured with nano-RP-LC-ESI-MS/MS. Peptide ratios were calculated using the integrated peak area of heavy and light peptides. As can be seen from the elution profiles, peptide pairs elute at almost the same time which is a prerequisite for reliable relative quantification. Red color shows d₀-dimethyl labeled peptide elution profile (light), green color shows d₂-dimethyl labeled peptide elution profile (heavy).

Heavy vs. light labeled digested casein peptides were mixed at ratios 1:1, 1:1.2, 1:1.5, 1:2, 1:3, 1:5, 1:10 and 1:20 (Fig. 4.7). The samples were measured three times using an Ettan nano flow HPLC (Amersham Biosystems) with a self-made reverse phase column (ID 75 μ m) coupled online to an LTQ tandem mass spectrometer to check if the measured peptide ratios correlate well with the theoretical ones. Figure 4.8 shows a good correlation and small standard deviations of standard peptides indicating a good analytical setup for relative quantitation.

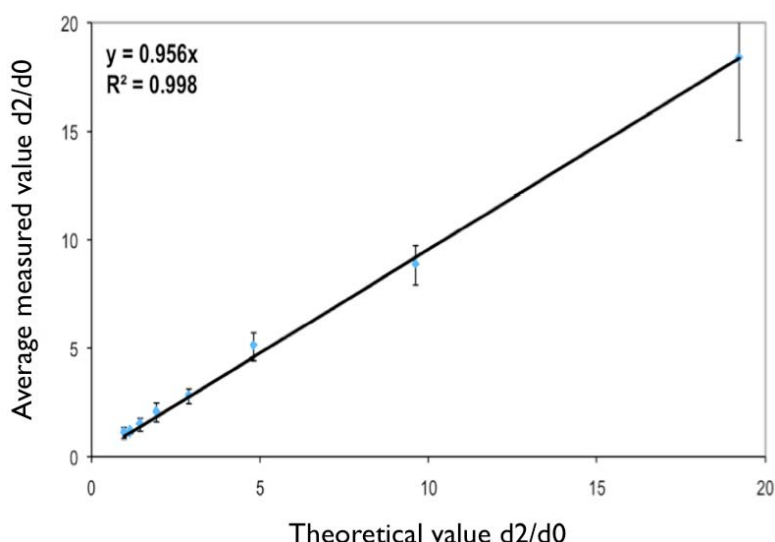


Figure 4.8: Good correlation between theoretical and measured peptide ratios after mixing heavy and light dimethyl labeled casein peptides in different ratios from 1:1 to 1:20 with each other.

4.2.2 PHOSHOPEPTIDE ENRICHMENT

Phosphorylation is among the most widespread post-translational modifications in nature. About 30% of the proteins are phosphorylated in a given mammalian cell at some point during their expression but phosphorylation is often substoichiometric. Therefore phosphopeptides derived from phosphorylated proteins have to be enriched as a prerequisite for their characterization by modern mass spectrometric methods. Three different phosphopeptide enrichment methods were tested: (1) immobilized metal affinity chromatography (IMAC), (2) phosphopeptide enrichment on titanium dioxide (TiO_2) and (3) calcium phosphate ($\text{Ca}_3(\text{PO}_4)_2$) precipitation.

4.2.2.1 Immobilized metal affinity chromatography (IMAC)

The IMAC phosphopeptide enrichment kit (Pierce) used according to the manufacturers instructions showed an inefficient removal of non phosphorylated peptides (Fig. 4.9).

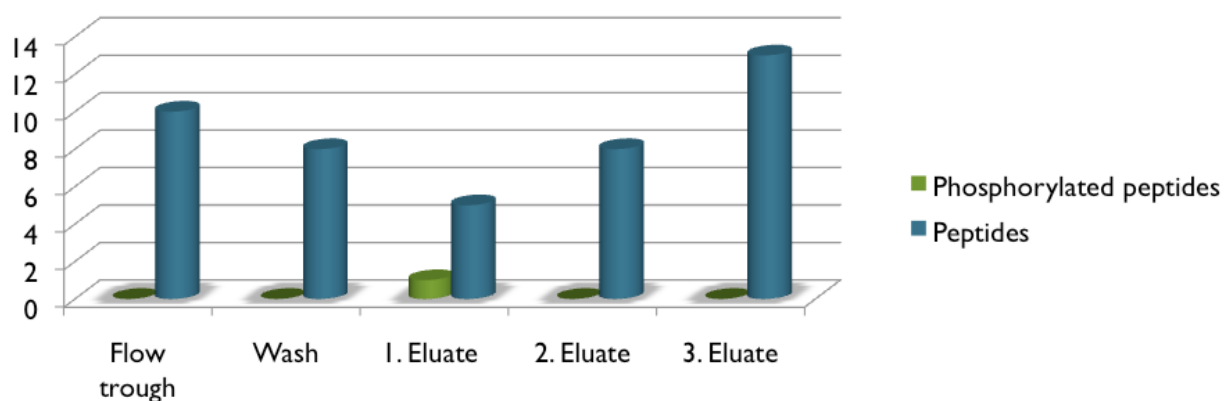


Figure 4.9: IMAC phosphopeptide enrichment kit (Pierce) removes only about 40% of non phosphorylated peptides from peptide mixture derived from a tryptic digest of casein. Due to the huge excess of the remaining non-phosphorylated peptides which suppress phosphopeptide signal intensity only one out of the four phosphorylated casein peptides was detected. (Analyzed with nanoRP-LC-ESI-MS/MS.) A part of non detected remaining phosphorylated and non-phosphorylated peptides stayed stuck on the IMAC column material.

Similar to peptide-IMAC, Phosphoprotein-IMAC (Chelating Sepharose Fast Flow, Amersham Biosciences) enrichment using heart homogenate of WT mice resulted in not sufficient enrichment. Furthermore, some phosphorylated proteins were unreproducibly lost during sample binding and washing steps which was controlled via SDS-PAGE and ProQ Diamond phosphoprotein stain. This methods were therefore not suitable for a quantitative analysis.

4.2.2.2 Titanium dioxide

Phosphopeptide enrichment using titanium dioxide filled tips was reported by Larsen et al. (2005). Here, 2,5-dihydroxy-bezoic acid (DHB) was applied in the binding buffer to improve selectivity by competition for binding sites on TiO_2 between non-phosphorylated peptides and DHB molecules, whereas phosphorylated peptide binding is unaffected. Applying this method with original TiO_2 filled TopTips resulted also in inefficient enrichment rates (detected phosphopeptide ratio was less than 1%). By exchanging the TiO_2 tip filling material to Titansphere (GL Sciences) which has a smaller particle size and possibly different surface properties resulted in a very good enrichment rate with only about 5% of non-phosphorylated detected peptides. The phosphorylated peptides identified by this method are listed in Table 4.1 - 4.8.

4.2.2.3 Calcium phosphate precipitation

Calcium phosphate precipitation was reported by Zhang et al. in 2007. The method was tested using the published protocol, which leads to a very good enrichment efficiency (Fig. 4.10) by removing all non phosphorylated peptides from a standard synthetic peptide and phosphopeptide mixture (list of used peptides is described in Table 3.3). Applied to dimethyl labeled cardiac phosphopeptides, about 60% purity could be obtained. The identified phosphorylated peptides are listed in Table 4.1 - 4.5.

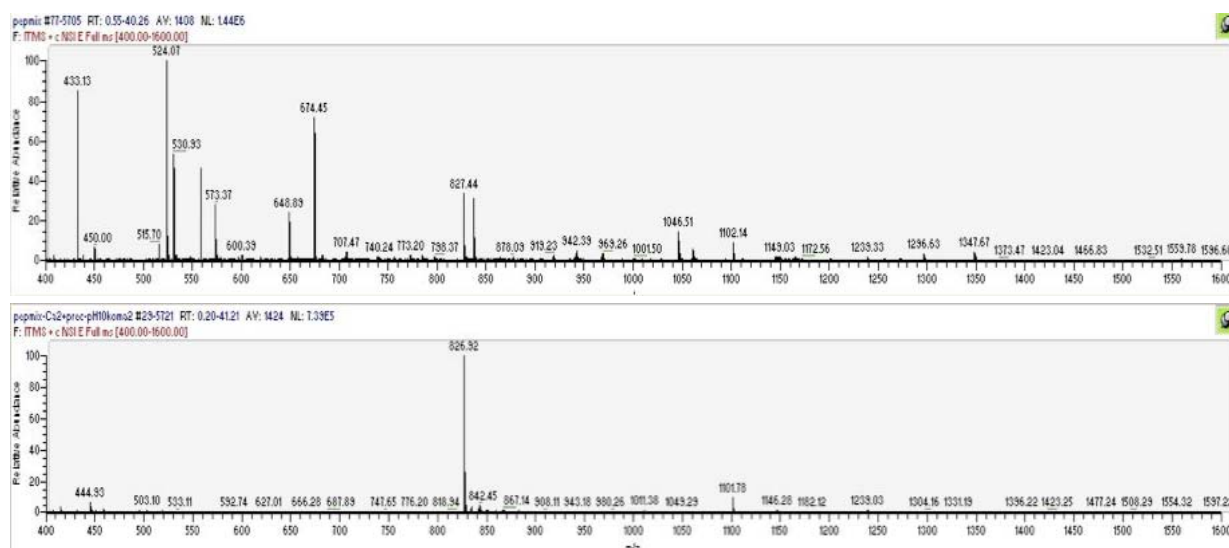


Figure 4.10. Efficiency of calcium phosphate precipitation. The upper spectrum shows peaks of standard synthetic peptide mixture. The lower spectrum shows the sample after phosphopeptide enrichment. The remaining high abundant peak belongs to a synthetic phosphopeptide (GTYSPpSAQEYCNPR, 1652.67 Da) while all other non-phosphorylated peptides are not detectable.

4.2.3 SCX FRACTIONATION

4.2.3.1 Multidimensional protein identification technology (MudPIT)

MudPIT was introduced in 2001 by the Yates group (Washburn et al., 2001) allowing for gel free LC-MS based complex proteome studies. This method permits the identification of up to 2000 proteins from one sample using a home made three phase nano HPLC column (Fig. 4.11). Furthermore, the identification of hydrophobic transmembrane proteins, which usually precipitate in the IP strip during the focusing step of the 2D-PAGE technique is also possible.

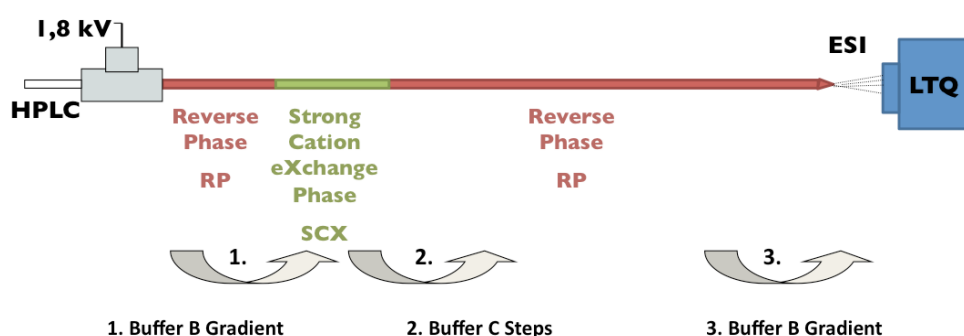


Figure 4.11: Workflow of the MudPIT nano flow 2D HPLC method. Separation efficiency is enhanced by two different particle surfaces within one column. First, the sample binds to the first reverse phase which enables desalting. In the second step, this sample is eluted to the strong cation exchange (SCX) material. Next, peptides are eluted step by step using buffer with increasing salt concentrations. After each salt step peptides are finally separated by an acetonitrile (MeCN) gradient and measured online in a tandem mass spectrometer.

To benefit from these advantages, MudPIT was established and used for the identification of the cardiac phosphoproteome. The number of identified peptides was increased about two times in

comparison to the already established one dimensional reverse phase separation method although just half of the sample amount was analyzed (Fig. 4.12). Phosphopeptides were enriched from the tryptic digest of the cardiac phosphoproteome using the immobilized metal affinity chromatography (IMAC) phosphopeptide enrichment kit (Pierce).

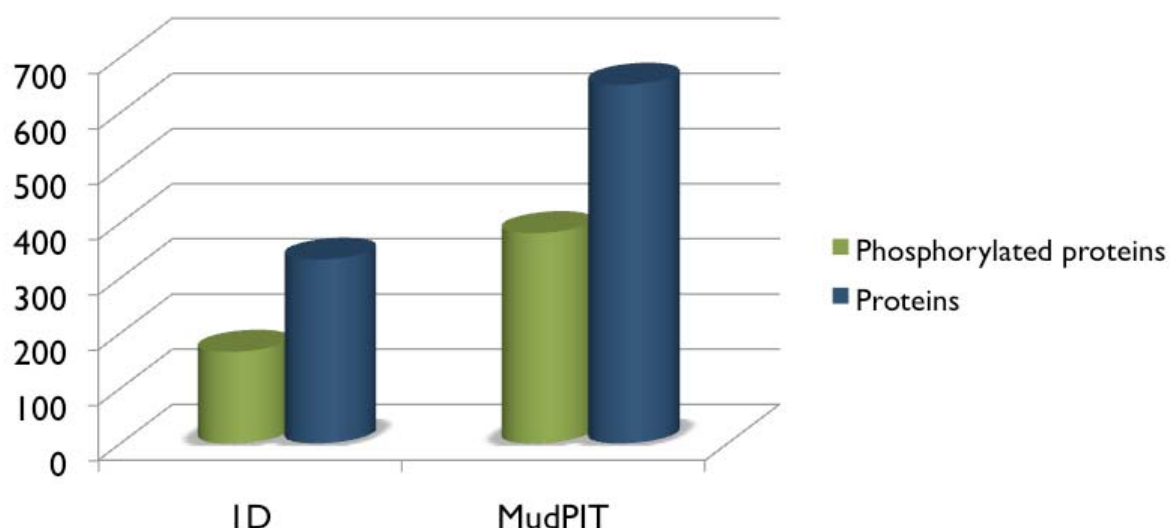


Figure 4.12: Comparison of number of phosphoproteins and total proteins identified by MS after separation by nano flow reverse phase one dimensional (ID) chromatography or MudPIT chromatography. Cardiac proteins were digested with trypsin in solution and phosphopeptides were enriched using IMAC.

Further optimization of the MudPIT separation technology would be possible by increasing the number of salt steps, fine tuning of salt step concentrations to get about equal number of eluting peptides in each fraction and by increasing the elution time of the second dimensional separation. These steps were not performed, since the self made three phase nano flow columns ending in a pulled tip seemed to be quite susceptible to small impurities which often lead to blockade and decreasing flow rates during separation.

4.2.3.2 Manual SCX fractionation using TopTip

To achieve better reproducibility, SCX material filled TopTip was introduced, which is a more robust setup for peptide fractionation. In addition, switching from the online fractionation technique MudPIT to offline SCX fractionation using TopTips allowed for a higher sample loading capacity.

This method was used to fractionate trypsin digested, stable isotope dimethyl labeled and titanium dioxide enriched cardiac phosphopeptide samples. The fractions were divided and analyzed with LTQ or LTQ Orbitrap XL mass spectrometers. Detected phosphorylated peptides are listed in Table 4.1 - 4.7.

4.2.3.3 Offline SCX fractionation using micro flow HPLC

By purchasing Ultimate 3000 (Dionex), a new nano and micro flow HPLC with autosampler and fraction collector, off line SCX fractionation under micro flow conditions became available (Fig. 3.4). Compared with the earlier used SCX fractionation methods, MudPIT and TopTip, HPLC fractionation offered peptide elution by salt gradient instead of salt steps, which improved separation efficiency. Further advantages of micro flow HPLC over nano flow MudPIT separation are the higher loading capacity (250 µg in nano flow HPLC, 100 µg in MudPIT) and the more robust technology with a better reproducibility. Robustness was also improved by inserting an online filter with a pore size of 0.5 µm between the autosampler and columns to prevent column blockade by possible sample impurity. Compared to the online MudPIT method, offline separation allowed the application of acetonitrile as a component of the elution buffer, to enhance peak sharpness and thereby, separation efficiency.

Buffers containing different sodium dihydrogen phosphate (NaH_2PO_4) and acetonitrile (MeCN) concentrations were tested to optimize sample binding. 5 mM NaH_2PO_4 and an increasing MeCN concentration gave the best sample binding and peak resolution. Peptide elution profiles were also optimized by applying different salt gradients.

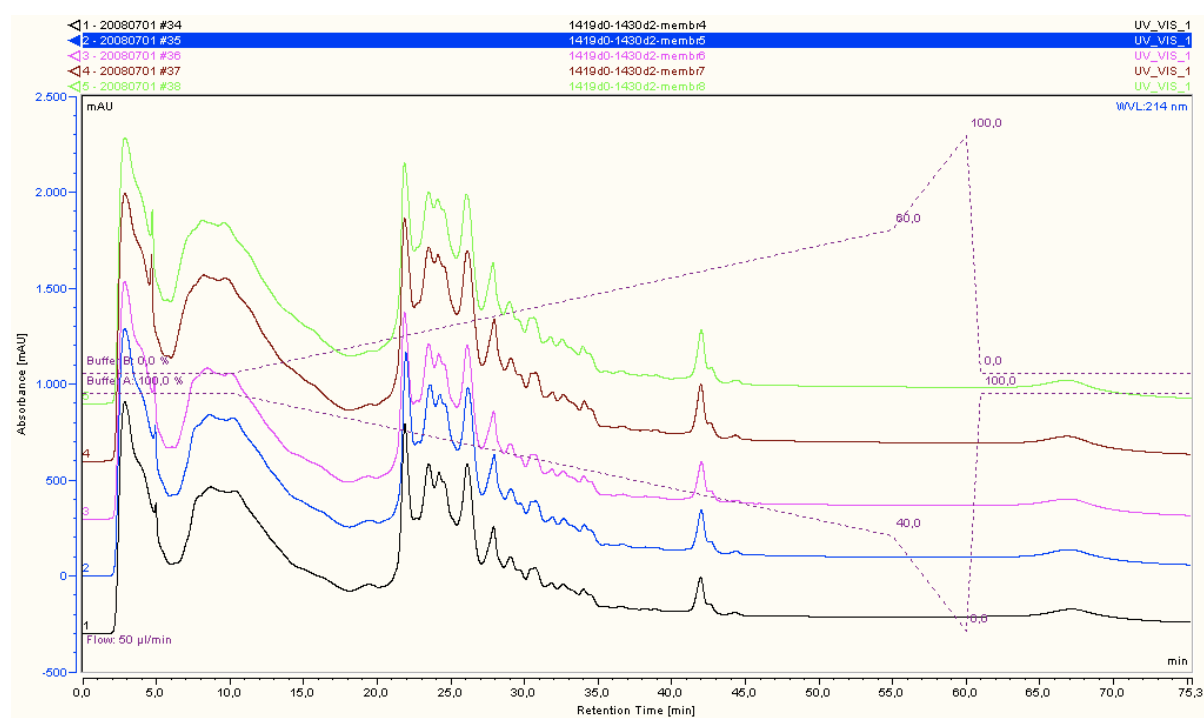


Figure 4.13: UV (214 nm) chromatograms reveal good reproducibility of SCX fractionation. Different colors show peptide elution profiles derived from repeated separation of a dimethyl labeled membrane fraction.

To handle larger sample amounts, aliquots from the same sample were fractionated under identical conditions and good reproducibility of the peptide elution profiles could be obtained (Fig. 4.13). Corresponding fractions were combined, phosphopeptides were enriched using titanium dioxide or calcium phosphate precipitation and analyzed using nanoLC-ESI-MS/MS.

4.2.4 NANO FLOW REVERSE PHASE CHROMATOGRAPHY

Nano flow reverse phase chromatography was used to desalt, concentrate and further separate prepared peptide samples before mass spectrometric analysis. HPLC was online coupled with a tandem MS using an electrospray ionization (ESI) interface which generates a very fine liquid aerosol through electrostatic charging from the eluting sample.

4.2.4.1 Ettan nano LC

An Ettan microLC system coupled with an A-905 autosampler was operated in nanoflow and used to perform MudPIT or ID reverse phase chromatography. Thereby, a Pepmap pre-column was coupled to a home made separation column, prepared from a pulled fused silica capillary packed with 3 μm Pepmap RP particles (75 μm I.D. x 15 cm). To minimize post column peak broadening by dead volumes, the separation column was coupled to the HPLC and to the ESI voltage by a T-piece (Upchurch) directly before the MS. This set up gave quite good HPLC performance with about 30 to 60 seconds peak width. A disadvantage of these pulled columns is that ESI spray stability sometimes degraded upon column tip aging. This problem could be fixed by applying a new column.

4.2.4.2 Ultimate 3000

In comparison to the Ettan nano LC the Ultimate 3000 offers several advantages like actively controlled flow rate, different possible buffer conditions for sample loading/washing and elution by using two different quaternary gradient pumps, a temperable column oven and UV detection at 214 nm, enabling easier trouble shooting and faster method development.

Optimization of nano flow reverse phase chromatography was performed in cooperation with Prof. Dr. Sickmann (ISAS, Dortmund). Briefly, commercially available Pepmap pre-column and separation column (Dionex) were exchanged with home made columns. As pre-column a 2 cm long, as separation column a 15 cm long (I.D. 75 μm ; O.D. 360 μm) packed fritted fused silica (kind gift of Prof. Sickmann) were used. In order to minimize peak broadening, the dead volume between the pre-column and the separation column and after separation column was minimized using special valve (Tube PEEK Gray 1/16 x .015, Upchurch Scientific) and fused silica connections (Teflon tubing 250 μm I.D., Dionex). Since samples were loaded in 0.1% TFA and eluted in 0.1% FA containing buffer, the dead volume could be controlled by the signal differences caused by differences in the UV sign of 0.1% TFA and 0.1% FA. This test called CARLA (current assay for real time liquid baseline analysis) was used every time after placing a new column or pre-column into the system. Using this set up the peak width could be reduced from about 60 to 20 seconds (Fig. 4.14) which enormously enhanced the separation power of the chromatographic system and thereby the sensitivity of peptide identification by mass spectrometry.

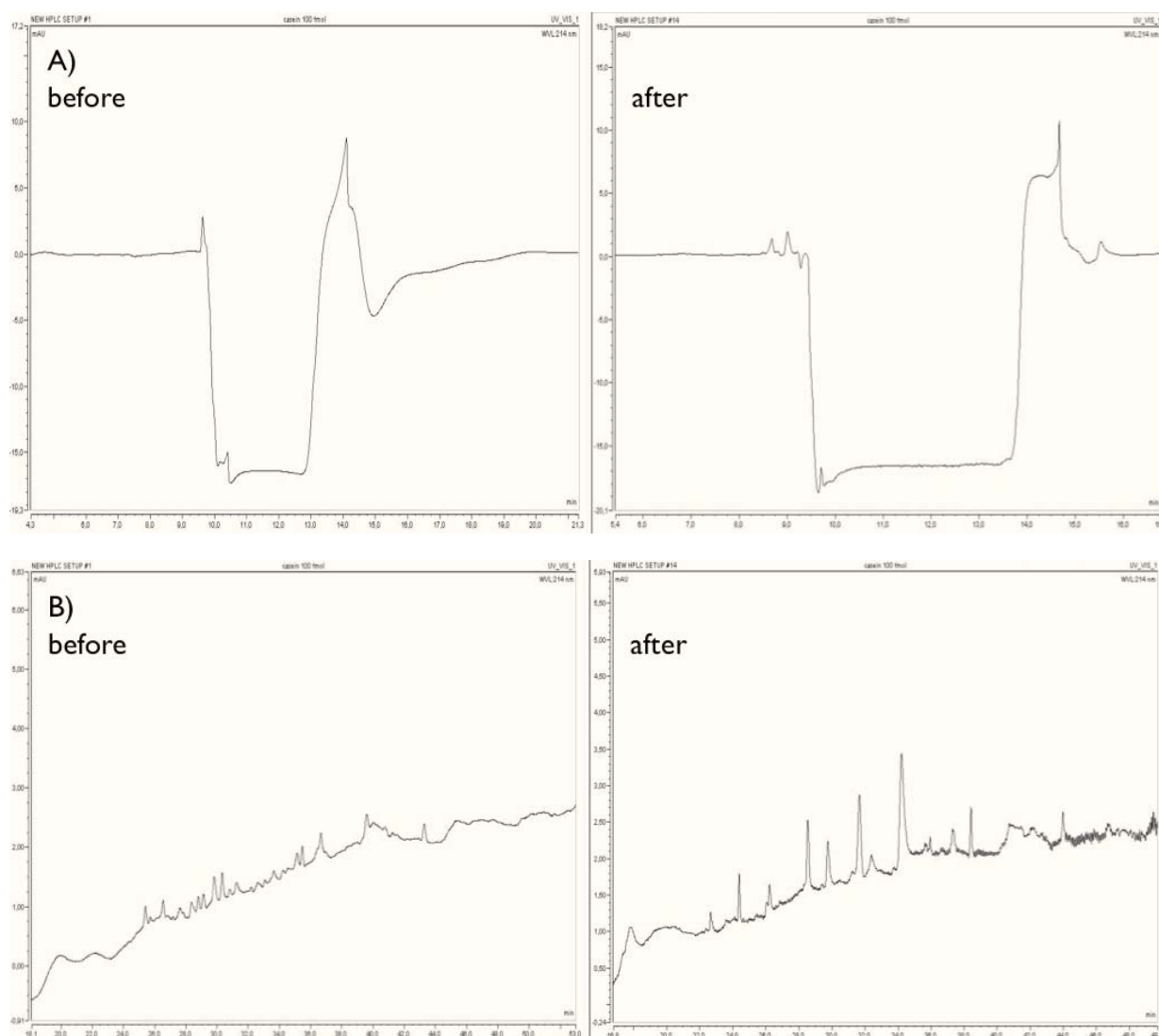


Figure 4.14: A) CARLA test. UV signal at 214 nm shows sharper changes between 0.1% FA and 0.1% TFA indicating minimized dead volume. B) UV peptide elution profile of 100 fmol digested casein shows sharper and higher peaks due to optimized HPLC performance enabling more sensitive MS detection.

Using the optimized setup, SCX fractions derived originally from one sample were separated and measured on the system. Figure 4.15 shows huge sample complexity as indicated by the UV signal of the reverse phase nanoHPLC separated SCX fractions derived from two dimethyl labeled heart samples. After this 2nd dimensional separation step, still more than one peptide elutes from the RP column at a specific point of time which can then be resolved by MS in the 3rd dimension.

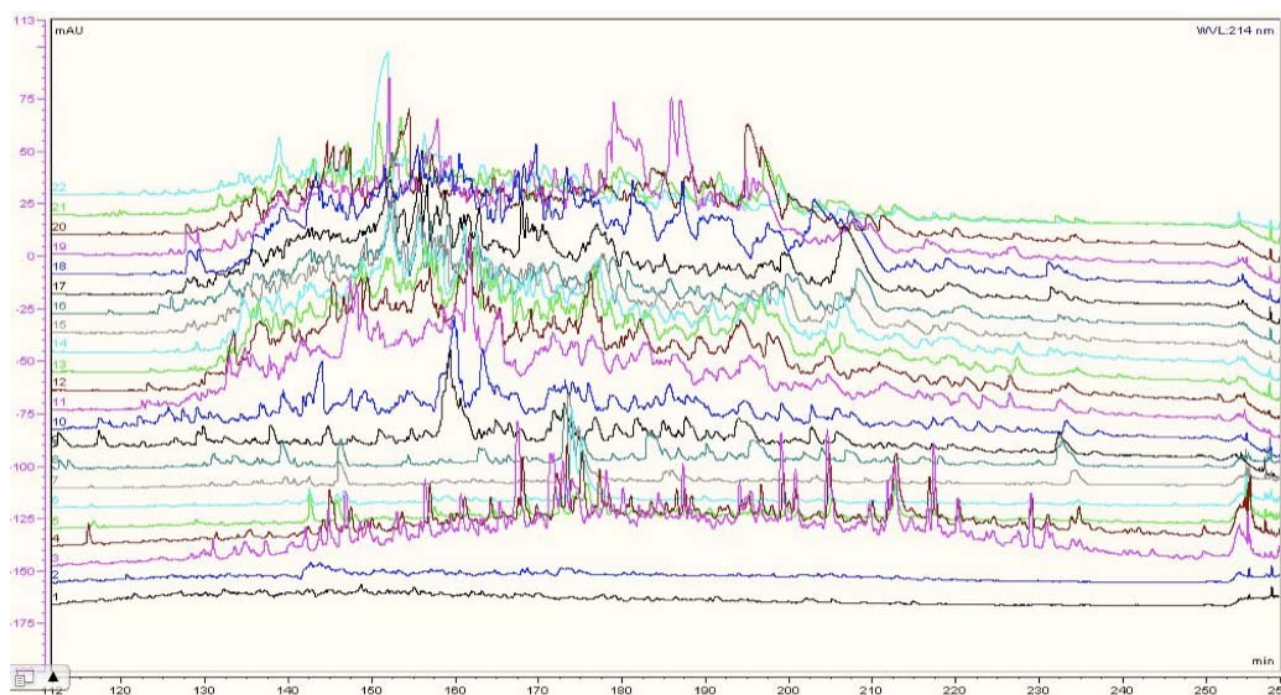


Figure 4.15 UV elution profile of different SCX fractions shows high sample complexity. First chromatogram (black) shows RP elution profile of the first SCX fraction, second chromatogram (blue) shows the RP elution profile of the second SCX fraction and so on.

4.3 QUANTITATIVE ANALYSIS OF iNOS DERIVED NO INDUCED CHANGES IN THE HEART PHOSPHOPROTEOME

The combination of stable isotope dimethyl labeling of primary amino groups with gel free peptide separation methods like phosphopeptide enrichment, fractionation on a strong cation exchange column and nano flow reverse phase liquid chromatography coupled with a tandem mass spectrometer, provided an excellent analytical platform to identify and relatively quantify differences in protein phosphorylation. In the following, the elaborated methods were applied to analyze changes in the heart phosphoproteome in a iNOS induced heart failure model.

4.3.1 REPEATED ANALYSIS FOR STATISTICAL VALIDATION - EXPERIMENTAL SETUP

In order to obtain reliable results, two biological (four months (± 2 weeks) old adult male iNOS^{+/myo^{-/-}} double transgenic mice pairs) and two technical replicates were measured of each membrane and cytosolic fraction (n=8) using enhanced mass resolution mode of a LTQ mass spectrometer (Fig 4.16).

Additionally, during the method evaluation phase a cytosolic fraction of a third mouse pair was measured using a LTQ Orbitrap XL high mass accuracy mass spectrometer in Bremen (kind offer of Thermo Scientific).

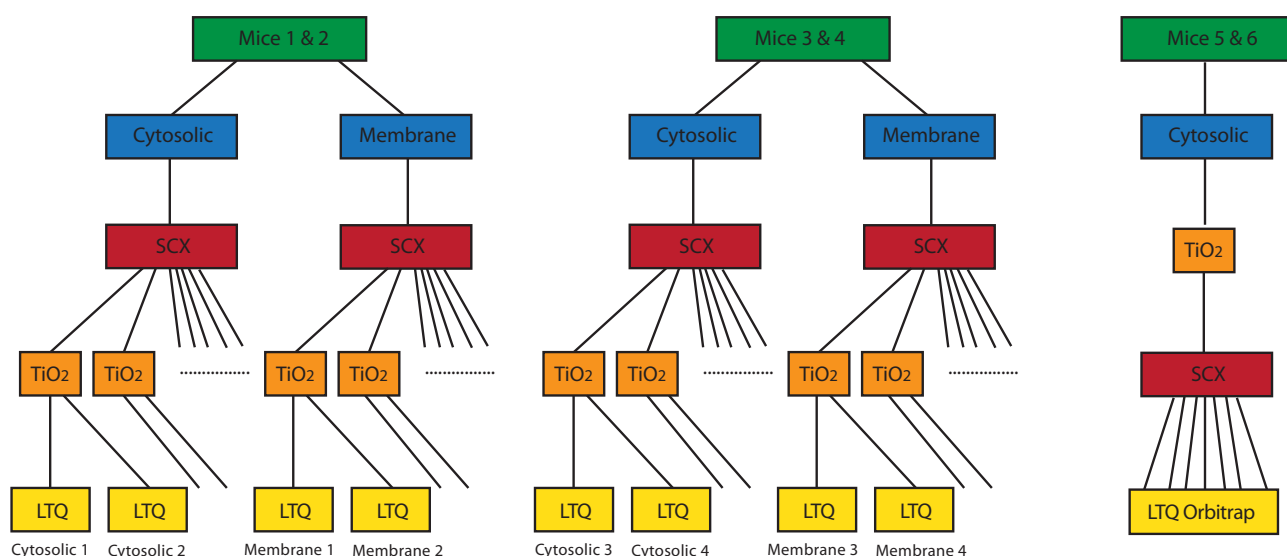


Figure 4.16: Overview of repeated experiments to analyze NO-induced changes in the cardiac phosphoproteome. Cytosolic: cytosolic fraction, Membrane: membrane fraction, SCX: fractionation using strong cation exchange column, TiO_2 : phosphopeptide enrichment on titanium dioxide particles, LTQ: nanoRP-LC-MS/MS measurements on Ultimate 3000 nanoHPLC online coupled with an LTQ, LTQ Orbitrap: nanoRP-LC-MS/MS measurements on Agilent 1100 nanoHPLC online coupled with an LTQ Orbitrap at Thermo Fischer Scientific, Bremen.

Proteins were identified by using MASCOT (version 2.2) software and peptide quantification was performed with a novel version of MSQuant modified to handle dimethyl labeled peptide pairs. Peptides showing a heavy/light peak area ratio ($\text{XIC}_\text{H}/\text{XIC}_\text{L}$) of >1.3 or <0.7 , thus a changed phosphorylation status were manually validated using QualBrowser software of XCalibur (version 2.2). This time consuming process is necessary to filter out false positive results derived from overlapping MS peaks of peptides eluting at the same time with a similar mass to charge value. Data of technically and biologically repeated experiments were summarized by a MATLAB script (written by Jan Heye Buß) and $\text{XIC}_\text{H}/\text{XIC}_\text{L}$ values representing means \pm S.D were counted (Table 4.1).

Table 4.1. Relative quantification and statistical values of repeated experiments on the example of two identified phosphopeptide. Since peaks were chosen for MS/MS identification based on their actual intensity, peptides were usually found in a few but not in every experiment. Missing values indicate that peptide identification did not occur. (XIC_L: integrated peak area of light (not treated with L-arg) peptide, XIC_H: integrated peak area of heavy (treated with L-arg) peptide, XIC_H/XIC_L values representing means \pm S.D, PTM score: indicating post translational modification counted by MSQuant, Mascot score: indicating validity of peptide identification, PTM max: highest PTM score, Mascot max: Mascot score measured in experiment with highest PTM score, Phos. site: position of phosphorylated amino acid within the protein sequence, cyt. 1 and cyt. 2: cytosolic fraction of mice 1&2, cyt 3 and cyt. 4: cytosolic fraction of mice 3&4, membr. 1 and membr. 2: membrane fraction of mice 1&2, membr. 3 and membr. 4: membrane fraction of mice 3&4).

Symbol	Protein							
	Peptide	PTM max	Mascot max	Phos. site	N/K	XIC _H /XIC _L		log ₂ (XIC _H /XIC _L)
Ndrp2	Isoform 2 of Protein NDRG2							
TApSLTSAApSIDGSR		186.87	107	318, 324	known	1.0548 +/- 0.11223		0.076966
	Cyt. 1	Cyt. 2	Membr. 1	Membr. 2	Cyt. 3	Cyt. 4	Membr. 3	Membr. 4
XIC ₁	24118409	9763103	1605377	902233	198397038	112916630	2550345	1196886
XIC ₃	27842454	8688657	1820844	902004	194496932	109505258	2775482	1462185
XIC ₃ /XIC ₁	1.1544	0.88995	1.1342	0.99975	0.98034	0.96979	1.0883	1.2217
Psite	332	332	324	338	324	332	332	324
PTM Score	95.32	132.5	133.88	86.08	186.87	92.94	68.35	84.15
Mascot Score	59	79	59	82	107	79	94	80
File	E:\2008\2008	E:\2008\2008	E:\2008\2008	E:\2008\2008	E:\2008\2008	E:\2008\2008	E:\2008\2008	E:\2008\2008
Symbol	Ndrp2	Ndrp2	Ndrp2	Ndrp2	Ndrp2	Ndrp2	Ndrp2	Ndrp2

Srl	Isoform 1 of Sarcalumenin precursor							
TQDIEAEApSEER		138.18	59	442	known	1.5893 +/- 0.24706		0.66835
	Cyt. 1	Cyt. 2	Membr. 1	Membr. 2	Cyt. 3	Cyt. 4	Membr. 3	Membr. 4
XIC ₁	2349567	188669	145215	310787				
XIC ₃	3777947	249248	219902	594744				
XIC ₃ /XIC ₁	1.6079	1.3211	1.5143	1.9137				
Psite	442	442	442	442				
PTM Score	128.91	46.43	118.33	138.18				
Mascot Score	60	64	54	59				
File	E:\2008\2008	E:\2008\2008	E:\2008\2008	E:\2008\2008				
Symbol	Srl	Srl	Srl	Srl				

4.3.2 COMPARISON OF PROTEIN EXPRESSION PROFILES OF iNOS⁺/MYO^{-/-} MICE

As can be seen in Fig. 4.17 non-phosphorylated peptides appeared in a ratio of one to one indicating the same protein expression level in both saline and L-arginine coperfused iNOS⁺/myo^{-/-} hearts as well as accurate sample preparation.

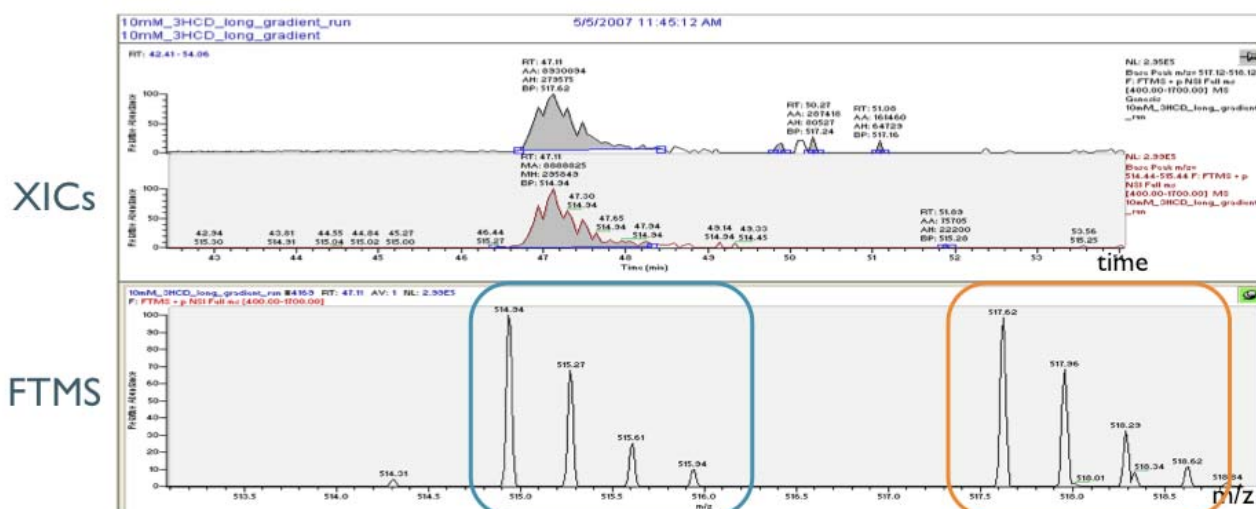


Figure 4.17: The protein expression pattern in arginine treated (blue) and untreated (orange) hearts is the same (ratio is 1). XIC peptide elution profile shows that heavy and light peptides elute at the same time which is an important criteria for relative quantification. (XIC: extracted ion chromatogram, FTMS: Fourier transformed mass spectrum).

Statistical analysis confirmed this finding: Fig. 4.18 shows that 300 non-phosphorylated heavy and light peptide ratios result in a mean \log_2 value of 0.009 (heavy/light peptide ratio is 1:1). Hence, differences in phosphopeptide ratios are due to changes in phosphorylation levels induced by *in situ* iNOS activation.

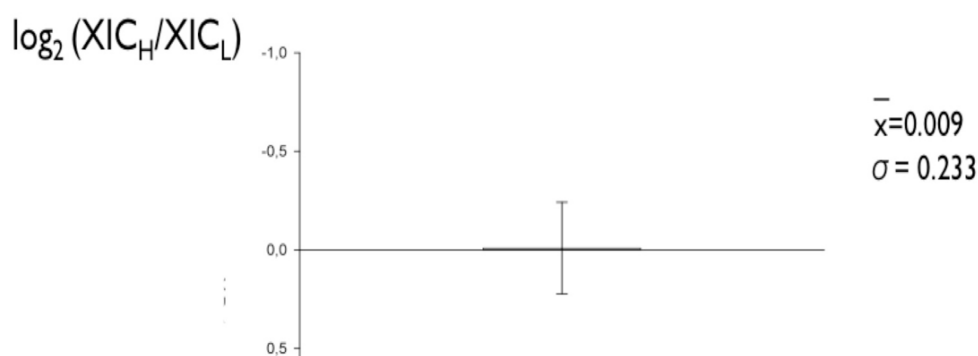


Figure 4.18: Mean \log_2 value of 300 non-phosphorylated heavy and light peptide ratios is 0.009 (heavy/light peptide ratio is 1:1) with a standard deviation of 0.233. Therefore changes in phosphopeptide ratios indicate differences in the phosphorylation level induced by *in situ* iNOS derived NO production. (XIC_H: extracted ion chromatogram of heavy; XIC_L: extracted ion chromatogram of light peptides)

4.3.3 IDENTIFIED CARDIAC PHOSPHOPROTEOME USING LTQ

Using LTQ, collision induced dissociation (CID) and CID with multistage activation were applied for peptide fragmentation. Compared with multistage activation, CID gives a high number of MS/MS spectra because of faster data acquisition. On the other hand, phosphorylated peptides lose a phosphate group during fragmentation in an ion trap. Therefore, a prominent ion corresponding to

a dephosphorylated peptide (neutral loss fragment, loss of 98 Da) is present in the MS/MS spectrum (Fig. 4.6, peak at 799 m/z). This inadequate fragmentation leads to a poor spectrum quality which results in lower identification scores. This means, that such a badly fragmented phosphopeptide spectrum often does not contain enough information to identify the amino acid sequence, or assignment of the phosphorylated residue is not possible.

This problem is solved by CID with multistage activation which works as a kind of pseudo MS/MS/MS experiment, where neutral loss peaks of a phosphopeptide get fragmented additionally. Therefore, the resulting spectrum contains peptide fragment information derived from the original peptide (MS/MS) and fragments from the neutral loss peak (MS/MS/MS) as a merged spectrum (pseudo MS/MS/MS) (Fig. 4.19). Thus, these structural information rich spectra enable easier phosphopeptide and phosphorylation site detection, due to peaks of neutral loss peptide fragments (-98 Da), which serve as an indicator for peptide phosphorylation. In the tests CID with multistage activation gave the best results, therefore this activation mode was used in the following.

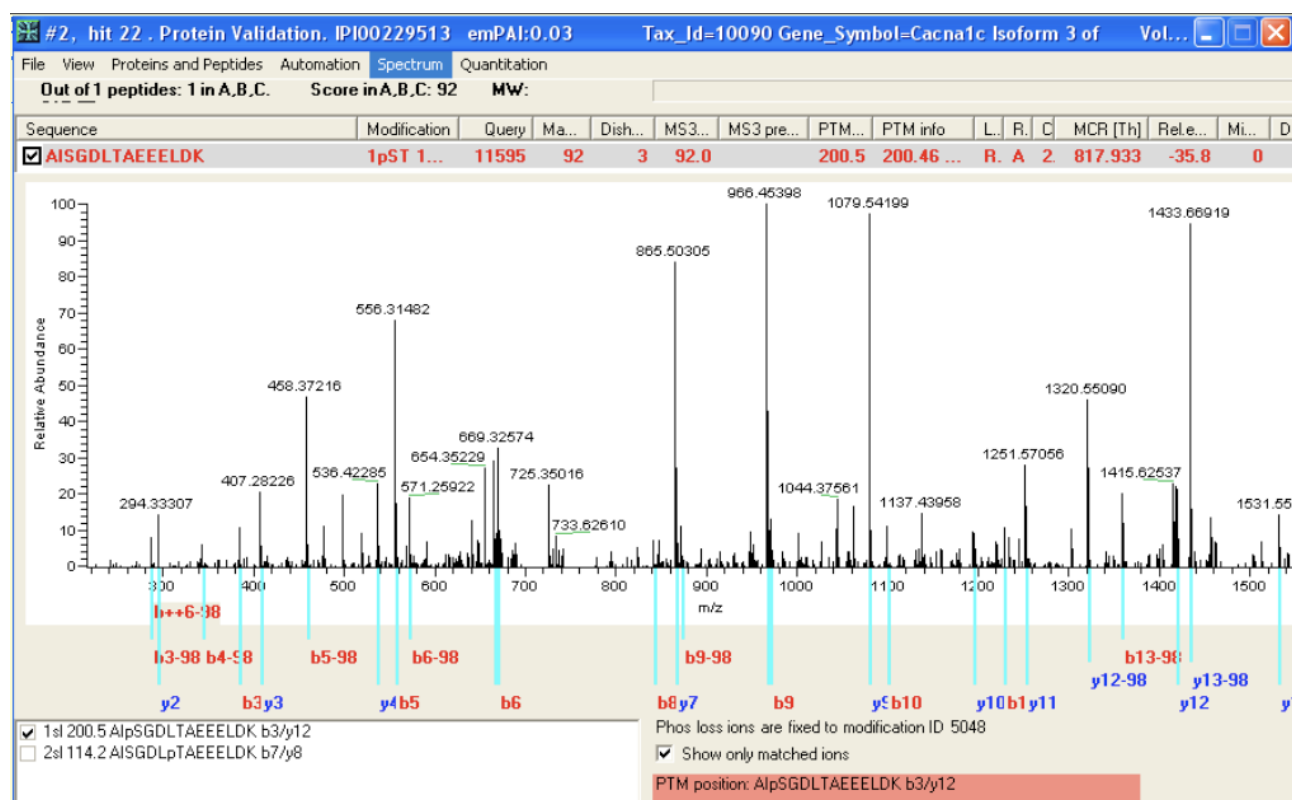


Figure 4.19: Multistage activation MS/MS spectra of a dimethyl labeled phosphopeptide AlpSGDLTAEELDK of voltage gated calcium channel ($\text{Ca}_v1.2$) α -1c subunit (Cacna1c) with a novel phosphorylation site at pSer-1670. Peptide fragments with a neutral loss of -98Da are typical for Ser and Thr phosphorylated peptide, increase the probability of phosphorylation site (PTM) and peptide identification (MASCOT) scores.

In order to maximize the number of identified phosphorylated peptides a relative large amount of sample, 7 mg and 3 mg protein was used for the analysis of the cytosolic and the membrane fraction, respectively. Since the identification rate of phosphorylated peptides was just about 1% of all peptides in the beginning, phosphopeptide enrichment had to be optimized. Additionally, strong

cation exchange fractionation and nano flow reverse phase HPLC was improved as described before.

As a result of these improvements 784 phosphorylation sites in 737 phosphorylated peptides could be identified and quantified, as listed in table 4.5-4.8. These peptides belong to 448 phosphorylated proteins. Phosphorylation site distribution was 80.5% Serine, 18.9% threonine and 0.6% tyrosine. Furthermore, most of the analyzed SCX fractionated and phosphopeptide enriched samples were found to contain 90-100% clean fraction of phosphorylated peptides which is a clear improvement compared to the earlier results.

Statistical analysis of 300 non-phosphorylated peptide ratios resulted in a mean \log_2 value of heavy and light peptide ratios ($\log_2(\text{XIC}_H/\text{XIC}_L)$) of 0.009 whereas the standard deviation is 0.233. To differentiate between regulated and not regulated phosphopeptides, a cutoff score about two times of the standard deviation, 0.5 and -0.5 was defined. By applying these criteria 51 enhanced phosphorylated and 44 decreased phosphorylated peptides were identified (Fig. 4.20).

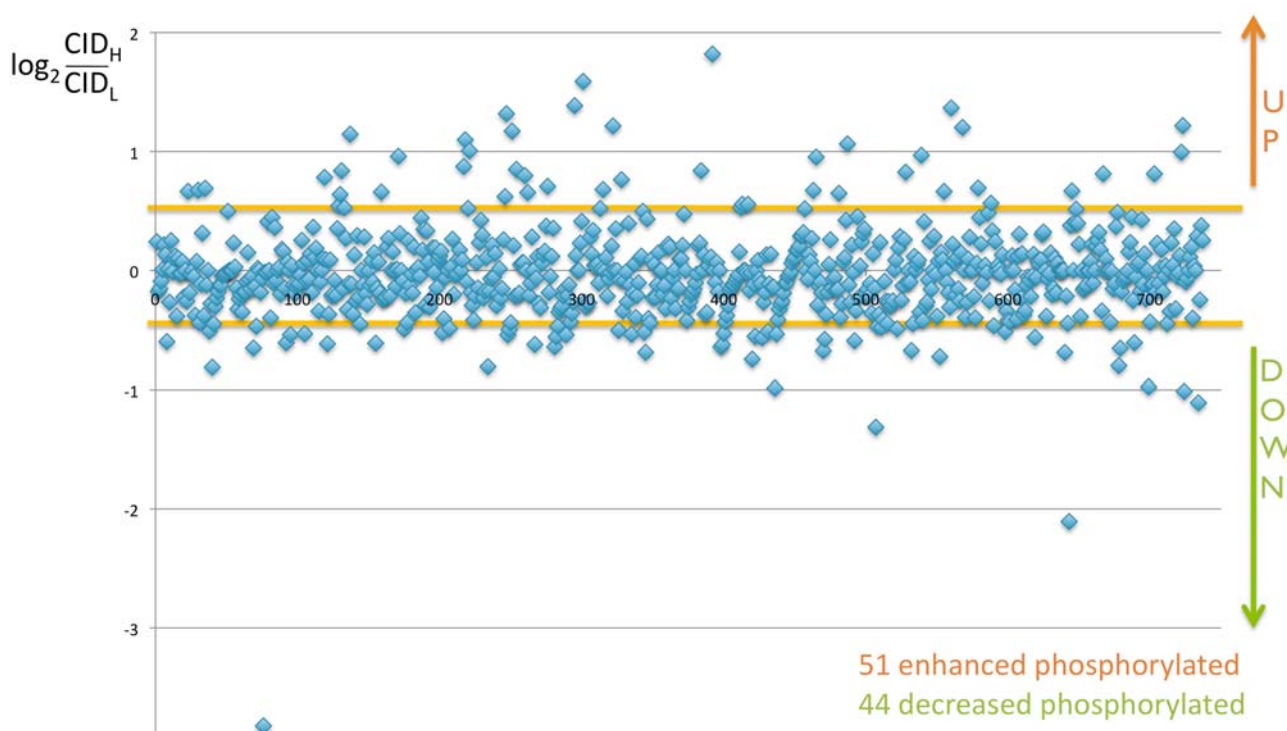


Figure 4.20: Identified and relatively quantified phosphopeptides measured by LTQ. X axis shows number of phosphorylated peptides, Y axis shows mean of $\log_2(\text{XIC}_H/\text{XIC}_L)$ values. If \log_2 ratio of peptide areas is 0, heavy (+L-arginine) and light (-L-arginine) labeled peptides have the same intensity and phosphorylation level. (XIC_L : integrated peak area of light (did not treated with L-arg) peptide, XIC_H : integrated peak area of heavy (with L-arg treated) peptide)

Identified proteins were located in all possible cellular compartments, indicating that the method is applicable for the analysis of both hydrophilic (cytosolic) and hydrophobic (integral to membrane) proteins (Fig. 4.21).

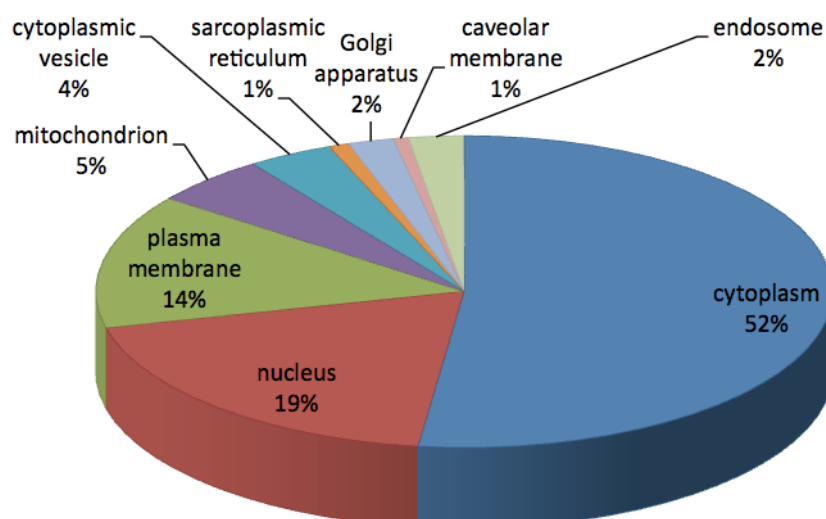


Figure 4.21. Subcellular distribution of the identified phosphoproteins. Determined using the identified gene symbol list fed into DAVID bioinformatic resources 2008 online tool available at <http://david.abcc.ncifcrf.gov/> (Dennis et al., 2003 and Huang et al., 2009).

4.3.3.1 Differentially regulated phosphoproteins upon enhanced NO formation

4.3.3.1.1 DEPHOSPHORYLATED CARDIAC PHOSHOPEPTIDES

In table 4.2 peptides are listed which become dephosphorylated upon iNOS-induced heart failure. Regulated proteins are ordered according to their function or localization. If the identified phosphorylation site is already known from the mouse, human or other species was checked on www.phosphosite.org. Already published phosphorylation sites are signed as known, the others as novel (Phosphosite database from March 2009).

Table 4.2: List of dephosphorylated peptides upon iNOS derived NO release (1 min), measured by LTQ. Blue color shows that other phosphorylated peptides were also identified from the same protein (not regulated), green color shows, that protein was found both enhanced and decreased phosphorylated at different sites. (XIC_L: integrated peak area of light (not treated with L-arg) peptide; XIC_H: integrated peak area of heavy (treated with L-arg) peptide; PTM score: indicating post translational modification counted by MSQuant; Mascot score: indicating validity of peptide identification). XIC_H/XIC_L values represent means \pm S.D.

Gene Symbol	Protein						
	Peptide	PTM max	Mascot max	Phos. site	N/K	XIC _H /XIC _L	log ₂ (XIC _H /XIC _L)
Cardiac contractile proteins							
Myh6	Myosin-6						
	EQpYEEEMoxEAK	4.3	55	1349	novel	0.64067	-0.64235
	YEESQpSELESSQK	6.48	64	1467	novel	0.6491 \pm 0.18729	-0.62349
	TLEDQANepYR	73.26	52	1261	novel	0.69251 \pm 0.076357	-0.53009
My17	Myosin regulatory light chain 2, atrial isoform						
	GSSNVFpSMoxFEQAQIQEFK	8.35	45	27	novel	0.59645 \pm 0.056703	-0.74553
My1c2b	Myosin regulatory light chain 2-B, smooth muscle isoform						
	ATSNVFAMFDQpSQIQEFK	7.38	94	19	novel	0.6814 \pm 0.192	-0.55342
Myo9b	Isoform I of Myosin-IXb						
	AQDKPESPpSGSTQIQR	30.04	60	1266	novel	0.67517	-0.56669

Sarcomeric proteins							
Nexn	Nexilin						
	TVpSQESLTPGK	148.5	53	296	novel	0.6261 +/- 0.022136	-0.67554
	SMoxVLDDDDpSPEIYK	123	52	288	known	0.66884 +/- 0.18194	-0.58027
Myot	Myotilin						
	SSpSRAEANDQDAIQEK	87.23	69	231	novel	0.70022 +/- 0.058362	-0.51411
Ttn	Isoform 1 of Titin						
	TApSPHFTVSK	55.83	41	814	novel	0.50877	-0.9749
Smpx	Small muscular protein						
	RKEpSTPETEEGAPTTSEEK	11.53	45	46	novel	0.67715 +/- 0.17698	-0.56244
Actin binding proteins							
Fhod3	Isoform 4 of FHL1/FH2 domain-containing protein 3						
	DAAPESSALHTTSSpTSQGR	75.9	48	429	novel	0.57102	-0.80837
Spnb2	Isoform 1 of Spectrin beta chain, brain 1						
	GDQVSQNGLPAEQGpSPR	93.14	54	2137	known	0.62004 +/- 0.041147	-0.68956
Microtubule plus-end tracking							
Clip1	Isoform 1 of CAP-Gly domain-containing linker protein 1						
	QLpSSSSGNTDAQAEEDER	56.99	89	1255	novel	0.65438	-0.61181
Membrane-cytoskeleton linker							
Ank3	Brain-specific ankyrin-G						
	EFDSDpSLR	124.1	59	959	known	0.63651	-0.65175
Calmodulin binding proteins							
Add3	Adducin 3						
	TEEVLPSPDGSPSKSPSK	156.6	57	681	known	0.56911 +/- 0.088358	-0.81322
Calcium homeostasis							
Srl	Isoform 1 of Sarcalumenin precursor						
	TQDIEAEApSEERQQR	31.65	41	442	known	0.23231	-2.1059
Cacnb2	Isoform 4 of Voltage-dependent L-type calcium channel subunit beta-2						
	QETFDpSETQESR	79.36	63	470	novel	0.65201	-0.61703
Metabolism							
Acyp2	Acylphosphatase						
	NTpSKGTVTGQVQGPEEK	7.99	40	56	novel	0.70204 +/- 0.047739	-0.51038
Atp5a1	ATP synthase subunit alpha, mitochondrial						
	TGTAEMoxpSSILEER	39.89	48	52	novel	0.65601	-0.60822
Kinases/Phosphatases							
Map3k3	Mitogen-activated protein kinase kinase kinase 3						
	SADpSENALTVQER	76.35	78	340	known	0.62044 +/- 0.014554	-0.68864
Ltbp2	latent transforming growth factor beta binding protein 2						
	GELDPVLEDNpSVETR	91.24	95	511	novel	0.69784	-0.51904
Ppp2r5d	Protein phosphatase 2A B56 delta subunit						
	DGGGENpTDEAQPQPQSQSPS SNK	11.53	61	34	novel	0.62724	-0.67292
Tns1	tensin 1						
	QGSPpTPALPEKR	7.99	47	1537	novel	0.57452 +/- 0.076165	-0.79958
	QGSPpTPALPEK	136.3	58	1537	novel	0.63586 +/- 0.13333	-0.65322
Cholesterol/HDL binding							
Apoa1bp	Apolipoprotein A-I-binding protein						
	RGpSETMAGAAVK	7.11	53	43	novel	0.070635 +/- 0.020244	-3.8235

Osbp	oxysterol binding protein	MoxLAESDDSGDEESVpSQTDK	8.3	73	198	novel	0.66386	-0.59106
Stress proteins								
Hsp90ab I	Heat shock protein HSP 90-beta	EKEIpSDDEAEEEEKGEK	36.54	45	226	known	0.64086 +/- 0.04904	-0.64192
		ElpSDDEAEEEEKGEK	205.7	96	226	known	0.67897 +/- 0.0011805	-0.55859
Hspb I	Isoform A of Heat shock protein beta-I	QLpSSGVSEIR	136.3	65	86	known	0.68723 +/- 0.13222	-0.54113
Vascular development								
Qk	Isoform 6 of Protein quaking	DANIKpSPTAQAPR	77.33	40	211	novel	0.60512	-0.7247
Transcriptional regulation								
Naca	Nascent polypeptide-associated complex subunit alpha, muscle-specific form	ADSCVSPNpTVSQPLKR	16.22	68	580	novel	0.50505 +/- 0.15562	-0.98549
		GAPVPSTGAPPpSPK	226.8	84	765	novel	0.69034 +/- 0.0063836	-0.53461
Pbxip I	Pre-B-cell leukemia transcription factor-interacting protein I	CSSpSDDDTDVDVEGLR	45.33	58	144	known	0.40256	-1.3127
Lmo7	LIM domain only 7	LAPpSPSEEPR	132.1	60	822	novel	0.70503 +/- 0.026764	-0.50424
Translation regulation								
LOC100047194	similar to Eukaryotic translation initiation factor 4 gamma 3	GpSSKDLLDNQSQEEQR	102.7	80	1157	novel	0.68921 +/- 0.054477	-0.53698
Eef1d	eukaryotic translation elongation factor I delta isoform a	ATAPQTQHVPSPMR	144.3	52	512	known	0.69571 +/- 0.028572	-0.52345
Splicing factor/mRNA binding								
Hnrnpc	Isoform C1 of Heterogeneous nuclear ribonucleoproteins C1/C2	DDEKEPEEGEDDRDSANGEDDpS	10.19	41	300	known	0.64964	-0.62228
Sfrs6	Putative uncharacterized protein	SHpSPLPAPPSK	6.97	49	303	known	0.69977 +/- 0.093888	-0.51505
Zranb2	37 kDa protein	EEpSDGEYDEFGR	55.87	51	130	known	0.46409	-1.1075
Protein with unknown function								
II10058 L19Rik	UPF0369 protein C6orf57 homolog	FDpSLEDSPeer	51.59	50	56	novel	0.66049 +/- 0.11196	-0.59838
Atxn2I	Isoform 2 of Ataxin-2-like protein	QGSGREpSPSLVSR	38.12	51	337	known	0.68776	-0.54002
BC005624	Uncharacterized protein C9orf78 homolog	RADpSEpSEEDEQESEEVR	49.18	59	15, 17	known	0.69113	-0.53298
Gm1614	hypothetical protein	TGpSLDESLSR	99.9	67	295	novel	0.68706 +/- 0.012313	-0.54149
Wdr20b	WD repeat-containing protein 20	SNSLPHSAVPsNAASK	9.82	51	439	novel	0.49576	-1.0123

4.3.3.1.2 CARDIAC PHOSHOPEPTIDES WITH INCREASED PHOSPHORYLATION

Peptides with an enhanced phosphorylation upon iNOS derived NO release are listed in table 4.3:

Table 4.3: Proteins found with an enhanced phosphorylation ordered according their function, binding partner or localization. Orange color shows that other phosphorylated peptides were also identified to the same protein (not regulated), green color shows, that protein was found both enhanced and decreased phosphorylated at different sites. (XIC_L: integrated peak area of light (did not treated with L-arg) peptide, XIC_H: integrated peak area of heavy (with L-arg treated) peptide, PTM score: indicating post translational modification counted by MSQuant, Mascot score: indicating validity of peptide identification). XIC_H/XIC_L values represent means \pm S.D.

Symbol	Protein	Peptide	PTM max	Mascot max	Phos. site	N/K	XIC _H /XIC _L	log ₂ (XIC _H /XIC _L)
Cardiac contractile proteins								
Mybpc3	Myosin binding protein C, cardiac							
		TpSLAGAGR	87.76	43	281	known	3.5294 \pm 0.015532	1.8194
Myh6	Myosin-6							
		EEQAEPDGpTEDADK	127.39	54	379	novel	1.4428	0.52888
		EALpSQLTR	163.84	56	1301	novel	1.4705 \pm 0.095962	0.55633
Myh9	myosin heavy chain IX							
		GTGDCpSDEEVDGK	158.32	44	1942	known	1.4707 \pm 0.70015	0.55651
Sarcomeric proteins								
Cmya5	Cardiomyopathy-associated protein 5							
		ETSpSPLSPEVEHR	83.21	49	772	novel	1.5787 \pm 0.63358	0.65874
Ldb3	Isoform 3 of LIM domain-binding protein 3							
		ASSEGAQGSVPSPK	246.51	105	179	novel	1.6023 \pm 0.69097	0.68019
Actin binding proteins								
Capzb	Isoform 1 of F-actin-capping protein subunit beta							
		ELpSQVLTQR	114.22	84	263	known	1.4413 \pm 0.13248	0.52734
Limch1	109 kDa protein							
		ETDDIDpSPKR	112.44	57	169	novel	2.3209 \pm 0.3239	1.2147
Lcp1	Plastin-2							
		GpSVSDEEMoxMoxELR	110.44	48	5	known	1.4344 \pm 0.089288	0.52046
Microtubule building protein								
Tubb2c	Tubulin beta-2C chain							
		GSQQpYRALpTVPELTQQMFDK	44.23	55	281, 285	novel	1.7562	0.81245
Mtap4	Isoform 1 of Microtubule-associated protein 4							
		VGpSTENIK	107.82	40	914	known	1.7884 \pm 0.73569	0.83865
Calcium homeostasis								
Canx	Calnexin precursor							
		SDAEEDGVTGpSQDEEDpSKPKAEDEILNR	46.32	42	563, 569	known	1.4581	0.5441
		pSDAEEDGVTGSQDEEDSKPK	230.41	108	553	known	1.5569 \pm 0.33227	0.6387
		QKpSDAEEDGVTGpSQDEEDSKPK	129.62	53	553	known	1.7877 \pm 0.21932	0.83813
Hrc	histidine rich calcium binding protein							
		EDENDDDEDGpSGEYR	212.83	65	272	novel	1.6321 \pm 0.42358	0.70677

Pln	Cardiac phospholamban						
	ASpTIEMoxPQQAR	124.07	43	17	known	1.7733 +/- 0.75328	0.82646
Srl	Isoform 1 of Sarcolumenin precursor						
	TQDIEAEApSEER	138.18	59	442	known	1.5893 +/- 0.24706	0.66835
GAP junction							
Gja1	Gap junction protein						
	MGQAGpSpTISNSHAQPF DFPDDSQNAK	18.07	42	325, 326	known	1.5375	0.62059
	QApSEQNWANYSAEQN R	121.12	48	306	known	2.4926	1.3176
Metabolism							
Acly	ATP-citrate synthase						
	TApSFSESR	109.94	60	455	known	1.6143 +/- 0.0071249	0.69091
Ndufa7	NADH dehydrogenase [ubiquinone] 1 alpha subcomplex subunit 7						
	ALVSGKAAEpSSAMoxAAT EK	26.16	44	84	novel	1.9365 +/- 0.16481	0.95345
Ion/Lipid/protein transport							
Abcc1	Multidrug resistance-associated protein 1						
	GSpSQLDVNEEVEALIVK	169.36	63	290	novel	1.5959	0.67435
Stard10	PCTP-like protein						
	AGGAGGEGpSDDDTSLT	43.11	51	284	known	1.4283	0.51427
Rab3ip	RAB3A-interacting protein						
	TLVLSSSPpSPTQEPLAAA K	131.09	69	218	known	1.5847	0.66422
Ranbp3	Ran-binding protein 3						
	TSpSLTHSEEK	64.66	47	58	known	2.5778	1.3661
Vps4b	Vacuolar protein sorting-associating protein 4B						
	GNDpSDGEAESDDPEK	216.43	112	102	known	1.992 +/- 0.16689	0.99419
	GNDpSDGEAESDDPEKK	98.83	58	102	known	2.3252 +/- 0.10326	1.2174
Kinases/Phosphatases							
Prkca	protein kinase C, alpha						
	VlpSPSEDR	59.16	54	319	known	1.9571	0.96869
Saps3	Isoform 1 of SAPS domain family member 3						
	IQQFDDGGpSDEEDIWEE K	141.4	73	588	known	1.4799 +/- 0.11775	0.56555
Transcriptional regulation							
Cbx3	Chromobox protein homolog 3						
	SLpSDSESDDSK	112.19	66	95	known	2.2129 +/- 0.049728	1.1459
Csrp3	Cysteine and glycine-rich protein 3						
	FGEpSEKCPR	8.88	41	117	novel	1.9455	0.96017
Hdac4	Isoform 1 of Histone deacetylase 4						
	QEPIEpSEEEAEATR	92.94	90	562	known	1.8017	0.84939
Hecw2	Isoform 1 of E3 ubiquitin-protein ligase HECW2						
	ANpSDTDLVTSESR	42.61	66	48	known	1.5755	0.65577
Hdgfrp2	Isoform 1 of Hepatoma-derived growth factor-related protein 2						
	LApSESANDDNEDS	75.39	41	659	known	1.7388	0.79807

Htatsf1	Isoform 1 of HIV Tat-specific factor 1 homolog						
	AEEGGEpSEGDApSEKDAK	91.94	42	441, 446	novel	2.6126 +/- 0.36142	1.3855
Irf2bp1	Isoform 1 of Interferon regulatory factor 2-binding protein 1						
	KApSPEPEGETAGK	82.21	52	384	novel	3.0093	1.5894
Lmo7	LIM domain only 7						
	EDSVVAETQLASHpSPEEQ R	104.54	66	813	known	1.6973 +/- 0.041912	0.76323
Naca	Nascent polypeptide-associated complex subunit alpha, muscle-specific form						
	AIEpTLLVSPAK	162.26	67	1859	novel	1.4323 +/- 0.23833	0.51837
Nr3c1	Isoform 2 of Glucocorticoid receptor						
	SSTPAAGCApTPTEK	194.78	50	159	known	1.5678	0.64871
Translation regulation							
Eif4b	Eukaryotic translation initiation factor 4B						
	SQpSSDTEQPSPTSGGGK	141.6	97	497	known	1.8329 +/- 0.22652	0.87415
	TGpSESSQTGASATSGR	86.2	53	422	known	2.1408	1.0981
Eif4ebp1	Eukaryotic translation initiation factor 4E-binding protein 1						
	DLPAIPGVTSPTpSDEPPMo xQASQSQLPSSPEDK	59.49	53	85	known	1.4361 +/- 0.082196	0.5222
Eif4g1	eukaryotic translation initiation factor 4, gamma 1 isoform b						
	AApSLTEDR	169.28	66	1205	known	2.0081 +/- 0.0072395	1.0058
Translation elongation							
Rplp0	60S acidic ribosomal protein P0						
	AEAKEEpSEEpSDEDMoxG FGLFD	102.05	67	304, 307	known	1.6173 +/- 0.56015	0.69359
Hypoxia-induced apoptosis							
Ndrp2	Isoform 1 of Protein NDRG2						
	SRpTASLpTSAASIDGSR	18.42	44	330, 334	known	1.5943	0.67295
RNA binding							
Rbm20	similar to hCG2036763						
	ETEGTDSPpSPER	152.77	49	1213	novel	2.3013 +/- 0.021505	1.2025
Protein with unknown function							
C130038G02Rik	Isoform 1 of Uncharacterized protein KIAA0774						
	QLpSEENANLQEYVEK	105.48	50	1286	novel	1.7201	0.7825
Gm1614	hypothetical protein						
	TpSPLGGAR	46.94	49	833	novel	2.2523	1.1714
Nucks1	Nuclear ubiquitous casein and cyclin-dependent kinases substrate						
	NSQEDpSEDpSEEKDVK	129.62	41	58, 61	known	2.0907	1.064
Tcp1112	T-complex protein 11-like protein 2						
	QCVSEDQQpSDSESR	165.71	61	16	novel	1.7568 +/- 0.24919	0.81296
5730494N06Rik	UPF0414 transmembrane protein C20orf30 homolog						
	LAPSTDDGYIDLQFK	6.75	76	24	known	1.5857	0.66508

4.3.3.2 Identified phosphoproteins which are not regulated by NO

Most of the identified phosphorylation sites did not reach level of significance upon iNOS derived NO release. These unaffected cardiac phosphopeptides are listed in Table 4.4.

Table 4.4. List of identified phosphopeptides. Relative quantification showed no or small changes upon iNOS derived NO activation. Orange color shows that protein was also found with significantly enhanced phosphorylation at a further phosphorylation site, blue with decreased phosphorylation and green shows both enhanced and decreased phosphorylated proteins. (XIC_L: integrated peak area of light (did not treated with L-arg) peptide, XIC_H: integrated peak area of heavy (with L-arg treated) peptide, PTM score: indicating post translational modification counted by MSQuant, Mascot score: indicating validity of peptide identification). XIC_H/XIC_L values represent means \pm S.D.

Symbol	Protein	PTM max	Mas cot max	Phos. site	N/K	XIC _H /XIC _L	log ₂ (XIC _H /XIC _L)
	Peptide						
Cardiac contractile proteins							
Dnm1l	Isoform 4 of Dynamin-1-like protein						
	SKPIPIMPApSPQK	7.53	47	492	known	0.81685	-0.29185
Dync1i2	Dynein cytoplasmic 1 intermediate chain 2						
	SVSpTPSEAGSQDSGDGAV GSR	85.14	82	95	known	0.98892 +/- 0.07049	-0.016068
	EDEEEEDDVApTPKPPVEPEE EK	131.14	59	174	novel	1.1408 +/- 0.055897	0.19003
	KPASVSPTTPTpSPTEGEAS	100.63	81	516	novel	0.90482 +/- 0.14056	-0.1443
Kif13b	kinesin family member 13B						
	APLLSEPASAVPpTSPFR	85.78	69	1653	novel	1.0305	0.043314
Mybpc3	myosin binding protein C, cardiac						
	RDpSKLEAPAEEDVWEILR	133.53	54	315	known	0.78339	-0.3522
	TpSDSHEDAGTLDFSSLLK	112.18	99	290	known	1.0662 +/- 0.048612	0.092507
	RTSDSHEDAGpTLDFSSLLK	11.26	67	298	novel	1.0814 +/- 0.084463	0.11287
Myh1	Myosin-1						
	pSELQAALAEAEASLEHEEG K	7.02	49	1545	novel	0.93293	-0.10015
Myh10	Myosin, heavy polypeptide 10, non-muscle						
	QLHIEGASLElpSDDDTESK	92.94	66	1987	known	1.0483	0.068095
Myh11	Myh11 protein						
	VIENTDGpSEEEEMoxDAR	194.4	109	1954	known	0.88363 +/- 0.16289	-0.17848
Myh6	Myosin-6						
	QAEEAEEQANTNLpSK	223.17	95	1896	novel	0.74088 +/- 0.086676	-0.43268
	LELQpSALEAEASLEHEEGK	173.79	121	1552	novel	0.76952 +/- 0.13336	-0.37796
	ADIAEpSQVNK	234.83	85	1917	known	0.81337 +/- 0.12838	-0.29801
	LAEQELIETpSER	168.54	55	1712	known	0.89089	-0.16669
	LQpTENGELAR	41.99	62	1284	novel	0.90351	-0.14639
	ALQEAHQALDDLQAEEDKVNpTLTK	163	72	1021	novel	0.92023	-0.11994
	VQLLHSQNpTSLINQK	8.11	84	1723	novel	0.92055	-0.11943
	LEDEEEMoxNAELpTAK	6.35	80	939	novel	0.93826	-0.091939
	ANpSEVAQWR	60.35	78	1368	novel	0.95416	-0.067694
	pSLSTELFK	175.58	62	1480	novel	0.97324 +/- 0.095001	-0.039138
	LEQQVDDLEGpSLEQEK	206.44	110	1039	known	1.1139 +/- 0.06962	0.15559
Myh9	15 days pregnant adult female amnion cDNA, RIKEN full-length enriched library, clone:M421002E03 product:myosin heavy chain IX, f... <Preview trun						
	KGTGDCpSDEEVDGK	168.61	43	1942	known	0.98729 +/- 0.12887	-0.018454

Myl2	Myosin regulatory light chain 2, ventricular/cardiac muscle isoform						
	RIEGGpSSNVFSMFEQTQIQ EFK	11.4	94	14	novel	0.89008 +/- 0.050413	-0.168
	IEGGSpSNVFSMoxFEQTQIQ QEFK	187.13	151	15	known	0.98687 +/- 0.13761	-0.019065
Myl7	Myosin regulatory light chain 2, atrial isoform						
	AAApTKQAQRGpSSNVFpS MoxFEQAQIQEFK	11.13	66	15, 22, 27	novel, known, novel	0.92269	-0.11609
Myo18b	myosin XVIIIb						
	ASpSDEGDLSLK	127.51	83	2303	novel	0.92743 +/- 0.15067	-0.10869
Tpm1	Isoform 1 of Tropomyosin alpha-1 chain						
	ATDAEADVApSLNR	208.53	113	87	known	0.96195 +/- 0.088106	-0.055968
	LVIIpSLER	102.85	44	174	known	1.0297 +/- 0.11032	0.042258
	AISEELDHALNDMoxpTSI	102.78	82	282	known	1.047 +/- 0.13976	0.066245
Sarcomeric proteins							
Cryab	Alpha-crystallin B chain						
	APpSWIDTGLSEMR	102.99	82	59	known	1.115 +/- 0.20871	0.15703
Hspbl	Isoform A of Heat shock protein beta-1						
	SPpSWEpFR	97.7	48	15	known	0.86481 +/- 0.12355	-0.20955
Jph2	Junctophilin-2						
	ETPQPEGGPpSPAGpTPPQ PK	116.6	40	479, 483	known	1.1 +/- 0.041786	0.13751
	RSDSAPPSPVpSApTVPEEEPP APR	19.9	40	600, 602	novel	1.2621 +/- 0.031094	0.33583
Ldb3	LIM domain binding 3 isoform c						
	VVANpSPANADYQER	164.4	51	112	novel	1.008	0.011462
Myom2	M-protein						
	RVpSASEEEEEVENENR	194.4	85	76	known	0.83051 +/- 0.09989	-0.26793
	LCAKRVPpSApSEEEEEVENEN R	24.09	48	76	known	0.87866	-0.18663
	VSApSEEEEEVENENR	182.59	70	78	novel	1.0957 +/- 0.0066003	0.13191
Myoz2	Myozenin-2						
	pSPNPENIAPGYSGPLK	62.16	51	116	novel	0.92504	-0.11242
	VDGSNLEGGSSQGPpTPP NTDPDR	46.29	75	107	known	1.1002 +/- 0.060933	0.13772
Pgm5	Phosphoglucomutase-like protein 5						
	AAGGIILTApSHCPGGPGGE FGVK	252.59	84	122	known	0.81915 +/- 0.029813	-0.28781
Smpx	Small muscular protein						
	ESpTPETEEGAPTTSEEK	85.78	81	37	novel	0.96046 +/- 0.0010218	-0.058198
	KEpSTPETEEGAPTTSEEK	10.61	43	36	novel	1.0563 +/- 0.09126	0.078986
Smtn	Adult male tongue cDNA, RIKEN full-length enriched library, clone:2310020N01 product:smoothelin, full insert sequence						
	STpSFGVpNANSIK	118.95	64	323	known	1.0388 +/- 0.040868	0.054895
	RSpSLMoxEPDPAEPSTTVE AANGAEQAR	29.03	44	142	novel	1.0643	0.0899
Actin binding proteins							
Ablim1	49 kDa protein						
	TLpSPTPSAEGYQDVR	87.07	58	475	known	0.92355	-0.11473
	QSLGEpSPR	67.76	46	470	known	1.2431	0.31395
Cap2	Adenylyl cyclase-associated protein 2						
	THTPSPpTSPK	61.7	48	310	novel	0.89694	-0.15692

Ctnna1	Catenin alpha-1						
	TPEELDDSDFEpTEDFDVR	66.94	75	641	known	1.2397 +/- 0.11258	0.30996
Epb4.112	Protein 4.1G						
	pSSHETLNVVEEK	6.05	44	595	novel	1.3394	0.42157
Fhod3	Isoform 1 of FH1/FH2 domain-containing protein 3						
	GAIpSPDVESQDK	180.45	69	921	novel	0.88766 +/- 0.15486	-0.17192
	GAIpSPDVESQDKVPDTPPAQLK	160.24	62	889	novel	0.95351 +/- 0.050329	-0.068681
	GAEpSQEEPVLLEPEER	260.41	50	751	novel	1.1595 +/- 0.088612	0.21352
Lmod2	Leiomodin-2						
	SLTEKpTPTGNFSR	11.36	50	59	novel	0.78948	-0.34103
	YEpSIDEELLASLSPEELK	158.88	75	15	novel	0.94255	-0.085364
Marcks	Myristoylated alanine-rich C-kinase substrate						
	AEDGAAPSPSSEpTPK	139.99	76	143	known	0.85267 +/- 0.1086	-0.22994
	AEDGAAPSPSSEpTPKK	7.31	83	143	known	1.0346	0.049046
Myo18a	Isoform 6 of Myosin-XVIIIa						
	LEGDPsDVDpSELEDR	126.39	63	1978, 1982	known	0.95071	-0.072922
Mypn	myopalladin						
	TPVDESDEIEHDEIPpTGK	75.56	81	991	novel	0.90427 +/- 0.076118	-0.14518
Nebi	116 kDa protein						
	pSHSGSTFGTGLGDDK	109.14	71	887	novel	0.81761 +/- 0.14005	-0.29051
	GFpTPVVDDPVTTER	129.17	45	800	novel	0.91281	-0.13161
	AMoxYDYSAQDEDEVpSFR	108.53	75	976	novel	0.93441 +/- 0.035739	-0.097865
Nexn	Nexilin						
	EMoxLApSDDEEESSPK	289.5	100	16	known	0.77259 +/- 0.17788	-0.37223
	NTpSVVDSEPVR	51.59	49	523	novel	0.88015 +/- 0.18477	-0.18418
	KREDEEEEGpSIVNGSTTEDEEQTR	116.03	86	495	novel	1.0354 +/- 0.17051	0.050212
Nrap	Isoform 2 of Nebulin-related-anchoring protein						
	GMoxApSPVGAEGGMoxTK	7.92	60	273	novel	0.76022 +/- 0.075253	-0.39552
Palld	Isoform 6 of Palladin						
	SRDPsGDENEPIQER	51.59	53	1129	known	0.86097 +/- 0.1367	-0.21596
	IApSDEEIQGTK	154.58	68	901	known	0.92724 +/- 0.077787	-0.10898
Phactr4	Isoform 3 of Phosphatase and actin regulator 4						
	SSpSPVLVEEEPER	99.9	55	128	known	1.0626	0.087558
Spnb2	Isoform 1 of Spectrin beta chain, brain 1						
	ESpSPVPpSPTLDR	31.65	43	2164, 2168	known	0.86094	-0.21601
Synpo	Isoform 1 of Synaptopodin						
	AApSPAKPSSLDLVPNLPR	159.74	68	833	known	0.90574 +/- 0.045567	-0.14283
	DRApSPAAAEAVPEWASCLK	85.7	64	672	known	0.91594	-0.12667
Synpo2	130 kDa protein						
	GCVApSPVEGGR	154.48	54	300	novel	0.99893 +/- 0.14524	-0.0015402
	AQpSPTPSLPASWK	89.11	52	895	known	1.0558 +/- 0.086096	0.078288
Tln2	taln 2						
	LDEGpTPPEPK	44.33	51	1844	known	0.73943 +/- 0.055551	-0.43551
Tnks1bp1	182 kDa tankyrase 1-binding protein						
	MoxQAESQpSPTNVDLEDK	9.82	50	1063	novel	0.89823	-0.15484
	MoxQAESQpSPTNVDLEDKER	40.88	56	1063	novel	0.92729 +/- 0.013496	-0.10891
	pSAEEGEVTESK	82.58	63	1657	known	1.2921	0.36969
	RASVSpTNQDTEENDQELGMoxK	7.78	59	890	known	1.4021 +/- 0.29435	0.48763

Tns1	tensin 1						
	AVNPTMAAPGpSPSLSHR	113.38	49	1363	novel	0.88272 +/- 0.045719	-0.17997
	AASDGQYENQpSPEATSPR	109.31	83	1062	known	0.93855 +/- 0.00057711	-0.091491
	TVGTNTPPpSPGFGR	129.17	52	1346	known	0.95118 +/- 0.11842	-0.072211
	SQpSFPDVEPQLPQAPTR	57.62	94	792	known	0.96292 +/- 0.089012	-0.054519
	QVMGPGSGPGFHGNVVS GH						
	PASAApTTPGSPSLGR	24.05	40	1393	novel	0.99682	-0.0045956
	HLGGSGSVVPGpSPSLDR	63.47	60	1468	known	1.1149 +/- 0.30778	0.15695
	NGTPGGSFVSPSPLSTpSSPIL						
Vcl	SADSTSVGSFSPSVSSDQGP						
	R	97.01	58	1234	novel	1.178	0.23631
	ETTS DPpSRTPEEEPLNLEGL						
	VAHR	64.83	47	1013	known	1.3652	0.4491
	Vinculin						
Vcl	DPNAPSPGDAGEQAIR	196.63	76	290	known	0.79989 +/- 0.027011	-0.32213
	pSLLDASEEAIKK	9.63	64	726	known	0.96638 +/- 0.10134	-0.049342
	GQGApSPVAMoxQK	148.55	45	346	novel	0.98537 +/- 0.32434	-0.021256
	pSLLDASEEAIK	116.6	77	721	known	1.0901 +/- 0.11092	0.12452
Actin filament turnover modulator							
Pdlim4	PDZ and LIM domain 4						
	RSpSVSGISLEDNR	50.4	68	119	known	0.74979 +/- 0.20618	-0.41544
Rcsd1	Isoform 2 of Capz-interacting protein						
	pSPDANMoxPEEEGVVR	142.38	66	303	novel	1.069	0.096249
	NpTCNSTEKPEELVRTPEEA						
Rras2	NAGEK	6.76	48	243	novel	1.2132	0.27885
	Ras-related protein R-Ras2						
Rras2	FQE QECPPpSPEPTR	112.86	55	186	known	0.92798 +/- 0.17334	-0.10784
Calcium homeostasis							
Ahnak	AHNAK nucleoprotein isoform 1						
	VQANLDPpTDINIEGPEAK	97.8	47	4950	novel	0.73253	-0.44904
	GHYEVpTGSDDEAGK	284.32	95	5607	known	0.80989 +/- 0.078089	-0.3042
	GGVTGSPEASISGpSKGDLK	158.45	81	5512	known	0.85019 +/- 0.097759	-0.23414
	GGVTGpSPEASISGSK	159.59	93	5504	known	0.8832 +/- 0.15543	-0.17918
	GDLGApSSPSMoxK	70.62	53	5098	novel	0.91729 +/- 0.19058	-0.12455
	AEpSPEMEVNLPK	188.48	64	893	novel	0.91762 +/- 0.03591	-0.12403
	EFSAPSpTPTGTLEFAGGDA						
	K	149.95	66	5567	known	0.96984 +/- 0.11196	-0.044182
	LRpSEDGVEGDLGETQSR	65.97	47	136	known	0.97533 +/- 0.15343	-0.036031
	ASLGpSLEGEVEAEApSSPK	216.54	108	5525	known	0.97766 +/- 0.10009	-0.032596
	LPSGSGPpSPTTGSAVDIR	64.77	84	217	known	0.98814 +/- 0.074366	-0.017206
	SSEVVLpSGDDEDYQR	130.59	55	116	novel	1.4114	0.49708
Atp2a2	Isoform SERCA2A of Sarcoplasmic/endoplasmic reticulum calcium ATPase 2						
	EFDELSPpSAQR	162.62	58	663	known	1.1181 +/- 0.10748	0.16111
Atp2b1	plasma membrane calcium ATPase 1						
	IEDSEPHIPLIDDTDAEDDAP						
Cacna1c	pTK	9.04	56	1173	novel	0.90147	-0.14964
	Isoform 2 of Voltage-dependent L-type calcium channel subunit alpha-1C						
Canx	AlpSGDLTAEEELDK	200.46	92	1659	novel	1.0645 +/- 0.13424	0.090108
	Calnexin						
Dnajc5	AEDEILNRpSPR	126.5	49	582	known	1.2762 +/- 0.083811	0.35183
	DnaJ homolog subfamily C member 5						
Dnajc5	SLpSTSGESLYHVLGLDK	174.32	58	10	known	1.2699	0.34472

Hrc	histidine rich calcium binding protein						
	EHDNEDLGDPsAENHLPR	101.96	45	129	novel	1.0424	0.059894
	EVGEENVpSEEVFR	210.56	69	104	known	1.095 +/- 0.21697	0.13095
	QAHpSEEEKEEEEEEEEEEE K	92.94	46	542	novel	1.1188	0.16191
	GDDEDlpSTEFCHK	208.09	81	474	novel	1.2948 +/- 0.11854	0.37276
Pln	Cardiac phospholamban						
	RApSpTIEMPQQAR	123.02	45	16	known	1.1967 +/- 0.27281	0.25901
Ryr2	ryanodine receptor 2, cardiac						
	RlpSQpTpSQVSIDAAHGYS R	42.54	55	2807, 2809, 2810	known, novel, novel	1.3974	0.48275
Srl	Isoform I of Sarcalumenin						
	AEVDTEpSGEKVEDQGEPR	187.7	78	304	known	1.2996 +/- 0.053886	0.37808
Strn	Striatin						
	FLESAAADFpSDEDEDED DGR	179.88	98	245	known	1.1649 +/- 0.043652	0.22018
Calcium binding protein							
Itsn1	195 kDa protein						
	LPEEPsPSEDEQQPEK	120.29	80	335	known	0.82342 +/- 0.08732	-0.28029
	SAFTPATATGSSPpSPVLGQ GEK	119.89	85	897	known	0.82866	-0.27116
D6Wsu1 16e	Isoform I of Protein FAM21						
	VpSPEVGSADVASIAQK	75.45	71	747	known	1.1893	0.25016
Vcan	Isoform VI of Versican core protein						
	LESHGSpSEESLQVQEK	84.24	55	1626	novel	1.2742 +/- 0.25484	0.34956
Zinc ion binding							
Mical1	Isoform I of MICAL-like protein 1						
	DPAPPSPTSTSPAVQPGEEA QGDDLpSPDSLSEQK	17.45	57	148	novel	0.91491	-0.1283
Morc2a	MORC family CW-type zinc finger protein 2A						
	SLAVpSDEEEAEEAEK	257.16	97	741	known	1.166	0.22156
Trim47	Isoform 2 of Tripartite motif-containing protein 47						
	GLGpSNEDGLQK	5.65	69	393	novel	0.88466	-0.17681
Removal of superoxide radicals & relaxation of vascular smooth muscle & regulation of blood pressure							
Sod1	Superoxide dismutase [Cu-Zn]						
	DGVANVpSIEDR	88.98	54	99	known	0.76548 +/- 0.092977	-0.38556
Electron transport chain							
Txndc1	Thioredoxin domain-containing protein 1 precursor						
	VEEEQEADEEDVpSEEEAED REGASK	109.31	108	245	known	0.92751	-0.10856
	KVEEEQEADEEDVpSEEEAE DR	179.89	99	245	known	1.0144 +/- 0.090342	0.020624
	VEEEQEADEEDVpSEEEAED R	226.45	86	245	known	1.1296 +/- 0.12805	0.1758
Microtubule associated protein							
Arhgef2	Isoform 5 of Rho guanine nucleotide exchange factor 2						
	EAQELGpSPEDR	78.77	67	902	known	1.2849 +/- 0.16877	0.36162
Eml1	Isoform 3 of Echinoderm microtubule-associated protein-like 1						
	EPAFSPALQpSPKPQK	101.78	43	185	novel	0.90313	-0.14699

Mapt	Isoform Tau-D of Microtubule-associated protein tau						
	SGYSSPGSPGpTPGSR	57.64	49	136	known	0.73633	-0.44157
	SPVVSgDpTSPR	104.65	62	303	known	1.0662 +/- 0.20905	0.092419
Mtap1a	Microtubule-associated protein 1A						
	EEpSEPEVKEDVIEK	6.45	51	882	known	0.85127 +/- 0.046385	-0.23231
	AELEEMoxEEVHPpSDEEEEE TK	132.5	49	905	known	0.95631 +/- 0.094156	-0.064457
Mtap1b	Microtubule-associated protein 1B						
	LGGDVpSPTQIDVSQFGSFK	165.76	145	1497	known	0.80087 +/- 0.064195	-0.32036
	SVSPGVpTQAVVEHCASPE EK	10.61	51	1297	known	0.89416	-0.1614
	GEAEQpSEEEGEEEDKAED R	228.51	100	1013	known	0.9012 +/- 0.050762	-0.15008
	EpSVVSGDDRAEEDMoxDD VLEK	5.99	40	989	known	1.0704	0.098087
	QGVDDIEKFEDGAGFEpS SETGDYEEK	7.45	45	933	known	1.0714	0.09947
	EEQpSPVKA EVAEK	79.97	47	614	known	1.1576 +/- 0.068953	0.21113
	FEDEGAGFEESpSETGDYEE K	131.94	77	933	known	1.3888 +/- 0.13523	0.47382
Mtap4	Isoform I of Microtubule-associated protein 4						
	NpTTPTGAAPPAGMoxTST R	53.11	49	846	novel	0.74769 +/- 0.028261	-0.41948
	GQSTVPPCpTASPEPVK	70.71	46	596	novel	0.80621 +/- 0.042073	-0.31077
	ALETMAEQTTDVVHpSPST DTTPGPDTEALAK	125.2	60	254	known	0.83336 +/- 0.0025179	-0.263
	DMoxpSPSAETEAPLAK	127.77	79	517	known	0.8683 +/- 0.10787	-0.20374
	LApTTVSAPDLK	7.35	58	898	known	0.87852 +/- 0.21274	-0.18686
	ATpSPSTLVSTGPSSR	57.64	75	785	known	0.89747 +/- 0.024036	-0.15606
	DMoxpSPLPESEVTLGK	131.14	56	475	known	0.92917 +/- 0.1226	-0.10598
	VGpSLDNVGHLPAGGAVK	141.19	58	1008	known	0.97927 +/- 0.098573	-0.030225
	DVTLPLEAERPLVTDMpTPSL ETEMTLGK	77.08	52	447	novel	1.1737	0.23108
Microtubule plus-end tracking protein							
Clasp2	CLIP-associating protein CLASP2 isoform b						
	SRpSDIDVNAAAGAK	137.02	77	376	known	1.1093 +/- 0.14282	0.14962
Clip1	148 kDa protein						
	TASEpSISNLSEAGSVK	216.69	84	194	known	0.90102 +/- 0.049062	-0.15037
Connect cytoskeletal structures to the plasma membrane							
Msn	Moesin						
	QRIDEFEpSMox	126.3	48	576	known	1.1471 +/- 0.037248	0.19805
Recycling or degradation of cell surface receptors							
Chmp2b	Charged multivesicular body protein 2b						
	ATIpSDEEIER	93.44	80	199	known	0.82095 +/- 0.035973	-0.28464
Regulation of cell shape							
Palmd	Adult male diencephalon cDNA, RIKEN full-length enriched library, clone:9330200H01 product:palmdelphin, full insert sequence						
	SGPQCSpSPTCQEETEDVR	145.42	63	385	known	0.77926 +/- 0.040651	-0.35981
	VIpSPGPNFQER	80.08	58	278	known	1.1021	0.14031

Receptor							
Igfr	Cation-independent mannose-6-phosphate receptor precursor						
	LVSFHDDpSDEDLLHI	188.7	105	2476	known	1.1727 +/- 0.036192	0.22989
	AEALSSLHGDDQDpSEDEV LTVPEVK	130.63	57	2401	known	1.3305	0.41195
Pgrmc1	Membrane-associated progesterone receptor component 1						
	EGEPTVYSDDEEPKDEpTAR	90.11	65	181	novel	0.83784 +/- 0.1591	-0.25526
Pgrmc2	Membrane-associated progesterone receptor component 2						
	LLKPGEEPSEYpTDEEDTK	142.84	50	205	known	1.0039 +/- 0.050669	0.0055619
Sort1	Isoform 1 of Sortilin precursor						
	SGYHDDpSDEDLLE	16.45	43	819	known	1.1076	0.14747
Intercellular junction							
Dsp	desmoplakin isoform 2						
	AEPSPDLR	36.16	52	22	known	0.80687	-0.3096
Tight junction							
Cxadr	Isoform 1 of Coxsackievirus and adenovirus receptor homolog						
	APQpSPTLAPAK	71.69	54	332	known	0.87434 +/- 0.15904	-0.19373
Mtdh	Protein LYRIC						
	NpSQPVKpTLPPAISAEPSITLSK	30.04	57	503, 508	novel, known	1.0944	0.13015
Adherens junction							
Milt4	Isoform 1 of Afadin						
	SSPNVANQPPpSPGGK	181.59	74	1167	known	0.79977 +/- 0.032499	-0.32235
Sorbs1	Isoform 1 of Sorbin and SH3 domain-containing protein 1						
	ESDGpTPGGLASLENER	69.17	74	435	novel	0.95367 +/- 0.086678	-0.068436
	DlpSPEIDLK	155.62	41	336	known	0.98149 +/- 0.084906	-0.026956
Tjp1	Tight junction protein ZO-1						
	AVPVpSPSAVEEDEDEDGHTVVATAR	62.06	53	1614	known	1.0708	0.098727
Xirp1	xin actin-binding repeat containing 1						
	GlPSLEEALPDVSATR	106.9	51	295	novel	1.1455	0.19593
Vesicle protein							
Ehbp111	tangerin isoform a						
	GQGSEPAITGGQVGPETP EPPpSPPETR	24.82	57	284	known	1.021	0.030015
	13 days embryo forelimb cDNA, RIKEN full-length enriched library, clone:5930429A15 product:EH DOMAIN-CONTAINING PROTEIN-2 homolo						
Ehd2	GPDEAIEDGEEGpSEDDAE WVVTK	240.94	86	438	known	1.199 +/- 0.17782	0.26187
	Isoform 2 of Epsin-1						
Epn1	TALPTSGpSSTGELELLAGEV PAR	66.06	65	419	novel	1.2297	0.29836
	Epsin-3						
Epn3	GDDpSPVANGAEPAGQR	99.44	51	257	novel	0.85157 +/- 0.033438	-0.2318
	TPVLPSGPPIADPWAPSpSPT R	58.27	54	387	novel	0.88585	-0.17486
Eps1511	epidermal growth factor receptor pathway substrate 15, related isoform a						
	pSTPSHGSVSSLNSTGSLSPK	10.34	57	238	known	1.0771 +/- 0.022076	0.10709

Sec3 Ia	SEC3I-like I						
	DSDQVAQpSDGEESPAEE QLLGER	167.05	67	620	known	1.0318 +/- 0.071255	0.045182
Syt2	Synaptotagmin-2						
	GGQDDDDAETGLpTEGEG EGEEKEPENLGK	71.99	55	128	known	1.166 +/- 0.010353	0.22159
Txlna	Isoform I of Alpha-taxilin						
	EQGVESPGAQPApSSPR	93.83	74	522	known	0.88367 +/- 0.051694	-0.17842
Txlnb	Beta-taxilin						
	TSEEEPEPSVpSENEEVDAEE ANSFQK	202.81	83	486	novel	1.1715 +/- 0.039464	0.22834
Uso I	Isoform 4 of General vesicular transport factor p115						
	DLGHPVEEEDepSGDQEDD DDEIDDGDKDQDI	58.9	44	334	known	0.96746 +/- 0.0018938	-0.047733
Vamp4	Vesicle-associated membrane protein 4						
	NLLEDDpSDEEEDFFLR	124.46	57	30	known	1.031 +/- 0.050255	0.04411
Chaperone							
Hsp90aa I	Heat shock protein HSP 90-alpha						
	EpSDDKPEIEDVGSDEEEEEK K	188.82	68	263	known	0.87931 +/- 0.12868	-0.18555
	ESDDKPEIEDVGpSDEEEEEK	190.18	85	263	known	0.96576 +/- 0.13045	-0.050257
	EVpSDDEAEEKEEK	257.57	56	231	known	1.0856 +/- 0.056636	0.11845
	DKEVpSDDEAEEK	154.48	44	231	known	1.2786 +/- 0.10735	0.35456
Hsp90ab I	Putative uncharacterized protein						
	EKEIpSDDEAEEEEK	0		225	known	0.72199 +/- 0.12572	-0.46995
	IEDVGpSDEEDDSGKDKK	127.12	71	255	known	0.78414 +/- 0.21449	-0.35081
	IEDVGpSDEEDDSGKDK	242.52	76	255	known	0.80002 +/- 0.13784	-0.32189
	IEDVGpSDEEDDSGK	220.93	107	255	known	0.81297 +/- 0.17149	-0.29873
	ElpSDDEAEEEEK	196.45	65	225	known	0.86077 +/- 0.03438	-0.2163
	PKIEDVGpSDEEDDSGK	0		255	known	0.89713	-0.15662
Nap114	Bone marrow stroma cell CRL-2028 SR-4987 cDNA, RIKEN full-length enriched library, clone:G430136P17 product:nucleosome assembly ... <Preview truncated at 128 charac						
	EFITGDVEPTDAESAWhpSE NEEEDKLAGDMK	160.81	94	125	known	0.94856 +/- 0.013652	-0.076196
Sgta	Isoform I of Small glutamine-rich tetratricopeptide repeat-containing protein alpha						
	APDRTPPpSEEDSAEAER	29.26	40	85	known	0.74758 +/- 0.045435	-0.41971
Metabolism							
Acot5	Acyl-coenzyme A thioesterase 5						
	ADpSHGELDLAR	169.58	59	56	known	0.91877	-0.12223
Aldoa	26 kDa protein						
	LQpSIGTENTEENR	67.78	55	46	known	0.78455 +/- 0.0558	-0.35006
	GILAADESTGpSIK	267.62	97	36	known	0.88025 +/- 0.12489	-0.18401
	LQpSIGTENTEENRR	47.14	44	46	known	0.88298 +/- 0.00086655	-0.17954
	RLQpSIGTENTEENR	69.17	81	46	known	0.93699	-0.093893
	GILAADESTGpSIKAR	130.59	62	46	known	1.1099 +/- 0.061037	0.15045
BC024814	Uncharacterized protein C16orf68 homolog						
	AApSDPNPAEPAR	33.77	60	120	novel	0.9413	-0.08727
Bckdha	branched chain ketoacid dehydrogenase E1, alpha polypeptide						
	IGHHSpTSDDSSAYR	80.25	58	340	known	0.94878 +/- 0.12525	-0.075849
	pSVDEVNYWDK	5.87	43	348	known	1.1023	0.14049

Brp	Isoform 1 of BRCA1-associated protein						
	EQSESVNTAPEpSPSK	171.83	86	116	known	0.93378 +/- 0.017106	-0.098842
Cav2	Caveolin-2						
	ADVQLFMoxADDAYpSHHp SGVDYADPEK	68.01	48	14, 17	known	0.92679 +/- 0.0080251	-0.10969
Ckm	Creatine kinase M-type						
	GQpSIDDmoxIPAQK	177.78	60	372	novel	0.91792 +/- 0.1812	-0.12356
Ckmt2	Creatine kinase, sarcomeric mitochondrial precursor						
	LGyILTCpPSNLGTGLR	124.72	62	319	novel	1.0584	0.081939
Comt	Isoform Membrane-bound of Catechol O-methyltransferase						
		6.8	54	260	novel	0.86194 +/- 0.076458	-0.21434
Cs	Citrate synthase, mitochondrial						
	EGSSIGAIDpSR	103.29	69	232	novel	0.9999 +/- 0.061286	-0.00014475
Ctps	CTP synthase 1						
	SGSSpSPDSEITELK	87.07	56	575	known	0.94 +/- 0.11003	-0.089267
Did	Dihydrolipoyl dehydrogenase						
	IDVSVEAApSGGK	151.01	79	297	novel	0.96669	-0.04888
Gfpt1	Isoform 1 of Glucosamine--fructose-6-phosphate aminotransferase [isomerizing] 1						
	VDpSTTCLFPVEEK	101.96	70	259	known	0.89864 +/- 0.005586	-0.15419
Gpam	Glycerol-3-phosphate acyltransferase, mitochondrial precursor						
	SDEDEDpSDFGEEQR	204.4	75	694	known	1.1553 +/- 0.015841	0.20833
Itpkb	68 kDa protein						
	VLAPCSPpSEER	111.98	42	202	novel	0.80936 +/- 0.0083328	-0.30515
Ldhd	L-lactate dehydrogenase B chain						
	LIAPSVADDEAAVPNNK	220.93	102	11	novel	1.0771	0.1072
Limch1	120 kDa protein						
	TINHQMepSPGER	156.43	53	984	known	0.86104 +/- 0.010923	-0.21585
	DDpSFDLSDFGSR	35.95	52	201	known	0.95045	-0.073311
	pSPEPEATLTFFFLDK	59.76	40	719	known	0.98896 +/- 0.067876	-0.01602
	SHpSTEPNVSSFPNDPSPMox K	97.05	44	471	known	1.1533 +/- 0.036019	0.20578
Lipe	lipase, hormone sensitive isoform 1						
	SVpSEAAALQPEGLGDTL K	140.41	68	602	known	1.2745 +/- 0.073283	0.34998
Pdha1	Pyruvate dehydrogenase E1 component subunit alpha, somatic form, mitochondrial						
	YGMoxGTpSVER	75.25	44	231	known	0.71762 +/- 0.2443	-0.47871
Pgam2	Phosphoglycerate mutase 2						
	HpYGGLTGLNK	4.34	42	92	known	0.83428	-0.26139
Pgm1;Pg m2	Phosphoglucomutase 2						
	AIGGIILTApSHNPGGPNGD FGIK	159.59	82	135	novel	0.81111 +/- 0.063375	-0.30203
Pkm2	Isoform M2 of Pyruvate kinase isozymes M1/M2						
	GSGpTAEVELK	8.88	49	129	novel	1.218 +/- 0.090363	0.28457
Ptges3;E NSMUS G000000 40078;L OCI000 48119	Prostaglandin E synthase 3						
	DWEDDpSDEDMoxSNFDR	175.48	65	113	known	1.2193 +/- 0.11335	0.28604
Serinc1	Serine incorporator 1						
	SDGpSLDDGDGIHR	84.85	48	364	known	0.9781	-0.031945
Sgpp1	Sphingosine-1-phosphate phosphatase 1						
	RNpSLTGEEGELVK	80.41	40	101	known	0.79092	-0.33839

Sucla2	Succinyl-CoA ligase [ADP-forming] subunit beta, mitochondrial INFDpSNSAYR	90.42	52	279	known	0.89445 +/- 0.084147	-0.16093
Ubiquitin conjugating system							
Sqstm1	Isoform 1 of Sequestosome-1 EVDPTGELQSLQMoxPESE GPSSLDpSQEGPTGLK	12.77	77	377	novel	0.73495 +/- 0.060423	-0.44429
Stub1	STIPI homology and U box-containing protein 1 LGpTGGGGSPDKPSAQEL K	11.4	56	15	novel	0.76416	-0.38805
Usp4	Ubiquitin carboxyl-terminal hydrolase EQLSEVEGSGEDDQGDDH SEpSAQK	116.19	78	633	novel	0.78736 +/- 0.057798	-0.3449
Usp5	Ubiquitin carboxyl-terminal hydrolase 5 GTGLQPGEEELPDIAAPLVp TPDEPK	63.77	61	623	known	1.1753 +/- 0.11207	0.23301
Usp10	Ubiquitin carboxyl-terminal hydrolase 10 TCDpSPQNPFVDFISGPVPDS PFPR	34.69	68	208	known	1.0281	0.039922
Protease							
Nrd1	Nardilysin, N-arginine dibasic convertase, NRD convertase 1 LGADEpSEEEGR	156.71	66	85	known	0.8236	-0.27999
Psmc1	26S proteasome non-ATPase regulatory subunit 1 TVGpTPIASVPGSTNTGTVP GSEK	86.22	54	273	known	1.1856	0.24565
Psmc4	Isoform Rpn10A of 26S proteasome non-ATPase regulatory subunit 4 AAAASAAEAGIApTPGTED SDDALK	73.86	55	250	known	0.89587	-0.15864
Usp24	Ubiquitin carboxyl-terminal hydrolase VSDQNpSPVLPK	98.51	51	2044	known	0.73367 +/- 0.068693	-0.44679
Hydrolase							
Dpysl3	Collapsin response mediator protein 4A EPAPEpSPKPAGVEIR	93.74	47	101	novel	1.0517 +/- 0.19867	0.072673
Transferase							
Dlst	Isoform 1 of Dihydrolipoyllysine-residue succinyltransferase component of 2-oxoglutarate dehydrogenase complex, mitochondrial NDVITVQTPAFAPSVTEGD VR	144.08	67	82	novel	1.3577 +/- 0.058081	0.4412
Nmt1	Glycylpeptide N-tetradecanoyltransferase 1 pSGLSPANDTGAK	128.91	69	47	novel	1.1961 +/- 0.23062	0.25836
Nsun2	88 kDa protein EGVILTENAApSPEQPGDE DAK	193.23	93	748	known	1.0504 +/- 0.12385	0.070967
Isomerase							
OTTMU SG00000 014964	1 cell embryo 1 cell cDNA, RIKEN full-length enriched library, clone:10C0028J24 product:Peptidyl- prolyl cis-trans isomerase NIMA... <Preview truncated at 128 characters> SGEEDFESLApSQFSDCSSA KARGDLGAFSR	33.2	55	104	novel	1.0265	0.037796
Ion/metabolite/lipid/protein transport							
Atp1a1	Sodium/potassium-transporting ATPase subunit alpha-1 precursor VDNpSSLTGESEPQTR	30.44	44	216	novel	1.1301	0.17649

Cln1a;LOC100040211;ENSMUSG00000056003	Putative uncharacterized protein						
	EPLpSDEDEEDNDDVEPISEFR	78.02	42	100	known	1.0501 +/- 0.023465	0.070463
ENSMUSG00000056003;LOC100040211;Cln1a	Chloride channel, nucleotide-sensitive, 1A						
	LGEESEKPELpSDEDEEDNDDVEPISEFR	112.66	78	100	known	1.1753 +/- 0.20607	0.23307
Slc12a4	Bone marrow macrophage cDNA, RIKEN full-length enriched library, clone:G530110M10 product:solute carrier family 12, member 4, fu... <Preview tru						
	LEpSLYSDEEEESVAGADK	173.42	80	969	known	1.2353 +/- 0.10842	0.30483
Slc16a1	Monocarboxylate transporter 1						
	SKEpSLQEAGK	8.25	54	213	known	0.85109 +/- 0.22772	-0.23262
	AAQSPQQHSSGDPTEEEpSPV	88.89	55	491	known	1.1027 +/- 0.084722	0.14105
Slc25a13	Calcium-binding mitochondrial carrier protein Aralar2						
	FGLGSIAGAVGApTAVYPIDLVKpTRMoxQNQR	31.59	62	345, 355	novel	0.77157	-0.37413
Slc25a4	ADP/ATP translocase 1						
	YFPpTQALNFAFK	5.86	58	84	known	0.79112	-0.33803
Slc2a4	solute carrier family 2 (facilitated glucose transporter), member 4						
	RpTPSLLEQEVKpSTELEYLGPDEND	117.17	66	488	known	0.91787 +/- 0.015469	-0.12364
	TPSLLEQEVKpSTELEYLGPDEND	25.44	60	499	novel	0.96319 +/- 0.0038125	-0.054104
Atp8a1	ATPase, aminophospholipid transporter (APLT), class I, type 8A, member 1 isoform a						
	TDDVSEKTPSLADQEEVR	76.35	42	29	known	1.0502	0.070605
Osbpl6	Isoform 1 of Oxysterol-binding protein-related protein 6						
	TApSSSTEPSVSR	125.91	49	44	known	1.3689 +/- 0.19066	0.45299
Pitpnc1	Isoform 1 of Cytoplasmic phosphatidylinositol transfer protein 1						
	SAPSpSAPSTPLSTDAPEFLSI PK	129.61	85	274	known	1.1409	0.19014
Mon1a	Isoform 2 of Vacuolar fusion protein MON1 homolog A						
	pSYEDLTELEDR	98.51	57	56	known	1.1479 +/- 0.051414	0.19896
Rab11fip5	RAB11 family interacting protein 5 (class I) isoform 1						
	TYpSDEASQLR	110.44	49	307	known	1.1105 +/- 0.13379	0.1512
Tom1;EG545878	Isoform 1 of Target of Myb protein 1						
	TVFNSETPpSR	132.63	55	176	known	0.8392 +/- 0.10256	-0.25291
Rras2	Ras-related protein R-Ras2						
	FQEQCPEPpSPEPTR	112.86	55	186	known	0.92798 +/- 0.17334	-0.10784
Sec62	Translocation protein SEC62						
	EELEQQpTDGDCDEEDDDKDGEVVK	165.71	73	375	known	1.0053 +/- 0.24444	0.0075548
Guanine nucleotide exchange factor							
Mcf2l	120 kDa protein						
	TSpSTGEEESLAILR	51.7	52	587	novel	0.92056 +/- 0.21555	-0.11942
Small GTPase mediated signal transduction							
Rab12	RAB12, member RAS oncogene family						
	RPAGGSLGAVpSPALSGGQAR	24.41	48	68	known	1.0654	0.09137
Rras2	Ras-related protein R-Ras2						
	FQEQCPEPpSPEPTR	112.86	55	186	known	0.92798 +/- 0.17334	-0.10784

Xabl	XPA-binding protein 1						
	GTLDEEDEEADpSDTDDID HR	109.59	59	338	known	1.0807 +/- 0.10006	0.11193
Guanylyl-nucleotide exchange factor activity							
Rapgef2	166 kDa protein						
	SETpSPVAPR	98.36	57	1022	known	1.1653	0.22072
Rapgef6	Rap guanine nucleotide exchange factor (GEF) 6						
	LADVADADpSEADENEQVS AV	60.88	83	1590	known	1.0557	0.078144
GTPase activator							
Arhgap1	Rho GTPase activating protein 1						
	SSSPEPVpTHLK	14.34	50	96	novel	0.75835	-0.39906
Arhgap2 6	13 days embryo lung cDNA, RIKEN full-length enriched library, clone:D430038K17 product:GRAF PROTEIN homolog						
	pSGDETPGSEAPGDK	7.42	54	41	novel	1.3618 +/- 0.046078	0.44557
Arhgap5	Rho GTPase activating protein 5						
	GGIDNPAITpSDQEVDDKK	66.59	52	1219	known	0.93163 +/- 0.12302	-0.10218
B230339 M05Rik	B230339M05Rik protein						
	SDpSAPPTPVNR	97.17	51	359	known	0.91575 +/- 0.0091466	-0.12697
Cdgap	Cdc42 GTPase-activating protein						
	DDSPSSLGpSPEEQPK	210.63	74	1242	novel	0.919	-0.12187
Ddef2	Isoform 2 of Development and differentiation-enhancing factor 2						
	LLHEDLDEpSDDDVDEK	115.19	54	555	known	0.97798 +/- 0.084692	-0.032128
Dock6	dedicator of cytokinesis 6						
	TGPEDVDDPQHCSGpSPED TPR	71.3	45	178	novel	1.2599	0.33335
Git2	ARF GTPase-activating protein GIT2						
	TVSTQHSTESQDNDQPDY DSVApSDEDTDVETR	106.89	49	396	known	1.1956 +/- 0.17976	0.25771
LOC547 385	similar to StAR-related lipid transfer protein 13						
	DRTpSLNESEATGVR	55.07	54	566	novel	0.93082 +/- 0.089415	-0.10342
Regulation of blood pressure							
Ace	Angiotensin-converting enzyme, somatic isoform precursor						
	GPQFGpSEVELR	144.21	64	1305	known	0.76818 +/- 0.21612	-0.38048
Add1	Isoform 2 of Alpha-adducin						
	GpSEENLDETR	37.78	53	586	known	0.82494	-0.27764
Cast	Isoform 2 of Calpastatin						
	SNDTSQpTPPGETVPR	73.13	78	460	known	0.79634 +/- 0.042181	-0.32855
Platelet derived growth factor binding							
Pdap1	28 kDa heat- and acid-stable phosphoprotein						
	SLDpSDEpSEDEDDDYQQK	11.13	83	60, 63	known	0.7215	-0.47092
Adaptor/scaffold protein							
Akap1	A-kinase anchor protein 1						
	SEpSSGNLPSVADTR	150.43	62	103	known	1.0205 +/- 0.058753	0.029257
Akap12	Isoform 1 of A-kinase anchor protein 12						
	GPSEAPQEAEAEAGATpSD GEK	122.79	99	583	known	0.90279 +/- 0.082385	-0.14754

Akap13	A kinase (PRKA) anchor protein 13						
	DEDEGIPpSENEEEKK	54.09	69	2308	novel	0.79886 +/- 0.16152	-0.32399
Ank1	Isoform Mu7 of Ankyrin-I						
	ELGESEGLpSDDEETISTR	90.55	69	55	novel	0.9482 +/- 0.3855	-0.076743
Ank2	ankyrin 2, brain isoform 2						
	GpSPIVQPEEEASEPK	135.9	63	855	known	0.89739 +/- 0.086507	-0.15619
Ank3	Brain-specific ankyrin-G						
	LSDGEYISDGEEGEDAITGD pTDK	13.03	62	880	novel	0.91157	-0.13358
Ap3d1	AP-3 complex subunit delta-1						
	VDIIPTEEMPENALPSDEDD KDPNDPYR	9.21	48	774	novel	0.87912	-0.18587
App11	DCC-interacting protein 13- alpha						
	VNQSALEAVTPpSPSFQQR	60.88	64	401	known	0.98855 +/- 0.21825	-0.01662
Cd2bp2	CD2 antigen cytoplasmic tail-binding protein 2						
	HSLDpSDEEDDDEEGSSK	165.85	81	49	known	0.85429 +/- 0.011205	-0.22721
D19Ert 721e	SAPK substrate protein 1						
	SpSPPATDPGPVPSSPSQEP TKR	63.19	56	188	novel	0.73721	-0.43985
Fnbp11	formin binding protein 1-like isoform 1						
	EpSPEGSYTDDANQEV	88.99	56	501	known	1.1034	0.14201
G3bp1	9 days embryo whole body cDNA, RIKEN full-length enriched library, clone:D030024B16 product:Ras-GTPase-activating protein SH3-do... <Preview truncated at 128 characters						
	STpSPAPADVAPAQEDLR	200.44	89	231	known	1.0105 +/- 0.073913	0.015003
Kpna3	10 days embryo whole body cDNA, RIKEN full-length enriched library, clone:2610027A11 product:karyopherin (importin) alpha 3, ful... <Preview truncated at						
	NVPQEELEDpSDVDADFK	211.22	91	60	known	1.0215 +/- 0.087315	0.030622
Kpna4	Importin subunit alpha-4						
	NVPQEDICEDpSDIDGDIYR	102.05	70	60	known	1.0375 +/- 0.10832	0.053151
LOC100 041194	similar to KIAA2019 protein						
	DMoxSPpTSTDTEVHR	43.11	48	413	known	0.83267	-0.26418
Mapk8ip 3	Isoform 1a of C-jun-amino-terminal kinase-interacting protein 3						
	TGpSSPTQGIVNK	5.96	63	333	known	0.75578	-0.40397
Pacsin2	Protein kinase C and casein kinase substrate in neurons protein 2						
	TQTYPTDWpSDDSNPF SSTDANGDSNPFDEDTTSG TEVR	76.1	63	399	known	1.2731 +/- 0.11719	0.34829
Pacsin3	Protein kinase C and casein kinase II substrate protein 3						
	DGpTAPPPQSPSPGSGQD EDWSDEESPRK	11.75	66	335	novel	0.87195	-0.19769
Ranbp3	Ran-binding protein 3						
	SPpSESAEETHLEEK	137.24	62	148	known	0.80699 +/- 0.030982	-0.30938
Raph1	similar to RAPH1 protein						
	TApSAGTVSDAEAR	136.6	90	192	novel	0.86496 +/- 0.20905	-0.20929
Slc9a3r1	Isoform 1 of Ezrin-radixin-moesin-binding phosphoprotein 50						
	SAPSSDTSEELNSQDSPK	179.53	90	285	known	0.85949 +/- 0.041456	-0.21845
Spag9	Isoform 1 of C-jun-amino-terminal kinase-interacting protein 4						
	ERPISLGIFPLPAGDGLLP DTQK	59.95	50	217	known	0.86832 +/- 0.055255	-0.20371
Trip10	Isoform 1 of Cdc42-interacting protein 4						
	VPSSSLGpTPDGRPELR	24.09	46	302	known	1.3427	0.42511
Wdr42a	Isoform 2 of WD repeat-containing protein 42A						
	GHGHpSDEEDEEQPR	93.31	44	100	known	0.93633	-0.094912

Protein kinases							
Aak1	Isoform 2 of AP2-associated protein kinase I						
	ILpSDVTHSAVFGVPASK	10.09	97	554	known	0.76981 +/- 0.084784	-0.37742
Bckdk	24 kDa protein						
	STpSATDTHHVELAR	68.67	56	33	known	0.87795 +/- 0.013567	-0.18779
Braf	Isoform 1 of B-Raf proto-oncogene serine/threonine-protein kinase						
	SASEPpSLNR	82.8	46	766	novel	0.78858 +/- 0.087094	-0.34268
Camk2d	calcium/calmodulin-dependent protein kinase II, delta isoform I						
	ESTESSNTpTIEDEDVKAR	79.3	48	371	known	0.77456 +/- 0.042514	-0.36855
	ESTESSNpTIEDEDVK	137.24	71	371	known	1.0629 +/- 0.24108	0.088026
Camk2g	Isoform 1 of Calcium/calmodulin-dependent protein kinase type II gamma chain						
	GpSTESCNTTTEDEDLK	115.13	88	381	known	0.86403 +/- 0.076717	-0.21085
	QEpTVECLR	64.21	46	287	known	0.87353 +/- 0.088096	-0.19507
	GpSTESCNTTTEDEDLKVR	92.94	55	381	known	0.9448 +/- 0.030312	-0.081925
Cdc42bp b	Serine/threonine-protein kinase MRCK beta						
	HSTPSNSSNPSPGPPSPNSP HR	116.14	72	1692	known	0.73162	-0.45083
Gsk3b	Glycogen synthase kinase-3 beta						
	GEPNVSpYICSR	162.16	66	216	known	0.86059 +/- 0.095645	-0.21661
Hspb8	Heat shock protein beta-8						
	pSPPPFPGEWVK	5.7	43	87	known	0.91979	-0.12062
Mapk14	Isoform 3 of Mitogen-activated protein kinase 14						
	HTDDEMoxpTGYVATR	35.95	50	180	known	1.35	0.43293
Mylk3	Isoform 1 of Putative myosin light chain kinase 3						
	DETVGTTDLQQGIDPGAV						
	pSPEPGK	164.34	57	432	novel	1.0601 +/- 0.035367	0.084181
Nek1	Nek1 protein						
	EQPGDEYpSEEEESVLK	98.83	43	1143	known	0.89856	-0.15431
Obscn	Obscurin, cytoskeletal calmodulin and titin-interacting RhoGEF						
	TGEADLSHTSpDDESR	100.63	89	5745	novel	0.88469 +/- 0.055899	-0.17675
Obscn	Isoform 1 of Obscurin						
	LQVPGGDpSDEETK	118.33	51	6503	novel	0.83053 +/- 0.086971	-0.26789
	EPpTLDSISELPEEDSR	115.5	57	5694	novel	1.1595 +/- 0.066612	0.21355
Oxsr1	16 kDa protein						
	TEDGGWEWpSDDEFDEES EEGR	96.77	84	68	known	1.2394 +/- 0.10163	0.30963
Pak2	Serine/threonine-protein kinase PAK 2						
	pSVIDPIAPVGDSNVDSGA K	11.66	56	197	known	0.89603	-0.15838
Pank2	Pantothenate kinase 2						
	ASpSAAPSGSGEAEVR	68.41	67	56	known	0.90144	-0.1497
Pdpk1	61 kDa protein						
	ANpSFVGTAQYVSPPELLTEK	87.27	83	217	known	0.93771	-0.092794
Pi4kb	Phosphatidylinositol 4-kinase beta						
	pTASNPKVENEDPVR	26.54	61	292	known	0.71143	-0.49121
Pkn1	Bone marrow macrophage cDNA, RIKEN full-length enriched library, clone:G530007J07 product:Cardiolipin/protease-activated protein... <Preview tr						
	TDVSNFDEEFTGEAPTLpSP PR	117	132	925	known	0.84014 +/- 0.04655	-0.2513
Pkn2	Isoform 1 of Serine/threonine-protein kinase N2						
	ASpSLGETDESELR	87.07	97	582	known	0.9144	-0.1291
Prkab2	5-AMP-activated protein kinase subunit beta-2						
	IMVGpSTDDPSVFLPDSK	151.18	50	38	known	0.73305 +/- 0.23031	-0.44803
Prkaca	Isoform 2 of cAMP-dependent protein kinase catalytic subunit alpha						
	TWTLCGpTPEYLAPEILSK	123.05	54	190	novel	1.0849 +/- 0.017399	0.11762

Prkar1a	2 days neonate thymus thymic cells cDNA, RIKEN full-length enriched library, clone:C920026H02 product:protein kinase, cAMP depen... <Preview truncated at 128 characters>						
	TDSREDEIpSPPPNPVVK	172.88	45	83	known	1.003 +/- 0.092868	0.0042501
	EDEIpSPPPNPVVK	267.92	91	83	known	1.0391 +/- 0.15656	0.055278
Prkar2a	cAMP-dependent protein kinase type II-alpha regulatory subunit						
	RVSVCAEpTFNPDEEEEDN DPR	205.13	80	96	known	1.0621 +/- 0.014425	0.086875
Prkca	protein kinase C, alpha						
	STLN PQWNEpSFTFK	7.78	54	226	known	0.78463	-0.34991
Raf1	Isoform 1 of RAF proto-oncogene serine/threonine-protein kinase						
	SAPSEPSLHR	37.14	49	621	known	0.87899	-0.18607
Spep	Isoform 1 of Striated muscle-specific serine/threonine protein kinase						
	GTPDPSPAQAAPR	82.58	65	2777	novel	0.87706 +/- 0.16338	-0.18925
	AVGPPAPTPPR	48.37	42	2741	novel	1.0427	0.060263
Stk39	STE20/SPS1-related proline-alanine-rich protein kinase						
	pTEDGDWEWSDDMoxD EK	230.61	82	397	novel	1.3165 +/- 0.33012	0.39674
Ttn	Isoform 1 of Titin						
	AVSPTEpTKPTEK	143.15	56	34488	novel	0.74014 +/- 0.0082241	-0.43413
	IELpSPSMEAPK	7.35	44	2078	known	0.91955 +/- 0.19866	-0.121
	VKSPEVPpTSHPK	5.77	43	34481	novel	0.92175	-0.11755
Protein phosphatases							
Ppp1r1l	protein phosphatase 1, regulatory (inhibitor) subunit 1 l						
	AFGESSpTESDEEEEGCSH K	119.96	59	80	known	0.93374 +/- 0.016939	-0.098901
Ppp1r2	22 kDa protein						
	EQEpSpSGEEDNDLSPEER	22.84	64	123	known	0.93518 +/- 0.17243	-0.096679
Ssh3	Isoform 2 of Protein phosphatase Slingshot homolog 3						
	QASVDDpSREEDKA	6.35	65	647	known	1.3216	0.40228
Cardiac myofibril assembly							
2310039 E09Rik	Isoform 1 of PTRF/SDPR family protein						
	LpSSVTEDEDQDAALTIVTV LDR	130.63	107	19	novel	0.99315	-0.0099236
	VEDDEpSLLLELK	5.59	50	353	novel	1.0733	0.10202
	GGYSPQEGGDPPpTPEPLK	157.55	68	334	novel	1.0868 +/- 0.1595	0.12006
Coronary vessel development							
Bves	Blood vessel epicardial substance						
	GSSSTASLPMoxSpSPQQR	68.41	42	323	novel	1.0695 +/- 0.018293	0.096892
Platelet derived growth factor binding							
Pdap1	28 kDa heat- and acid-stable phosphoprotein						
	SLDPSEpSEDEDDDYQQK	11.13	83	60, 63	known	0.7215	-0.47092
Lipid/protein binding							
Osbp	oxysterol binding protein						
	GDMpSDEDDNEFFDAPEII TMPENLGHK	73.86	51	349	known	0.79042	-0.3393
2310047 M10Rik; 9330160 F10Rik	NOD-derived CD11c +ve dendritic cells cDNA, RIKEN full-length enriched library, clone:F630002E15 product:hypothetical Proline-ri... <Preview truncated at 128 characters>						
	TLpSGEEEEAESVGVSSR	39.99	64	43	novel	0.98067	-0.028159

Fnbp4	formin binding protein 4 TGRDSPENGEP TAIGAEDSEK	9.83	61	539	novel	0.81383 +/- 0.092751	-0.29719
Integral membrane protein							
Armcl10	Isoform 1 of Armadillo repeat-containing protein 10 SAEDLP TDGSYDDILNAEQ LK	9.7	109	48	known	0.94277 +/- 0.05841	-0.08502
Mxra7	Matrix-remodeling-associated protein 7 VAPEEPSEAEPPAAEGR	165.98	65	79	known	0.77557 +/- 0.17329	-0.36668
Nedd4	E3 ubiquitin-protein ligase NEDD4 RQlpSEDVDGPDNR	76.59	45	309	known	0.878 +/- 0.24914	-0.18771
Phospholipid biosynthetic process							
Cds2	Phosphatidate cytidyltransferase 2 LDGETApSDSESR	121.25	61	32	known	1.2154 +/- 0.27403	0.28145
Transporter							
Aqp1	Aquaporin-1 VWTSGQVEEYDL DADDIN pSR	157.2	120	262	known	1.3278	0.40908
Ligand gated channel							
AA407270	Protein GRINL1A EIGVGCDLLPpSPTGR	130.59	60	435	novel	0.96525	-0.051028
Transcriptional regulation							
I810007M14Rik	Isoform A of GC-rich sequence DNA-binding factor homolog EDENDApSDEDDDEKR	100.6	63	316	known	1.1896	0.25044
Atf7ip	Isoform 1 of Activating transcription factor 7-interacting protein 1 SKpSEDMoxDSVESK	38.7	47	593	novel	0.87124	-0.19886
Bclaf1	Isoform 2 of Bcl-2-associated transcription factor 1 ADGDWDDQEVLDFpSD KESAK	164.34	85	381	known	1.0789	0.10955
Cc2d1a	99 kDa protein LANHDEGP SDDEEETPK	7.31	61	390	novel	0.92333	-0.11508
Csrp3	Cysteine and glycine-rich protein 3 GIGFGQGAGCLSTD TGEH LGLQFQQpSPKPAR	103.75	101	95	novel	0.91021 +/- 0.12862	-0.13572
	GIGFGQGAGCLSTD TGEH LGLQFQQpSPK	166.77	110	95	novel	1.0071 +/- 0.25457	0.010219
Ctr9	Isoform 1 of RNA polymerase-associated protein CTR9 homolog GEEGSEEEpTENGPKPK	74.45	73	975	novel	0.7108	-0.49248
Ddx21	Nucleolar RNA helicase 2 EIITEEPSEEEAD MoxPKPK	138.18	70	118	known	1.1448 +/- 0.09575	0.19511
Dek	Protein DEK EEpSEEEEDDEDDDEE DEE EEKEK	218.57	126	33	known	0.78165 +/- 0.091499	-0.35541
Hmgal	Isoform HMG-I of High mobility group protein HMG-I/HMG-Y EEEEGISQEpSSEEEQ	33.03	68	102	known	0.86388	-0.2111
	KLEKEEEEGISQEpSSEEEQ	34.45	63	102	known	0.92848 +/- 0.27993	-0.10706

Htatsf1	Isoform 1 of HIV Tat-specific factor 1 homolog						
	EFEEDpSDEKEEGDDDEEE VVYER	41.49	58	621	known	0.74001	-0.43438
	LFDDpSDEKEDEEDTDGK	176.42	70	679	known	0.77853 +/- 0.078211	-0.36118
	VLDEEGpSER	136.78	72	613	known	0.83088 +/- 0.029035	-0.2673
Irf2bp2	similar to interferon regulatory factor 2 binding protein 2						
	RPASVpSSAAAEHEAR	74.47	49	421	novel	0.83087	-0.26731
Iwsl	Isoform 1 of IVSI homolog						
	IDpSDDDEEKEGDEEK	174.32	67	321	known	1.2133 +/- 0.064338	0.27898
Lmo7	LIM domain only 7						
	STpTELNDPLIEK	63.65	40	1448	known	0.94778	-0.07738
Mbd2	Isoform 1 of Methyl-CpG-binding domain protein 2						
	AADTEEVDIDMoxDpSGDE A	11.36	54	410	known	0.85525	-0.22559
Mecp2	Isoform A of Methyl-CpG-binding protein 2						
	AEpTSESSGSAPAVPEASASP K	61.69	42	78	novel	0.86938 +/- 0.10897	-0.20194
Myt2	Isoform 2 of Histone acetyltransferase MYST2						
	NAGSSSDGpTEDSDFSTDLE HTDSSSEDGTSR	36.09	57	17	novel	0.90797	-0.13929
Naca	Nascent polypeptide-associated complex subunit alpha, muscle-specific form						
	VDPIMSDVTPTpSPKK	59.04	44	822	novel	0.75035 +/- 0.086049	-0.41437
	ADpSPPAVIR	155.24	60	565	novel	0.79666 +/- 0.024087	-0.32796
	DAPTTLAESpSPK	145.8	70	1492	novel	0.82195 +/- 0.10684	-0.28287
	EASVLpSPTATSSGK	132.5	62	1744	novel	0.83563 +/- 0.020765	-0.25907
	EAPATPSVGVIASVGEIpSPSP K	137.23	49	1206	novel	0.87584	-0.19127
	GAPNALAESpAPSPK	219.64	58	1285	novel	0.92727 +/- 0.039828	-0.10894
	VDPIMSDVTPTpTSPK	145.8	67	821	novel	0.93053 +/- 0.072803	-0.10388
	LISAVQpSPK	8.25	59	808	novel	0.96475	-0.051766
	DVpSPSQFPK	130.1	41	929	novel	0.97423 +/- 0.19704	-0.037665
	DSHISPVS DACSTGTTpTPQ ASEK	81.22	44	1769	novel	0.99045 +/- 0.25969	-0.013839
	QIPpTPEDAVTILAGSPLSPK	181.83	101	1163	novel	1.0438 +/- 0.047096	0.061849
	LLAVDSGAAPSDDKGSSAV pTNELCSPPGSSNVAGTSLSPK	118.76	66	350	novel	1.0642	0.089711
	VQGEAVpSNIQENTQTPTV QEESEEEVEDETGVVK	16.14	79	2138	novel	1.079 +/- 0.047717	0.10972
	SVPAVTpSLSPKAPVAPSNE ATIVPTEIPTSLK	79.32	44	849	novel	1.1231	0.16753
	SVpTDPAMoxAPR	65.28	43	590	novel	1.1276	0.17325
	GPVpSPPAR	97.7	41	257	novel	1.1517	0.20377
	GSSAVTNELCpSPPGSSNVA GTSLSPK	180.05	99	355	novel	1.2215 +/- 0.040534	0.28871
	DPApSPVTSLVVPAAHK	128.51	69	442	novel	1.2228 +/- 0.073126	0.29015
	ETPTpTPSPEGVTAAPIEIPIS SK	123.75	102	1398	novel	1.2468 +/- 0.10742	0.31827
Nolc1	nucleolar and coiled-body phosphoprotein 1 isoform A						
	AAKESEEEEEEEpTEEK	258.62	106	562	novel	0.8955 +/- 0.10192	-0.15923
	nucleolar and coiled-body phosphoprotein 1 isoform D						
	EpSEEEEEEEETEEK	141.4	75	562	known	0.89344	-0.16256
Optn	Optineurin						
	LNSGGpSSEDSFVEIR	13.25	58	183	novel	0.9878	-0.017712
Psip1	Isoform 1 of PC4 and SFRS1-interacting protein						
	QSNASpSDVEEEK	121.25	56	106	known	0.83181 +/- 0.16245	-0.26567
	EDTDQEEKApSNEDVTK	174.97	53	129	known	0.94549	-0.080869

Ptrf	Polymerase I and transcript release factor						
	ATEPSGpTGSDLIK	183.32	84	42	known	0.9771 +/- 0.22166	-0.033421
Purb	Transcriptional activator protein Pur-beta						
	RGGGpSGGGDEpSEGEEVD ED	166.32	47	310, 316	known	1.0562 +/- 0.14504	0.078865
Rbl	0 day neonate cerebellum cDNA, RIKEN full-length enriched library, clone:C230007M09 product:retinoblastoma 1, full insert sequen.						
	EDDPAQDpSGPEELPLAR	93.98	75	31	known	1.0774	0.10753
Rdbp	Isoform 1 of Negative elongation factor E						
	SMoxpSAEDDLQEPSR	81.22	57	115	known	0.85822 +/- 0.037123	-0.22058
Rere	Arginine-glutamic acid dipeptide repeats protein						
	ApSPINEDIR	61.59	66	600	known	0.7584 +/- 0.071876	-0.39897
Sdpr	Serum deprivation-response protein						
	DEEALEDpSAEEK	181.19	64	218	known	0.72467 +/- 0.1959	-0.4646
	RGNNsAVGSNADLpTIEED EEEEPVALQQAQQVR	66.15	63	368	known	1.1836 +/- 0.086548	0.24321
Sin3a	Isoform 5 of Paired amphipathic helix protein Sin3a						
	GDLpSDVEEEEEEMoxDVD EATGAPK	11.4	51	833	known	0.75243	-0.41037
Sltm	Isoform 2 of SAFB-like transcription modulator						
	DVQDAIAQpSPEK	7.26	64	271	known	0.96839 +/- 0.055658	-0.046344
Smarcc2	SWI/SNF-related matrix-associated actin-dependent regulator of chromatin c2 isoform 2						
	GGpTMoxTDLDEQDDESM oxETTgKDEDENSTGNK	9.83	45	376	known	1.0985	0.13558
Snip1	Smad nuclear-interacting protein 1						
	KEDEDEEEEEEMoxVpSDS	32.64	48	381	novel	1.2512 +/- 0.042	0.32331
Tcfe2a	Isoform E47 of Transcription factor E2-alpha						
	TSSpTDEVLSLEEK	93.45	71	528	known	1.1266	0.17192
Tcof1	Tcof1 protein						
	KLpSGDLEAGAPK	108.94	61	1143	known	0.78956 +/- 0.35349	-0.34089
Trp53bp1	Isoform 1 of Tumor suppressor p53-binding protein 1						
	SEDRPSPQVSVAAYETK	54.98	44	262	known	0.92105	-0.11865
	TEEDRENTQIDDTEPLpSPV SNSK	117	50	546	known	1.1021 +/- 0.013138	0.14027
Tsc22d3	Isoform 3 of TSC22 domain family protein 3						
	QDpSMoxEPVVR	134.47	59	71	known	0.84688 +/- 0.090126	-0.23978
Yap1	65 kDa Yes-associated protein						
	QASpTDAGTAGALTPQHVR	68.07	123	99	known	0.7576 +/- 0.033282	-0.40049
	QpSSFEIPDDVPLPAGWEMAK	9.94	56	148	known	1.0252	0.035959
Zfp768	Zinc finger protein 768						
	FQEGAEMoxPLpSPEEK	174.32	71	210	novel	1.2211	0.28818
Translation regulation							
I30000101Rik	Activated spleen cDNA, RIKEN full-length enriched library, clone:F830210J11 product:Putative eukaryotic translation initiation f... <Preview truncated at 128						
	AVEDMoxGpSPQTAK	116.6	66	1338	novel	1.0074	0.010572
Aarsd1;1700113122Rik	Alanyl-tRNA synthetase domain containing 1						
	RPPPAMoxDDLDDpSDS	39.89	63	95	novel	1.0538 +/- 0.035533	0.075653
Abcf1	ATP-binding cassette, sub-family F (GCN20), member 1						
	SKPAAADSEGEEDpTAK	226.01	108	194	novel	0.73743 +/- 0.13878	-0.43942

Eef1b2	Elongation factor 1-beta						
	DDDDIDLFGSDDEEEpSEEA KK	111.75	68	106	known	1.0632 +/- 0.0020454	0.088367
	YGPSSVEDTTGpSGAADAK DDDDIDLFGSDDEEESEEA K	101.38	91	106	known	1.0877 +/- 0.17053	0.12127
	DDDDIDLFGpSDDEEESEEA K	276.89	98	106	known	1.1189 +/- 0.19713	0.16211
Eef1d	Eef1d protein						
	VMLPNSPEALGQATPGpTSS GPGASSGPGGDHSELIVR	54.05	50	58	novel	0.75426	-0.40686
	GATPAEDDEDKDIDLFGpS DEEEDK	82.68	64	138	known	0.95797 +/- 0.18203	-0.061952
	GATPAEDDEDKDIDLFGpS DEEEDKEAAR	193.97	130	541	known	1.0058 +/- 0.058027	0.0083783
Eif2b5	Translation initiation factor eIF-2B subunit epsilon						
	AGpSPQLDDIR	142.65	65	540	known	0.86937 +/- 0.12438	-0.20196
Eif3b	Eif3b protein						
	AKPAAQSEETATpSPAAPSP TPQSAER	37.35	75	75, 79	known	0.97257 +/- 0.14365	-0.040132
	GHPSAGAE EEGGpSDGpSA AEAEPR	40.77	54	120, 123	known	0.98092 +/- 0.024968	-0.027797
Eif3c	Eukaryotic translation initiation factor 3 subunit C						
	QPLLLpSEDEEDTKR	147.33	61	39	known	1.0664 +/- 0.20875	0.092742
	QPLLLpSEDEEDTK	192.41	68	39	known	1.1268 +/- 0.027854	0.17222
Eif3g	Eukaryotic translation initiation factor 3 subunit G						
	GIPLPpTGDTSPPELLPGDP LPPPK	126.26	45	42	known	1.0623 +/- 0.061258	0.087253
Eif4ebp1	Eukaryotic translation initiation factor 4E-binding protein 1						
	TPPKDLPAIPGVTSPTSDEPP MQApSQSQLPSSPEDK	17.31	64	93	known	0.93472	-0.097392
Eif4g2	eukaryotic translation initiation factor 4, gamma 2 isoform 1						
	pTQTPPLGQTPQLGLK	8.47	54	505	known	0.87981 +/- 0.11279	-0.18473
Eif4g3	Eukaryotic translation initiation factor 4 gamma, 3						
	AESEpSDGQAEETADPQSL HSGR	69.3	88	472	known	0.81613 +/- 0.039435	-0.29314
Eif5b	eukaryotic translation initiation factor 5B						
	TARPNSEAPLpSGSEDADDS NK	199.91	85	137	known	0.749 +/- 0.060103	-0.41697
	SVPTVDpSGNEDDDSSFK	202.67	54	215	known	0.86058 +/- 0.097727	-0.21662
	TSFDENDpSELEDKDSK	142.85	57	114	known	1.0464 +/- 0.064783	0.06544
LOC100 047194	similar to Eukaryotic translation initiation factor 4 gamma 3						
	EEDAPPVPSPTSCTAASGPSL TDNpSDICK	11.53	55	337	novel	0.87374 +/- 0.029594	-0.19472
	EQTRpTPDEVLEAEAEPK	33.69	49	520	novel	1.0384	0.054383
Pum2	Isoform 3 of Pumilio homolog 2						
	QApSPTEVVER	130.17	58	125	known	0.76544	-0.38564
Rplp2;W dr89	60S acidic ribosomal protein P2						
	KEESEEpSDDDMoxGFLFD	181.59	73	102	known	1.3607 +/- 0.35792	0.44433
Rps3	40S ribosomal protein S3						
	DEILPTpTPISEQK	102.99	57	221	known	1.1674 +/- 0.0061371	0.22326
Cell cycle proteins							
Ccnd2	G1/S-specific cyclin-D2						
	SVEDPDQATpTPTDVR	56.96	58	280	known	0.83787 +/- 0.0047808	-0.2552

Ccny;LO C100044 842	Isoform 1 of Cyclin-Y						
	SAPsADNLILPR	70.19	44	326	known	1.2247	0.29248
Clasp1	CLIP-associating protein 1 isoform 2						
	SRpSDIDVNAAASAK	142.84	71	600	known	0.93552 +/- 0.081175	-0.096157
Dnajc2	DnaJ homolog subfamily C member 2						
	NAPSTSFQLEDK	178.9	72	47	known	1.1256 +/- 0.16657	0.17066
Numa1	Nuclear mitotic apparatus protein 1						
	TQPDGTSVPGEPApSPISQR	70.63	65	1739	known	0.91901 +/- 0.064554	-0.12185
Rsrc2	arginine/serine-rich coiled-coil 2 isoform 1						
	EQSDISlpSPR	113.57	80	32	novel	1.0309 +/- 0.040057	0.043943
Sash1	SAM and SH3 domain-containing protein 1						
	SHpSLDDLQGDADV GK	301.64	94	831	known	1.2596	0.33296
Tacc2	transforming, acidic coiled-coil containing protein 2 isoform c						
	SSDpSEEFETPESTTPVK	143.95	121	1842	known	0.92862 +/- 0.11678	-0.10684
	LDNpTPApSPPRSPTEPSDTP IAK	11	44	2210, 2213	known	0.9992	-0.001157
	GPEGpSPLPR	111.87	52	86	novel	1.1525 +/- 0.1492	0.20482
	ETQQEPGEESPVPSEEHLAP EpTK	81.95	57	2057	novel	1.1902 +/- 0.18088	0.25116
Zzef1	Isoform 2 of Zinc finger ZZ-type and EF-hand domain-containing protein 1						
	GDQEEELDRPVpSSPGAE QK	105.48	42	2406	novel	1.1916	0.25288
Cell growth/development/differentiation							
Cluap1	Clusterin-associated protein 1						
	KPEPLDEpSDNDF	110.44	65	409	known	0.87795	-0.18778
Cobll1	Isoform 3 of Cordon-bleu protein-like 1						
	EQTApSAPATPLVSK	172.1	93	267	known	0.8436 +/- 0.058375	-0.24536
	TLpSSPTGTETNPPK	153.46	92	863	known	0.85242 +/- 0.0053911	-0.23036
	ADDDIIQKPAEpTSPPPVAP K	92.33	55	956	known	0.85499	-0.22602
	ENHLTApSPGPDQK	59.74	63	595	known	1.1484	0.19964
Gap43	Neuromodulin						
	EGDGSATTDAAPApTSPK	94.92	61	95	known	0.85047 +/- 0.03733	-0.23366
Hdgf	Hepatoma-derived growth factor						
	RAGDVLEDpSPK	130.17	44	165	known	0.86536 +/- 0.046582	-0.20863
	AGDVLEDpSPK	208.39	65	165	known	0.87597 +/- 0.034113	-0.19105
	AGDVLEDpSPKRPK	116.07	53	165	known	1.0357 +/- 0.21708	0.050571
	NSTPpSEPDSGQGPPAEEEE GEEEAKEEAQAQGV R	51.4	63	170	known	1.0454 +/- 0.14867	0.064078
Hn1	Hematological and neurological expressed 1 protein						
	SNpSSEASSGDFDLK	188.7	93	87	known	0.99985 +/- 0.12436	-0.00022133
Uhrf1bp1	UHRF1 (ICBP90) binding protein 1						
	DGpSGENLAASQER	100.6	75	929	novel	0.8832	-0.17919
DNA repair							
Oxr1	Isoform 2 of Oxidation resistance protein 1						
	VVpSSTSEEEAFTEK	7.53	71	113	known	1.1811	0.24008
Rad23a	9.5 days embryo parthenogenote cDNA, RIKEN full-length enriched library, clone: B130049A16 product: similar to UV EXCISION REPAIR ... <Preview truncate						
	EDKpSPSEESTTTTSPESISGS VPSSGSSGR	37.1	44	123	known	0.93364	-0.099062

Sod1	Superoxide dismutase [Cu-Zn] DGVANVPsIEDR	88.98	54	99	known	0.76548 +/- 0.092977	-0.38556
Apoptosis							
Akt1s1	Proline-rich AKT1 substrate 1 SSDEENGPPpSSPDLDLR	77.08	59	213	known	0.84662 +/- 0.055273	-0.24022
	EDEEDEDEPTETEpTSGER	23.14	60	116	novel	0.86855	-0.20333
Bag3	BAG family molecular chaperone regulator 3 AAPpSPAPAEPAPK	170.3	60	404	novel	0.87296 +/- 0.008777	-0.19602
	SQpSPAASDCSSSSSASLPSS GR	89.78	66	177	known	0.9071 +/- 0.11052	-0.14066
	SGpTPVHCPSPIR	74.47	64	291	known	0.91826 +/- 0.15245	-0.12302
	VSSAIPCPSPSPAPSAVPpSPP K	189.26	69	390	known	0.92668 +/- 0.016695	-0.10986
	TEAAAApTPQR	82.37	40	132	novel	0.97349	-0.038768
	AApTPPNPSNPADSAGNLV AP	11.93	43	560	novel	1.1923 +/- 0.043771	0.2538
Bat3	NOD-derived CD11c +ve dendritic cells cDNA, RIKEN full-length enriched library, clone:F630021C15 product:HLA-B-associated transc... <Preview truncated at 128 charact						
	ENApSPAPGTTAEEAMoxSR	169.1	98	1030	known	1.0404 +/- 0.2426	0.057131
Bcl2l13	BCL2-like 13 TSPTTPpSVFVELGEELEAVT ARPEAVER	68.78	80	343	known	1.2861 +/- 0.49696	0.36297
Birc6	baculoviral IAP repeat-containing 6 LEGDSDDLLEDpSDSEEHSR	95.78	62	455	known	1.1382 +/- 0.019141	0.18676
Casp7	Caspase-7 VDSpSSEDGVDAKPDR	11.36	53	17	known	1.2057	0.26992
Ccdc6	coiled-coil domain containing 6 QLpSESSSLEMoxDDER	131.14	76	316	known	1.0949 +/- 0.095738	0.13085
Huwl1	HECT, UBA and WWE domain containing 1 GSGTApSDDEFENLR	162.52	64	1907	known	1.0921 +/- 0.1266	0.12713
LOC100042570	similar to E1B 19K/Bcl-2-binding protein homolog NSTLpSEEDYIER	81.16	69	88	novel	1.3149 +/- 0.29185	0.39498
Ndrp2	Isoform 2 of Protein NDRG2 TApSLTSAApSIDGSR	186.87	107	324	known	1.0548 +/- 0.11223	0.076966
	pTLSQSSSGTLPSGPPGHT MEVpSC	44.93	58	339, 361	known, novel	1.2046 +/- 0.10854	0.26853
Pdcd5	22 kDa protein KVMoxDpSDEDDADY	79.97	49	198	known	0.773	-0.37146
Pdcl3	Phosducin-like protein 3 TYEDMoxTLEEELENEDEFpS EEDER	65.41	48	65	novel	1.1776	0.23579
Pea15a	Isoform 1 of Astrocytic phosphoprotein PEA-15 QPpSEEEIHK	139.18	59	116	known	0.73417 +/- 0.010315	-0.44582
Rtn4	Isoform 2 of Reticulon-4 DDSPKEYpTDLEVSNNK	7.31	43	746	known	0.98737	-0.018342
Sept4	M-Septin ESGpTDFPIPAVPPGTDPETE K	36.2	50	335	known	1.1822	0.2415
Sh3kbp1	Isoform 3 of SH3 domain-containing kinase-binding protein 1 ASpSPSLFSTEGKPK	80.25	45	550	known	0.89386 +/- 0.013932	-0.16188
DNA binding							
Chracl	Chromatin accessibility complex protein 1 REEEEDNEDDGpSDLGEAL A	6.97	75	122	known	0.99826 +/- 0.033536	-0.0025175

Hmgn1; LOC100 044391	Non-histone chromosomal protein HMG-14						
	QADVADQQTTTELPAENGE TENQSPApSEEEKEAK	99.84	49	87	known	1.215	0.28093
Pds5b	Isoform 1 of Sister chromatid cohesion protein PDS5 homolog B						
	AESPEpTSAVESTQSTPQK	11.26	69	1367	known	0.83672 +/- 0.086215	-0.25719
Tmpo	thymopoietin isoform epsilon						
	SSpTPLPTVSSSAENTR	136.8	64	163	known	0.9954 +/- 0.26297	-0.0066567
DNA replication							
Dtd1	Isoform 1 of D-tyrosyl-tRNA(Tyr) deacylase 1						
	SASpSGAEGDVSSSEREP	61.58	118	197	known	0.84786 +/- 0.090683	-0.2381
	SASpSGAEGDVSSER	70.01	66	197	known	1.1408	0.19001
Mcm3	DNA replication licensing factor MCM3						
	ASEDESLEDEEEKSQEDpT EQK	11.93	81	685	novel	1.1092	0.14957
RNA binding							
Ascc3l1	Activating signal cointegrator 1 complex subunit 3-like 1						
	EEApSDDDMoxEGDEAVVR	101.78	84	225	known	1.0187 +/- 0.079813	0.02667
Denr	Density-regulated protein						
	LTVENpSPKQETGITEGQGP VGEEEEK	59.04	51	73	known	1.0191	0.027313
EG54495 4	similar to heterogeneous nuclear ribonucleoprotein A1, isoform 2						
	SEpSPKEPEQLR	196.45	58	6	known	0.71294 +/- 0.070191	-0.48814
Fxr1	Isoform C of Fragile X mental retardation syndrome-related protein 1						
	AINGPpTSASGDEIPK	7.76	58	613	novel	0.87166 +/- 0.1185	-0.19816
HnrnpC	Isoform 5 of Heterogeneous nuclear ribonucleoproteins C1/C2						
	MoxESEAGADDpSAEEGDL LDDDDNEDRGDDQLELK	84.93	86	261	known	0.95518 +/- 0.06428	-0.066154
HnrnpH 1	2 days neonate thymus thymic cells cDNA, RIKEN full-length enriched library, clone:E430005G16 product:heterogeneous nuclear ribo... <Preview truncated at 128 charac						
	HTGPNpSPDTANDGFVR	36.27	48	104	known	1.0856	0.1185
HnrnpK	Isoform 1 of Heterogeneous nuclear ribonucleoprotein K						
	DYDDMoxpSPR	84.26	46	284	known	0.82506	-0.27743
Hrb	Isoform 1 of Nucleoporin-like protein RIP						
	GpTPSQpSPVVGR	132.04	52	177, 181	known	0.80468 +/- 0.051655	-0.31351
Larp2	Adult male testis cDNA, RIKEN full-length enriched library, clone:4930423D11 product:hypothetical Arginine-rich region containin... <Preview truncated at 128						
	LDGPTENIpSEDEAQSSSQR	141.57	64	60	known	0.92905 +/- 0.2525	-0.10617
LOC100 046246; Carhsp1	Calcium-regulated heat stable protein 1						
	GNVVPpSPLPTR	69.57	41	42	known	0.91952	-0.12105
Ncl	Nucleolin						
	KEDpSDEDEDEDEDDpSD EDEDEDEDEFEPIVK	10.59	47	145, 157	known	1.0972	0.13389
Nol5	Nucleolar protein 5						
	EEpLpSEEEpCTSTAVPSPEK	112.18	67	509	known	0.90169 +/- 0.19556	-0.1493
Nol5a	Nucleolar protein 5A						
	EEVApSEPEEAASPTTPK EELApSDLEEMoxATSSAK	178.06 220.49	84 98	536 513	known known	0.94883 +/- 0.23595 0.96134 +/- 0.21177	-0.07578 -0.056885
Prkra	Interferon-inducible double stranded RNA-dependent protein kinase activator A						
	EDpSGTFSLGK	82.37	59	18	known	0.74663 +/- 0.25351	-0.42154
Prr8	Isoform 1 of RNA-binding protein 33						
	DIKEEpSDEEDDDDEESGR	58.9	85	243	known	0.81293 +/- 0.019231	-0.2988

Rbm16	Rbm16 protein						
	ASEPVKEPVQTAQpSPAPVE K	95.78	55	617	known	0.89798 +/- 0.11379	-0.15525
Rbm20	similar to hCG2036763						
	GSPEDGSHEApSPLEGK	12.22	59	1052	novel	0.83739 +/- 0.036818	-0.25603
	pSPEFTEAELK	5.65	57	1092	novel	1.1066 +/- 0.12148	0.14607
Rbm25	Rbm25 protein						
	LGASNSPGQPNpSVK	8.11	77	681	known	0.75964 +/- 0.0019999	-0.39661
	QEPEpSEEEEEKQEK	155.41	59	581	known	0.82964 +/- 0.055199	-0.26945
Safb2	Scaffold attachment factor B2						
	APTAALpSPEPQDSK	177.21	77	387	known	0.83727 +/- 0.23565	-0.25624
Zranb2	37 kDa protein						
	EVEDKEpSEGEEDDEDLS K	212.11	88	153	known	0.84202 +/- 0.08686	-0.24807
	YNLDApSEEDSNK	217.32	103	198	known	1.2989	0.37726
mRNA/RNA processing							
Apobec2	Probable C->U-editing enzyme APOBEC-2						
	EEAAEAAAPApSQNGDDLE NLEDPEK	81.85	59	15	novel	0.98921	-0.015645
Dbr1	Lariat debranching enzyme						
	CGEpTVESGDEKDLAK	6.8	59	505	novel	0.91557 +/- 0.017508	-0.12725
Ddx10	Probable ATP-dependent RNA helicase DDX10						
	LASGDGDDEEQDEETDEEp TEDHLGK	107.52	58	587	known	0.87694 +/- 0.051437	-0.18945
Fip111	66 kDa protein						
	DHSPTpSVFNSDEER	67.54	53	491	known	0.96282 +/- 0.0050563	-0.054658
Skiv2l;Skiv19	superkiller viralicidic activity 2-like						
	ApSSLEDLVK	179.98	78	253	known	1.088 +/- 0.33255	0.1217
Splicing							
Prpf3	U4/U6 small nuclear ribonucleoprotein Prp3						
	GDDDEEpSDEEAVKK	141.46	60	619	known	1.3277 +/- 0.16335	0.40891
Sf3a1	Splicing factor 3 subunit 1						
	FGEpSEEVEMoxEVESDEED QEK	165.85	72	329	novel	1.0955 +/- 0.18068	0.13153
Sfrs11	splicing factor, arginine/serine-rich 11 isoform 3						
	DYDEEEQGYDpSEKEK	14.89	53	374	known	0.82353	-0.28011
Protein with unknown function							
-	51 kDa protein						
	pSGSPSDNSGAEEMoxEVSL AK	119.96	60	124	novel	0.9394 +/- 0.010559	-0.090189
-	37 kDa protein						
	GAAQNIIPASpTGA AK	39.28	40	215	novel	1.0045	0.006465
I110004 F10Rik	Small acidic protein						
	pSASPDDDLGSSNWEAADL GNEER	57.85	135	15	known	1.0959 +/- 0.20723	0.13218
I700021 F05Rik	Uncharacterized protein C6orf203 homolog						
	EADEEDpSDEETSYPER	156.56	71	106	known	0.83091 +/- 0.11873	-0.26724
2310046 A06Rik	hypothetical protein LOC69642						
	IPEPTDKpSPETVNR	119.91	81	61	novel	0.76588 +/- 0.02316	-0.3848
2310046 A06Rik	similar to 2310046A06Rik protein						
	AEYVFIVDpSDGEDEATCR	193.32	100	85	known	1.0742 +/- 0.067651	0.10325
2410004 B18Rik	Uncharacterized protein C1orf52 homolog						
	LLPEGEETVpSDDDKDER	216.69	114	156	known	0.9827 +/- 0.051121	-0.025172

2410166	Isoform 1 of Protein FAM54B						
I05Rik	ASpSFADMoxMoxGILK	107.4	54	235	known	1.0528	0.074221
3425401	similar to Uncharacterized protein C10orf71						
B19Rik	SVpSQETETER	124.74	51	677	novel	0.85648	-0.2235
4930535	Isoform 2 of Uncharacterized protein KIAA0460						
B03Rik	DVEDMoxELSDVEDDGpSK	8.71	62	355	novel	0.83597	-0.25848
6330577	17 days embryo stomach cDNA, RIKEN full-length enriched library, clone:1920015M04 product:hypothetical Proline-rich region profi... <Preview truncated at 128 characters>						
E15Rik	ENPPpSPPTpSPAAPQPR	119.96	55	67, 71 or 83, 84	known	0.87759 +/- 0.12495	-0.18839
8030462	RIKEN cDNA 8030462N17 gene						
N17Rik	RDpSSEQLASTESDKPTTG R	100.09	61	66	known	0.97885 +/- 0.18959	-0.030843
AK157302	hypothetical protein LOC432732						
	TKGDPsDEEVIQDGV R	161.53	65	73	novel	1.1738 +/- 0.030085	0.23122
Anks1	Isoform 2 of Ankyrin repeat and SAM domain-containing protein 1A						
	SEpSLNCSIGK	9.78	43	642	known	0.72232	-0.46929
	pSPSFASEWDEIEK	6.15	67	656	known	1.0118	0.016907
Atxn2l	Isoform 2 of Ataxin-2-like protein						
	EVDGLLTSDPMGpSPVSSK	127.37	64	591	known	1.0295	0.041952
BC031781	Uncharacterized protein C1orf55 homolog						
	EDGIDAVEVAADRPgSPR	38.7	51	269	known	1.059	0.08277
Camsap III	Isoform 2 of Calmodulin-regulated spectrin-associated protein 1-like protein 1						
	LDGEpSDKEQFDDQK	7.26	44	1120	novel	0.86515	-0.20898
Ccdc25	Coiled-coil domain-containing protein 25						
	VENMoxSSNQDGNdpSDE FMox	26.4	46	195	known	0.77478	-0.36815
Chchd2	Coiled-coil-helix-coiled-coil-helix domain-containing protein 2, mitochondrial						
	RAPAAQPPAAAAPSavgpSP AAAPR	57.19	76	45	known	0.87369	-0.19481
Gm1614	hypothetical protein						
	pSPDVDTPAQPR	118.15	47	637	known	0.70779 +/- 0.056957	-0.49861
	NApSVEEVVSR	64.66	46	501	novel	0.73719	-0.4399
LOC10039888	similar to Pr22 isoform 1						
	ESVPDFLPpSPPK	149.28	58	38	known	0.99016 +/- 0.1701	-0.014267
LOC10047790	similar to beta-2-syntrophin						
	GPAGEApSASPPVR	110.79	61	88	known	0.76006 +/- 0.10648	-0.39581
LOC10048389; ENSMUSG0000047016	similar to G protein pathway suppressor 1						
	EGpSQGELTPANSQSR	64.46	93	470	known	0.86412 +/- 0.05801	-0.2107
LOC633594	Putative uncharacterized protein						
	DETVGTDDLQGGIDPGAV pSPEPGKDHAAGGPR	122.81	87	432	novel	1.0757 +/- 0.13153	0.10527
	LSSGPLPQLGPLTPDSDT HSGDALPR	122.81	76	317	novel	1.0874 +/- 0.10463	0.12095
LOC665298	similar to acidic ribosomal phosphoprotein P1 isoform 1						
	KEESEpSEDDMoxGFLFD	218.74	65	104	novel	1.4117 +/- 0.332	0.49743
Nucks1	Nuclear ubiquitous casein and cyclin-dependent kinases substrate						
	VVDYSQFQEpSDDADEDYGR	171.83	49	19	known	1.0778 +/- 0.01463	0.10805
	EEDEEAepSPEKK	7.75	55	214	known	1.3393 +/- 0.02431	0.42146

OTTMU SG00000 014672;L OCI000 47184	similar to proteasome alpha7/C8 subunit						
	ESLKEEDEpSDDDNMox	171.11	63	249	novel	0.85241 +/- 0.15417	-0.23037
Rilpl1	14 kDa protein						
	LQGEHSQNGEEEEAEIQPQ PDGEESlpSDAEK	11.31	43	79	novel	1.0432	0.061029
Sh3bgr	Protein						
	SGENEAQKEDpSED TGELSE SQEK	135.59	85	27	novel	0.7417 +/- 0.068676	-0.4311
Sh3bp5l	SH3 domain-binding protein 5-like						
	SEVVEDEGPRpSPVAEEPGGS GSNSSETK	123.5	63	30	novel	1.09 +/- 0.11965	0.12427
Slc7a6os	Protein SLC7A6OS						
	EFDYDSPHGLDpSD	125.91	62	305	known	0.94448	-0.08241
Smtnl2	Smoothelin-like protein 2						
	SpSVEHDEASDLEVR	148.96	95	131	novel	1.2345 +/- 0.011884	0.30397
Wdr44	Isoform 1 of WD repeat-containing protein 44						
	EAENTANQAGNEpSPVQEL R	115.13	58	50	known	0.95531 +/- 0.39785	-0.065963

4.3.3.3 Not quantifiable phosphopeptides

The relatively low mass resolution of the LTQ mass spectrometer resulted in several peptide pairs which could not be quantified although measurements were taken out in the enhanced scan mode. A few peptides of the complex sample were eluting at the same time with a very similar mass to charge (m/z) value, e.g. the mass of the heavy labeled peptide of the lighter peptide pair have had sometimes an indistinguishable mass from the light labeled peptide of the heavy peptide pair. This could lead to false positive results in the regulated peptide list, which was eliminated by manual validation of each regulated peptide pair using the QualBrowser software. Table 4.5 shows the list of these non quantifiable peptides.

Table 4.5. List of identified phosphopeptides. Relative quantification was not possible due to peak overlapping with a neighbor peptide eluting at the same time with a very similar mass to charge value. Orange color shows that protein was also found with significantly enhanced phosphorylation at a further phosphorylation site, blue with decreased phosphorylation and green shows both enhanced and decreased phosphorylated proteins. (XIC_L: integrated peak area of light (did not treated with L-arg) peptide, XIC_H: integrated peak area of heavy (with L-arg treated) peptide, PTM score: indicating post translational modification counted by MSQuant, Mascot score: indicating validity of peptide identification, NaN: not quantifiable.

Symbol	Protein						
	Peptide	PTM max	Mascot max	Phos. site	N/K	XIC _H / XIC _L	log ₂ (XIC _H /XIC _L)
Cardiac contractile proteins							
Acta1	Actin, alpha skeletal muscle						
	KDLYANNVMpSGGTTMYPGIADR	48.04	60	302	novel	NaN	NaN
Mybpc3	myosin binding protein C, cardiac						
	DGpSDITANDK	76.28	45	55	novel	NaN	NaN
	DASPDDQGSYAVIAGpSSK	134.44	130	80	novel	NaN	NaN

Myh13	Myosin, heavy polypeptide 13, skeletal muscle						
	NDLQLQVQpSEpTENLMoxDAEER	8.4	42	897, 899	novel	NaN	NaN
Myh6	Myosin-6						
	SDLpSRELEEISER	36.48	40	1142	novel	NaN	NaN
	VLpSKANSEVAQWR	46.77	42	1364	novel	NaN	NaN
Actin binding protein							
Ctnnd1	107 kDa protein						
	VGGpSSVDLHR	61.85	53	268	known	NaN	NaN
Synpo	Isoform 1 of Synaptopodin						
	AGLPPpSPALPR	110.71	43	854	known	NaN	NaN
Tln1	Talin-1						
	VLVQNAAGpSQEK	5.68	50	2040	novel	NaN	NaN
Actin filament turnover modulator							
Cdc42e p4	Cdc42 effector protein 4						
	EADDESLEQASApSK	220.47	118	64	known	NaN	NaN
Rcsd1	Isoform 1 of Capz-interacting protein						
	LQANLAFDPAALLPGApSPK	6.72	44	105	novel	NaN	NaN
	VKSpSPLIEK	88.83	40	83	novel	NaN	NaN
Sarcomeric proteins							
Ldb3	Isoform 3 of LIM domain-binding protein 3						
	DPALDTNGSLApTPpSPSPEAR	100.09	122	119	novel	NaN	NaN
Calcium homeostasis							
Ahnak	AHNAK nucleoprotein isoform 1						
	AEAPLPpSPK	78.04	41	4890	known	NaN	NaN
	FKAEAPLPpSPK	86.23	46	4890	known	NaN	NaN
	VSVApTPDVSLESEGAVK	166.32	62	5169	novel	NaN	NaN
Calcium binding							
Efh2	EF-hand domain-containing protein D2						
	ADLNQIGIGEPQpSPSR	66.9	44	74	known	NaN	NaN
Microtubule associated proteins							
Mtap1a	Isoform 1 of Microtubule-associated protein 1A						
	ALALVPGpTPTR	136.27	50	2182	known	NaN	NaN
Mtap1b	microtubule-associated protein 1B						
	RSEpSPFEGK	95.03	51	1422	known	NaN	NaN
Mtap7d1	Microtubule-associated protein 7 domain containing 1						
	AAEEKEPAAPASPSPVPSPpTPAQPK	8	50	522	known	NaN	NaN
Intermediate filament							
Lmna	Isoform A of Lamin-A/C						
	SGAQASSTPLpSPTR	86.08	52	22	known	NaN	NaN
Tight junction protein							
Tjp1	Tight junction protein ZO-1						
	pSREDLSAQPVQTK	8	44	617	known	NaN	NaN

Vesicle protein							
Stx4a	Syntaxin-4						
	QGDNIpSDEDEVR	150.34	79	15	known	NaN	NaN
Protein kinase							
Mylk	myosin, light polypeptide kinase						
	KSpSTGSPTSPINAEK	111.46	81	1804	known	NaN	NaN
Speg	Isoform 1 of Striated muscle-specific serine/threonine protein kinase						
	ATpSEGESLR	71.39	63	2499	novel	NaN	NaN
	SSpSFSQGEAEPR	54.09	51	2135	novel	NaN	NaN
	AApSVELPQR	71.82	51	2042	novel	NaN	NaN
	AVGPPAPpTPPRK	5.02	55	2741	novel	NaN	NaN
Protein phosphatase							
Ppp1r1 2b	Isoform 1 of Protein phosphatase 1 regulatory subunit 12B						
	YPTQPDKPTTPVpSPSASR	67.67	45	729	novel	NaN +/- 0	NaN
Metabolism							
Limch1	120 kDa protein						
	CpSPTVALVEFSSNPQLK	7.53	41	660	known	NaN	NaN
Mdh1	Malate dehydrogenase, cytoplasmic						
	KLSpSAMSAK	92.11	40	242	known	NaN	NaN
Mdh2	Malate dehydrogenase, mitochondrial						
	IQEAGpTEVVK	72.63	53	235	novel	NaN	NaN
Antigen processing and presentation							
Ap3b1	AP-3 complex subunit beta-1						
	NFYEpSEEEEEK	146.19	54	276	known	NaN	NaN
Regulation of GTPase mediated signal transduction							
A23006 7G2IRi k	Isoform 1 of 250 kDa substrate of Akt						
	SSpSTSDITER	134.43	67	765	known	NaN	NaN
Rabgap 1	Isoform 1 of Rab GTPase-activating protein 1						
	GVSEDEpTDEEKETLK	125.91	51	991	known	NaN	NaN
Protease							
Psm4	Isoform Rpn10C of 26S proteasome non-ATPase regulatory subunit 4						
	AAAASAAEAGIApTPGTEGER	70.89	53	250	known	NaN	NaN
Usp24	similar to hCG33036, isoform 5						
	CGTRSpSMoxIGpSSR	11.2	50	1832, 1836	novel	NaN	NaN
Ubiquinone biosynthetic process							
Coq9	Ubiquinone biosynthesis protein COQ9, mitochondrial precursor						
	YTDQpSGEEEEEDYESEQLQHR	67.67	50	81	known	NaN +/- 0	NaN
Integral membrane protein							
Aqp1	Aquaporin-1						
	SSDFTDRMKVWpTSGQVEEYDLDA DDINSR	63.64	107	246	known	NaN	NaN

Armcl0	Isoform 1 of Armadillo repeat-containing protein 10						
	pSAEDLTDSYDDILNAEQLKK	119.96	56	43	known	NaN	NaN
Rrp12	RRP12-like protein						
	GDSIEILADpSEDEDEEEER	113.98	51	1081	known	NaN	NaN
Tgoln1; LOC10038890	Trans-Golgi network integral membrane protein 1 precursor						
		9.96	43	210	novel	NaN	NaN
Transcriptional regulation							
Dek	23 kDa protein						
	EEpSEEEEDDEDDDEDEEEEEK	7.75	44	33	known	NaN	NaN
Hdgfrp2	Isoform 1 of Hepatoma-derived growth factor-related protein 2						
	GGpSpSGEELEDEEPVK	6.44	44	366, 367	known	NaN	NaN
Naca	Nascent polypeptide-associated complex subunit alpha, muscle-specific form						
	ESpSpSQSASSLEVLSEDVTK	23.93	41	522	novel	NaN	NaN
Sdpr	Serum deprivation-response protein						
	EGSpSVENETK	124.3	52	308	novel	NaN	NaN
Tsc22d4	TSC22 domain family protein 4						
	VEVESGGSAAApTPPLSR	61.22	62	223	known	NaN	NaN
Ybx1	Nuclease-sensitive element-binding protein 1						
	NEGSEpSAPEGQAQQR	142.74	76	174	known	NaN	NaN
Translation regulation							
Eif3c	Eukaryotic translation initiation factor 3 subunit C						
	PVSGNYGKQPLLPSEDEEDTKR	38.22	40	39	known	NaN	NaN
DNA repair							
Atrx	3 days neonate thymus cDNA, RIKEN full-length enriched library, clone:A630055L09 product:X-linked nuclear protein, full insert s... <						
	YVEpSDDEKPTDENVNEK	6.29	41	92	known	NaN +/- 0	NaN
RNA binding protein							
Rbm20	similar to hCG2036763						
	QSpSPFLDDCK	153.19	44	1032	novel	NaN	NaN
Srrm2	Isoform 1 of Serine/arginine repetitive matrix protein 2						
	NSGPVSEVNTGFpSPEVK	194.93	73	1305	known	NaN	NaN
Apoptosis							
Bnip2	Putative uncharacterized protein						
	KGpSITEYTATEEK	7.2	70	114	known	NaN	NaN
Huwe1	HECT, UBA and WWE domain containing 1						
	DLSMoxpSEEDQMoxMoxR	30.87	44	1369	novel	NaN	NaN
	IALPAPRGSGpTApSDDEFENLR	54.35	55	1905, 1907	known	NaN	NaN
Ndrp2	Isoform 2 of Protein NDRG2						
	LSRSRpTASLTSAASIDGSR	32.77	52	316	known	NaN	NaN
Protein with unknown function							
342540 IB19Rik	similar to Uncharacterized protein C10orf71						
	KApSAEDLSAR		48	813	novel	NaN	NaN
Brd3	Isoform 1 of Bromodomain-containing protein 3						
	SEpSPPLSEPK	104.65	44	262	known	NaN	NaN
Sh3bgr	Protein						
	EDSEDGELpSESQEK	103.16	56	34	novel	NaN	NaN

Sh3bp5 I	SH3 domain-binding protein 5-like						
	GLSDHApSLDGQELGAQSR	66.23	93	361	novel	NaN	NaN
Wdr44	Isoform I of WD repeat-containing protein 44						
	EYVSNDATQpSDDEEKLQSQQTDT DGGR	126.68	76	405	known	NaN	NaN

4.3.4 IDENTIFIED CARDIAC PHOSPHOPROTEOME USING LTQ ORBITRAP XL

At an early point of time of method establishment, Thermo Fischer Scientific enabled me to perform some measurement on the novel LTQ Orbitrap XL mass spectrometer in Bremen.

Main advantage to use LTQ Orbitrap XL that it has a mass resolution up to 100.000 which enables high mass accuracy measurements to minimize the errors of relative quantification and identification of false negatively or positively regulated phosphorylation sites. Using LTQ Orbitrap XL with a mass resolution of 60.000 (at $m/z=400$), 42 phosphorylation sites (19 novel, based on data mining using Phosphosite Plus at www.phosphosite.org, state March 2009) on 35 cardiac phosphoproteins from as little as 200 μ g dimethyl labeled cytosolic protein fraction could be identified. HCD (higher-energy C-trap dissociation), CID and CID with multistage activation were applied for peptide fragmentation. Using HCD fragmentation (which is available only in LTQ Orbitrap XL but not in LTQ), large peptides with up to 5 positive charges and three phosphorylation sites could be identified.

The relatively low number of identified phosphopeptides derived from an insufficient phosphopeptide enrichment (at this point of time methods were not fully established yet). Using the original titanium dioxide filled TopTips, a high number of non-phosphorylated peptides remained in the sample, which suppressed the ion signal intensity of phosphorylated peptides (Chapter 4.2.2.2). Furthermore, compared to the phosphorylated peptides, non-phosphorylated peptides were present in much higher concentrations in the sample, therefore they have had higher signal intensities in the MS spectra. Although the data dependent setup in the MS analysis method selected the first, second, third and fourth highest peaks for the MS/MS fragmentation, together with dynamic exclusion for the already analyzed peaks almost every time peaks of non-phosphorylated peptides were chosen for the identification by MS/MS.

Proteins and phosphorylation sites were identified by the SEQUEST algorithm. Peptides were accepted with XCorr vs. Charge state scores over 1.5, 2.0, 2.5 and 3.0 for one, two, three and four times charged peptides, respectively. As an additional criterium, peptide probability scores had to be over $3 \cdot 10^3$. Phosphorylated peptides were manually validated and quantified using the QualBrowser software based on the integrated peak area of heavy and light peptide pairs with a mass accuracy of 5 ppm.

As expected, most of the identified phosphorylation sites are not influenced by iNOS derived NO, however 10 (23.8%) and 3 (7.1%) phosphorylated peptides were found to be enhanced or decreased phosphorylated respectively (Fig. 4.22).

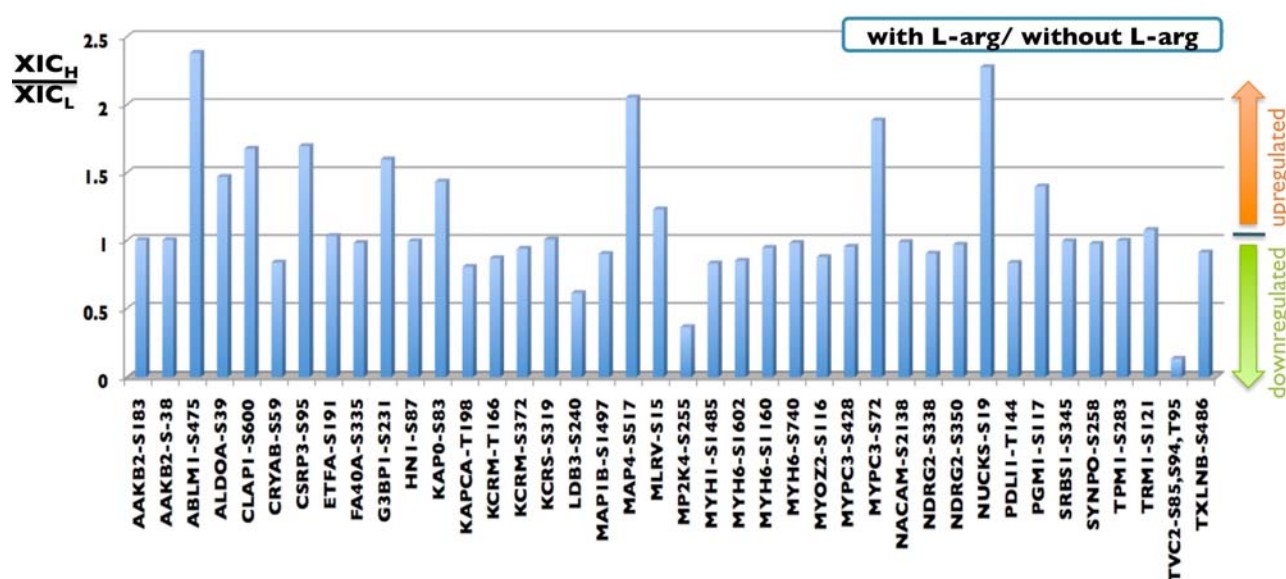


Figure 4.22: Protein phosphorylation site specific changes induced by iNOS derived NO in a heart failure model. X axis shows protein symbol, phosphorylated amino acid and phosphorylation site; Y axis shows ratio of integrated peak area (XIC) of heavy (+L-arg) vs. light (-L-arg) labeled peptide.

4.3.4.1 Identified novel and known phosphorylation sites - not regulated by NO

Three novel phosphorylation sites at Ser-740 (Fig. 4.19), at Ser-1160 and at Ser-1602 were identified in **myosin-6** (Fig. 4.23 and Fig. 4.24).

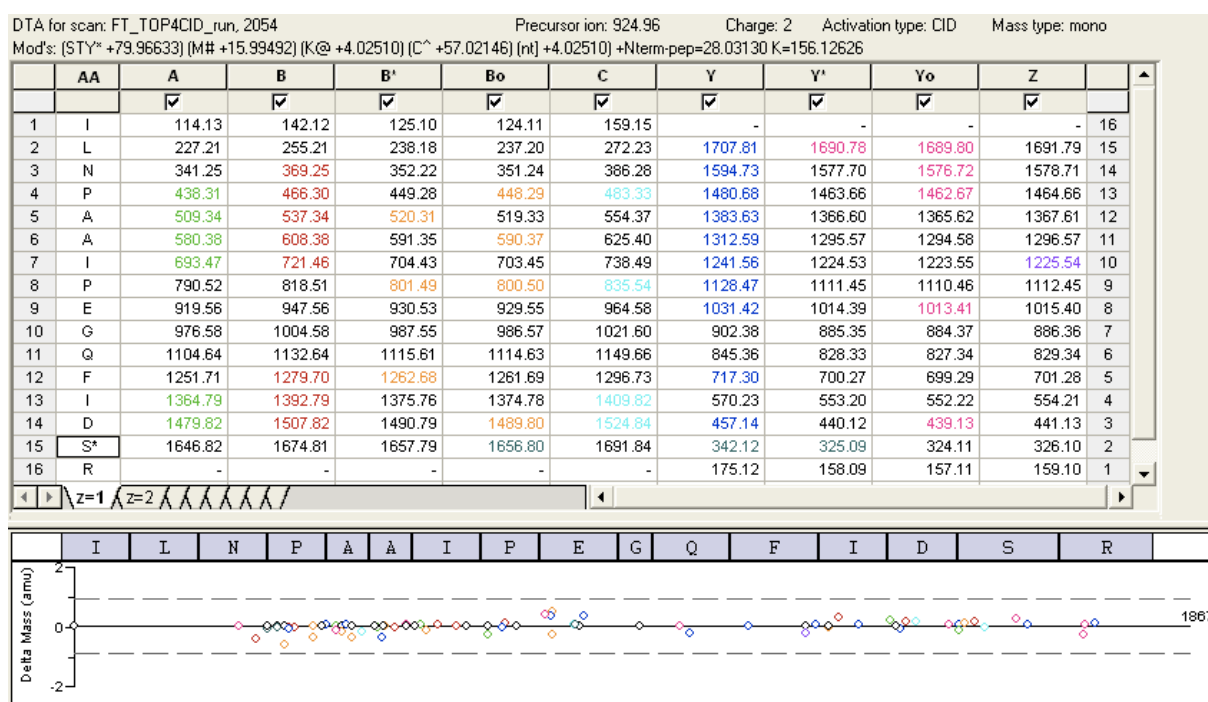


Figure 4.23: The table lists possible ILNPAAIPEGQFIDS*R. (*: phosphorylation) peptide fragment masses where the colored numbers show identified peptide fragments generated by CID with multistage activation. Colored dots show mass differences between measured and theoretical peptide fragments.

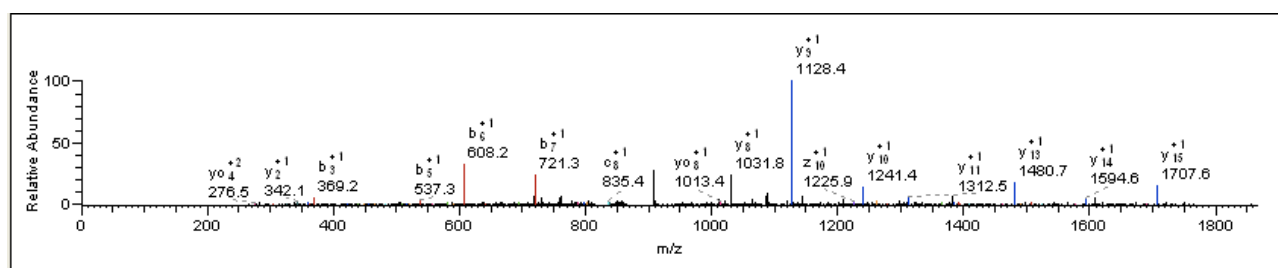


Fig. 4.24: Novel phosphorylation site at serine 740 in myosin-6 (MYH6) found in peptide ILNPAAIPEGQFIDS*R. (*: phosphorylation) MS/MS spectrum shows peptide fragments of the phosphorylated peptide fragmented by CID with multistage activation. (Identified peaks are colored.)

Other actin binding contractile proteins, like **cardiac myosin binding protein c** and **myosin-I** showed also novel phosphorylation sites at Ser-420 and at Ser-1485, respectively. Further novel phosphorylation sites could be identified in cytoskeletal actin binding but not contractile proteins, like **myozenin 2** (Ser-116), **PDZ and LIM domain protein I** (Ser-144).

Ser-191 located in the electron transfer flavoprotein (ETF) domain was also identified as a novel phosphorylation site in **electron transfer flavoprotein subunit alpha, mitochondrial precursor**. This protein serves as a specific electron acceptor for several dehydrogenases and transfers electrons to the main mitochondrial respiratory chain via ETF-ubiquinone oxidoreductase.

Novel phosphorylation sites were also identified in enzymes of energy transduction, like **creatine kinase M type** (Thr-166, Ser-342) and **creatine kinase, sarcomeric mitochondrial precursor** (Ser-319). These proteins reversibly catalyze the transfer of phosphate between ATP and phosphocreatine, providing a spatial and temporal buffer of ATP concentration in tissues with high, fluctuating energy demand like muscle and brain.

Phosphorylation of Ser-486 could be identified in **beta taxilin**, a protein which promotes motor nerve regeneration which is possibly involved in intracellular vesicle traffic. Interestingly, this protein is known to be specifically expressed in skeletal muscle and not in the heart.

Table 4.6 shows list of identified phosphopeptides which are not regulated by NO.

Table 4.6: List of identified novel and known phosphorylation sites which are not regulated upon iNOS derived NO release (after one minute). Symbols of variable amino acid modifications: *: phosphorylation; #: methionine oxidation; ^: carbamidomethylation of cysteine; J: d2-dimethyl labeling of N-terminal amino acids; @: d2-dimethyl labeling of lysine (K). (XIC_L: integrated peak area of light (not treated with L-arg) peptide, XIC_H: integrated peak area of heavy (treated with L-arg) peptide. Orange color shows that protein was also found with significantly enhanced phosphorylation at a further phosphorylation site, blue with decreased phosphorylation and green shows both enhanced and decreased phosphorylated proteins.

Symbol	Protein name				
	Peptide	Phos. site	Novel/ known	XIC ₃ /XIC ₁	log ₂ (XIC ₃ /XIC ₁)
KAPCA	cAMP-dependent protein kinase, alpha-catalytic subunit (EC 2.7.11.1) (PKA C-alpha)				
	R.TWT*LC^GTPEYLAPEIILSK.G	T-198	known	0.80	-0.31
MYHI	Myosin-I (Myosin heavy chain I) (Myosin heavy chain 2x) (MyHC-2x) (Myosin heavy chain, skeletal muscle, adult I)				
	R.SLS*TELFK.I	S-1485	novel	0.83	-0.27

PDLII	PDZ and LIM domain protein I (Elfin) (LIM domain protein CLP-36) (C-terminal LIM domain protein I)	R.VITNQYNS*PTGLYSSENISNFNNAVESK.T	S-144	novel	0.83	-0.26
CRYAB	Alpha crystallin B chain (Alpha(B)-crystallin) (P23)	R.APS*WIDTGLSEMR.L	S-59	known	0.84	-0.26
MYH6	Myosin-6 (Myosin heavy chain 6) (Myosin heavy chain, cardiac muscle alpha isoform) (MyHC-alpha)	R.MVDSLQTS*LDAETR.S	S-1602	novel	0.85	-0.23
KCRM	Creatine kinase M-type (EC 2.7.3.2) (Creatine kinase M chain) (M-CK)	K.LSVEALNSLT*GEFK.G	T-166	novel	0.87	-0.20
MYOZ2	Myozenin-2 (Calsarcin-1) (FATZ-related protein 2)	R.S*PPNPENIAPGYSGPLK.E	S-116	novel	0.88	-0.19
MAPIB	Microtubule-associated protein 1B (MAP 1B) (MAPI.2) (MAPI(X)) [Contains: MAPI light chain LC1]	K.LGGDV3*PTQIDVSQFGSK.E	S-1497	known	0.90	-0.15
NDRG2	Protein NDRG2 (Protein Ndr2)	R.TASLTSAAS*IDGSR.S	S-338	known	0.90	-0.15
TXLNB	Beta-taxilin (Muscle-derived protein 77)	R.TSEEEPEPS*VSENEEVDAAEANSFQK.A	S-486	novel	0.91	-0.14
KCRM	Creatine kinase M-type (EC 2.7.3.2) (Creatine kinase M chain) (M-CK)	K.GQS*IDDMIPAQK.-	S-372	novel	0.94	-0.09
MYH6	Myosin-6 (Myosin heavy chain 6) (Myosin heavy chain, cardiac muscle alpha isoform) (MyHC-alpha)	R.LEEAGGA(TS)*VQIEMNK.K	S-1160	novel	0.95	-0.08
MYPC3	Myosin-binding protein C, cardiac-type (Cardiac MyBP-C) (C-protein, cardiac muscle isoform)	R.TLTIS*QC*SLADDAAYQC*VVGGEK.C	S-420	novel	0.95	-0.07
NDRG2	Protein NDRG2 (Protein Ndr2)	R.TJLS*QSSESGTLPSGPPGHTMEVSC^.-	S-350	known	0.97	-0.05
SYNPO	Synaptopodin	K.VAS*EEEEVPLVVYLK.E	S-258	known	0.97	-0.04
FA40A	Protein FAM40A	R.AAS*PPASASDLIEQQQK.R	S-335	known	0.98	-0.03
MYH6	Myosin-6 (Myosin heavy chain 6) (Myosin heavy chain, cardiac muscle alpha isoform) (MyHC-alpha)	R.ILNPAAIPEGQFIDS*R.K	S-740	novel	0.98	-0.03
NACAM	Nascent polypeptide-associated complex subunit alpha, muscle-specific form (Alpha-NAC, muscle-specific form)	K.VQGEAVSNIQENTQTPTVQEESE*EEEEVD ETGVEVK.D	S-2138	known	0.99	-0.02
HNI	Hematological and neurological expressed 1 protein	R.SNS*SEASSGDFLDLK.G	S-87	known	0.99	-0.01
SRBS1	Sorbin and SH3 domain-containing protein 1 (Ponsin) (c-Cbl-associated protein) (CAP) (SH3 domain protein 5)	R.DIS*PEEIDLK.N	S-345	known	0.99	-0.01
TPM1	Tropomyosin-1 alpha chain (Alpha-tropomyosin)	K.AISEELDHALNDM#TS*I.-	S-283	known	1.00	-0.00
AAKB2	5'-AMP-activated protein kinase subunit beta-2 (AMPK beta-2 chain)	R.DLSSS*PPGPYQGEMYVFR.S	S-183	known	1.00	0.00
		K.IJMVGS*TDDPSVFSLPDSK@.L	S-38	known	1.00	0.00
KCRS	Creatine kinase, sarcomeric mitochondrial precursor (EC 2.7.3.2) (S-MtCK)	R.LGYILTC*PS*NLGTGLR.A	S-319	novel	1.01	0.01
ETFA	Electron transfer flavoprotein subunit alpha, mitochondrial precursor (Alpha-ETF)	K.APSS*SSVGISEWLDQK.L	S-191	novel	1.03	0.04
TRMI	N(2),N(2)-dimethylguanosine tRNA methyltransferase (EC 2.1.1.32) (tRNA(guanine-26,N(2)-N(2)) methyltransferase)	K.IAVDLS*DQEEETAGK.N	S121	known	1.08	0.11

4.3.4.2 Proteins with decreased phosphorylation upon enhanced NO formation

T-cell receptor gamma chain V region V108B precursor was identified with three novel phosphorylation sites within one peptide. Upon adding L-arginine into the perfusion buffer,

the intensity of the phosphorylated peptide decreased by 87%. This change represents the dephosphorylation rate of the whole peptide, corresponding to the total intensity difference of all identified phosphorylation sites within the peptide. To overcome this drawback and specifically address the regulation of single phosphorylation sites it is advantageous to enrich mainly single phosphorylated peptides in combination with stable isotope dimethyl labeling.

The dual specificity **mitogen-activated protein kinase kinase 4 (MAPKK4)** was found to be dephosphorylated by 63% at the known phosphorylation site Ser-255. This stress activated Ser/Thr protein kinase is activated by phosphorylation at Ser-255 and Thr-259 by Src homology domain containing proline-rich kinase (SPRK) and MAP kinase kinase kinase 1 (MEKK-1) which leads to activation of JUN kinases JNK1 and JNK2 as well as p38MAPK. Decreased phosphorylation could occur due to oxidative stress which inhibits MEKK1 by site-specific glutathionylation in the ATP-binding domain (Cross et al., 2004).

Ser-240 in **lim domain binding protein 3 (LDB3)** which is also known as protein cypher or protein oracle was also dephosphorylated upon L-arg treatment. Ser-240 is a novel phosphorylation site, therefore its function is unknown. LDB3 may couple protein kinase C-mediated signaling via its LIM domains to the cytoskeleton, furthermore it is interacting with ACTN2, MYOZ1, MYOZ2 and MYOZ3. Mutation of LDB3 gene can lead to myofibrillar and cardiac myopathies which are defined by the presence of foci of myofibril dissolution, accumulation of myofibrillar degradation products and ectopic expression of multiple proteins.

Table 4.7 shows dephosphorylated cardiac phosphopeptides after one minute L-arg perfusion:

Table 4.7: List of dephosphorylated protein phosphorylation sites upon 1 minute L-arginine perfusion of iNOS⁺/myo⁻ mouse hearts. Symbols of variable amino acid modifications: *: phosphorylation of serine, threonine or tyrosine; ^: carbamidomethylation of cysteine. XIC_L: integrated peak area of light (not treated with L-arg) peptide, XIC_H: integrated peak area of heavy (treated with L-arg) peptide. Green color shows proteins which are listed also in other tables in this work.

Symbol	Protein name				
	Peptide	Phos. site	Novel/known	XIC _H /XIC _L	log ₂ (XIC _H /XIC _L)
TVC2	T-cell receptor gamma chain V region V108B precursor (Fragment)				
	K.KIEAS*KDFQTSTS*T*LKINYLK.K	S-85, S-94, T-95	novel	0.13	-2.90
MP2K4	Dual specificity mitogen-activated protein kinase kinase 4 (EC 2.7.12.2) (MAP kinase kinase 4) (MAPKK 4)				
	K.LC^DFGISGQLVDS*IAK.T	S-255	known	0.37	-1.45
LDB3	LIM domain-binding protein 3 (Z-band alternatively spliced PDZ-motif protein) (Protein cypher) (Protein oracle)				
	K.DLAVIDSAS*PVYQAVIK.T	S-240	novel	0.61	-0.71

4.3.4.3 Proteins showing increased phosphorylation upon enhanced NO formation

One of the upregulated proteins is the **CLIP-associating protein 1 (Clasp1)** which showed an enhanced phosphorylation at serine 600 upon iNOS derived NO activation (Fig 4.25). Clasp1 is a microtubule plus-end tracking protein, promoting the stabilization of dynamic microtubules. In migrating cells Clasp1 is required for the polarization of the cytoplasmic microtubule arrays

towards the leading edge of the cell. CLASPI is highly expressed in brain and heart and localized to microtubule plus ends. Serine 600 is located in a so called HEAT repeat region which is a tandemly repeated, 37-47 amino acid long module occurring in numerous cytoplasmic proteins. Arrays of heat repeats consist of a rod-like helical structure formed by 3 to 36 units and appear to function as protein-protein interaction surfaces. Many HEAT repeat-containing proteins are involved in intracellular transport processes.

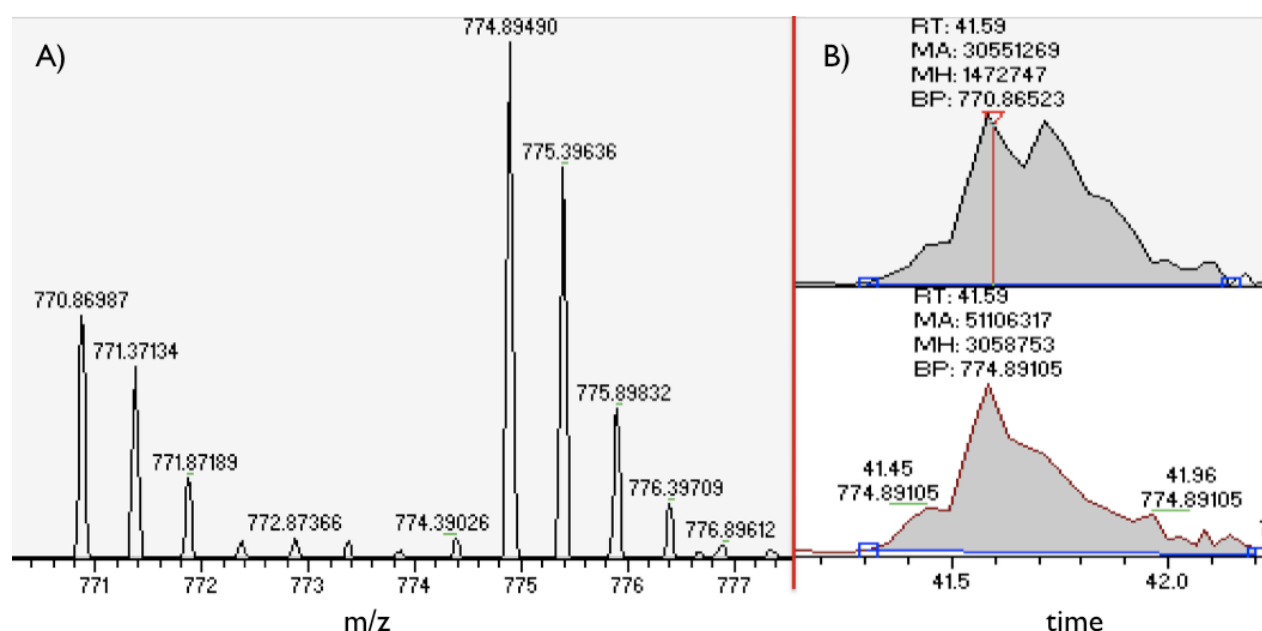


Figure 4.25. CLIP-associating protein I (ClaspI) phosphorylation at serine 600 is upregulated upon iNOS derived NO release. A) MS spectrum of 2⁺ charged peptide pair SRS**DIDVNAAASAK*. Monoisotopic 2⁺ charged base peak of heavy peptide m/z 774.89490 shows two times higher peak intensity than light peptide m/z 770.86987. B) Extracted ion chromatogram of light (upper panel) and heavy (lower panel) labeled peptides. (RT: retention time, MA: integrated peak area, MH: peak height, BP: base peak)

Phosphorylation of Ser-83 of the **cAMP-dependent protein kinase type I-alpha regulatory subunit** (PKA1a or PRKARIA) was increased 1.42 times upon L-arginine co-perfusion. PKA is activated by cAMP, a signaling molecule, which is important for a variety of cellular functions. Activated PKA transduces its signal through phosphorylation of downstream target proteins. PRKARIA interacts with AKAP4, its complex with RFC2 may be involved in cell survival. NO is known to inhibit cAMP degradation thereby leading to an enhanced PKA activity. Ser-83 is localized in one of the four regulatory subunits of the protein, and therefore could play an important role in the regulation of PKA activity.

Differential analysis of iNOS derived NO activation in myo^{-/-}/iNOS⁺ mouse hearts led to the identification of two novel phosphorylation site at Ser-72 and at Ser-420 in the thick filament protein **cardiac myosin binding protein-c (mypc3)**. Figure 4.26 shows an enhanced phosphorylation at Ser-72 whereas phosphorylation at Ser-420 did not change. Furthermore, as a kind of technical loading control, a non-phosphorylated peptide also shows the same intensity for both heavy (H) and light (L) labeled peptides indicating identical protein expression levels in

matched heart samples. This experiment shows that quantitative mass spectrometry can be used as a kind of modern western blot. Interestingly, Ser-72 is located near to the myosin head, therefore its phosphorylation may also influence cardiac contractility.

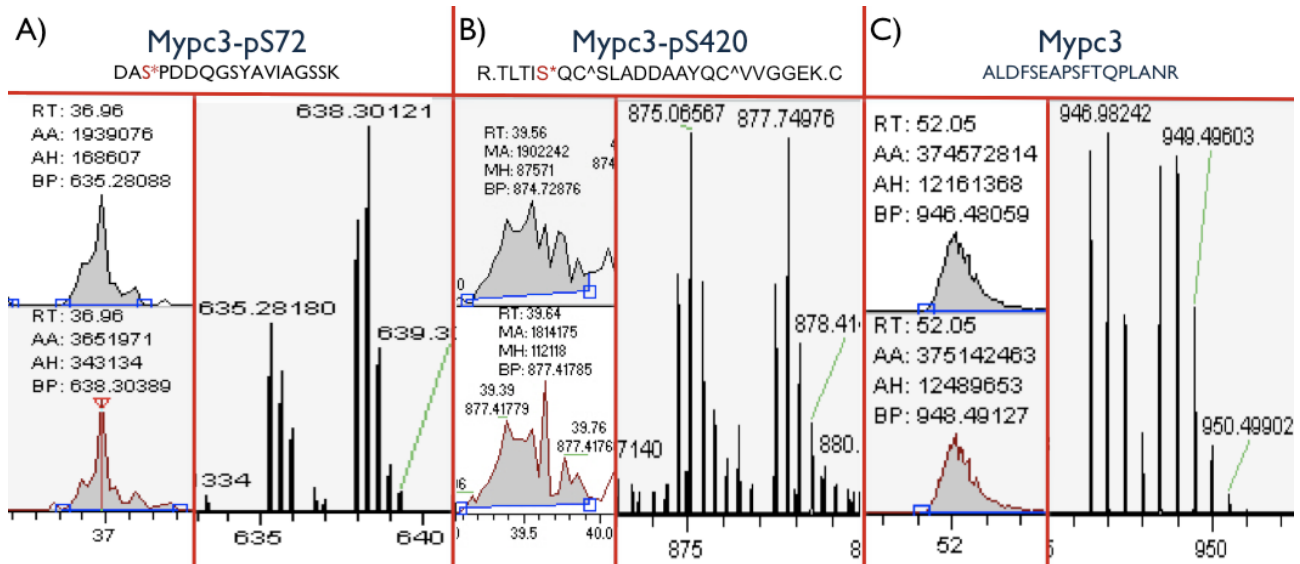


Figure 4.26: Comparing intensity ratios of H/L labeled peptide pairs with (A and B) and without (C) phosphorylation there is a clear evidence that Mypc3 is expressed in the same amount in both H and L labeled mouse heart (C) whereas phosphorylated peptide DAS*PDDQGSYAVIAGSSK shows a strongly enhanced phosphorylation upon NO activation (A). At the same time, an other phosphorylation site Ser-420 in the phosphorylated peptide TLTIS*QC^SLADDAAYQC^VVGGEK shows no changes upon iNOS derived NO release (B). (*: phosphorylation, ^: carbamidomethylation, RT: retention time, AA, MA: integrated peak area, MH: peak height, BP: base peak)

Three additional cytoskeletal proteins showed an increased phosphorylation upon L-arg treatment. **Actin binding LIM protein (ABLIM1)** and **cysteine and serine rich protein 3 (CSR3 or MLP)** both contain zinc binding LIM domains, an important side for protein-protein interactions. CSR3 is a positive regulator of myogenesis and interacts with lactate dehydrogenase D (LDHD). It is also known that downregulated CSR3-calcineurin signaling predisposes to adverse remodeling after myocardial infarct (Heineke et al., 2005). Deletion of CSR3 leads to diastolic dysfunction and by growing older to dilated cardiomyopathy (Lorenzen-Schmidt et al., 2005). These mice also give evidence for an increased ventricular vulnerability due to significant prolongation of atrial and ventricular conduction (Gardiwal et al., 2007). In humans, CSR3-expression is downregulated both in ischemic and dilative cardiomyopathy.

CSR3 was identified as novel phosphoprotein, with a novel phosphorylation site between the two LIM domains at Ser-95, which showed a 1.7 times enhanced phosphorylation upon iNOS derived NO release.

ABLIM1 is a known phosphoprotein which is phosphorylated upon DNA damage possibly by the tumor suppressor serine/threonine-protein kinases ATM or ATR. Ser-475 is known from phosphoproteomic studies of the brain. In the present study, phosphorylation was found to be increased by about 2.4 times, located between the N-terminal domain of four double zinc finger

motifs and the C-terminal cytoskeletal Villin headpiece domain (VHP). VHP is 50% identical to dematin, an F-actin-bundling protein of the erythroid cytoskeleton.

Microtubule associated protein 4 (MAP4) is regulated by phosphorylation at Ser-760 to control microtubule assembly. Like ABLIM1, MAP4 also gets phosphorylated upon genotoxic stresses by ATM or ATR. The phosphorylation site Ser-517 is known from brain and liver samples. Now it was found also in the heart and identified as a 2 times enhanced phosphorylation site upon 1 minute L-arg treatment (Fig. 4.27). Other non-phosphorylated peptides derived from MAP4 underline that the analysis started from the same protein amount in both heavy and light labeled mouse hearts.

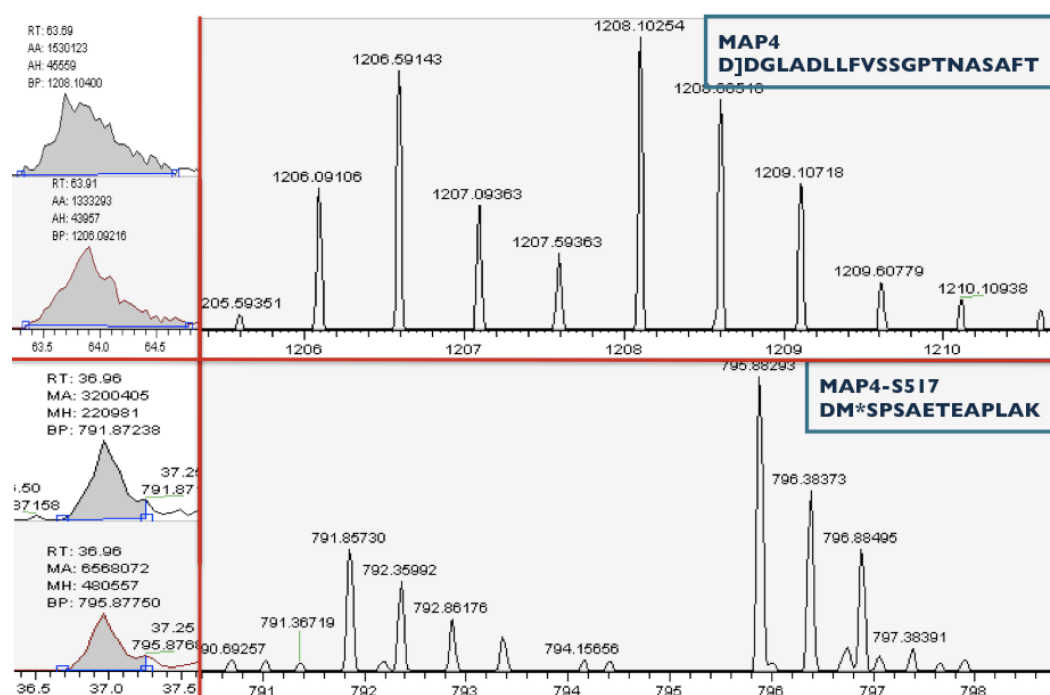


Figure 4.27: 1 minute L-arg treatment leads to a two times enhanced phosphorylation at Ser-517 in MAP4.

The cytoplasmic protein **phosphoglucosyltransferase-1 (PGMT1)** participates in both breakdown and synthesis of glucose by converting alpha-D-glucose 1-phosphate into alpha-D-glucose 6-phosphate. A known phosphorylation site of PGMT1 Ser-117 was found to be upregulated by factor of 1.4. This phosphorylation site was already identified by MS in HeLa cells.

Another glycolytic enzyme, **fructose-bisphosphate aldolase A (ALDOA)** which catalyses D-fructose 1,6-bisphosphate conversion into glyceraldehyde phosphate and D-glyceraldehyde 3-phosphate was also found to be increased phosphorylated at Ser-39 by 1.47 times.

Two other phosphorylation sites, one in **Ras GTPase-activating protein-binding protein 1 (G3BPI)** and an other in **Nuclear ubiquitous casein and cyclin-dependent kinases substrate (NUCKS)** were also found to become enhanced phosphorylated upon L-arg perfusion in iNOS⁺/myo^{-/-} mouse hearts. G3BPI phosphorylation at Ser-231 was already described in MS based phosphoproteome studies in different tissues, like liver, brain and in myoblast cell line,

but there is nothing known about its regulation. For detailed information about protein phosphorylation sites with enhanced phosphorylation upon iNOS derived NO release see table 4.8.

Table 4.8: List of phosphorylation sites found to be upregulated upon iNOS derived NO activation. Symbols of variable amino acid modifications: *: phosphorylation; #: methionine oxidation; ^: carbamidomethylation of cysteine;]: d2-dimethyl labeling of N-terminal amino acids; @: d2-dimethyl labeling of lysine (K). (XIC_L: integrated peak area of light (not treated with L-arg) peptide, XIC_H: integrated peak area of heavy (treated with L-arg) peptide. Orange color shows proteins which are listed in other tables, too.

Symbol	Protein name	Phos. site	Novel/ known	XIC _H / XIC _L	log ₂ (XIC _H / XIC _L)
PGMI	Phosphoglucosyltransferase-1 (EC 5.4.2.2) (Glucose phosphomutase 1) (PGM 1)				
	K.AIGGIILTAS*HNPGGPNGDFGIK.F	S-117	known	1.40	0.48
KAP0	cAMP-dependent protein kinase type I-alpha regulatory subunit				
	R.EDEIS*PPPPNPVVK.G	S-83	known	1.43	0.52
ALDOA	Fructose-bisphosphate aldolase A (EC 4.1.2.13) (Muscle-type aldolase) (Aldolase 1)				
	K.GILAADESTGS*IAK.R	S-39	known	1.47	0.55
G3BP1	Ras GTPase-activating protein-binding protein 1 (EC 3.6.1.-) (G3BP-1) (ATP-dependent DNA helicase VIII) (HDH-VIII)				
	K.STS*PAPADVAPAQEDLR.T	S-231	known	1.60	0.67
CLAPI	CLIP-associating protein 1 (Cytoplasmic linker-associated protein 1)				
	R.S]RS*DIVNAAASAK@.S	S-600	known	1.68	0.74
CSR3	Cysteine and glycine-rich protein 3 (Cysteine-rich protein 3) (CRP3) (LIM domain protein, cardiac)				
	K.GIGFGQGAGC^LSTDTGEHLGLQFQQ S*PKPAR.A	S-95	novel	1.69	0.76
MYPC3	Myosin-binding protein C, cardiac-type (Cardiac MyBP-C) (C-protein, cardiac muscle isoform)				
	R.DAS*PDDQGSYAVIAGSSK.V	S-72	novel	1.88	0.91
MAP4	Microtubule-associated protein 4 (MAP 4)				
	K.DMS*PSAETEAPLAK.N	S-517	known	2.05	1.04
NUCKS	Nuclear ubiquitous casein and cyclin-dependent kinases substrate (JC7)				
	K.G] IGFGQGAGC^LSTDT*GEHLGLQFQQSP K@PAR.A	S-19	known	2.27	1.19
ABLMI	Actin-binding LIM protein 1 (Actin-binding LIM protein family member 1) (abLIM-1)				
	R.T]LS*PTPSAEGYQDVR.D	S-475	known	2.38	1.25

5 DISCUSSION

5.1 GEL BASED PRELIMINARY STUDIES

In the present study I have elaborated methods which for the first time permit the analysis of the global cardiac phosphoproteome as influenced by endogenously formed NO. Before discussing the results obtained in a functional context, the initial gel based studies and same methodological aspect shall be considered.

In preliminary studies in myoglobin deficient (myo^{-/-} mice) hearts, I could show dephosphorylation of the Cytochrome c oxidase subunit Vb (COX5B) after perfusion with the NO donor SNAP (Fig. 4.2). COX5B is one of the nuclear-coded polypeptide chains of cytochrome C oxidase, the terminal oxidase of the mitochondrial electron transport (complex IV). NO is known to inhibit complex IV of the respiratory chain complex IV due to competition with oxygen at the heme groups at nanomolar concentrations (Brown et al., 1995).

In hearts with cardiac iNOS overexpression (iNOS⁺), during myoglobin blockade with CO, the observed functional and energetic impairment was considered to be due to the inhibitory action of NO on heme enzymes of the mitochondrial respiratory chain (Wunderlich et al., 2003). Furthermore, a reduced phosphorylation potential of the respiratory chain was predicted in a mouse model of cardiac iNOS overexpression together with lack of myoglobin (iNOS⁺/myo^{-/-} double mutant) showing in addition diminished oxygen consumption, decreased cardiac creatine phosphate levels and increased [P_i] and [ADP] (Gödecke et al., 2003). Thus, when myoglobin is lacking, SNAP-derived NO is likely to increase superoxide leakage from the electron transport chain, leading to peroxynitrite formation and protein phosphatase PPI and PP2A activation. This could explain the observed COX5B dephosphorylation.

Since the position of protein spots using the 2D-PAGE technique is determined by protein charge (1st dimension - horizontal) and size (2nd dimension - vertical), alterations in protein phosphorylation status can be detected by a spot shift in the horizontal and vertical position. The introduction of a strong negatively charged phosphate group on serine, threonine or tyrosine residues shifts the protein spot position by about 0.3 pH units to the acidic site. Furthermore, molecular mass is increased by 80 Da with each additional phosphate group. Therefore each additional phosphate group shifts protein spot position slightly left and up while each lost phosphorylation elicits the opposite effect.

Preliminary experiments were performed using 2D-PAGE based spot shift analysis to detect changes in protein phosphorylation level upon administration of the NO donor SNAP compared with the NOS inhibitor ETU. A drawback of 2D-PAGE is that this technique provides only a limited resolution and detection of site specific changes of protein phosphorylation is not possible. For example, although 2D-PAGE shows a protein spot shift, a sign of dephosphorylation upon SNAP perfusion, nanoHPLC-MS/MS analysis of the digested protein spot revealed phosphorylation at Ser-30 and at Ser-33 after both ETU (NOS inhibitor) and SNAP (NO donor) administration. Thus, 2D-PAGE based analysis does not provide information about which amino acid residue was phosphorylated or dephosphorylated. Furthermore, phosphorylation level can not be measured site specifically. There is in addition the possibility of further undetected COX5B phosphorylation sites, alterations of which could also induce protein spot shift during 2D-PAGE separation.

On the other hand, dephosphorylation of COX5B is underlined by the decreased MASCOT identification score of doubly phosphorylated peptide after SNAP perfusion, possibly a sign of reduced phosphopeptide amount, intensity and peptide phosphorylation level.

5.2 NEWLY ESTABLISHED METHODS FOR IMPROVED PHOSPHOPROTEOME ANALYSIS

In order to be able to introduce stable isotope dimethyl labeling method into the analytical workflow, labeling efficiency was optimized in the present study until unlabeled N-terminus or lysine residue could no longer be detected in standard and also in complex cardiac peptide mixtures (Fig. 4.8). The method was further validated by calibration using heavy and light dimethyl labeled digested casein as standard phosphoprotein mixed in different ratios with each other. Results showed a very good linear correlation between measured and theoretical heavy and light labeled peptide ratios. The small standard deviation suggests that dimethyl labeling is a valid method for the differential quantitation of phosphopeptides in tissue samples (Fig 4. 9 and 4.10).

Stable isotope dimethyl labeling was combined in the present study with phosphopeptide enrichment and peptide fractionation using SCX chromatography followed by nano flow RP-LC separation, on-line coupled with electrospray ionization to a tandem mass spectrometer (nanoRP-LC-ESI-MS/MS). Each step of this procedure was individually validated and finally enabled site specific detection and relative quantification of phosphorylated peptides to obtain a deeper insight into the cardiac signaling of NO.

5.3 STUDY MODEL: NO-INDUCED HEART FAILURE IN MICE

Use was made of the double transgenic mouse model ($iNOS^{+}/myo^{-/-}$) in which endogenously formed NO is responsible for heart failure. This model is characterized in-vivo by decreased left ventricular developed pressure (LVDP), contractility (dP/dt_{max}), ejection fraction and stroke volume (Gödecke et al., 2003). End-systolic and end-diastolic volumes were increased, resulting in a leftward shifted pressure volume loop, a sign of ventricular dilatation. In this model cardiac NO production was increase 40-fold. Thus, NO-induced heart failure includes nitrosative stress (peroxynitrite ($ONOO^{-}$) nitroxyl (NO^{-}) formation) and reactivated fetal gene expression program resulting in cardiac hypertrophy.

It is well known that extracellular L-arginine is required for NO synthesis by eNOS and iNOS (MacKenzie et al., 2003). I have therefore used the isolated mouse heart from $iNOS^{+}/myo^{-/-}$ mice perfused with or without L-arginine for the differential analysis of the cardiac phosphoproteome. Perfusion of hearts with L-arginine in a final concentration of 200 μ M - which is similar to in-vivo conditions – resulted in an immediate NO-induced decrease of the perfusion pressure (vasodilatation) which reached maximal values already after 1 min. Concomitantly cardiac contractile force (LVDP) and contractility (dP/dt_{max}) decreased by 29.1% and by 30.3%, respectively (n=6). Under the same conditions, as a sign of inhibited cytochrome c oxidase, O_2 consumption decreased by 16.4% and the ATP level decreased by 3.3%. Additionally, the AMP level was increased by 42.7% and the ADP level by 17.3%. Interestingly, the phosphocreatine (pCr) level

decreased stronger than ATP, by 11.3% and free phosphate (Pi/ATP) increased by 55.8%, showing a decreased cardiac energy pool under activated iNOS derived NO release (unpublished results by Dr. Ulrich Flögel).

This model has several advantages for the study of NO-induced phosphorylation of the heart. Firstly, NO is produced by the heart in sufficient amounts to induce stable and consistent functional effects (decrease in contractility and vasodilatation) Secondly, only one minute of L-arginine perfusion is required to reach a new functional steady state characterized by vasodilatation and reduced cardiac contractility. Thirdly, the short exposure time to endogenously formed NO assured, that the protein composition in the absence and presence of L-arginine can be considered to be the same

In an attempt to measure the global phosphoproteome I have used iNOS⁺/myo^{-/-} hearts perfused with and without L-arginine as a convenient model. As MS-based analysis technique I have applied the dimethyl labeling technique (Hsu et al., 2003) which was adapted and validated for the tissue examined.

5.4 OVERVIEW OF RESULTS

In repeated experiments this technique enabled me to identify a total of 826 phosphorylation sites (246 novel) in 772 phosphorylated peptides which relate to 475 proteins. In NO-induced heart failure 61 were upregulated (16 novel) and 47 downregulated (31 novel).

Distribution of phosphorylated amino acids were as follows: 671 Serine (81.2%), 150 Threonine (18.2%) and 5 Tyrosine (0.6%). Hunter described relative abundances of 90%, 10%, and 0.05% for phosphoserine (pS), phosphothreonine (pT), and phosphotyrosine (pY) in normally growing HBL-100 cells (Hunter and Sefton, 1980). A more recent mass spectrometry based phosphoproteome study suggests a distribution of pS, pT, and pY sites is 86.4%, 11.8%, and 1.8%, in stimulated HeLa cells (Olsen et al., 2006). This later published pS, pT and pY ratios are close to my finding.

5.5 NOVEL VS. KNOWN TARGETS OF iNOS-DERIVED NO SIGNALING

NO release resulted in increased phosphorylation of 64 serine (9.5% of serines), 9 threonine (6.0% of threonines) and 1 tyrosine (20% of tyrosines) and in decreased phosphorylation of 43 serine (6.4% of serines), 7 threonine (4.7% of threonines) and 2 tyrosine (40% of tyrosines), suggesting an important role of tyrosine phosphorylation upon NO. On the other hand, the fact that dynamic changes in tyrosine phosphorylation occur much faster and from a lower basal level compared to serine/threonine phosphorylation (Olsen et al., 2006) could result in higher changed pY ratios after one minute iNOS activation.

It has to be kept in mind that the isolated heart analyzed is comprised of endothelial cells, vascular smooth muscle cells, connective tissue and atrial but mostly ventricular cardiomyocytes. While ventricular cardiomyocytes are by far the dominant cell fraction on a weight basis, endothelial cells comprise about 2.8 % of the total heart (Anversa et al., 1983). The fraction of vascular smooth

muscle cells is most likely even lower. If not otherwise indicated the phosphoproteins identified in this study are to all likelihood of cardiomyocytic origin.

5.5.1 NO-INDUCED VASCULAR SMOOTH MUSCLE RELAXATION

In vascular smooth muscle cells (VSMC), NO works classically via the NO/cGMP/PKG signaling pathway, activating/inhibiting downstream targets by PKG induced phosphorylation, leading to decreased cytosolic Ca^{2+} concentration and VSMC relaxation (schematically shown in Fig. 5.1).

Although relative ratio of vascular smooth muscle in the heart is likely to be very low, I was able to identify a novel phosphorylation site in a protein specific for smooth muscle, called **Myosin regulatory light chain 2-B, smooth muscle isoform** (Mylc2b or **MRLC2**). This protein plays an important role in regulation of smooth muscle cell contraction and relaxation. In the presence of calcium and calmodulin, Myosin light chain kinase (MLCK) phosphorylates MRLC2 at Ser-19 and Thr-20, increasing the actin-activated myosin ATPase activity which leading to contraction. MRLC2 dephosphorylation is activated by the NO/cGMP/PKG pathway which in turn activates Myosin light chain phosphatase mediated relaxation. Myosin is a hexamer of two heavy and four light chains.

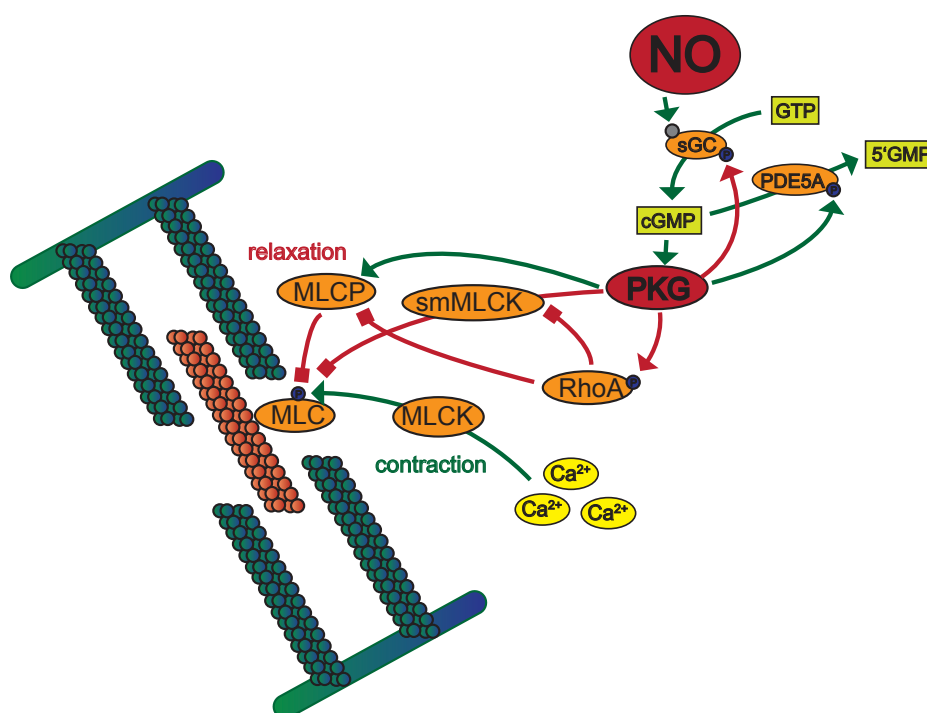


Fig 5.1: NO/cGMP/PKG signaling in vascular smooth muscle cells. PKG phosphorylates numerous targets and thereby activates (green arrow) or inhibits protein activity (red arrow), leading to vascular smooth muscle relaxation. Red blunt arrow means inactivation; red blunt arrow showing to a P represent inactivation by protein dephosphorylation and small grey bubble shows heme-nitrosylation. NO: nitric oxide, sGC: soluble guanylyl cyclase, GTP: guanosine triphosphate; cGMP: cyclic guanylyl monophosphate; PKG: cGMP dependent protein kinase; PDE5A: Phosphodiesterase 5A; 5'GMP: guanosine monophosphate; smMLCK: smooth muscle myosin light chain kinase; MLCK: Ca-independent MLC kinase; MLCP: Myosin light chain phosphatase; MLC: myosin light chain.

Results obtained in the present study shows MRLC2 dephosphorylation at the novel phosphorylation site Ser-29 by 47% (identified in an isoform specific peptide - blasted against non-redundant Swissprot sequences). Decreased phosphorylation at Ser-29 very likely contributed to the observed NO-induced **VSMC relaxation** leading to drop in perfusion pressure.

Although atrial cardiomyocytes are also a low abundant cell population in the heart, the present study identified an atrial specific phosphorylated peptide of the **myosin regulatory light chain 2, atrial isoform (Myl7)**, peptide was blasted against non-redundant Swissprot sequences). In this protein a novel phosphorylation site at Ser-27 was identified, which was decreased by 67% upon iNOS derived NO release, presumably taking part in NO-induced relaxation of atrial cardiomyocytes.

5.5.2 CALCIUM HOMEOSTASIS DURING EXCITATION-CONTRACTION COUPLING

As schematically shown in Fig. 5.2 the action potential reaches the contractile myocytes through gap junctions which triggers the L-type Ca^{2+} channels ($\text{Ca}_v1.2$, or LTCC) causing a relatively small net flux of Ca^{2+} ($I_{\text{Ca}2+}$) into the cardiac myocytes.

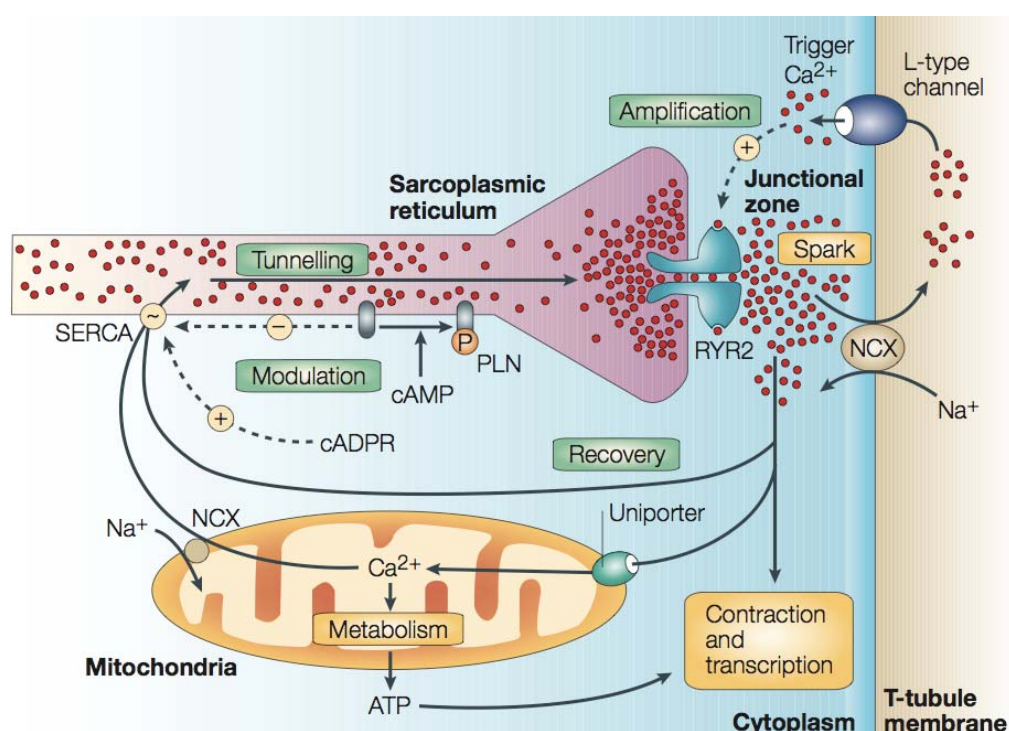


Figure. 5.2: Cardiac calcium signaling. Depolarization trigger L-type channel on the T-tubule membrane to introduce a small pulse of trigger Ca^{2+} , which then diffuse across the narrow gap of the junctional zone to activate ryanodine receptor 2 (RYR2) to generate a Ca^{2+} spark (Ca^{2+} is shown as red circles). This localized Ca^{2+} diffuses out to the sarcomere, to activate contraction and perhaps also gene transcription. Recovery occurs as Ca^{2+} is pumped out of the cell by the $\text{Na}^+/\text{Ca}^{2+}$ exchanger (NCX) or is returned to the sarcoplasmic reticulum (SR) by sarcoplasmic Ca^{2+} ATPase (SERCA). SERCA acts at the non-junctional region of the SR. A proportion of Ca^{2+} stimulates mitochondrial metabolism to provide ATP necessary for contraction and transcription. The SERCA pumped returning Ca^{2+} 'tunnels' back to the junctional zone to be used again in the next contraction. Ca^{2+} circulation is modulated by several factors, for example second messengers such as cyclic AMP (cAMP) removes the inhibitory action of phospholamban (PLN), or cyclic ADP ribose (cADPR) activates SERCA to pump Ca^{2+} into the SR thereby increases releasable Ca^{2+} for the next cycle. (Figure was taken from Berridge et al., 2003)

This increased intracellular calcium ion concentration triggers the release of a larger amount of Ca^{2+} from the sarcoplasmic reticulum (SR) via ryanodine receptor 2 (RyR2, or Cardiac Ca^{2+} release channel) in a process called Ca^{2+} -induced Ca^{2+} release. The cytoplasmic calcium binds to troponin C allowing the myosin head to bind to the actin filament by moving the tropomyosin complex off the actin binding site. Following ATP hydrolysis, the myosin head pulls the actin filament to the centre of the sarcomere leading to muscle contraction. Between beats (diastole) Ca^{2+} is transported out of the cytosol allowing myofilament deactivation and relaxation. Sarcoplasmic/endoplasmic reticulum calcium ATPase 2 (SERCA2a) pumps Ca^{2+} into the SR or it is transported out of the cell by the sarcolemmal Na^+ - Ca^{2+} exchanger (NCX) or by plasma membrane Ca^{2+} ATPase.

Cardiac gap junctions are essential for conduction of the electrical impulse from one cell to the other, which enables coordinated contraction of the heart. **Connexin-43 (Cx43, or Gja1)** is the primary gap junction protein in the ventricles. The presence of Cx43 prevents post-infarct arrhythmias by improving intercellular coupling. Transplantation of skeletal myoblasts genetically engineered to express Cx43 into the myocardial infarct has a protective potential, suggesting strategies for cardiac cell-based therapy. (Roell et al., 2007). Various kinases, including PKA, PKC, p34cdc2(cyclin B kinase), casein kinase I (CKI), MAPK and Src were reported to phosphorylate Cx43 and thereby regulate its cellular localization and channel conductance (Solan et al., 2009). Interestingly, NO depresses Cx43 expression level after myocardial infarction (Jackson et al., 2008).

In the NO-induced heart failure model studied I found three phosphorylation sites to be increased: Ser-305 (+149%), Ser-324 and Thr-325 (+54% both). Interestingly, Ser-305 was reported to be fully dephosphorylated after 7 min of ischemia, whereas Ser-324 remained phosphorylated (Axelsen et al., 2006). Ser-324 is known to be a CKI δ target, phosphorylation of which is present only in gap junctions and may regulate gap junction assembly and influence channel permselectivity (Cooper et al., 2002; Lampe et al., 2006; Solan et al., 2007). Thus, iNOS derived NO most likely influenced electrical impulse conduction through connexin-43 in the heart.

L-type Ca^{2+} channel ($\text{Ca}_v1.2$), the regulatory protein of the cardiac excitation-contraction (E-C) coupling, contributes to the plateau phase of the cardiac action potential, have pacemaker activity in nodal cells and modulates gene expression. Neurotransmitters and hormones can regulate cardiac contraction through Ca^{2+} current modulation by cAMP and cGMP dependent phosphorylation of $\text{Ca}_v1.2$. In cardiac myocytes, PKG is able to phosphorylate **α_{1c} subunit of $\text{Ca}_v1.2$ (Cacna1c)** at Ser528, Ser533, and Ser1928 (Yang et al., 2007). In the present study, I identified a novel phosphorylation site at Ser-1659 of isoform 2 of Cacna1c. This site, however remained unchanged upon iNOS-induced NO-formation.

On the other hand I found decreased phosphorylation of Isoform 4 of **$\text{Ca}_v1.2$ subunit β -2 (Cacnb2)** at Ser-470 (novel). Cacnb2 contributes to the channel activity by increasing peak calcium current, shifts the voltage dependencies of activation and inactivation, modulates G protein inhibition and controls the targeting of the alpha-1 subunit. Interestingly, β_{2a} subunit is phosphorylated by PKG at Ser-522 (rabbit, equal to Ser-463 Cacnb2 isoform 4, mouse) leading to channel inhibition and reduced $\text{Ca}_v1.2$ current (Yang et al., 2007). In contrast, Cacnb2 is known to

be activated by CaMKII dependent phosphorylation at Thr-498, increasing channel open probability (P_0) to dynamically increase Ca^{2+} current (I_{Ca}) and augment cellular Ca^{2+} signaling (Grueter et al., 2006 and 2008). Thr-498 (isoform 2, rat is equal to Thr-467, Cacnb2 isoform 4, mouse) phosphorylation site is only three amino acid far away from the identified novel phosphorylation site Ser-470, therefore it could have similar way of action. Decreased phosphorylation upon iNOS derived NO release may decrease Ca^{2+} current into cardiac myocytes and possibly contributes to the reduced contractility.

Interestingly, NO has been shown to have variable effects - inhibition, activation or both - on $\text{Cav}1.2$ current in the heart, depending on species, age and cardiac myoglobin content. The observed dephosphorylation may derive from NO dependent G protein-coupled receptor kinase I (substrate motif: XX[pS/pT]E) or Casein Kinase I (substrate motif: [pS/pT]XX[S/T]) inactivation all of which could target Ser-470.

In the myocardium, **Ahnak** interacts with L-type Ca^{2+} channel subunit β -2 via multipoint attachment mediated by ahnak's carboxyl terminal domains C1 and C2 (aa4646-5288 and aa 5262-5643)(Alvarez et al., 2004). Furthermore, Ile5236Thr mutation of the Ahnak C1 domain decrease ahnak-C1/ $\text{Cav}1.2$ - β -2 interaction, increasing cytosolic Ca^{2+} current (I_{CaL}) by 60% (Haase et al., 2005). Thus, ahnak-C1/ $\text{Cav}1.2$ - β -2 interaction inactivates L-type Ca^{2+} channel, which inhibition is slowed down by PKA phosphorylation (Fig. 5.3.A) or by mutation at Ile5236Thr. This changes results in blunted β -adrenergic responsiveness, triggering the fight or flight response of the heart. Patients with cardiac hypertrophy (Schröder et al., 1998). Interestingly, ahnak protein provides a link between $\text{Cav}1.2$ and the actin based cytoskeleton. (Hohaus et al., 2002). The endogenous carboxyl-terminal 72 kDa ahnak fragment (C2) is localized to the intercalated discs and close to the Z-line of cardiomyocytes, induces actin bundling and stabilizes muscle contraction (Haase et al., 2004).

Ahnak can be phosphorylated by PKA and PKB (=Akt), leading to attenuated interaction and increased I_{CaL} . A recent report shows that Ahnak can activate PKC by dissociating the PKC-protein phosphatase 2A complex (Lee et al., 2008). Phospholipase C-gamma1 (IP_3 synthesis, leading to contraction) can be also activated through Ahnak -mediated PKC stimulation. (Lee et al., 2004).

In this the large, propeller like protein I identified 11 phosphorylation sites (4 novel), of which one was enhanced (in the head region, at Ser-116) and the other was decreased (near to the C-terminus, within the C1 domain, at Thr-4950) phosphorylated upon iNOS derived NO release. Although changes in phosphorylation level were slightly under the cut off score for regulation (tendency, not significant change) they could have relevant functional effects such as decreased I_{CaL} (Fig. 5.3.B), altered response to β -adrenergic regulation and ahnak's stabilizing effect on muscle contractility could be affected.

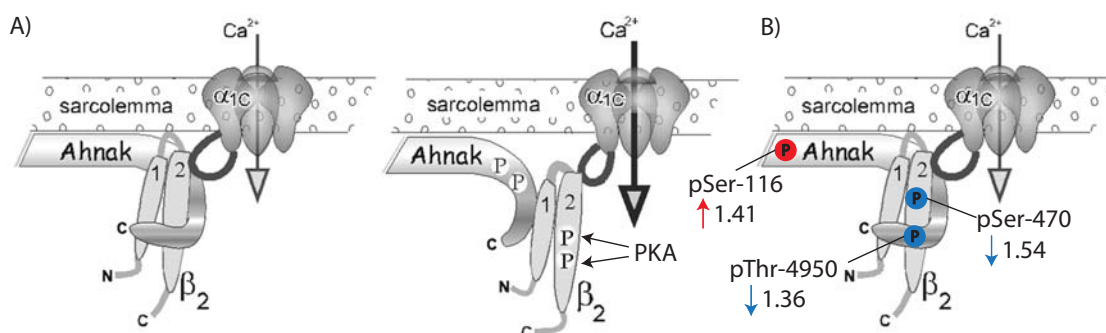


Fig. 5.3: A) Proposed model for sympathetic control of I_{CaL} by ahnak/ Ca^{2+} channel binding. Under basal conditions (left panel), α_{1C} subunit of $Ca_v1.2$ is re-primed by strong ahnak-CI/ β_2 subunit binding, resulting normal I_{CaL} . Upon sympathetic stimulation, PKA phosphorylates β_2 subunit of $Ca_v1.2$ at Ser-478 and 479, leading to attenuated ahnak-CI/ β_2 binding and increased I_{CaL} . Additionally, Ile5236Thr mutation have the same effect also. B) iNOS derived NO release induced decreased phosphorylation of Ser-470 $Ca_v1.2$ - β_2 subunit together with decreased phosphorylation of Thr-4950 ahnak-CI and increased phosphorylation at the ahnak-N-terminal region Ser-116 which may result in a reduced I_{CaL} . (Fig. was modified from Haase et al., 2005).

During relaxation, **SERCA2A** (cardiac specific isoform of SERCA, SERCAI is skeletal muscle isoform) transports Ca^{2+} into the SR thereby decreasing cytoplasmic calcium levels leading to relaxation and increasing the SR Ca^{2+} available for next contraction. Upon iNOS derived NO release, no change was detected at the phosphorylation site Ser-663. This phosphorylation site is known from brain and cell (HeLa, TERT20) based studies, this work provide the first evidence for SERCA2a-Ser-663 phosphorylation in the heart.

Activity of SERCA2A is known to be influenced by interaction and binding partners like **Cardiac phospholamban (PLB)**, Histidine rich calcium binding protein (Hrc) and Calnexin precursor (Canx). Unphosphorylated Plb protein inhibits SERCA2A activity due to binding to SERCA, whereas PLB phosphorylation at Ser-16 by PKA or PKG or at Thr-17 by CaMKII relieves this inhibition. Thus, PLB is one of the important factors in the regulation of myocardial relaxation and contractility. I could identify 77% increased phosphorylation at Thr-17 upon iNOS derived NO release. In the presence of Ca^{2+} and calmodulin, CaMKII autophosphorylates itself at Thr-286 leading to kinase activation resulting in concomitant PLB-Thr17 phosphorylation, SERCA2a activation and Ca^{2+} transport into the SR. Frequency-dependent increase of cardiac contractility was shown upon PLB-Thr17 phosphorylation (Zhao et al. 2004). In discrepancy with this finding, Mills et al. (2006) reported that Thr-17 phosphorylation reduces cardiac adrenergic contractile responsiveness in chronic pressure-overload induced hypertrophy. Therefore, this PLB-Thr17 phosphorylation is possibly a part of secondary compensatory mechanisms, working against total heart holdup induced by huge amount of NO-release by iNOS, or a part of heart failure pathophysiology. Interestingly, PLB-Thr17 phosphorylation and CaMKII activity vary in the different heart failure models. As Fig. 5.4 shows, other molecules of the excitation-contraction coupling are also CaMKII targets.

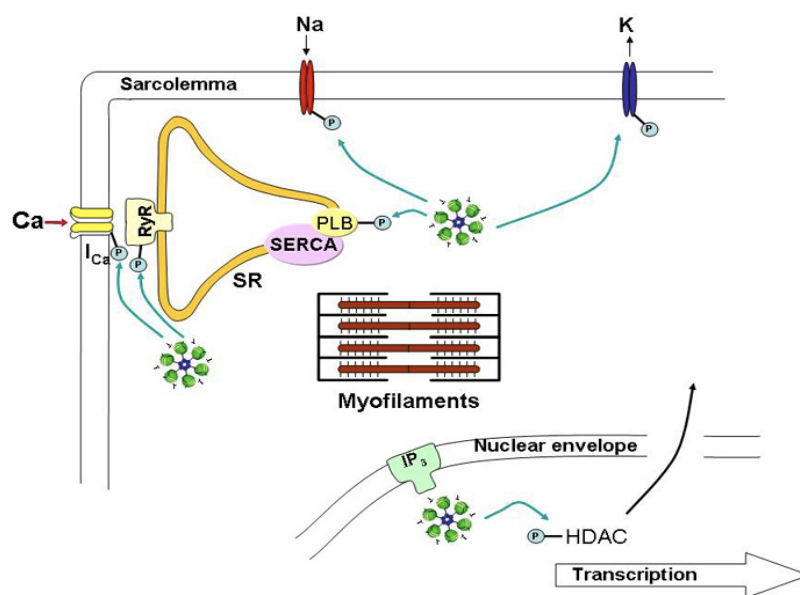


Fig. 5.4: Simple scheme of the effects of CaMKII on excitation-contraction coupling (ECC) and excitation-transcription coupling (ETC). CaMKII phosphorylates Ca-handling proteins such as phospholamban (PLB), SR Ca release channels (RyR), and L-type Ca channels responsible for Ca influx (I_{Ca}). In addition, Na and K channels are regulated by CaMKII. In addition, CaMKII may be activated by local Ca^{2+} -release in the nucleus through IP_3 receptors thereby phosphorylating HDAC leading to nuclear export and transcription (Figure was taken from Mailer et al., 2009).

This work identified furthermore a double phosphorylated PLB peptide with phosphorylation at Ser-16 and Thr-17. This peptide showed only 20% enhanced phosphorylation upon iNOS activation. If we take into account, that signal intensity of singly phosphorylated peptide with pThr-17 showed 77% increase, than it seems to be logic that first CaMKII dependent phosphorylation takes place at Thr-17 upon increased cytosolic Ca concentrations, followed by PKA phosphorylation of the Ser-16 PLB residue. The other possible mechanism would be, that NO-release induces very fast phosphorylation of both Ser-16 and Thr-17 residues, followed by Ser-16 dephosphorylation leading to the 20% increased double phosphorylated and the 77% increased single phosphorylated peptides. To ensure this hypotheses, time resolved experiments would be necessary.

Sarcalumenin (SRL), is another important SERCA2a cofactor and Ca^{2+} -shuttle and ion-binding protein, locating in the lumen of the sarcoplasmic reticulum. Yoshida and his colleagues (2005) reported an impaired Ca^{2+} store function in sarcalumenin-deficient mice ($Srl^{-/-}$) due to weakened Ca^{2+} uptake activity (-30%) into the SR. This finding suggest, that Srl contributes to Ca^{2+} buffering and maintenance of Ca^{2+} pump proteins. Furthermore, impaired Ca^{2+} transients lead to slowed contraction and relaxation in sarcalumenin lacking cardiac myocytes and to impaired cardiac function in $Srl^{-/-}$ mice. Shimura et al. (2008) showed that SRL coimmunoprecipitates and enhances SERCA2a half-life in transfected HEK293 cells, suggesting an essential role of SRL in preserving cardiac function under biomechanical stresses such as pressure overload. Interestingly, SRL protein expression was found to be reduced in cardiac Duchenne muscular dystrophy fibers (Lohan et al., 2004).

Present study shows an increased phosphorylation at Ser-442 (+60%) and at Ser-304 (+30%) of Isoform I of Sarcalumenin (SRL) upon iNOS derived NO release. Ser-442 phosphorylation site is

located in a G protein-coupled receptor kinase I substrate motif XX[pS/pT]E and in a Casein Kinase II (CKII) substrate motif (pSX[E/S/T]. Hadad et al., (1999) showed that SRL can be phosphorylated in the endogenous SR phosphorylation system by CKII. Unfortunately, except for an MS based study to discover novel phosphorylation sites in liver (Dai et al., 2007), there is no information about SRL phosphorylation and its functional consequences.

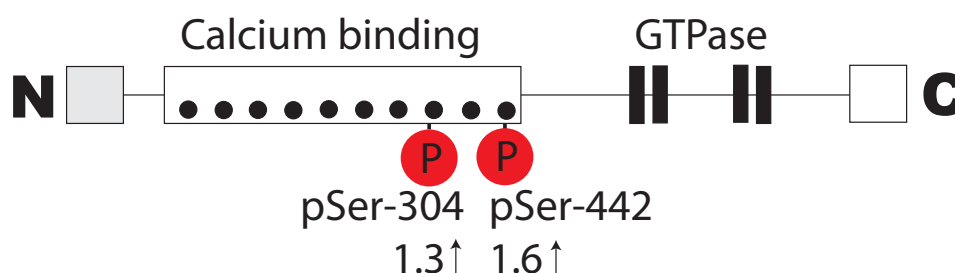


Fig. 5.5: Schematic view of sarcalumenin (SRL) calcium binding protein of the sarcoplasmic reticulum. Ser-304 and Ser-442 are enhanced phosphorylated upon iNOS derived NO release, by 1.3 and 1.6 times respectively. Thus, NO induce introduction of two negatively charged phosphogroups into the Srl Ca^{2+} binding domain thereby inducing sarcalumenins Ca^{2+} binding properties and enhance the Ca^{2+} storage capacity of the sarcoplasmic reticulum.

Taking into account that oxidative phosphorylation mostly changes protein conformation, interaction and activity, the observed increased Ser-442 and Ser-304 phosphorylation sites located in the Ca^{2+} binding domain (aa 21-459) of the protein (Fig. 5.5), most presumably alters sarcalumenins Ca^{2+} binding capacity, its effect on SERCA2a activity thus, speed of Ca^{2+} uptake into the SR and cardiac contractility thereby contributing to the observed experimental effects of iNOS derived NO release.

CKII also targets an other SERCA2a cofactor, the **Histidine rich Ca^{2+} binding protein (HRC)**. Hrc is located in the SR lumen where it binds Ca^{2+} with low affinity and high capacity. At higher Ca^{2+} concentrations its dissociating into dimers or trimers from the original pentameric structure (Suk et al., 1999), possibly to increase its Ca^{2+} binding properties. HRC overexpression leads to increased SR Ca^{2+} storage capacity (Kim et al., 2003), to ventricular dysfunction, associated with depressed maximal SR Ca^{2+} uptake rates (Gregory et al., 2006). Interestingly, cardiac specific HRC overexpression protects against ischemia/reperfusion-induced cardiac injury possibly by inhibition of apoptotic cell death (Zhou et al., 2007). In details, decreased free SR Ca^{2+} content and subsequent oscillatory Ca^{2+} release could result in attenuated cytosolic Ca^{2+} preventing mitochondrial Ca^{2+} overload which in turn decrease PTP opening probability and repress mitochondrial-mediated apoptotic and necrotic cell death.

On the other hand in mice lacking the histidine-rich calcium-binding protein showed reduced skeletal muscle and fat mass, upregulated triadin expression and an exaggerated response to cardiac hypertrophy induction by isoproterenol (Jaehnig et al., 2006). Furthermore, Ser96Ala HRC variant was associated with life-threatening ventricular arrhythmias in idiopathic dilated cardiomyopathy patients (Arvanitis et al., 2008).

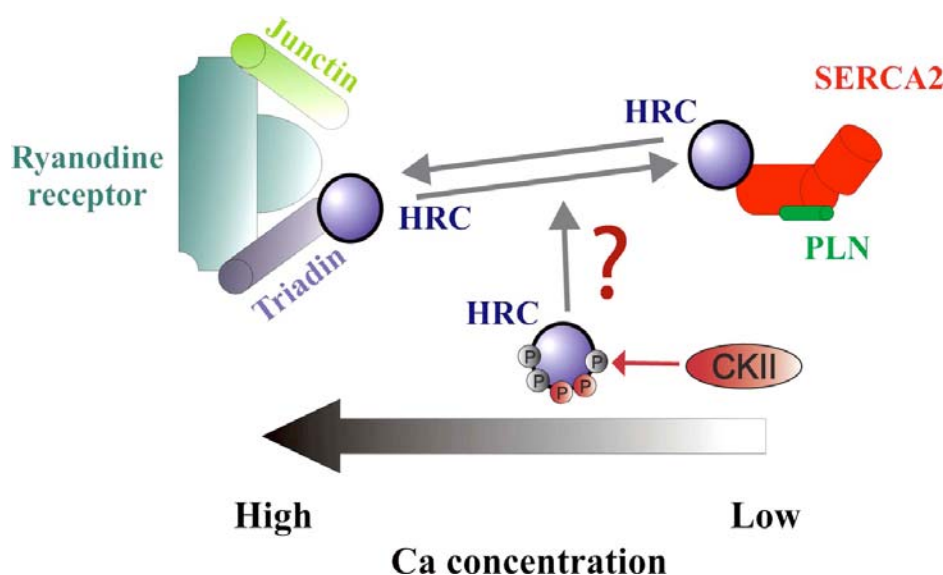


Fig. 5.6: In the SR lumen of cardiac myocytes, HRC may interact with SERCA2a and triadin (RyR2 cofactor) on a calcium concentration dependent manner, possibly playing a critical coordinating role in cardiac SR Ca^{2+} handling. Upon iNOS derived NO release two phosphorylation site was found to be increased phosphorylated (red) and three other phosphorylation site was not influenced (gray). Ser-272 is possibly a target of CKII, an endogenous protein kinase of the SR (modified from Arvanitis et al., 2007).

As figure 5.6 shows, HRC was described as a possible mediator between SERCA2a (Ca^{2+} uptake into the SR) and Ryanodine (Ca^{2+} release into the cytosol) receptor, due to its Ca^{2+} -dependent direct binding to SERCA2a and triadin (Fig. 5.6). Thus, HRC may play a critical role in coordinating sarcoplasmic reticulum Ca^{2+} uptake and release (Arvanitis et al., 2007). Up to date, four phosphorylation sites of HRC were detected in large scale phosphoproteome studies, no additional functional information is available.

In the present study I identified five HRC phosphorylation sites, four novel and one known in the hypertrophy model *iNOS⁺/myo^{-/-}* mouse heart. NO induced phosphorylation in the Ca^{2+} binding domain of the protein, at Ser-272 by 1.6 times and at Ser-474 residue by 1.3 times. Three further phosphorylation sites at Ser-104, Ser-129, and Ser-572 (outside of the Ca^{2+} binding domain) showed no changes under this conditions. Ser-272 is predicted to be phosphorylated by CKII or β -adrenergic receptor kinase, alike published by Hadad et al. (1999). HRC phosphorylation can take place if Ca^{2+} , high concentrations of NaF and additional GTP or ATP are present, furthermore if ryanodine binding is inhibited parallel to the phosphorylation of SRL and HRC.

Due to the additional negatively charged phosphate groups, phosphorylation may increase Ca^{2+} binding capacity of HRC (Fig. 5.7) and therefore may contribute to its action in the SR and as antiapoptotic protein. Furthermore, Ca^{2+} uptake into the SR may also positively influenced upon NO-induced phosphorylation, leading to decreased cytosolic calcium concentrations and reduced contractility.

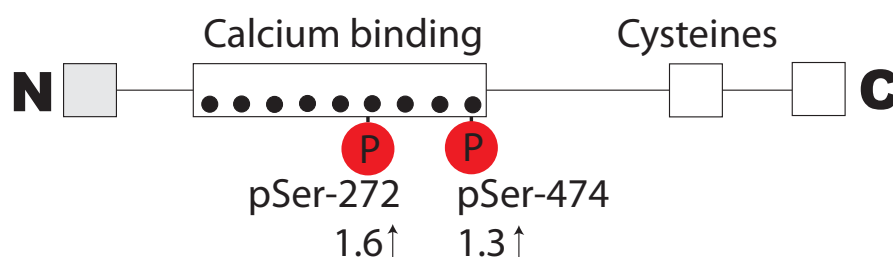


Figure 5.7: NO induced phosphorylation of histidine rich calcium binding protein in the Ca^{2+} binding domain, at Ser-272 and Ser474. Similar to sarcalumenin, the additional negatively charged phosphate groups most likely enhance the positively charged calcium ion affinity capacity and thereby the SR Ca^{2+} storage.

The **ryanodine receptor** (RyR2) on the sarcoplasmic reticulum (SR) regulates Ca^{2+} homeostasis in cardiac myocytes by releasing calcium from the sarcoplasmic reticulum into the cytosol. In the healthy heart, Ca^{2+} influx and efflux is in a balance giving progressively stable Ca^{2+} levels in the cell and in the SR. In diastole, there is still a small SR Ca^{2+} leak via the RyR2, which Ca^{2+} leakage is increased under pathological conditions in failing heart leading to reduced systolic function by a decreased SR Ca^{2+} content and to arrhythmogenic inward current via the sodium/calcium exchanger (NCX), developing delayed afterdepolarizations. RyR2 can be phosphorylated by PKG, PKA, PKC and CaM (Takasago et al., 1991, targeted amino acid is not determined). Marx et al. (2000) has shown that RyR2 is hyperphosphorylated by PKA in failing hearts may be due to decreased level of associated phosphates PPI and PP2A. On the other hand, PPI expression levels were shown to be higher in failing hearts. Hyperphosphorylated RyR2 dissociates the regulatory subunit FKBP12.6 from the channel increasing RyR2 Ca^{2+} sensitivity leading to a RyR2 activation at resting levels of cytosolic Ca^{2+} . However, other groups disputed these findings. In summary, it is unclear if PKA phosphorylation influence RyR function (Lim et al., 2008).

In failing (CMI) hearts, an enhanced Ser-2808 phosphorylation of RyR2 was reported by Xiao et al., 2006. The calcium release channel can be phosphorylated at Ser-2808 by PKGI, PKA and CaMKII. In the present study, I could identify a triple phosphorylated peptide RlpSQpTpSQVSDAAHG YSPR from this region with a phosphorylation at Ser-2808 (known), Thr-2810 (novel) and Ser-2811 (novel). This peptide shown about 40% enhanced signal intensity (means 40% summarized phosphorylation enhancement for all three sites) upon iNOS derived NO release, slightly under the cut off score for regulation. Xiao and his colleagues shown an already high phosphorylation degree for Ser-2808 in native mouse RyR under normal conditions, which could explain that intensity changes upon activation couldn't reach a significant level just a tendency for regulation. Furthermore technical setup determines only summarized changes of all phosphorylation excluding the possibility to measure site specific changes of phosphorylation dynamics. Thus, phosphopeptide enrichment methods resulting mostly in single phosphorylated peptides is of advantage. Therefore, titanium dioxide phosphopeptide enrichment method was preferred over immobilized metal affinity chromatography (IMAC), which result multiple phosphorylated peptides in a higher rate.

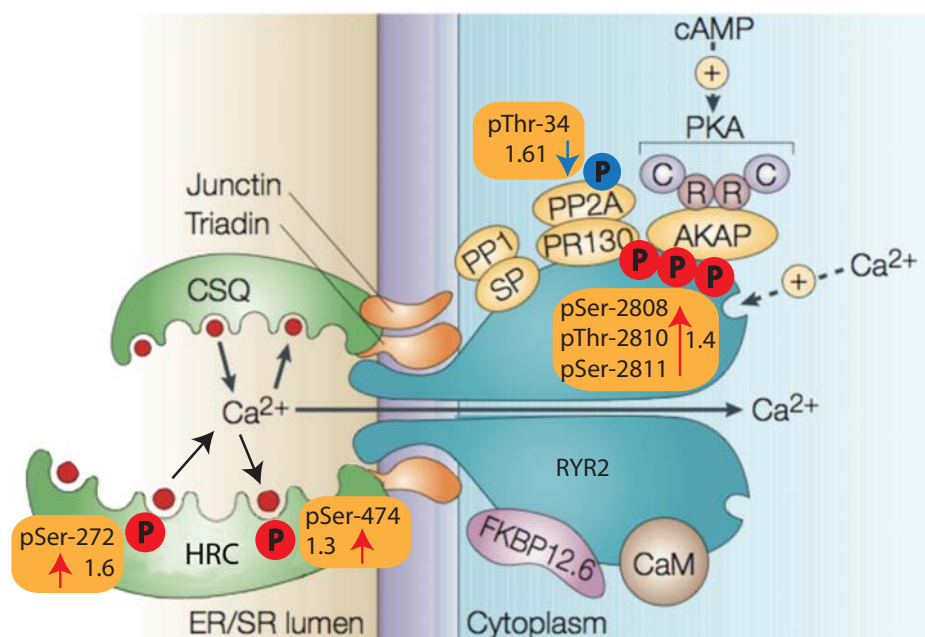


Fig. 5.8: The Ryanodine receptor 2 (RyR2) Ca^{2+} -release complex in cardiac cells. Various proteins modulate channel opening potential, like the Ca^{2+} binding protein calsequestrin (CSQ) and possibly the histidine rich calcium binding protein (HRC). Interaction between RyR2 and CSQ is facilitated by the transmembrane proteins triadin and junctin, between RyR2 and HRC only by triadin. RyR2 can be reversibly phosphorylated by PKA (attached through the A kinase anchoring protein (AKAP)) and dephosphorylated by protein phosphatase 2A (PP2A) (attached through the isoleucine-zipper-binding scaffolding protein (PR130)), and by protein phosphatase 1 (PP1) (attached through spinophilin (SP)). RyR2 is also modulated by calmodulin (CaM) and by FK506-binding protein 12.6 (FKBP12.6). iNOS derived NO induced phosphorylation of RyR2, HRC and dephosphorylation of PP2A (Figure was modified from Berridge et al., 2003).

In summary, enhanced RyR2 phosphorylation at Ser-2808, at Thr-2810 and at Ser-2811 upon iNOS derived NO release could possibly contribute to the hyperphosphorylated “leaky channel” syndrome, leading to cardiac dysfunction obtained in heart failure (Fig. 5.8).

Interestingly, whereas RyR2 phosphorylation increased about 40%, **B56 delta subunit of protein phosphatase 2A (PP2A)** was dephosphorylated about 60% at the novel phosphorylation site Thr-34. PP2A can build a macromolecular complex with RyR2 and other proteins (Fig. 5.7), therefore dephosphorylation of the PP2A regulatory subunit B56 delta may inhibit its phosphatase activity leading to an increased RyR2 phosphorylation. Similarly, it was already reported, that PKA activates PP2A B56 delta by phosphorylation at Ser-566 (Ahn et al., 2007).

5.5.3 NO-TARGETED CONTRACTILE PROTEINS

As shown in Fig. 5.9, during the contraction/relaxation cycle Ca^{2+} binds to troponin C resulting in the conformational change in troponin, which in turn, releases α -tropomyosin from its position and thereby uncovers the actin myosin binding site.

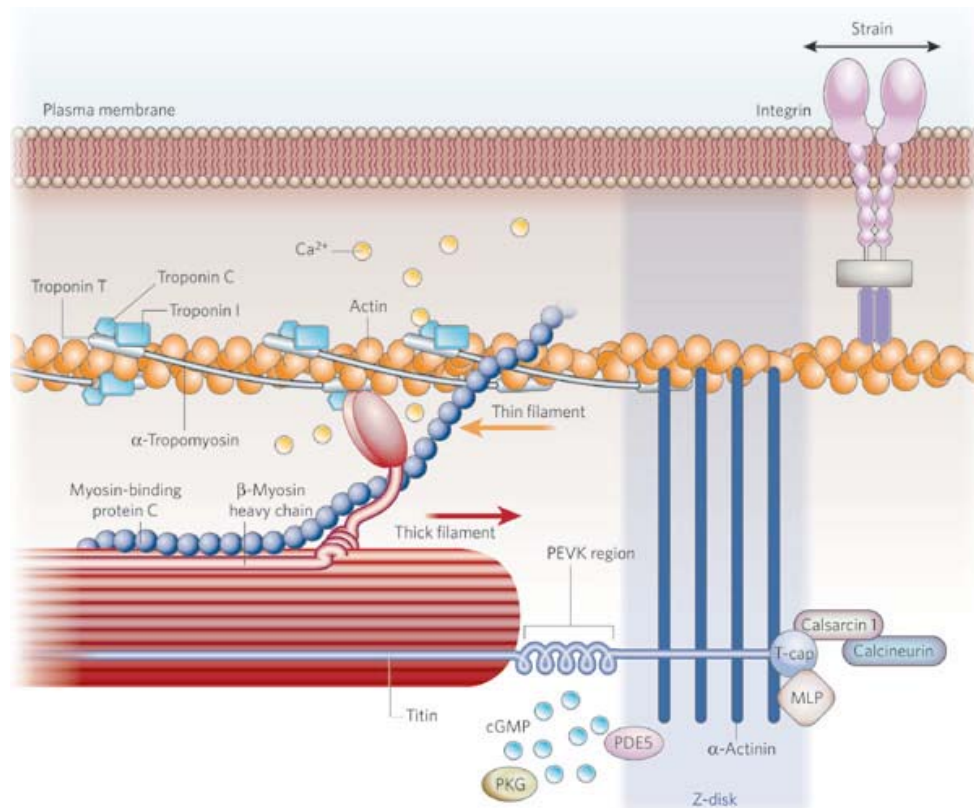


Fig. 5.9: Structural and motor proteins of cardiac contraction. Integrins transduce mechanical stimuli to the sarcomeric Z-disc where calsarcin 1, muscle lim protein (MLP or CSRP3) and titin cap (T-cap) are localized. These proteins interacting with α -actinin, titin, actin and other proteins to couple the input from the integrin to the contractile filaments. Ca^{2+} - troponin C interaction allows myosin head to bind actin, forming the force-generating crossbridges. Regulatory proteins of the thin filament, like troponin T, troponin C, troponin I and myosin binding protein C as well as titin can be regulated by phosphorylation/dephosphorylation. For example, PDE5 regulated cGMP pools activate PKG, reducing myofilament Ca^{2+} sensitivity resulting in depressed contraction. In the failing heart titin phosphorylations was shown to cause contractile dysfunction. (from Mudd et al., 2008).

Once the head region of myosin heavy chain (MHC) is properly attached to the actin subunit, bound inorganic phosphate (P_i) is released. This strengthens the binding of MHC to actin and triggers the formation of force-generating crossbridges which moves the actin filament and leads to sarcomere shortening. ADP then dissociates and ATP binds to the anti nucleotide binding site causing the myosin head to detach from the actin filament. On the detached head ATP is hydrolyzed, and the resulting energy is used to move the myosin head conformation back into the prestroke state. This contractile cycle is repeated as long as Ca^{2+} and ATP are present. When Ca^{2+} is pumped back into the sarcoplasmic reticulum (SR), the tropomyosin conformation changes into its previous state, thereby blocking the myosin binding sites of actin, finally leading to muscle relaxation.

The phosphorylation state of the following proteins was found to be altered in the NO-induced heart failure model:

α -MHC (Myosin-6, Myh6) and its isoform **β -MHC (Myosin-7, Myh7)** display an almost identical (93%) amino acid sequence. Muscle myosin is a hexameric protein that consists of 2 heavy chain subunits (MHC), 2 alkali light chain subunits (MLC) and 2 regulatory light chain subunits (MLC-2). Normally, α -MHC is the protein predominantly expressed in adult mouse hearts, while β -

MHC is observable only in distinct heart areas such as at the tip of papillary muscles and at the base close to the valvular annulus (Krenz et al., 2007). In the human heart, β -MHC is predominantly expressed (93%) which reaches 100% in heart failure patients. Interestingly, β -MHC has a lower actomyosin ATPase activity and a lower actin filament sliding velocity, however, energy consumption is more economical. α -MHC is an actin based ATPase motor activity supports movement toward the (-) end of actin (Fig. 5.10).

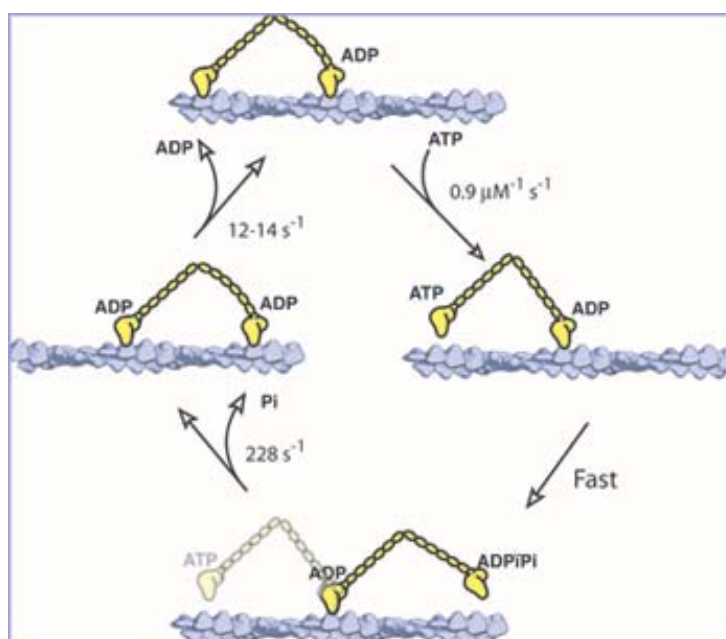


Fig. 5.10: ATP-driven Myosin heavy chain (Myh6) movement on actin. First, calcium binds to the troponin complex allowing myosin to bind actin followed by ATP hydrolysis providing energy for force transduction by Myh6. Novel Myh6 phosphorylations may regulate its contractile function upon iNOS derived NO.

Already in 2000, contractile and cytoskeletal proteins have been proposed to be NO/cGMP/PKG dependent targets (Lucas et al., 2000). In present study I was able to show that iNOS derived NO release increases the phosphorylation of α -MHC at Thr-379 by 44%. This site is localized in the second myosin head domain, which is situated close to the actin-binding interface of the myosin head. Therefore, Thr-379 phosphorylation might influence actin binding, modulate actin-activated ATPase activity and thereby could play an important role in the actin filament based movement. An other novel phosphorylation site is at Ser-1301 (tail region) which was enhanced by 47%. While Thr-379 could be phosphorylated by G protein-coupled receptor kinase I, Ser-1301 may be the substrate of the DNA dependent protein kinase, the ATM kinase (ATM: Ataxia telangiectasia mutated) or Casein kinase I and II.

On the other hand, I have found NO-induced dephosphorylation of Myosin-6 at the novel phosphorylation sites Tyr-1349 (- 54%), Ser-1467 (- 54%) and Tyr-1261 (- 44%) in the C-terminal tail region. This region is required for the interaction of **α -MHC** with other proteins. Tyr-1349 is a predicted target of Syk and Src kinase, and SHP1 phosphatase; Ser-1467 is a predicted target of

Casein kinase I and II, β -Adrenergic Receptor kinase, G protein-coupled receptor kinase I and ATM kinase; Tyr-1261 may be phosphorylated by EGFR kinase and TC-PTP phosphatase.

This study provides the first evidence that there are 21 phosphorylation sites in cardiac α -MHC, of five sites are linked to NO-induced changes of phosphorylation. These findings suggest that these sites may play a role in the regulating myocardial contractile function.

Interestingly, a recent paper showed regulator effects O-linked modification of α -MHC serine and threonine residues by beta-N-acetyl-D-glucosamine (Ramirez-Correa et al., 2008).

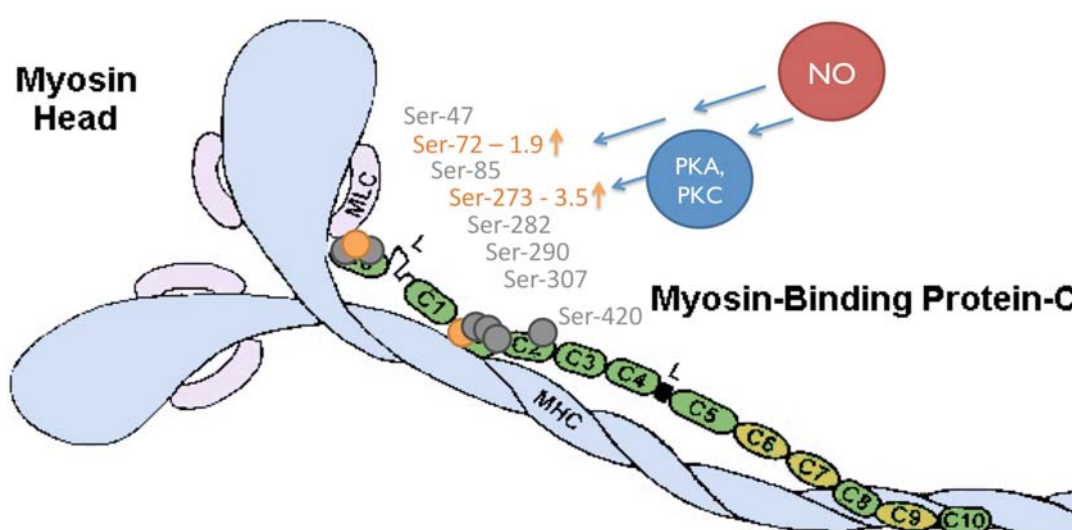


Figure 5.11. Myosin binding protein C (green) binds to myosin heavy chain (MHC, blue) near to the myosin head and the regulatory myosin light chain (MLC, violet). iNOS derived NO release leads to an enhanced myosin binding protein C phosphorylation (orange) at Ser-273 by PKA and PKC which may prevent MHC neck-binding and protects from ischemic injury. Near to the myosin head binding site an additional novel phosphorylation site was identified with enhanced phosphorylation (1.9 times), which may contribute to the negative inotropic effects of NO. Further six phosphorylation sites (grey) were not altered in the NO-induced decreased contractile force..

The thick filament protein **myosin binding protein-C** (MYPC3) has both structural and regulatory functions. Mutations of the cardiac MYPC3 gene were associated with familial hypertrophic cardiomyopathy. MYPC3 mechanically stabilizes the actomyosin cross-bridge post power stroke state, thereby maintaining ejection phase duration and building an energy-consuming viscous load which inhibits premature LV relaxation (Palmer et al., 2004). MYPC3 phosphorylation (at the PKA and PKC targeted Ser-273, Ser-282 and Ser 302) was reported to be decreased during the development of heart failure or hypertrophy. Therefore MYPC3 phosphorylation is essential for normal cardiac function (Sadayappan et al., 2006). It was also reported, that phosphorylation accelerates the kinetics of force development (Stelzer et al., 2007) and can protect the myocardium from ischemic injury (Sadayappan et al., 2006).

In the present study I found enhanced phosphorylation of MYPC3 at Ser-72 (+90%) and at Ser-273 (3.5 times). Ser-72 is located near to the myosin head, therefore its phosphorylation may influence cardiac contractility. According to the PhosphoMotif Finder of the human protein reference

database (Amarchy et al, 2007, http://www.hprd.org/PhosphoMotif_finder), numerous kinases such as calmodulin dependent protein kinase II, PKA, GSK-3, ERK1, ERK2, CDK5, pyruvate dehydrogenase kinase and casein kinase II could be responsible for the phosphorylation of Ser-72 (Table 5.2).

Position in query protein	Sequence in query protein	Corresponding motif described in the literature (phosphorylated residues in red)	Features of motif described in the literature
69 - 72	RDAS	RXXpS	Calmodulin-dependent protein kinase II substrate motif
69 - 72	RDAS	RXXpS	PKA kinase substrate motif
69 - 72	RDAS	RXX[pS/pT]	Calmodulin-dependent protein kinase II substrate motif
69 - 72	RDAS	[R/K]XX[pS/pT]	PKC kinase substrate motif
70 - 73	DASP	XXpSP	GSK-3, ERK1, ERK2, CDK5 substrate motif
71 - 73	ASP	X[pS/pT]P	GSK-3, ERK1, ERK2, CDK5 substrate motif
71 - 77	ASPDDQG	XpSXXDXX	Pyruvate dehydrogenase kinase substrate motif
72 - 73	SP	pSP	ERK1, ERK2 Kinase substrate motif
72 - 75	SPDD	pSXX[E/D]	Casein kinase II substrate motif
72 - 75	SPDD	[pS/pT]XX[E/D]	Casein Kinase II substrate motif
72 - 75	SPDD	[pS/pT]XX[E/D/pS*/pY*]	Casein Kinase II substrate motif
72 - 75	SPDD	[pS/pT]XX[E/D]	Casein Kinase II substrate motif

Table 5.2: Kinase prediction for the novel phosphorylation site Ser-72 of Mypc3 based on phosphorylation motifs using PhosphoMotif Finder.

Ser-273, on the other hand, is located at a myosin- binding interface and can be phosphorylated by PKA and PKC. Mimicked phosphorylation at Ser-273, Ser-282 and Ser-302 (all together) prevents MYPC3-MHC interaction, thereby protecting hearts from ischemia-reperfusion injury. Therefore, the measured increased phosphorylation at Ser-273 already after 1 minute of NO-formation by iNOS may have contributed to the cardioprotective effects of nitric oxide. This site is predicted to be phosphorylated by PKA, PKC, PAK2, PKC epsilon, Casein kinase I and II, and by Calmodulin dependent protein kinase II.

Titin is the largest known protein, consisting of 35,213 amino acids. Titin connects the Z-disc (titin N-terminal with actin) to the A-band (titin C-terminal with myosin) in the sarcomere and plays an important role in contraction and elasticity of the muscle. For example, upon stretch some of titin's 300 globular protein domains can unfold in a one-by-one fashion, permitting titin to retain its elastic properties over a very wide length range. The first unfolding region, called PEVK is rich in proline, glutamate, valine and lysine. Interestingly, myosin binding to the titin C-terminal at the A-band has kinase activity, which may contribute to the numerous identified novel myosin phosphorylation sites. Furthermore, titin can interact with many sarcomeric proteins, including myosin binding protein C at the region of the M line. Mutations at this site have been reported to be associated with familiar hypertrophic cardiomyopathy.

Recently it was shown that PKA and PKG-mediated phosphorylation at Ser-469 reduces titin-based stiffness, thereby improving diastolic function of the heart. In addition, left ventricular tissue of human hearts with end-stage DCM displays a lower titin phosphorylation rate compared with healthy donors (Krüger et al., 2009).

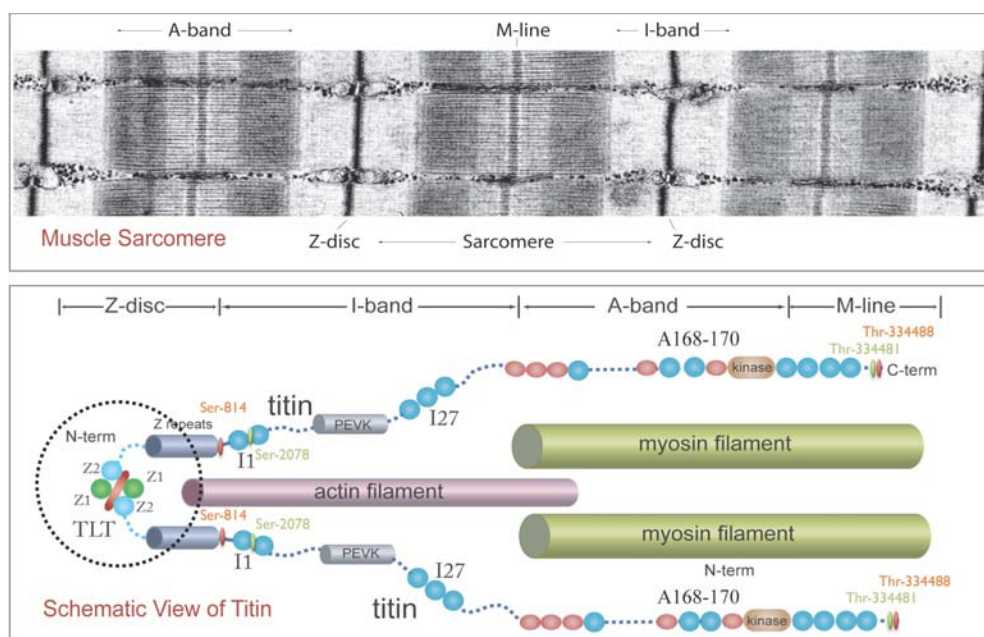


Fig. 5.12: Muscle sarcomere and Titin structure. Identified phosphorylation sites in NO-induced decrease in contractility are included. Orange: dephosphorylated sites; Green: unchanged phosphorylation sites (modified from www.ks.uiuc.edu/Research/zl2/TITIN-OVERVIEW.jpg).

In the present study I found a decrease in titin (N2A or isoform I) phosphorylation at Ser-814 by 50%. This site is located between the 6th Z-repeat region and the 3rd Ig-like domain (Fig. 5.12). (Identified peptide is also present in other titin isoforms.) As shown in Table. 5.3 there are numerous predicted kinases all of which may regulate titin phosphorylation at Ser-814. This provides a rich tableau of regulatory possibilities.

809 - 814	RPRTAS	RXXRX[pS/pT]	Akt kinase substrate motif
809 - 814	RPRTAS	[R/K]X[R/K][S/T]XpS	Akt kinase substrate motif
809 - 814	RPRTAS	[R/K]XRXpS	MAPKAPK1 kinase substrate motif
811 - 814	RTAS	RXXpS	Calmodulin-dependent protein kinase II substrate motif
811 - 814	RTAS	RXXpS	PKA kinase substrate motif
812 - 815	TASP	XXpSP	GSK-3, ERK1, ERK2, CDK5 substrate motif
813 - 815	ASP	X[pS/pT]P	GSK-3, ERK1, ERK2, CDK5 substrate motif
813 - 818	ASPHFT	X[pS/pT]XXX[A/P/S/T]	G protein-coupled receptor kinase 1 substrate motif
814 - 815	SP	pSP	ERK1, ERK2 Kinase substrate motif
814 - 818	SPHFT	pSXXX[pS/pT]	MAPKAPK2 kinase substrate motif
814 - 818	SPHFT	pSPXX[pS*/pT*]	Casein Kinase I substrate motif
814 - 819	SPHFTV	[pS/pT]XXX[S/T][M/L/V/I/F]	Casein Kinase I substrate motif

Table. 5.3: Predicted kinases for phosphorylation site Ser-814 of titin isoform I according to Phosphomotif finder.

I was able to identify three additional phosphorylation sites, one at Ser-2078 located between the 9. and 10. Ig-like domain at the N-terminus and two novel phosphorylation sites at Thr-34481 and Thr-34488, which are located close to the C-terminal regulatory tail between the 15. TPR repeat and the 141. Ig-like domain. Interestingly, Thr-34488 was found to be dephosphorylated (-35%) when endogenous NO-formation was enhanced. Thr-34488 dephosphorylation may influence titin kinase activity, which requires both Tyr-33203 phosphorylation and Ca^{2+} /calmodulin binding to the

C-terminal regulatory tail, resulting in unblocked catalytic aspartate residue and ATP binding, respectively.

5.5.4 MITOCHONDRIAL RESPIRATION

The components of the electron transport chain, summarized in Fig. 5.13, are: NADH-coenzyme Q reductase (complex I), succinate-coenzyme Q reductase (complex II), coenzyme Q-cytochrome c reductase (complex III), cytochrome c oxidase (complex IV) and ATP synthase.

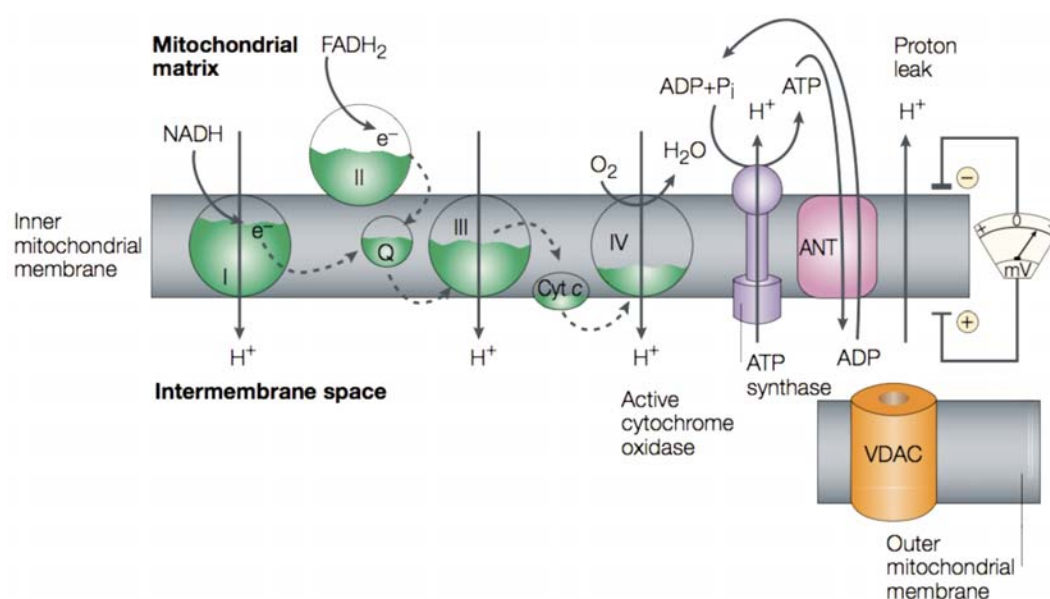


Figure 5.13: Mitochondrial electron transport chain. I,II, III, IV: protein complexes of the electron-transport chain; Cyt c: cytochrome c; FADH₂: Flavin-adenine dinucleotide (reduced); NADH: nicotinamide-adenine dinucleotide (reduced); Q: ubiquinone; VDAC: voltage-dependent anion channel; ANT: adenosine nucleotide translocator; membrane potential is indicated by a voltmeter (from Moncada et al.; 2002).

Complex I-IV pump protons out of the mitochondrial matrix, generating the membrane potential ($\Delta\Psi_m \sim 150\text{-}180\text{mV}$) and a pH gradient. This proton-motive force then drives the ATP synthesis, which is the main pathway for the return of protons into the matrix. Fuel of the process is provided by glycolysis, TCA cycle and fatty acid oxidation in form of electrons carried by NADH and FADH₂. This process generates 34 molecules of ATP from each glucose, and serves as the main energy source for cardiac contraction. Normally there is an equilibrium between energy consuming (contraction) and energy generating reactions in the heart. The regulation of mitochondrial respiration is therefore important to match the energy requirements.

NO is known to inhibit cytochrome oxidase potently and reversibly by binding to its heme centers (Fig. 5.14). This, in turn, leads to drop in the electron flux and in proton transfer. Resulting fall in the membrane potential, proton leak closure and reversal of the ATP synthase. Thus, ATP synthase now hydrolyses cytoplasmic ATP and extrudes protons, thereby restoring membrane potential and proton leak. In this state, increased glycolysis rates are necessary to ensure sufficient ATP supply to

feed ATPase (see more in chapter 5.4.5). These changes lead to a slight hyperpolarization of the inner mitochondrial membrane which favors superoxide anion generation by complex I and III of the electron transport chain (increased reduction state). Superoxide anions induce superoxide dismutase (SOD) to convert O_2^- to hydrogen peroxide (H_2O_2). Enhanced NO and O_2^- generation results in a depletion of the glutathione pool and $ONOO^-$ formation. Which in turn, induce the permeability transition pore, resulting in collapse of the membrane potential, swelling, outer mitochondrial membrane rupture, release of mitochondrial pro-apoptotic factors and cell death.

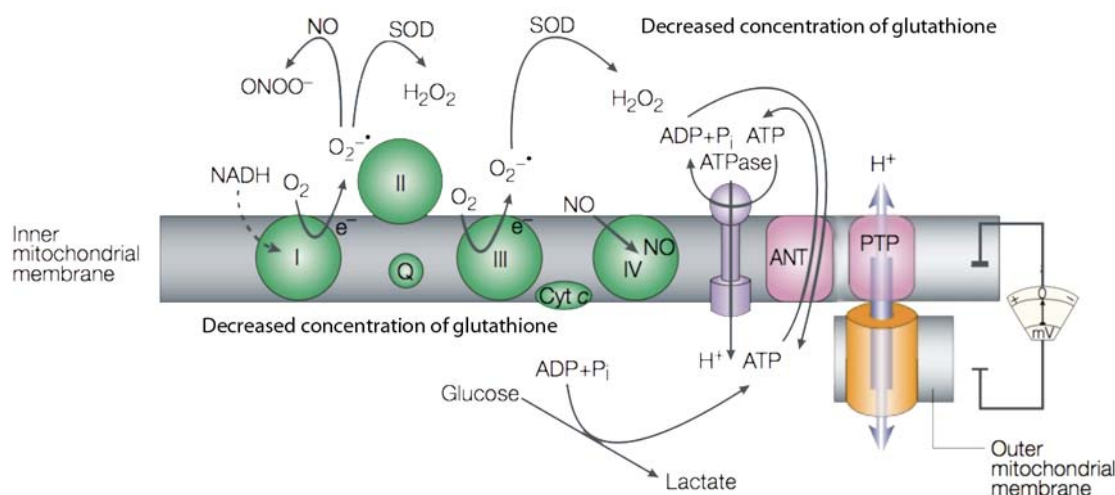


Figure 5.14: NO-inhibits complex IV, uncouples the electron transport of the mitochondrial respiratory chain complexes I, II and III and thereby induces superoxide (O_2^-) production. Superoxide can be converted into the hydrogen peroxide by superoxide dismutase (SOD). In this state, ATP synthase works reversely trying to restore the normal membrane potential by pumping H^+ into the intermembrane space by using ATP produced by glucose metabolism. At higher and prolonged concentrations of NO and at reduced glutathione pool NO and O_2^- form peroxynitrite ($ONOO^-$) which in turn reacts with the surrounding proteins by nitration and S-nitrosylation. $ONOO^-$ and maybe NO itself can cause direct induction of the mitochondrial permeability transition pore (PTP) which leads to mitochondrial depolarization, swelling, membrane rupture and apoptosis. ANT: adenosine nucleotide translocator; Cyt c: cytochrome c; FADH₂: flavin-adenine dinucleotide (reduced); NADH: nicotinamide-adenine dinucleotide (reduced); Q: ubiquinone; VDAC: voltage-dependent anion channel; I, II, III and IV refer to the protein complexes of the electron-transport chain. (Figure was modified from Moncada et al.; 2002).

In the present study I have found the following mitochondrial phosphoproteins:

Electron transfer flavoprotein subunit alpha, mitochondrial precursor (ETF) serves as a specific electron acceptor for several dehydrogenases and transfers electrons to the main mitochondrial respiratory chain via ETF-ubiquinone oxidoreductase (Q in Fig. 5.13). In the present study a novel phosphorylation site of ETF at Ser-191 was identified. Phosphorylation of Ser-191, however; was not altered after enhanced NO formation.

The mitochondrial respiratory complex I (NADH-coenzyme Q reductase) is composed from 45 subunits and transfers electrons from NADH to the respiratory chain, thereby serving as a link between glycolysis, the TCA cycle, fatty acid oxidation, and the electron transport chain. Interestingly, the mitochondrial respiratory complex I is well known to be inhibited by NO, most probably mediated by peroxynitrite induced S-nitrosylation and nitration. Peroxynitrite is formed in

the reaction of nitric oxide and superoxide, which is produced mainly by the mitochondrial respiratory chain complexes I and III. However oxygen normally serves as the ultimate electron acceptor and is reduced to water; NO induced electron leak to oxygen results in superoxide anion generation. Therefore, NO started process is self-supporting and leads to huge amount of peroxynitrite generation, DNA damage, apoptosis or necrosis. Further post translational modifications of complex I include oxidation, glutathionylation and phosphorylation known to play important regulatory roles. Pyruvate dehydrogenase kinase (PDH kinase) and PKA-driven phosphorylation of a few subunits of complex I have been reported. Phosphorylation can regulate electron flow through complex I and the production of oxygen free radicals (Raha et al., 2002). For example, under increased energy requirements phosphorylation of NADH dehydrogenase (ubiquinone) Fe-S protein 4 (Ndufs4) by PKA promotes the NADH-ubiquinone oxidoreductase activity of complex I and lower the cellular level of ROS (Piccoli et al., 2006; Papa et al., 2008). In contrast, during starvation PDH kinase phosphorylates complex I possibly at Ndusb7 subunit and thereby decrease enzyme activity and increase superoxide production (Raha et al., 2002).

Phosphorylation of **NADH dehydrogenase I [ubiquinone] alpha subcomplex subunit 7 (Ndufa7)** was found to be increased 1.93 fold at a novel phosphorylation site Ser-84 (Fig 5.14). According to phosphomotif finder, Ndufa7-Ser84 can be phosphorylated by PKA, β -Adrenergic receptor kinase or G protein coupled receptor kinase I. iNOS derived NO induced Ndufa7-Ser84 phosphorylation may contribute to the inhibition of the mitochondrial respiratory complex I and increase superoxide production. Oxidative and nitrosative stress result than in decreased ATP synthesis, reduced contractility and possibly apoptosis and necrosis.

Cytochrome c oxidase subunit Vb (COX5B), a subunit of the terminal oxidase of the mitochondrial electron transport (**complex IV**), was found to be dephosphorylated after SNAP (NO-donor) perfusion in isolated Myo^{-/-} mouse heart. (In 2D-PAGE based analysis as described in chapter 5.1. Unfortunately, gel free experiments were unable to find COX5B derived phosphorylated peptides.) Observed COX5B dephosphorylation may contribute to the known NO induced cytochrome c oxidase inhibition, leading to superoxide leakage from the electron transport chain (Fig 5.14).

Superoxide dismutase [Cu-Zn] (SodI) converts the toxic superoxide radical into the hydrogen peroxide (H₂O₂), serving as an alternative process for nitric oxide mediated peroxynitrite formation and nitrosative stress.

Interestingly, I found SodI to be slightly (-30%) dephosphorylated at the known phosphorylation site Ser-99 (Fig. 5.14). Function of this phosphorylation site is not yet to be uncovered. According to PhosphoMotif Finder, SodI-Ser99 is postulated to be phosphorylated by casein kinase II and pyruvate dehydrogenase kinase. Protein phosphatase 2B is a SodI binding partner (Agbas et al., 2007) therefore it is possibly responsible for the observed dephosphorylation after iNOS activation. Since large amount of iNOS derived NO leads most probably to increased superoxide and H₂O₂ levels and SodI can be activated by superoxide and H₂O₂ (Inarrea et al., 2007). Thus, the observed dephosphorylation may contribute to increased SodI activity and be involved in the cardioprotective effects of NO.

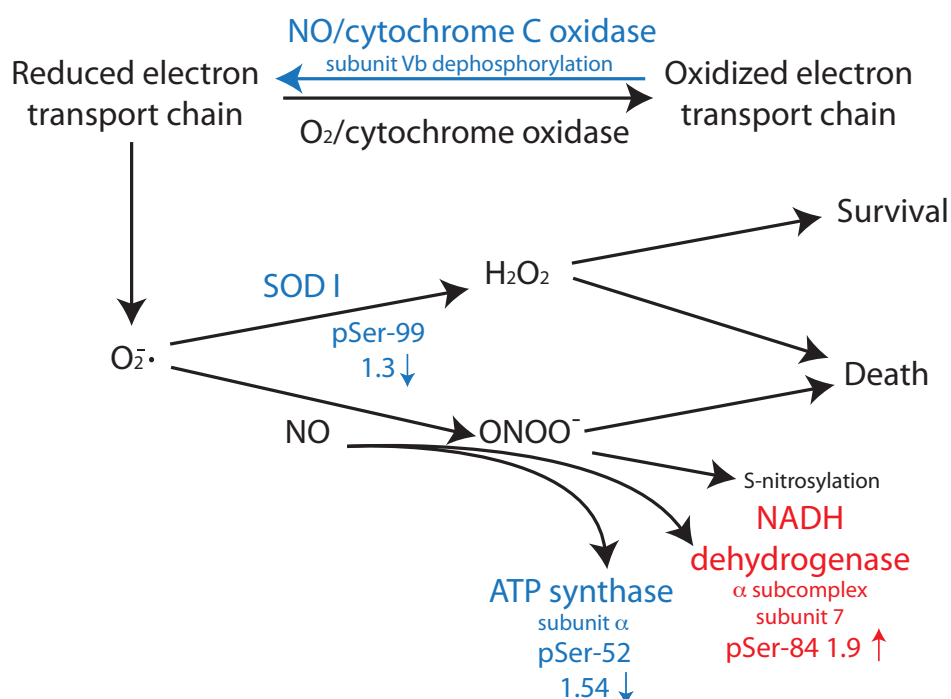


Figure 5.14: Inhibition of cytochrome oxidase by nitric oxide (NO) reduces the electron transport chain and thereby favors the formation of superoxide anions ($O_2^{\cdot-}$) by complex I and III of the electron transport chain. Superoxide dismutase (SOD) converts superoxide anions into hydrogen peroxide (H_2O_2), which can activate mechanisms leading to cell protection of death, depending on its concentration. On the other hand, if SOD is impaired or saturated with higher amount of superoxide anion, peroxynitrite ($ONOO^-$) can be formed in the reaction with NO, resulting in macromolecular damage and cell death. In present study I could show (in red and blue), that iNOS derived NO induces dephosphorylation of SOD I at Ser-99 (1.3 times) and of ATP synthase subunit α at Ser-52 (1.54 times). Additionally an enhanced phosphorylation of NADH dehydrogenase (complex I) α subcomplex, subunit 7 (Ndufa7) at Ser-84 (1.9 times) was found. Furthermore, compared to NOS inhibition with ETU, cytochrome c oxidase (complex IV) subunit Vb (COX5B) was found to be dephosphorylated upon 1 minute SNAP activation. This data provides the first evidence of NO induced phosphorylation/dephosphorylation events on the mitochondrial respiratory chain, which may play an important regulatory role beside protein S-nitrosylation, nitration and simple inhibition by NO binding to the heme catalytic core.

ATP synthase subunit alpha, mitochondrial (Atp5a1), the regulatory subunit of the mitochondrial respiration **complex V**, produces ATP from ADP in the presence of a proton gradient across the membrane.

In the present study I found the novel phosphorylation of Atp5a1 at Ser-52 to be decrease by 54%, when NO-production was enhanced. Phosphorylation at this site may influence regulatory subunit conformation, and thereby ATP synthase activity. Thus, Ser-52 phosphorylation may contribute to the NO-induced inhibition of the mitochondrial respiration.

5.5.5 GLYCOLYSIS AND PYRUVATE METABOLISM

NO-induced inhibition of the mitochondrial respiratory chain has been shown to lead to an induction of the glycolytic pathway (Almeida, et al., 2004; Cicad et al., 2004), to ensure sufficient amount of ATP supply for complex V of the mitochondrial respiratory chain (Fig. 5.14). In the following a few NO regulated enzyme of glycolysis and pyruvate metabolism will be discussed.

Phosphoglucomutase-I (PGMI), is an important regulatory enzyme in cellular glucose utilization and energy homeostasis. It participates in both the breakdown and synthesis of glucose by interconversion of alpha-D-glucose 1-phosphate (Glc-1P) and alpha-D-glucose 6-phosphate (Glc-6P) (Fig. 5.17), resulting in an equilibrium of about 95% Glc-6P. The catalytic center of PGMI is known to be phosphorylated at a serine residue which activates the enzyme (phosphorylated amino acid residue is not known). Furthermore, PGMI can be activated by p21-activated kinase 1 (Pak1) induced phosphorylation at Thr-466 (Gururaj et al., 2004).

The present study shows an enhanced phosphorylation at Ser-117 (+40%). Whether this phosphorylation site may serve as a molecular switch between NO induced glucose synthesis and breakdown remains to be determined.

As shown in Fig. 5.17, another glycolytic enzyme, **fructose-bisphosphate aldolase A (ALDOA)** catalyses the conversion of D-fructose 1,6-bisphosphate to dihydroxyacetone phosphate and D-glyceraldehyde 3-phosphate. Phosphorylation of ALDOA at Ser-39 was found to be enhanced 1.4 fold. This phosphorylation site is known from brain and tumor based phosphoproteome studies, however its function is still unclear. Therefore, phosphorylation of Ser-39 may play an important regulatory role, providing a target of NO-induced enzyme activation by phosphorylation.

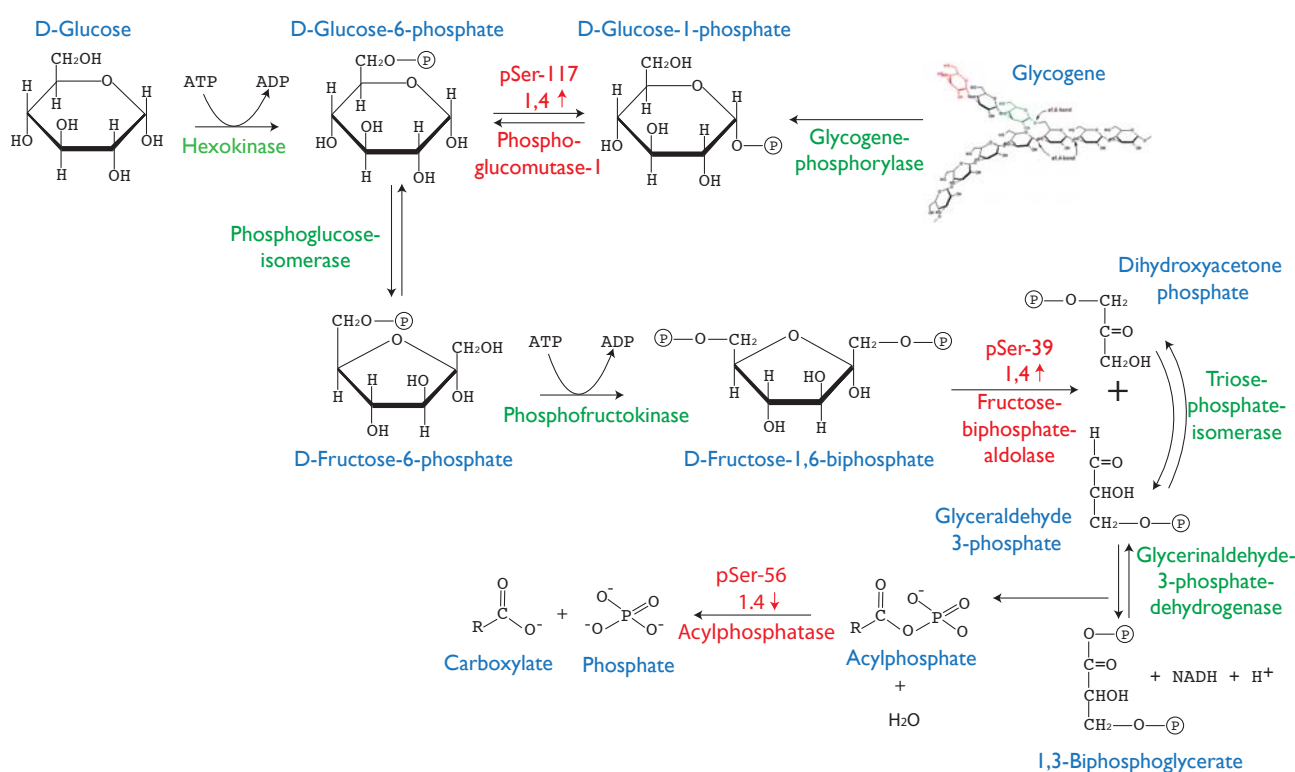


Fig. 5.17: First steps of glycolysis and glycogenolysis (catabolism of glycogen). Enzymes of key metabolic trafficking points are shown in red, because they were found to be regulated upon iNOS derived NO release. Phosphoglucomutase-I Ser-117 and fructose-bisphosphate aldolase Ser-39 showed a 1.4 times enhanced phosphorylation after one minute NO activation. Additionally, acylphosphatase, which catabolize an intermediate of glycerinaldehyde-3-phosphate dehydrogenase is dephosphorylated at Ser-56 by 1.4 times after NO activation. It is still remain to explore, if NO-regulated phosphorylation sites have enzyme activator or inhibitory effects.

Acylphosphatase (Acyp2, EC 3.6.1.7) is an enzyme of the glucose and pyruvate metabolism, which can hydrolyze the phosphoenzyme intermediate acylphosphate to carboxylate and phosphate (Fig. 5.17). Acylphosphates ($R\text{-COO-PO}_3^-$) are produced by different membrane pumps, for example by the $\text{Ca}^{2+}/\text{Mg}^{2+}$ -ATPase of the sarcoplasmic reticulum. Furthermore, acylphosphate is a product of pyruvate oxidase (from pyruvate), phosphate acetyltransferase (from acetyl-CoA) and an intermediate product of glyceraldehyde-3-phosphate dehydrogenase (from glyceraldehyde 3-phosphate) as well (As shown in Fig. 5.17). Interestingly, acylphosphate has a higher potential to transfer the phosphate group to an other molecule, than ATP. Therefore, its hydrolysis by Acyp2 breakdown phosphorylation reactions of acylphosphate. Up to date, there is no post translational modification described for Acyp2.

In the present study I have identified a novel Acyp phosphorylation site at Ser-56 which was upregulated 1.43 fold when NO-formation was enhanced. Therefore, this newly discovered novel phosphorylation site may play a role in the NO-dependent regulation of acylphosphate hydrolysis.

Pyruvate dehydrogenase (PDH) catalyzes the overall conversion of pyruvate (a product of glycolysis in the cytosol) to acetyl-CoA (rate limiting substrate of the Szent-Györgyi-Krebs or TCA cycle) to NADH (fuel of mitochondrial respiration) and CO_2 (Fig. 5.18). PDH regulation is crucial in determining the relative contribution of glucose oxidation to energy production. **E1 component of the alpha subunit of Mitochondrial pyruvate dehydrogenase (Pdh1)** is a regulatory subunit of PDH and its phosphorylation by pyruvate dehydrogenase kinase is known to lead to enzyme inhibition (Korotchkina et al., 2001).

As depicted in Fig 5.18 the enhanced cardiac NO-formation results in the decreased phosphorylation of PDH at Ser-232 (-30%) which enhances enzyme activity. Thus, acetyl-CoA, the rate limiting substrate of the Szent-Györgyi-Krebs cycle (TCA cycle), is possibly produced in higher amounts, leading to a faster TCA cycle rate. Furthermore, the produced NADH serves as a fuel of mitochondrial respiration, the supply of which could also be improved upon NO stimulation.

ATP citrate lyase (Acly) is a homotetramer that catalyzes the formation of acetyl-CoA and oxaloacetate in the cytosol, which is the key step for the biosynthesis of fatty acids, cholesterol and acetylcholine, as well as for glucogenesis (Fig. 5.18). Acly is phosphorylated by GSK-3 on Thr-446 and on Ser-450 and Ser-455 by PKA and Akt. Phosphorylation on Ser-455 abolishes the homotropic allosteric regulation (activation of protein by an effector molecule at a site, which differ from protein's active site) by citrate and enhances the catalytic activity of the enzyme (Potapova et al., 2000).

In the present study NO increased the phosphorylation of Acly at Ser-455 by 60 %, which to all likelihood enhanced the catalytic activity of this enzyme. Bauer et al. (2005) reported that Acly knockdown cells (in growing hematopoietic cells) display impaired glucose-dependent lipid synthesis, elevation of mitochondrial membrane potential and decreased cytokine-stimulated cell proliferation. Therefore, NO-induced increased Acly activity may lead to cardiac hypertrophy in iNOS overexpressing, myoglobin deficient double transgenic mouse hearts. Furthermore, decreased mitochondrial membrane potential could depress ATP synthesis by complex V of the mitochondrial respiratory chain, leading to impaired cardiac energetics and reduced contractility.

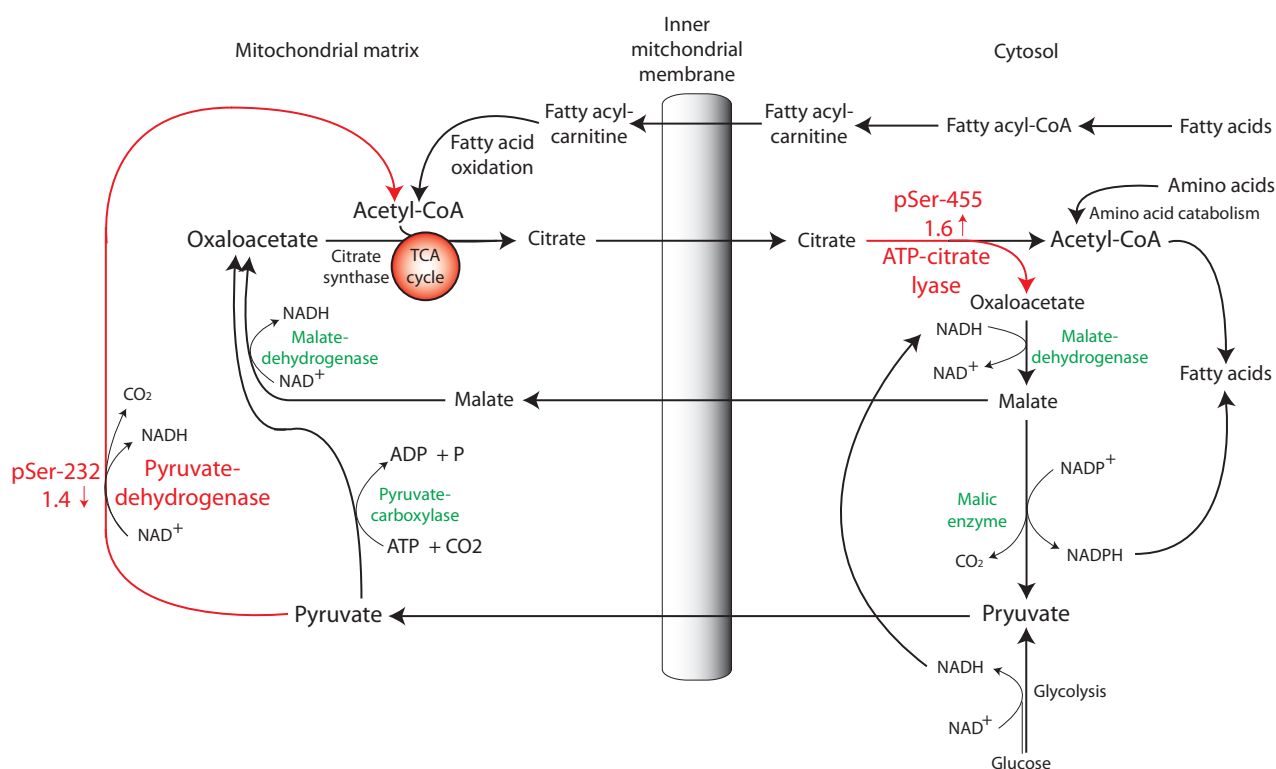


Figure 5.18: Figure 5.13: Citrate-malate-pyruvate shuttle in the cell. NO activation resulted in the acetyl-CoA producing pyruvate dehydrogenase dephosphorylation at Ser-232. Thereby NO enhances enzyme activity and production of the TCA cycle's rate limiting substrate. On the other hand, NO enhances ATP citrate lyase phosphorylation at Ser-455 and thereby activates the enzyme. Thus, changes in the phosphorylation state of key-enzymes by NO enhances metabolic activity and ensures sufficient supply of glycolytic ATP to fuel the reversal working mitochondrial ATPase under nitrosative stress.

Taken together, chapter 5.4.4 and 5.4.5 provides clear evidence for iNOS derived NO induced changes in the phosphorylation state of proteins of mitochondrial respiration, glycolysis and pyruvate metabolism. The function of most of the modulated phosphorylation sites are not known, but dephosphorylation of pyruvate dehydrogenase at Ser-232 and phosphorylation of ATP-citrate lyase at Ser-455 enhances catalytic activity of the enzymes. This novel information fit well to already published data by Almeida et al., (2004) and Cicad et al. (2004), where NO-induced inhibition of cytochrome c oxidase and the mitochondrial respiratory chain was found to induce the glycolytic pathway, to compensate decreased respiratory ATP production and protect cells from apoptosis. This processes are mediated by the energy charge-sensitive AMP-activated protein kinase (AMPK), resulting in induced GLUT3 mediated glucose uptake and activation of 6-phosphofructo-2-kinase/fructose-2,6-bis-phosphatase (PFK2). Similar processes, such as AMPK mediated PFK2-Ser466 phosphorylation and enzyme activation were described in the heart in response to ischemia (Marsin et al., 2000).

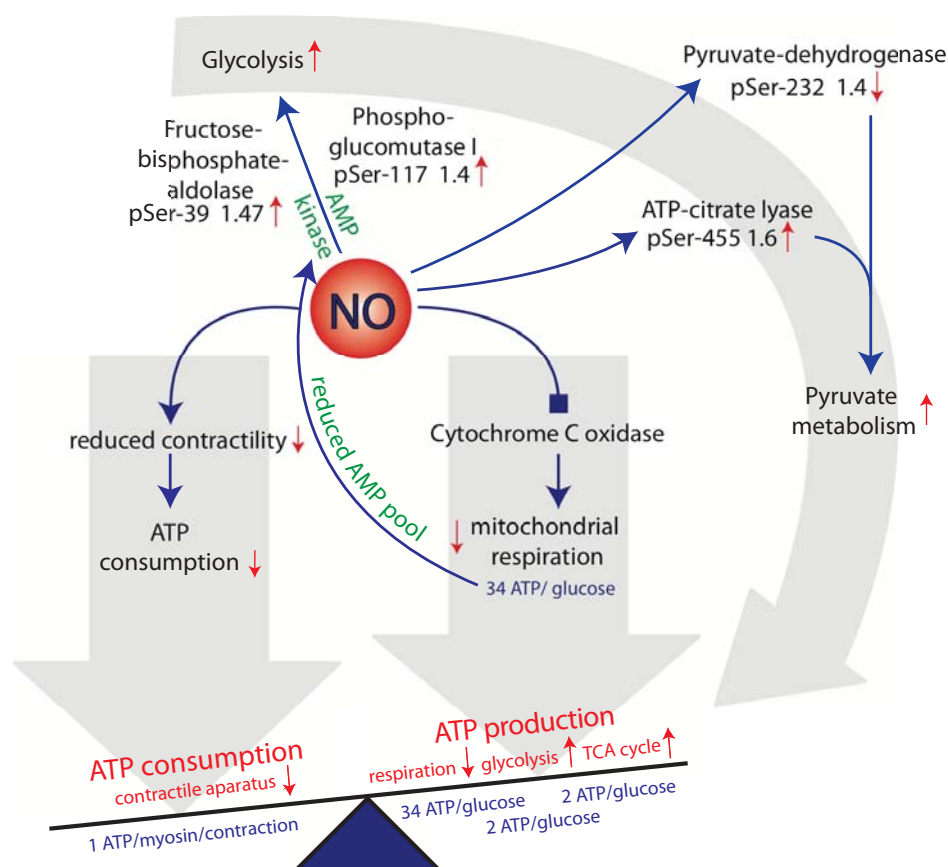


Figure 5.19: NO-induced downstream processes led on one hand to reduced cardiac contractile force and decreased ATP consumption, on the other hand to inhibited cytochrome C oxidase and mitochondrial respiration, thus reduced ATP production. Increased AMP/ATP (by 42.72%) and ADP/ATP (by 17.27%) level induces AMP kinase which in turn activates PFK2 and possibly other glycolytic enzymes like fructose-bisphosphate-aldolase and phosphoglucomutase-I. NO activated furthermore enzymes of pyruvate metabolisms like pyruvate-dehydrogenase and ATP-citrate lyase mediated by phosphorylation or dephosphorylation. In summary, there is a decreased cardiac energy (phosphocreatine -11.34%, ATP -3.34%) pool due to the still huge needs of contraction (1 ATP/myosin/contraction, decreased by 30%) and slightly inhibited mitochondrial respiration and ATP production (28-34 ATP/glucose depending on cellular condition) in opposite to the small compensatory mechanism of activated glycolytic (2 ATP/glucose) and pyruvate metabolic (rate limited step of the TCA cycle, 2 ATP/glucose) processes. Additional anaerobic ATP production from ADP and phosphocreatine (pCr) is implied by the decreased pCr pool (-11.34%)

Interestingly, phosphorylation of **5-AMP-activated protein kinase subunit beta-2 (AMPK-β2)** was found to be decreased at Ser-38 (-37%) after NO stimulation. Under this conditions, AMP/ATP level was measured to be increased by 42.72% and ADP/ATP by 17.27% (Gödecke et al., 2003), both of which activate AMPK. pSer-38 is known from phosphoproteome studies (Dephoure et al., 2008; Daub et al., 2008) but its function is remains to be explored.

5.5.6 TRANSCRIPTIONAL REGULATION FROM THE VIEW OF NO SIGNALING

The study was performed on a failing heart with cardiac hypertrophy. It is therefore not surprising that I have found changes in the phosphorylation pattern of various proteins active in transcriptional regulation.

Histone deacetylase 4 (HDAC4) acts by deacetylating lysine residues at the N-terminal part of core histones H2A, H2B, H3 and H4. Histones are chief protein components of chromatin, and act as spools around DNA winds. Therefore its regulation by HDAC4 plays an important role in transcriptional control, cell cycle progression and developmental events. Backs and his colleges (2006) reported, that phosphorylation of HDAC4 by CaMKII results in hypertrophic growth in cardiac myocytes by reactivation of the fetal gene expression program. This process can be blocked by a signal-resistant HDAC4 mutant.

In the present work, Isoform I of Histone deacetylase 4 (HDAC4) was found to be enhanced phosphorylated by 1.8 times at Ser-562, after one minute of NO stimulation.

Interestingly, HDAC4 region 529–657, locating around the NO regulated phosphorylation site Ser-562 has been shown to be CaMKII-responsive. Additionally, Little et al. (2007) reported HDAC4 Ser-210 residue as a special target of delta B isoform of calcium/calmodulin-dependent protein kinase II (CaMKIIdeltaB). Unfortunately, the authors did not examine CaMKII effects on Ser-562 residue. For this site NetPhosK (<http://www.cbs.dtu.dk/services/NetPhosK/>) predicts CKII (Casein kinase II) as the most presumptive responsible kinase, although the shown CaMKII phosphorylation sites at Ser-467 and Ser-632 of HDAC4 are also predicted for other kinases, for PKA and for RSK, respectively. The phosphomotif finder, a more recent kinase/phosphatase motif prediction program, predicts that Casein kinase II (CK2), G protein-coupled receptor kinase I and β -Adrenergic Receptor kinase could be responsible for Ser-562 phosphorylation. The known CaMKII target site Ser-632 is predicted to be phosphorylated by Casein kinase I and II, and by G protein-coupled receptor kinase I, whereas which is likely to the other known CaMKII target site Ser-467 there is no matching kinase. This search indicates the limitations of current kinase prediction programs based on known and predicted kinase substrate motifs.

Taking together, iNOS derived NO induced phosphorylation at Ser-562, which is mediated most likely by CK2 or CaMKII kinase and plays a role in the pathophysiology of hypertrophic gene expression processes in iNOS⁺/myo^{-/-} mouse heart (Fig. 5.19).

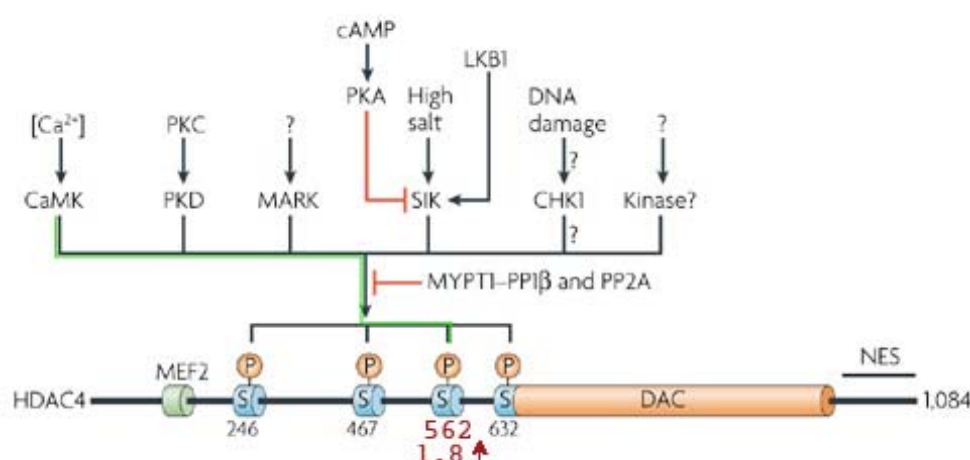


Figure 5.19: NO-induced phosphorylation at Ser-562 (red) on a background of known kinases and phosphorylation sites of Hdac4 (modified from Yang & Seto, 2008).

Isoform 2 of Glucocorticoid receptor (Nr3c1) is a transcription factor that binds glucocorticoid response elements as a modulator of other transcription factors. Furthermore, it affects inflammatory responses, cellular proliferation and differentiation and acts as a coactivator of STAT5-dependent transcription after growth hormone stimulation, therefore it has an essential role in body growth control. Glucocorticoid receptor becomes hyperphosphorylated in the presence of glucocorticoid, its phosphorylation level at Ser-211 is correlates with its transcriptional activity.

iNOS derived NO induced Nr3c1 phosphorylation at Thr-159 by 1.6 times, which is an already known phosphorylation site in mouse Nr3c1 and have no homologues in the human receptor (Bodwell et al., 1991). This phosphorylation site is located in a consensus sequence for proline-directed kinase and p34cdc2 kinase and possibly have a role in protein transactivation. Krstic et al. (1997) identified rat Nr3c1 Thr-171 (identical to Thr-159 in the mouse Nr3c1) as MAPK target.

Very recently, activated steroidogenesis and increased glucocorticoid levels were described in hypertrophied hearts. In addition, glucocorticoid have potential to augment cardiac hypertrophy and progression of heart failure *via* glucocorticoid receptor (Ohtani et al., 2009). Thus, NO induced glucocorticoid receptor phosphorylation and activation most likely contribute to the observed pathological phenotype (hypertrophy) of the iNOS⁺/myo^{-/-} mouse hearts.

Further transcription factors regulated by iNOS derived NO include the following:

- The DNA binding **Chromobox protein homolog 3 (Cbx3)**, which is phosphorylated during interphase and possibly hyperphosphorylated during mitosis by PIM1, was found to be enhanced phosphorylated at Ser-95 by 2.2 times.
- **Cysteine and glycine-rich protein 3 (Csrp3)**, missense mutations of which segregating with hypertrophic cardiomyopathy (HCM), dilated cardiomyopathy (DCM) and mild skeletal muscle disease in humans (Geier et al., 2008). Interestingly, mice lacking Csrp3 develop cardiomyopathy, additionally, NO induce Csrp3 downregulation in failing hearts (Heineke et al., 2003). I have found that there is an enhanced Csrp3 phosphorylation after NO stimulation at the novel phosphorylation sites Ser-95 and Ser-117 by 1.69 and 1.9 times, respectively. These may inactivate Csrp3 protein and thereby may contribute to the pathophysiology of heart failure.
- **Isoform 1 of Hepatoma-derived growth factor-related protein 2 (hdgfrp2)**, was found to be increased phosphorylated at the Akt substrate Ser-659 by 1.7 times by NO. This site is located close to the C-terminal and was also found to be phosphorylated in tumors (Zanivan et al., 2008).
- **LIM domain only 7 (Lmo7)** protein containing an alponin homology (CH), a PDZ and a LIM domain regulates transcription of many genes, and may transmit mechanical signals from focal adhesions. Animal model with deletion in the Lmo7 gene showed muscular degeneration and growth retardation, furthermore, Lmo7 is upregulated in several types of cancer, showing its potential in growth regulation. NO induced Lmo7 phosphorylation at Ser-813 by 1.7 times and dephosphorylation at Ser-822 by 1.43 times.

5.5.7 APOPTOSIS AND NO

As already mentioned in chapter 1.4.4, NO induced mitochondrial dysfunction leads to oxidative (O_2^- , H_2O_2 , OH^\cdot , etc.) and nitrosative ($ONOO^\cdot$) stress, which in turn reacts with surrounding proteins, DNA and lipids by oxidation and by S-nitrosylation. Downstream signaling of this processes lead to apoptosis and cell death.

Although the present study successfully identified 15 phosphoproteins playing a role in apoptosis, only one protein, called Protein NDRG2 showed significant changes in its phosphorylation level after one minute of NO-stimulation. Therefore, induction of apoptotic proteins are likely to be brought about by other post translational modifications like S-nitrosylation. Additionally, phosphorylation changes may take place at a later point of time.

Isoform 1 of Protein NDRG2 or N-myc downstream-regulated gene 2 (**Ndrg2**) plays a role in hypoxia-induced apoptosis, mediated by HIF-1 (Wang et al., 2008). Furthermore, NDRG2 is not expressed or strongly down-regulated in various cancer types. Recently, it was shown, that induced NDRG2 expression suppressed NFkB activity and attenuates invasive potential of highly malignant tumor cells (Kim et al., 2009).

Phosphorylation of NDRG2 peptide near to the protein C-terminus was found to be enhanced at Ser-330 and at Thr-334 by 1.6 times after one minute NO stimulation, while other phosphorylation sites at Ser-318, Ser-339 and Ser-361 were not affected. Ser-330 and Ser-334 were both described as AKT kinase substrate, additionally, Ser-334 can be targeted by SGK1 (serum- and glucocorticoid-induced kinase 1) in skeletal muscle (Murray et al., 2004).

Interestingly, NDRG2 phosphorylation by SGK1 transforms the protein into an excellent substrate for GSK3, at Ser342, Ser352 and Ser361 in the repeat region. Thus, one minute NO stimulation resulted in an intermediate state of NDRG2 phosphorylation, which primes it for phosphorylation by GSK3 at a later point of time.

5.5.8 BEYOND NO INDUCED PHOSPHORYLATION - KINASES AND PHOSPHATASES

In order to obtain an even broader overview about the observed phosphorylation/dephosphorylation processes induced by iNOS derived NO, predicted kinases for each up- or downregulated phosphorylation sites were collected using PhosphoMotif Finder.

Two groups were generated according to the iNOS derived NO induced changes in the phosphorylation level. Fig. 5.20 shows number of predicted kinases of enhanced (up, orange) or decreased (down, blue) phosphorylated sites, after normalization. As one can see, Calmodulin dependent protein kinase 2 and 4, casein II kinase, chk1 kinase, PKA, PKC and pyruvate dehydrogenase kinase has a much higher frequency in the group of enhanced phosphorylated peptides, than in the decreased phosphorylated group. On the other hand, DNA dependent protein kinase and MAPKAP2 has a higher frequency in the dephosphorylated group, similarly to the two predicted phosphatases SHP1 and TC-PTP.

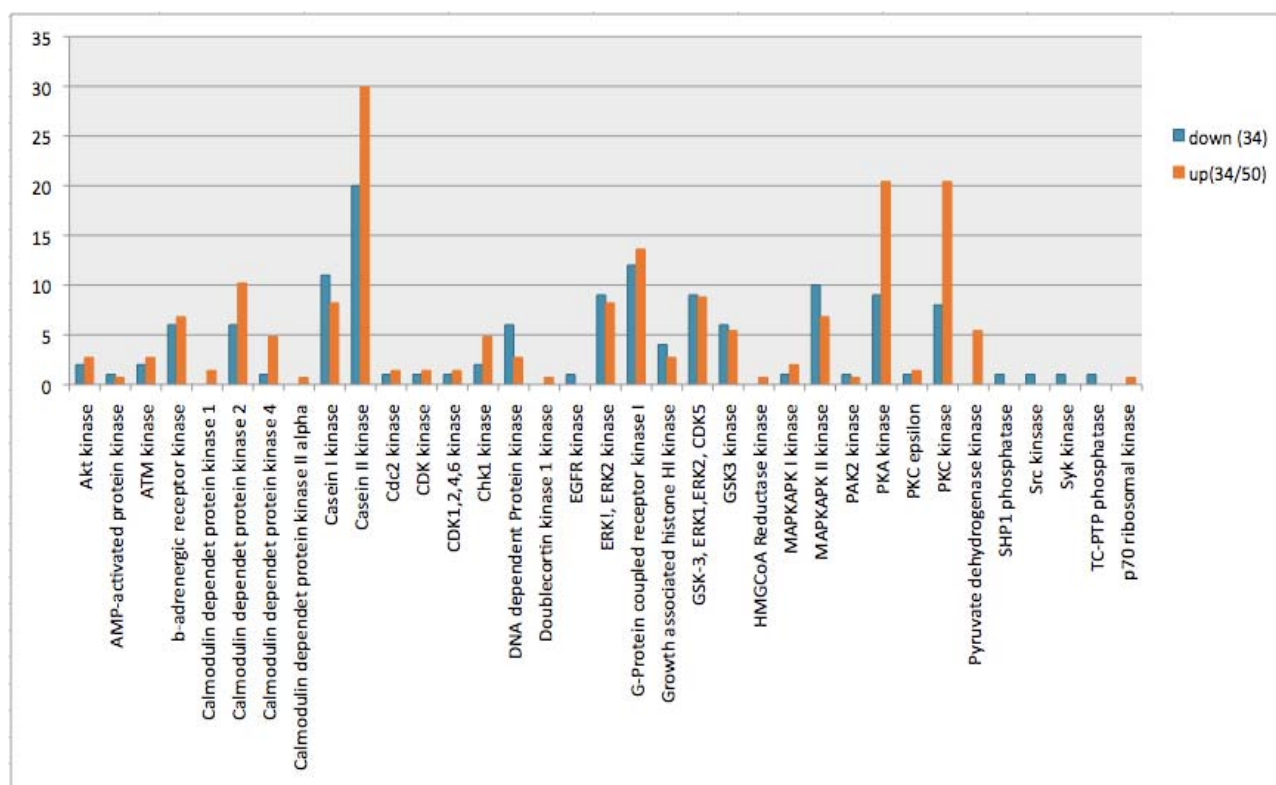


Figure 5.20: Summarized chart of predicted kinases (according to Phosphomotif Finder) of regulated phosphorylation sites upon one minute iNOS-derived NO release. Blue color shows predicted kinases of peptides with decreased phosphorylation (kinases were possibly inactivated leading to protein dephosphorylation), orange color shows predicted kinases of peptides with enhanced phosphorylation (possibly increased kinase activity). To obtain comparable results, number of predicted kinases and phosphatases were normalized according to the number of up (50) and downregulated (34) peptides. Interestingly, calmodulin dependent protein kinase 2 and 4, casein II kinase, PKA, PKC and pyruvate dehydrogenase shows a higher frequency in the group of enhanced phosphorylated peptides, therefore, possibly iNOS derived NO release lead to its activation.

Pyruvate dehydrogenase kinase shows the strongest changes between the increased and decreased phosphorylated groups. This kinase can be stimulated by ATP, NADH and acetyl-CoA and inhibited by ADP, NAD⁺, CoA-SH and pyruvate. Thus, the perfusion using pyruvate containing Krebs-Henseleit buffer very likely inhibited pyruvate dehydrogenase kinase. Following L-arginine activation of iNOS possibly induced various processes leading to pyruvate dehydrogenase kinase activation and phosphorylation of predicted downstream targets like 60S acidic ribosomal protein P0 or multidrug resistance associated protein 1.

Casein II kinase (CK2) showed also an increased frequency in the group of enhanced phosphorylated peptides. CK2 is a serine/threonine-selective protein kinase, that is implicated in cell cycle control, DNA repair, but also can regulate circadian rhythm and other cellular processes. Interestingly, activation of this kinase by angiotensin II can lead to cardiac hypertrophy (Hauck et al., 2008). Additionally, the angiotensin II producing **angiotensin-converting enzyme, somatic isoform precursor (ACE)** was found to be dephosphorylated at the C-terminal only known phosphorylation site Ser-1305 (-23%), after one minute of NO stimulation.

Calmodulin inhibitor (CaMI) and calmodulin kinase inhibitor induced Ser-1305 dephosphorylation is known to activate ACE cleavage secretion (Chattopadhyay et al., 2005). Interestingly, a

hypertrophic transcription factor **Histone deacetylase 4 (HDAC4)** was enhanced phosphorylated in a CK2 kinase substrate motif located Ser-562, by 1.8 times after one minute iNOS activation (see more about in chapter I.4.6).

Taking together, iNOS derived NO induced angiotensin II production, which in turn activated CK2 mediated hypertrophic signaling possibly due to HDAC4 phosphorylation at Ser-562 in double transgenic iNOS⁺/myo^{-/-} mice (Fig. 5.21).

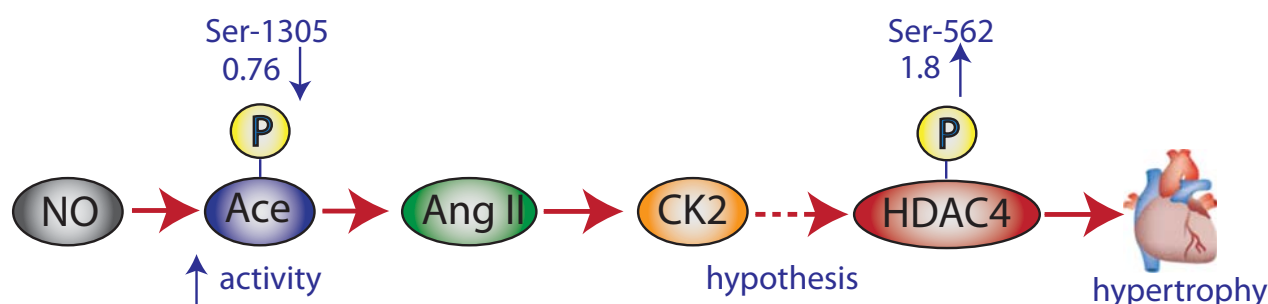


Fig. 5.21. Possible mechanism of hypertrophy development in iNOS⁺/myo^{-/-} mouse heart. Nitric oxide induced the major cardiac growth factor angiotensin II (Ang II) production by dephosphorylation and activation of angiotensin converting enzyme (Ace) at Ser-1305. Upon hypertrophic stimuli via angiotensin II, casein kinase 2 (CK2) dependent phosphorylation induces histone deacetylase 4 (HDAC4) phosphorylation at Ser-562 (predicted by PhosphoMotif finder and hypothesis after Force, 2008) which in turn may result in enzyme activation and hypertrophic growth.

As a further sign of increased CK2 activity, known CK2 substrates were found to be enhanced phosphorylated like histidine rich calcium binding protein at Ser-272 (+60%) and at Ser-474 (+30%), sarcalumenin at Ser-304 (+30%) and at Ser-442 (+60%) and nuclear ubiquitous casein and cyclin-dependent kinases substrate at Ser-58 and at Ser 61 (+109%).

The summarized data of predicted kinases (Fig. 5.20) show an enhanced frequency of protein kinase A (PKA) and protein kinase C (PKC) in the group of enhanced phosphorylated peptides by a factor 2.27 and 2.55, respectively.

In addition, enhanced phosphorylation of **protein kinase C, α (PKC- α or Prkca)** was found at Ser-319 (+96%) while phosphorylation of Ser-226 was slightly (-22%) decreased after NO stimulation, providing a further factor of PKC regulation upon iNOS derived NO release. However, there is no information about the functional relevance of this phosphorylation sites.

The fact, that PKC is a calcium stimulated enzyme but it can be also activated by diacylglycerol (DAG), the synthesis of which is stimulated by the NO/cGMP/PKG signaling pathway, gives additional evidence for enhanced PKC- α activation after one minute iNOS derived NO release.

PKC- α is the dominant PKC isoform in mouse and rabbit cardiac muscle and its activity and expression is known to be increased in the failing heart. Interestingly, hearts of mice lacking PKC- α contract more forcefully under resting and β -adrenergic-stimulated conditions than hearts with PKC- α . On the other hand, PKC- α overexpression depressed systolic function and contractility in both intact hearts and isolated cells (Braz et al., 2004). Functional changes occurs due to PKC- α

induced phospholamban (PLB) dephosphorylation at Ser-16 mediated by protein phosphatase 1 (PPI). Dephosphorylated PLB inhibits SERCA Ca^{2+} uptake into the SR, leading to reduced Ca^{2+} pools for the next contraction resulting in depressed contractility.

In addition, PKC- α -null mice crossed with a cardiomyopathy model lacking cysteine and glycine rich protein (CSRFP3) showed a normal phenotype, indicating a PPI independent PKC- α signaling in cardiomyopathy.

As described in chapter 5.4.2, iNOS derived NO release resulted in increased phosphorylation of PLB Thr-17 and in no changes of the doubly phosphorylated (Ser-16 and Thr-17) PLB peptide. This may indicate that Ser-16 dephosphorylation occurs concomitantly with induced Thr-17 phosphorylation, resulting a non-changed intensity of the doubly phosphorylated peptide. Thus, PKA target Ser-16 phosphorylation site could have been dephosphorylated upon PKC- α induced PPI.

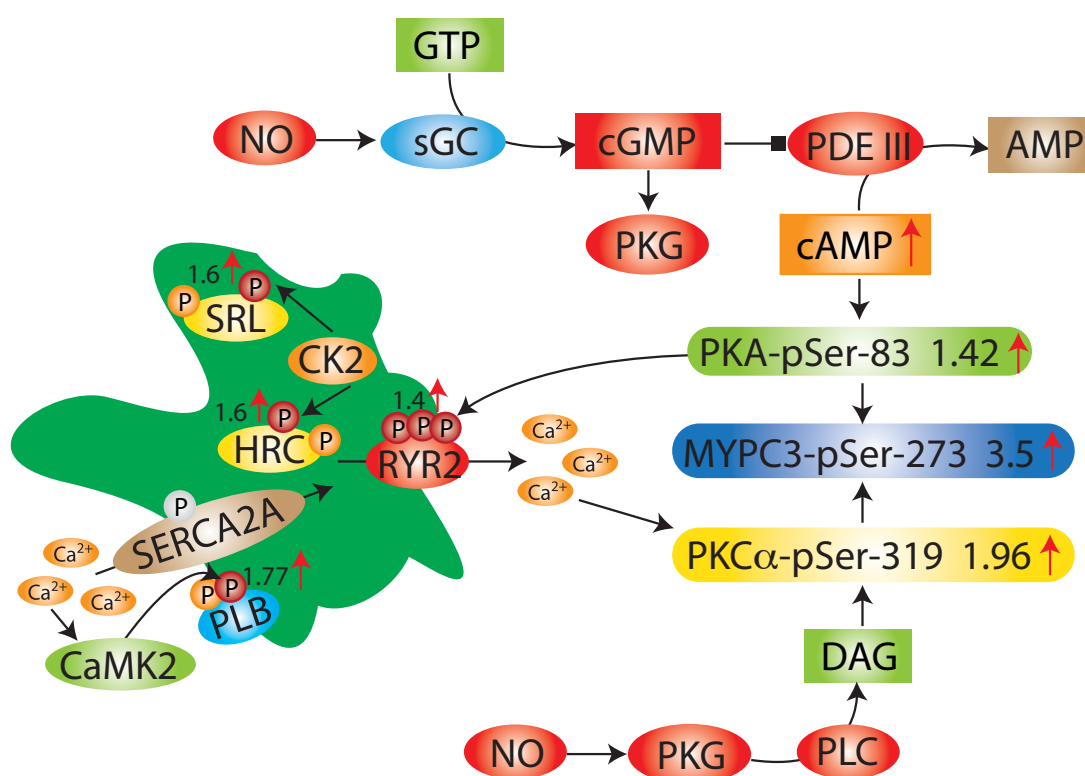


Figure 5.22: Nitric oxide (sGC) activates soluble guanylyl cyclase (sGC) converts guanylyl triphosphate (GTP) into cyclic guanylyl monophosphate (cGMP). This inhibits phosphodiesterase III (PDEIII) cyclic adenosine monophosphate (cAMP) conversion into adenosine monophosphate (AMP). Increasing cAMP levels activate protein kinase A (PKA), which can phosphorylate for example myosin binding protein c (MYPC3) the ryanodine receptor (RYR2) and phospholamban (PLB). iNOS derived NO release followed phosphoproteome study showed an enhanced phosphorylation (red) of PKA at Ser-83, of MYPC3 at Ser-273 (cardioprotective) and of RYR2 at Ser-2808, Thr-2810 and Ser-2811 (induce Ca^{2+} release into the cytosol). Additionally, the NO/cGMP/PKG pathway can activate diacylglycerol (DAG) synthesis over phospholipase C (PLC) which in turn induce PKC α and its downstream signaling like MYPC3 phosphorylation at Ser-273 and protein phosphatase I (PPI) activation which in turn dephosphorylates PLB at Ser-16. Interestingly, the CaMKII target PLB-Thr-17 showed an increased phosphorylation after iNOS derived NO release, which suppresses SERCA2A inhibition by PLB, and result in an induced Ca^{2+} transport into the sarcoplasmic reticulum (SR). Interestingly, SERCA2A phosphorylation (gray) was not affected upon iNOS derived NO release. Endogenous SR enzyme casein kinase II phosphorylates Ca^{2+} storage proteins sarcalumenin (SRL) and histidine rich calcium binding protein (HRC), which may enhance its Ca^{2+} binding capacity.

On the other hand, CaMKII induced PLB phosphorylation at its target site Thr-17, resulting in possibly increased SERCA activity. Furthermore, Thr-17 phosphorylation by CaMKII is known to be induced by electrical spacing in a frequency dependent manner (Hagemann et al., 2000). Furthermore, similar to my results, Said et al. (2003) measured also about two times increased Thr-17 phosphorylation and a decreased or non changed Ser-16 PLB phosphorylation in an ischemia-reperfusion model only one minute after reperfusion. This paper shows also that Thr-17 phosphorylation is essential for the mechanical recovery of cardiac functions. Thus, as a secondary effect, CaMKII-activation and PLB Thr-17 phosphorylation may contribute to the new steady state by partial functional recovery of the depressed heart function induced by NO stimulation.

According to a recent publication, PKA induced PLB phosphorylation at Ser-16 and subsequent increased SERCA Ca^{2+} load does not increase SR calcium release (Kawashima et al., 2009). Possibly phosphorylation of the neighbor site Thr-17 may also not influence SR calcium release, which would result in reduced cytosolic Ca^{2+} concentrations and increased SR calcium storage. In support of this hypothesis, I identified four enhanced phosphorylation sites in the Ca^{2+} ion binding region of two SR Ca^{2+} binding proteins, histidine rich calcium binding protein (HRC) and sarcalumenin (SRL). Hereby, the additional negatively charged phosphate groups have most likely enhanced the binding capacity of the proteins to positively charged calcium ions. Interestingly, changes in the phosphorylation level are almost the same, indicating that the same upstream kinase may targets these sites. In support of this hypothesis, phosphorylation sites HRC-272 and SRL-Ser442 both are located in a casein kinase 2 substrate motif and increased similarly, by factor 1.63 and 1.59 respectively. Interestingly, an early study described HRC and SRL as CK2 target within the SR, but without the identification of the phosphorylated amino acid residues (Shoshan-Barmatz et al., 1996). This study shows also, that both HRC and SRL associate with the ryanodine receptor 2 (RYR2) therefore, possibly regulate RYR2 mediated Ca^{2+} release into the cytosol.

A triple phosphorylated (pSer-2808, pThr-2810 and pSer-2811) peptide of RYR2 showed an increased signal intensity after iNOS derived NO release. Ser-2808 phosphorylation is known to reduce binding affinity of the channel-stabilizing subunit calstabin 2, resulting in leaky RYR2 and progressive cardiac dysfunction after myocardial infarction (Wehrens et al., 2006). Although the functional relevance of the other two novel phosphorylation site, pThr-2810 and pSer-2811 is not known, their phosphorylation most likely contributes to the pSer-2808 induced RYR2 activation. Therefore, RYR2 hyperphosphorylation and diastolic calcium 'leak' most likely contribute to impaired contractility upon iNOS derived NO release and to heart failure development in iNOS^{+/} myo^{-/-} mouse hearts.

cAMP dependent protein kinase (PKA) I-alpha regulatory subunit (PKA I α or PKARIA) is activated by cAMP, a signaling molecule, which is important for a variety of cellular functions. Activated PKA transduces its signal through phosphorylation of downstream target proteins. PRKARIA interacts with AKAP4, its complex with RFC2 may be involved in cell survival. NO is known to inhibit cAMP degradation thereby leading to an enhanced PKA activity. On the other hand, PKA can be phosphorylated by PKG-I at Ser-99 (Ser-100 in mouse; Hashimoto et al., 1981) but it is not phosphorylated by the catalytic subunit of cAMP-dependent protein kinase.

Using LTQ Orbitrap, I could identify an increased (+42%) Ser-83 PKA α phosphorylation after one minute of NO stimulation. While phosphorylation of Isoform 2 of cAMP-dependent protein kinase catalytic subunit alpha at Thr-190 and of cAMP-dependent protein kinase type II-alpha regulatory subunit at Thr-96 did not change. As a sign of increased PKA activity, an enhanced protein phosphorylation was measured at phosphorylation sites which are known PKA targets, like pSer-273 (+250%) of myosin binding protein C and Ser-2808 (+40%) of ryanodine receptor 2. However, this sites can be phosphorylated by other kinases, like PKC as well.

Dual specificity mitogen-activated protein kinase kinase 4 (EC 2.7.12.2) (MAP kinase kinase 4) (MAPKK 4) is also known as APK/Erk kinase (**SEK1**), or Jun kinase kinase (JNKK). In response to various cellular stresses and inflammatory cytokines, SEK1 activates the MAP kinase homologues SAPK, JNK and p38MAPK (Yan et al., 1994; Fleming et al., 2000). Interestingly, SEK1 expression is significantly reduced in heart failure patients and it has a key role in preventing the transition from an adaptive to maladaptive cardiac hypertrophy (Liu et al., 2009).

After one minute iNOS derived NO release SEK1 was found to be dephosphorylated at Ser-255 by 2.7 times. Decreased phosphorylation could occur due to oxidative stress which inhibits MAP kinase kinase kinase I (MEKK1) by site-specific glutathionylation in the ATP-binding domain (Cross et al., 2004). Additionally, MLK3 kinase mediated Ser-255 phosphorylation results in enzymatic activation (Deacon et al., 1997). Therefore, NO induced dephosphorylation inactivates SEK1, suppresses stress-activated signal transduction and may play a role in pathological hypertrophic remodeling.

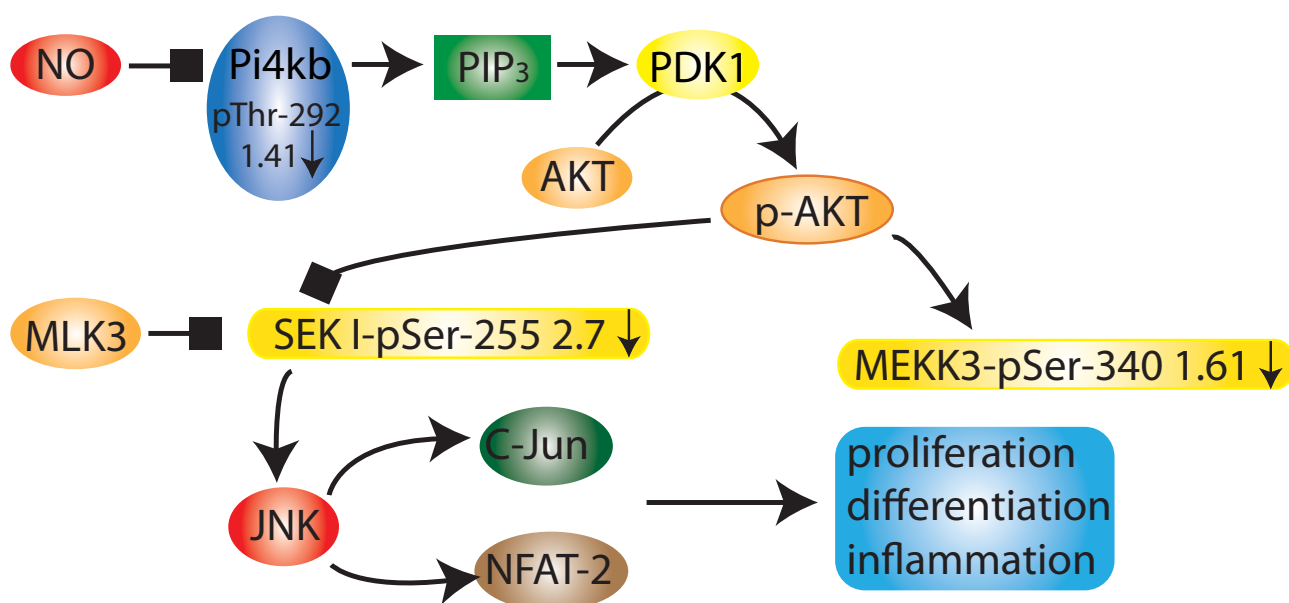


Figure 5.23: NO induced dephosphorylation of Phosphatidylinositol 4-kinase beta (Pi4kb) and thereby most likely decreased its activity to produce phosphatidylinositol-1,4,5,-triphosphate (PIP₃). Thus, reduced PIP₃ concentration leads to a decreased phosphoinositide-dependent kinase-I (PDK1) and Akt activity. Which led to a decreased mitogen-activated protein kinase kinase 3 (MEKK3) phosphorylation at Ser-340 (1.61 times). Additionally, reduced Akt activity leads to a depressed inhibition of SEK1 pathway (by phosphorylation at Ser80, not measured). On the other hand, MLK3 kinase target Ser-255 was found to be decreased phosphorylated by 2.7 times, which leads to decreased SEK1 activity and depressed downstream processes which play a role in proliferation, differentiation and inflammation.

Mitogen-activated protein kinase kinase kinase 3 (Map3k3 or **MEKK3**) is a protein kinase of the STE11 family. MEKK1-4 are important regulators of NF- κ B transcription factor which is an essential mediator of pro-inflammatory signals involved in immunity (Matitau et al., 2008). Similar to SEK1, MEKK3 is phosphorylated and activated also by MLK3 and additionally by TAK1. MEKK3 induces activation of mitogen-activated protein kinase kinase 5 (MEK5) by phosphorylation.

iNOS derived NO release resulted in dephosphorylation of Ser-340 by -61% which may decrease protein activity. Ser-340 is substrate of Akt (according to Phosphosite Plus, (2008) MS CS 5389), the key molecule in the signaling cascade of physiological hypertrophy which is suppressed by p38 MAPK (Taniike et al., 2008). Therefore, NO may induce p38 MAPK activity which in turn decrease Akt mediated Ser-340 MEKK3 phosphorylation leading to suppressed MEKK3 activity and downstream signaling,

Interestingly, phosphorylation of an other MAPK enzyme **Isoform 3 of Mitogen-activated protein kinase 14** at Thr-180 (+35%) were not strongly influenced by iNOS derived NO release.

Phosphatidylinositol 4-kinase beta (Pi4kb) phosphorylates phosphatidylinositol (PI) in the first committed step in the production of the second messenger phosphatidylinositol-1,4,5,-trisphosphate (PIP₃). Pi4kb is located at the mitochondrial and rough endoplasmic reticulum membranes. Ser-294 is a known PKD1 and 2 target, phosphorylation of which is protected by PI4KIIIbeta-14-3-3 interaction which stabilizes lipid kinase activity (Hausser A, et al., 2006).

I could identify dephosphorylation of the novel phosphorylation site Thr-292 by -41% after one minute of NO stimulaiton. Since Thr-292 is very close to Ser-294, phosphorylation of these sites may have similar roles in enzyme activation. Therefore, iNOS derived NO induced dephosphorylation may contribute to a decreased enzyme activity, and reduced PIP₃ production, which leads to suppressed PIP₃-PDK1 (phosphoinositide-dependent kinase-1)-Akt (v-Akt murine thymoma viral oncogene or PKB, protein kinase-B)-pAKT signaling (Scheid et al., 2002). Therefore, it seems to be a logic consequence, that phosphorylation of Akt targetes like MEKK3 Ser-340 and titin Ser-814 were also decreased. On the other hand, further Akt targets like isoform I of hepatoma-derived growth factor-related protein 2 at Ser-659 (+70%, Akt target), ATP citrate lyase at Ser-455 (+60%, target of PKA and Akt) and isoform I of protein NDRG2 at Ser-330 and at Thr-334 (+60%, Ser-330 is Akt target, Thr-334 is Akt and SGK1 target) were identified with an increased phosphorylation rate. However, other kinases could also be responsible for the observed phosphorylations after iNOS derived NO release.

5.6 SUMMARY

The present study gives the first global account of the NO-induced changes in the heart phosphoproteome. I was able to identify 826 phosphorylation sites (246 novel), in 772 phosphorylated peptides, of which 69 were upregulated (16 novel) and 50 downregulated (31 novel). This regulated phosphorylation sites are located in proteins playing a role in Ca²⁺ homeostasis, cardiac contractility, glucose and pyruvate metabolism, mitochondrial respiration and

transcriptional regulation. Furthermore, phosphorylation state of some kinases and phosphatases like PKA, PKC α , SEK1, MEKK3, Pi4kb and PP2A were also altered.

Fig. 5.24. shows a summary of the observed targets of NO-regulated protein phosphorylation sites in double transgenic iNOS⁺/myo^{-/-} mouse heart. iNOS derived NO most likely bound to the heme catalytic core of cytochrome C oxidase, which can explain the decrease in mitochondrial O₂ consumption (-16.4%) and ATP synthesis such as the decrease of the ATP pool (-3.3%) and the pCr/ATP ratio (-11.3%). Since under such conditions the AMP/ATP ratio (+42.7%), the ADP/ATP ratio (+11.3%) and the P_i/ATP ratio (+55.8%) were increased, changes in the cellular AMP and ADP pool might have activated AMP kinase, leading to increased ATP production by activation of glycolysis and TCA cycle by stimulation of pyruvate metabolism. Additionally, I found altered phosphorylation level of mitochondrial proteins like complex I, IV, ATP synthase and SOD1.

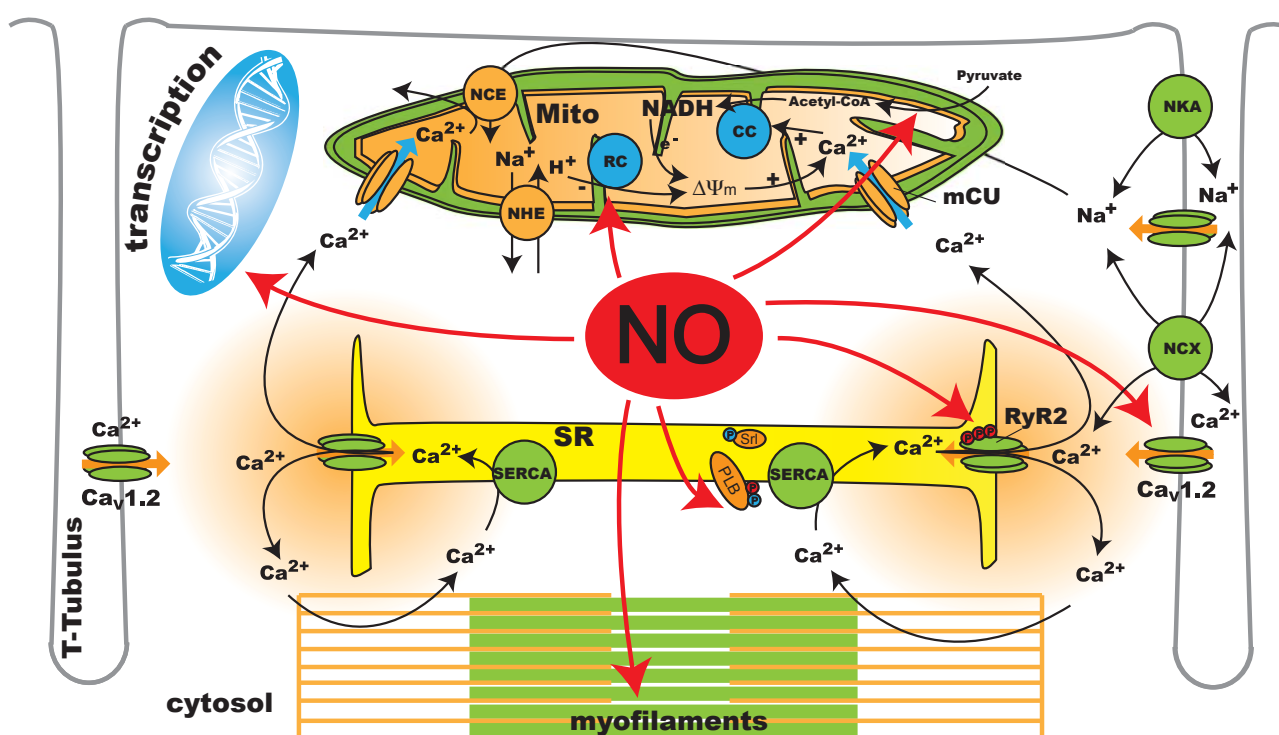


Figure 5.24: Schematic overview of iNOS derived NO induced changes in the cardiac phosphoproteome after one minute activation by L-arginine coperfusion. RC: respiratory chain, CC: Krebs Cycle, NKA: sodium potassium pump, NCX: sodium calcium exchanger, Cav1.2: L-type calcium channel, PLB: phospholamban, SERCA: sarcoplasmic reticulum Ca²⁺ ATPase, Srl: sarcalumenin, RyR2: ryanodine receptor

Interestingly, activity of proteins involved in calcium homeostasis like SERCA2A and RYR2 was induced by increased phosphorylation of PLB at Thr-17 (by CaMKII) or by RYR2 PKA phosphorylation. This should result in increased Ca^{2+} -cycling, possibly as a part of compensatory mechanism against NO-induced decreased contractility (-30%). On the other hand, dephosphorylation of additional proteins of Ca^{2+} homeostasis like Ahnak and L-type calcium channel $\text{Ca}_v1.2\text{-}\beta_2$, may decrease Ca^{2+} current I_{CaL} and might have served as mediator of iNOS induced negative inotropic effects.

Proteins of the contractile apparatus like myosin-6 and myosin binding protein c (by PKA) showed very strong changes in their phosphorylation state upon iNOS derived NO release, which may have additionally altered the contractile state. Surprisingly, in myosin-6, a major contractile protein of the mouse heart, I could identify 21 novel phosphorylation sites underlining the importance of protein phosphorylation in cardiac contraction. Additionally, the main cardiac gap junction protein connexin-43 which conducts electrical signals and is therefore important for cardiac rhythm generation was found to be enhanced phosphorylated. Furthermore, numerous transcription factors, some of which are involved in development of cardiac hypertrophy, were also altered.

Taking together, this study has identified numerous novel NO-dependent phosphorylation sites, which are likely to influence up- and downstream processes. While some phosphorylation sites can be directly related to the cardiodepressant action of NO, the functional relevance of many novel phosphorylation sites remain to be elucidated.

6 OUTLOOK

Future studies must examine the functional relevance of the identified novel phosphorylation sites e.g. by targeted point mutations of proteins. Generation of phosphorylation site specific antibodies or introducing multiple isotope label would enable to establish time courses to better understand phosphorylation kinetics in up- and downstream processes. The application of multiple labeling will certainly further increase sample complexity and this makes it indispensable to use mass spectrometer with high mass accuracy such as LTQ Orbitrap XL.

In addition to iNOS activation by L-arginine, targeted pharmacological activation or inhibition of relevant kinases such as AMPK, PKA, CK2, pyruvate dehydrogenase kinase, PKC α and phosphatases like PP2A could enable to test the role of downstream processes of iNOS derived NO.

Improving speed, sensitivity and mass accuracy of mass spectrometers, new fragmentation methods and introducing automated data analysis technologies will open another horizon for the analysis of biological processes. The growing need for understanding complex proteomics data will hopefully lead to improved computational modeling and prediction of signaling pathways in a systems biology approach.

7 REFERENCES

- Aebersold R, Mann M. (2003) Mass spectrometry-based proteomics. *Nature*. 422(6928):198-207.
- Afanas'ev I. (2009) Superoxide and nitric oxide in senescence and aging. *Front Biosci*. 14:3899-912. Review.
- Agbas A, Hui D, Wang X, Tek V, Zaidi A, Michaelis EK. (2007) Activation of brain calcineurin (Cn) by Cu-Zn superoxide dismutase (SOD1) depends on direct SOD1-Cn protein interactions occurring in vitro and in vivo. *Biochem J*. 405(1):51-9.
- Ahn JH, McAvoy T, Rakhilin SV, Nishi A, Greengard P, Nairn AC. (2007) Protein kinase A activates protein phosphatase 2A by phosphorylation of the B56delta subunit. *Proc Natl Acad Sci U S A* 104, 2979-84
- Almeida A, Moncada S, Bolaños JP. (2004) Nitric oxide switches on glycolysis through the AMP protein kinase and 6-phosphofructo-2-kinase pathway. *Nat Cell Biol*. 6(1):45-51.
- Alms GR, Sanz P, Carlson M, Haystead TA. (1999) Reg1p targets protein phosphatase 1 to dephosphorylate hexokinase II in *Saccharomyces cerevisiae*: characterizing the effects of a phosphatase subunit on the yeast proteome. *EMBO J*. 18(15):4157-68.
- Alvarez J, Hamplova J, Hohaus A, Morano I, Haase H, Vassort G. (2004) Calcium current in rat cardiomyocytes is modulated by the carboxyl-terminal ahnak domain. *J Biol Chem*. 279 (13):12456-61.
- Amanchy R, Periaswamy B, Mathivanan S, Reddy R, Tattikota SG, Pandey A. (2007) A curated compendium of phosphorylation motifs. *Nat Biotechnol*. 25(3):285-6.
- Anversa P, Levicky V, Beghi C, McDonald SL, Kikkawa Y. (1983) Morphometry of exercise-induced right ventricular hypertrophy in the rat. *Circ Res*. 52(1):57-64.
- Aponte AM, Phillips D, Hopper RK, Johnson DT, Harris RA, Blinova K, Boja ES, French S, Balaban RS. (2009) Use of (32)P To Study Dynamics of the Mitochondrial Phosphoproteome. *J Proteome Res*. 8(6):2679-2695.
- Arnold WP, Mittal CK, Katsuki S, Murad F. (1977) Nitric oxide activates guanylate cyclase and increases guanosine 3':5'-cyclic monophosphate levels in various tissue preparations. *PNAS*. 74, 3203-7.
- Arvanitis DA, Vafiadaki E, Fan GC, Mitton BA, Gregory KN, Del Monte F, Kontogianni-Konstantopoulos A, Sanoudou D, Kranias EG. Histidine-rich Ca-binding protein interacts with sarcoplasmic reticulum Ca-ATPase. (2007) *Am J Physiol Heart Circ Physiol*. 293(3):H1581-9.

- Arvanitis DA, Sanoudou D, Kolokathis F, Vafiadaki E, Papalouka V, Kontrogianni-Konstantopoulos A, Theodorakis GN, Paraskevaidis IA, Adamopoulos S, Dorn GW 2nd, Kremastinos DT, Kranias EG. (2008) The Ser96Ala variant in histidine-rich calcium-binding protein is associated with life-threatening ventricular arrhythmias in idiopathic dilated cardiomyopathy. *Eur Heart J*.29(20):2514-25.
- Axelsen LN, Stahlhut M, Mohammed S, Larsen BD, Nielsen MS, Holstein-Rathlou NH, Andersen S, Jensen ON, Hennan JK, Kjølbye AL. (2006) Identification of ischemia-regulated phosphorylation sites in connexin43: A possible target for the antiarrhythmic peptide analogue rotigaptide (ZPI23). *J Mol Cell Cardiol* 40, 790-8.
- Backs J, Song K, Bezprozvannaya S, Chang S, Olson EN. (2006) CaM kinase II selectively signals to histone deacetylase 4 during cardiomyocyte hypertrophy. *J Clin Invest*. 116(7):1853-64.
- Bailey A, Pope TW, Moore SA, Campbell CL. (2007) The tragedy of TRIUMPH for nitric oxide synthesis inhibition in cardiogenic shock: where do we go from here? *Am J Cardiovasc Drugs*. 7, 337-45.
- Bantscheff M, Schirle M, Sweetman G, Rick J, Kuster B. (2007) Quantitative mass spectrometry in proteomics: a critical review. *Anal Bioanal Chem* 389:1017–1031.
- Bauer DE, Hatzivassiliou G, Zhao F, Andreadis C, Thompson CB. (2005) ATP citrate lyase is an important component of cell growth and transformation. *Oncogene*. 24(41):6314-22.
- Beal MF. (2005) Less stress, longer life. *Nat Med*. 11(6):598-9.
- Beall A, Bagwell D, Woodrum D, Stoming TA, Kato K, Suzuki A, Rasmussen H, Brophy CM. (1999) The small heat shock-related protein, HSP20, is phosphorylated on serine 16 during cyclic nucleotide-dependent relaxation. *J Biol Chem* 274, 11344-51.
- Berridge MJ, Bootman MD, Roderick HL. (2003) Calcium signalling: dynamics, homeostasis and remodelling. *Nat Rev Mol Cell Biol*. 4(7):517-29.
- Bodwell JE, Ortí E, Coull JM, Pappin DJ, Smith LI, Swift F. (1991) Identification of phosphorylated sites in the mouse glucocorticoid receptor. *J Biol Chem*. 266(12):7549-55.
- Braugher JM, Mittal CK, Murad F. (1979) Effects of thiols, sugars, and proteins on nitric oxide activation of guanylate cyclase. *J Biol. Chem*. 254, 12450-4.
- Braz JC, Gregory K, Pathak A, Zhao W, Sahin B, Klevitsky R, Kimball TF, Lorenz JN, Nairn AC, Liggett SB, Bodi I, Wang S, Schwartz A, Lakatta EG, DePaoli-Roach AA, Robbins J, Hewett TE, Bibb JA, Westfall MV, Kranias EG, Molkentin JD. PKC- α regulates cardiac contractility and propensity toward heart failure. *Nat Med*. 10(3):248-54.
- Breckenridge MT, Dulyaninova NG, Egelhoff TT (2008) Multiple Regulatory Steps Control Mammalian Nonmuscle Myosin II Assembly in Live Cells. *Mol Biol Cell* 20(1):338-47.

- Brown GC, Cooper CE. (1994) Nanomolar concentrations of nitric oxide reversibly inhibit synaptosomal respiration by competing with oxygen at cytochrome oxidase. *FEBS Lett.* 356(2-3):295-8.
- Bryan NS, Bian K, Murad F. (2009) Discovery of the nitric oxide signaling pathway and targets for drug development. *Front Biosci.* 14:1-18. Review.
- Butler AR, Megson IL, Wright PG. (1998) Diffusion of nitric oxide and scavenging by blood in the vasculature. *Biochim Biophys Acta.* 1425, 168-76.
- Butt E, Gambaryan S, Göttfert N, Galler A, Marcus K, Meyer HE. (2003) Actin binding of human LIM and SH3 protein is regulated by cGMP- and cAMP-dependent protein kinase phosphorylation on serine 146. *J Biol Chem* 278, 15601-7
- Casteel DE, Zhuang S, Gudi T, Tang J, Vuica M, Desiderio S, Pilz RB. (2002) cGMP-dependent protein kinase I beta physically and functionally interacts with the transcriptional regulator TFII-I. *J Biol Chem.* 277(35):32003-14.
- Cidad P, Almeida A, Bolaños JP. (2004) Inhibition of mitochondrial respiration by nitric oxide rapidly stimulates cytoprotective GLUT3-mediated glucose uptake through 5'-AMP-activated protein kinase. *Biochem J.* 384(Pt 3):629-36.
- Chattopadhyay S, Santhamma KR, Sengupta S, McCue B, Kinter M, Sen GC, Sen I. (2005) Calmodulin binds to the cytoplasmic domain of angiotensin-converting enzyme and regulates its phosphorylation and cleavage secretion. *J Biol Chem.* 2005 Oct 7;280(40):33847-55.
- Chen EI, Cociorva D, Norris JL, Yates JR 3rd. (2007) Optimization of Mass Spectrometry-Compatible Surfactants for Shotgun Proteomics. *J. Proteome Res.* 7, 2529 -2538.
- Chen G, Pramanik BN. (2009) Application of LC/MS to proteomics studies: current status and future prospects. *Drug Discov Today.* 14(9-10):465-71.
- Chu G, Egnaczyk GF, Zhao W, Jo SH, Fan GC, Maggio JE, Xiao RP, Kranias EG. (2004) Phosphoproteome analysis of cardiomyocytes subjected to beta-adrenergic stimulation: identification and characterization of a cardiac heat shock protein p20. *Circ Res.* 94(2):184-93.
- Cooper CD, Lampe PD (2002) Casein kinase I regulates connexin-43 gap junction assembly. *J Biol Chem* 277, 44962-8
- Cross RL, Cunningham D, Tamura JK. (1984) Binding change mechanism for ATP synthesis by oxidative phosphorylation and photophosphorylation. *Curr Top Cell Regul.* 24:335-44
- Cross JV, Templeton DJ. (2004) Oxidative stress inhibits MEKK1 by site-specific glutathionylation in the ATP-binding domain. *Biochem J.* 1;381(Pt 3):675-83.

- Dai J, Jin WH, Sheng QH, Shieh CH, Wu JR, Zeng R. (2007) Protein phosphorylation and expression profiling by Yin-yang multidimensional liquid chromatography (Yin-yang MDLC) mass spectrometry. *J Proteome Res* 6, 250-62
- D'Atri LP, Malaver E, Romaniuk MA, Pozner RG, Negrotto S, Schattner M. (2009) Nitric oxide: news from stem cells to platelets. *Curr Med Chem*. 16(4):417-29. Review.
- Daub H, Olsen JV, Bairlein M, Gnad F, Oppermann FS, Körner R, Greff Z, Kéri G, Stemmann O, Mann M. (2008) Kinase-selective enrichment enables quantitative phosphoproteomics of the kinome across the cell cycle. *Mol Cell* 31, 438-48
- Deacon K, Blank JL (1997) Characterization of the mitogen-activated protein kinase kinase 4 (MKK4)/c-Jun NH2-terminal kinase 1 and MKK3/p38 pathways regulated by MEK kinases 2 and 3. MEK kinase 3 activates MKK3 but does not cause activation of p38 kinase in vivo. *J Biol Chem*. 272, 14489-96.
- Dennis G Jr, Sherman BT, Hosack DA, Yang J, Gao W, Lane HC, Lempicki RA. (2003) DAVID: Database for Annotation, Visualization, and Integrated Discovery. *Genome Biol*. 4(5):P3.
- Dephoure N, Zhou C, Villén J, Beausoleil SA, Bakalarski CE, Elledge SJ, Gygi SP. (2008) A quantitative atlas of mitotic phosphorylation. *Proc Natl Acad Sci U S A* 105, 10762-7.
- DeRubertis FR, Craven PA. (1976) Calcium-independent modulation of cyclic GMP and activation of guanylate cyclase by nitrosamies. *Science*. 193, 897-899.
- Dole M., Mack L. L., Hines R. L., Mobley R. C., Ferguson L. D., Alice M. B. (1968). Molecular beams of macroions. *Journal of Chemical Physics* 49 (5): 2240–2249.
- Duval M, Le Boeuf F, Huot J, Gratton JP. (2007) Src-mediated phosphorylation of Hsp90 in response to vascular endothelial growth factor (VEGF) is required for VEGF receptor-2 signaling to endothelial NO synthase. *Mol Biol Cell*. 18(11):4659-68.
- Endo S, Nairn AC, Greengard P, Ito M (2003) Thr123 of rat G-substrate contributes to its action as a protein phosphatase inhibitor. *Neurosci Res* 45, 79-8
- Evgenov OV, Pacher P, Schmidt PM, Haskó G, Schmidt HH, Stasch JP. (2006) NO-independent stimulators and activators of soluble guanylate cyclase: discovery and therapeutic potential. *Nat Rev Drug Discov*. 5(9):755-68.
- Feng J, Zhu M, Schaub MC, Gehrig P, Roschitzki B, Lucchinetti E, Zaugg M. (2008) Phosphoproteome analysis of isoflurane-protected heart mitochondria: phosphorylation of adenine nucleotide translocator-1 on Tyr194 regulates mitochondrial function. *Cardiovasc Res*. 80 (1):20-9.
- Fenn, J. B.; Mann, M.; Meng, C. K.; Wong, S. F.; Whitehouse, C. M. (1989). Electrospray ionization for mass spectrometry of large biomolecules. *Science* 246: 64–71.
- Fleming I, Busse R. (1999) Signal transduction of eNOS activation. *Cardiovasc Res*. 43, 532-41.

- Fleming Y, Armstrong CG, Morrice N, Paterson A, Goedert M, Cohen P. (2000) Synergistic activation of stress - activated protein kinase 1/ c- Jun N-terminal kinase (SAPK/JNK) isoforms by mitogen-activated protein kinase kinase 4 MKK4 and MKK7. *Biochem J.* 352:145–154.
- Flögel U, Merx MW, Godecke A, Decking UK, Schrader J. (2001) Myoglobin: A scavenger of bioactive NO. *Proc Natl Acad Sci.* 98, 735-40.
- Flögel U, Gödecke A, Klotz LO, Schrader J. (2004) Role of myoglobin in the antioxidant defense of the heart. *FASEB J.* 18, 1156-8
- Flögel U, Laussmann T, Gödecke A, Abanador N, Schäfers M, Fingas CD, Metzger S, Levkau B, Jacoby C, Schrader J. (2005) Lack of myoglobin causes a switch in cardiac substrate selection. *Circ Res.* 96(8):e68-75.
- Flynn CR, Smoke CC, Furnish E, Komalavilas P, Thresher J, Yi Z, Mandarino LJ, Brophy CM. (2007) Phosphorylation and activation of a transducible recombinant form of human HSP20 in *Escherichia coli*. *Protein Expr Purif* 52, 50-8
- Force, T. (2008) The weakness of a big heart *Nature Medicine* 14, 244 - 245.
- Fuchsgott RF, Zawadzki JV. (1980) The obligatory role of endothelial cells in the relaxation of arterial smooth muscle by acetylcholine. *Nature.* 288, 373-376
- Fukao M, Mason HS, Britton FC, Kenyon JL, Horowitz B, Keef KD. (1999) Cyclic GMP-dependent protein kinase activates cloned BKCa channels expressed in mammalian cells by direct phosphorylation at serine 1072. *J Biol Chem* 274, 10927-35
- Fulton D, Gratton JP, McCabe TJ, Fontana J, Fujio Y, Walsh K, Franke TF, Papapetropoulos A, Sessa WC. (1999) Regulation of endothelium-derived nitric oxide production by the protein kinase Akt. *Nature.* 399, 597-601.
- Galkina E, Ley K. (2009) Immune and inflammatory mechanisms of atherosclerosis. *Annu Rev Immunol.* 2009;27:165-97. Review.
- Gao F, Gao E, Yue TL, Ohlstein EH, Lopez BL, Christopher TA, Ma XL. (2002) Nitric oxide mediates the antiapoptotic effect of insulin in myocardial ischemia-reperfusion: the roles of PI3-kinase, Akt, and endothelial nitric oxide synthase phosphorylation. *Circulation.* 105(12): 1497-502.
- Gardiwal A, Klein G, Kraemer K, Durgac T, Koenig T, Niehaus M, Heineke J, Mohammadi B, Krampfl K, Schaefer A, Wollert KC, Korte T. (2007) Reduced delayed rectifier K⁺ current, altered electrophysiology, and increased ventricular vulnerability in MLP-deficient mice. *J Card Fail.* 13(8):687-93
- Garton AJ, Campbell DG, Carling D, Hardie DG, Colbran RJ, Yeaman SJ. (1989) Phosphorylation of bovine hormone-sensitive lipase by the AMP-activated protein kinase. A possible antilipolytic mechanism. *Eur J Biochem* 179, 249-54

- Geier C, Gehmlich K, Ehler E, Hassfeld S, Perrot A, Hayess K, Cardim N, Wenzel K, Erdmann B, Krackhardt F, Posch MG, Osterziel KJ, Bublak A, Nägele H, Scheffold T, Dietz R, Chien KR, Spuler S, Fürst DO, Nürnberg P, Ozcelik C. (2008) Beyond the sarcomere: CSRP3 mutations cause hypertrophic cardiomyopathy. *Hum Mol Genet.* 17(18):2753-65.
- Gerber SA, Rush J, Stemman O, Kirschner MW, Gygi SP. (2003) Absolute quantification of proteins and phosphoproteins from cell lysates by tandem MS. *Proc Natl Acad Sci.* 100(12): 6940-5.
- Gladwin MT. (2006) Role of the red blood cell in nitric oxide homeostasis and hypoxic vasodilation. *Adv Exp Med Biol.* 588:189-205.
- Glass DB, Krebs EG (1979) Comparison of the substrate specificity of adenosine 3':5'-monophosphate- and guanosine 3':5'-monophosphate-dependent protein kinases. Kinetic studies using synthetic peptides corresponding to phosphorylation sites in histone H2B. *J Biol Chem* 254, 9728-38
- Gödecke A, Flögel U, Zanger K, Ding Z, Hirchenhain J, Decking UK, Schrader J. (1999) Disruption of myoglobin in mice induces multiple compensatory mechanisms. *PNAS.* 96, 10495-10500.
- Gregory K.N., Ginsburg K.S., Bodi I., Hahn H., Marreez Y.M., Song Q., et al. (2006) Histidine-rich Ca binding protein: a regulator of sarcoplasmic reticulum calcium sequestration and cardiac function. *J Mol Cell Cardiol* 40:653–665
- Gruetter CA, Barry BK, McNamara DB, Gruetter DY, Kadowitz PJ, Ignarro L. (1979) Relaxation of bovine coronary artery and activation of coronary arterial guanylate cyclase by nitric oxide, nitroprusside and a carcinogenic nitrosoamine. *J Cyclic Nucleotide Res.* 5, 211-24.
- Grueter CE, Abiria SA, Dzhura I, Wu Y, Ham AJ, Mohler PJ, Anderson ME, Colbran RJ. (2006) L-type Ca²⁺ channel facilitation mediated by phosphorylation of the beta subunit by CaMKII. *Mol Cell* 23, 641-50.
- Grueter CE, Abiria SA, Wu Y, Anderson ME, Colbran RJ. (2008) Differential Regulated Interactions of Calcium/Calmodulin-Dependent Protein Kinase II with Isoforms of Voltage-Gated Calcium Channel beta Subunits. *Biochemistry* 47, 1760-7.
- Gururaj A, Barnes CJ, Vadlamudi RK, Kumar R. (2004) Regulation of phosphoglucomutase I phosphorylation and activity by a signaling kinase. *Oncogene.* 23(49):8118-27.
- Gygi SP, Rist B, Gerber SA, Turecek F, Gelb MH, Aebersold R. (1999) Quantitative analysis of complex protein mixtures using isotope-coded affinity tags. *Nat Biotechnol.* 17(10): 994-9.
- Haase H, Pagel I, Khalina Y, Zacharzowsky U, Person V, Lutsch G, Petzhold D, Kott M, Schaper J, Morano I. (2004) The carboxyl-terminal ahnak domain induces actin bundling and stabilizes muscle contraction. *FASEB J.* 18(7):839-41.

- Haase H, Alvarez J, Petzhold D, Doller A, Behlke J, Erdmann J, Hetzer R, Regitz-Zagrosek V, Vassort G, Morano I. (2005) Ahnak is critical for cardiac Ca(V)1.2 calcium channel function and its beta-adrenergic regulation. *FASEB J.* 19(14):1969-77.
- Hadad N, Meyer HE, Varsanyi M, Fleischer S, Shoshan-Barmatz V. (1999) Cardiac sarcalumenin: phosphorylation, comparison with the skeletal muscle sarcalumenin and modulation of ryanodine receptor. *J Membr Biol.* 170(1):39-49.
- Hagemann D, Kuschel M, Kuramochi T, Zhu W, Cheng H, Xiao RP. (2000) Frequency-encoding Thr17 phospholamban phosphorylation is independent of Ser16 phosphorylation in cardiac myocytes. *J Biol Chem.* 275(29):22532-6.
- Hashimoto E, Takio K, Krebs EG (1981) Studies on the site in the regulatory subunit of type I cAMP-dependent protein kinase phosphorylated by cGMP-dependent protein kinase. *J Biol Chem* 256, 5604-7.
- Hauck L, Harms C, An J, Rohne J, Gertz K, Dietz R, Endres M, von Harsdorf R. (2008) Protein kinase CK2 links extracellular growth factor signaling with the control of p27(Kip1) stability in the heart. *Nat Med.* 2008 Mar; 14(3):315-24.
- Haug LS, Jensen V, Hvalby O, Walaas SI, Ostvold AC. (1999) Phosphorylation of the inositol 1,4,5-trisphosphate receptor by cyclic nucleotide-dependent kinases in vitro and in rat cerebellar slices in situ. *J Biol Chem* 274, 7467-73
- Hausser A, Link G, Hoene M, Russo C, Selchow O, Pfizenmaier K. (2006) Phospho-specific binding of 14-3-3 proteins to phosphatidylinositol 4-kinase III beta protects from dephosphorylation and stabilizes lipid kinase activity. *J Cell Sci* 119, 3613-21
- Heineke J, Kempf T, Kraft T, Hilfiker A, Morawietz H, Scheubel RJ, Caroni P, Lohmann SM, Drexler H, Wollert KC. (2003) Downregulation of cytoskeletal muscle LIM protein by nitric oxide: impact on cardiac myocyte hypertrophy. *Circulation.* 107(10):1424-32.
- Heineke J, Ruetten H, Willenbockel C, Gross SC, Naguib M, Schaefer A, Kempf T, Hilfiker-Kleiner D, Caroni P, Kraft T, Kaiser RA, Molkentin JD, Drexler H, Wollert KC. (2005) Attenuation of cardiac remodeling after myocardial infarction by muscle LIM protein-calcineurin signaling at the sarcomeric Z-disc. *Proc Natl Acad Sci.* 102(5):1655-60
- Heller M, Mattou H, Menzel C, Yao X. (2003) Trypsin catalyzed 16O-to-18O exchange for comparative proteomics: tandem mass spectrometry comparison using MALDI-TOF, ESI-QTOF, and ESI-ion trap mass spectrometers. *J Am Soc Mass Spectrom.* 14(7):704-18.
- Heger J, Gödecke A, Flögel U, Merx MW, Molojavyi A, Kühn-Velten WN, Schrader J. (2002) Cardiac-specific overexpression of inducible nitric oxide synthase does not result in severe cardiac dysfunction. *Circ. Res.* 90, 93-99.

- Hilger M, Bonaldi T, Gnad F, Mann M. (2009) Systems-wide analysis of a phosphatase knock down by quantitative proteomics and phosphoproteomics. *Mol Cell Proteomics*. 2009 May 9. [Epub ahead of print]
- Hohaus A, Person V, Behlke J, Schaper J, Morano I, Haase H. (2002) The carboxyl-terminal region of ahnak provides a link between cardiac L-type Ca^{2+} channels and the actin-based cytoskeleton. *FASEB J*. 16(10):1205-16.
- Horio S, Ogawa M, Kawakami N, Fujimoto K, Fukui H. (2004) Identification of amino acid residues responsible for agonist-induced down-regulation of histamine $\text{H}(1)$ receptors. *J Pharmacol Sci* 94, 410-9
- Hsu JL, Huang SY, Chow NH, and Chen SH. (2003) Stable-Isotope Dimethyl Labeling for Quantitative Proteomics. *Anal. Chem*. 75, 6843 -6852.
- Huang SY, Tsai ML, Chen GY, Wu CJ, Chen SH. (2007) A systematic MS-based approach for identifying in vitro substrates of PKA and PKG in rat uteri. *J Proteome Res*. 6(7):2674-84.
- Huang J, Zhou H, Mahavadi S, Sriwai W, Murthy KS. (2007) Inhibition of $\text{G}\alpha_{\text{q}}$ -dependent PLC- $\beta 1$ activity by PKG and PKA is mediated by phosphorylation of RGS4 and GRK2. *Am J Physiol Cell Physiol* 292, C200-8.
- Huang DW, Sherman BT, Lempicki RA. (2009) Systematic and integrative analysis of large gene lists using DAVID Bioinformatics Resources. *Nature Protoc*. 4(1):44-57.
- Hunter T, Sefton BM. (1980) Transforming gene product of Rous sarcoma virus phosphorylates tyrosine. *Proc Natl Acad Sci U S A*. 77(3):1311-5.
- Ignarro LJ, Buga GM, Wood KS, Byrns RE, Chaudhuri G. (1987) Endothelium-derived relaxing factor produced and released from artery and vein is nitric oxide. *PNAS*. 84, 9265-9.
- Ignarro LJ. (2007) Heart mtNOS, a key mediator of oxidative injury in ischemia/reperfusion. *J Mol Cell Cardiol*. 43, 409-10.
- Iñarraa P, Moini H, Han D, Rettori D, Aguiló I, Alava MA, Iturralde M, Cadenas E. (2007) Mitochondrial respiratory chain and thioredoxin reductase regulate intermembrane Cu,Zn-superoxide dismutase activity: implications for mitochondrial energy metabolism and apoptosis. *Biochem J*. 405(1):173-9.
- Iribarne J.V. and Thomson B. A. (1976). On the evaporation of small ions from charged droplets. *Journal of Chemical Physics* 64 (6): 2287–2294.
- Jackson PE, Feng QP, Jones DL.(2008) Nitric oxide depresses connexin 43 after myocardial infarction in mice. *Acta Physiol (Oxf)*. 194(1):23-33.
- Jaehnig EJ, Heidt AB, Greene SB, Cornelissen I, Black BL. (2006) Increased susceptibility to isoproterenol-induced cardiac hypertrophy and impaired weight gain in mice lacking the histidine-rich calcium-binding protein. *Mol Cell Biol*. 26(24):9315-26.

- Joshi MS, Ferguson TB Jr, Han TH, Hyduke DR, Liao JC, Rassaf T, Bryan N, Feelisch M, Lancaster JR Jr. (2002) Nitric oxide is consumed, rather than conserved, by reaction with oxyhemoglobin under physiological conditions. *PNAS*. 99, 10341-6.
- Kang D, Ghoo YS, Suh M, Kang C. (2002) Highly Sensitive and Fast Protein Detection with Coomassie Brilliant Blue in Sodium Dodecyl Sulfate-Polyacrylamide Gel Electrophoresis. *Bull Kor Chem S*. 23, 1511
- Katsuki S, Arnold WP, Murad F. (1977) Effects of sodium nitroprusside, nitroglycerin, and sodium azide on levels of cyclic nucleotides and mechanical activity of various tissues. *J Cyclic Nucleotide Res*. 3, 239-47.
- Kawashima H, Satoh H, Saotome M, Urushida T, Katoh H, Hayashi H (2009) Protein Phosphatase Inhibitor-1 Augments a Protein Kinase A-Dependent Increase in the Ca(2+) Loading of the Sarcoplasmic Reticulum Without Changing its Ca(2+) Release. *Circ J*. 2009 Apr 20. [Epub ahead of print]
- Keicher C, Gambaryan S, Schulze E, Marcus K, Meyer HE, Butt E.(2004) Phosphorylation of mouse LASP-1 on threonine 156 by cAMP- and cGMP-dependent protein kinase. *Biochem Biophys Res Commun* 324, 308-16.
- Kelm M, Schäfer S, Dahmann R, Dolu B, Perings S, Decking UK, Schrader J, Strauer BE. (1997) Nitric oxide induced contractile dysfunction is related to a reduction in myocardial energy generation. *Cardiovasc Res*. 36, 185-94.
- Kim E, Shin DW, Hong CS, Jeong D, Kim DH, Park WJ. (2003) Increased Ca²⁺ storage capacity in the sarcoplasmic reticulum by overexpression of HRC (histidine-rich Ca²⁺ binding protein). *Biochem Biophys Res Commun*. 300(1):192-6.
- Kim A, Kim MJ, Yang Y, Kim JW, Yeom YI, Lim JS. (2009) Suppression of NF- κ B activity by NDRG2 expression attenuates the invasive potential of highly malignant tumor cells. *Carcinogenesis*. 2009 Mar 31. [Epub ahead of print] PMID: 19336468
- Kirkpatrick DS, Gerber SA, Gygi SP. (2005) The absolute quantification strategy: a general procedure for the quantification of proteins and post-translational modifications. *Methods*. 35(3):265-73.
- Köcher T, Superti-Furga G. Mass spectrometry-based functional proteomics: from molecular machines to protein networks. (2007) *Nat Methods*. 4(10):807-15.
- Korotchkina LG, Patel MS (1995) Mutagenesis studies of the phosphorylation sites of recombinant human pyruvate dehydrogenase. Site-specific regulation. *J Biol Chem* 270, 14297-304
- Korotchkina LG, Patel MS (2001) Probing the mechanism of inactivation of human pyruvate dehydrogenase by phosphorylation of three sites. *J Biol Chem* 276, 5731-8

- Krenz M, Sadayappan S, Osinska HE, Henry JA, Beck S, Warshaw DM, Robbins J. (2007) Distribution and structure-function relationship of myosin heavy chain isoforms in the adult mouse heart. *J Biol Chem.* 282(33):24057-64.
- Krstic MD, Rogatsky I, Yamamoto KR, Garabedian MJ. (1997) Mitogen-activated and cyclin-dependent protein kinases selectively and differentially modulate transcriptional enhancement by the glucocorticoid receptor. *Mol Cell Biol.* 17(7):3947-54.
- Krüger M, Kratchmarova I, Blagoev B, Tseng YH, Kahn CR, Mann M. (2008) Dissection of the insulin signaling pathway via quantitative phosphoproteomics. *Proc Natl Acad Sci.* 105(7):2451-6.
- Krüger M, Moser M, Ussar S, Thievensen I, Lubner CA, Forner F, Schmidt S, Zanivan S, Fässler R, Mann M (2008) SILAC mouse for quantitative proteomics uncovers kindlin-3 as an essential factor for red blood cell function. *Cell.* 134(2):353-64
- Krüger M, Kötter S, Grützner A, Lang P, Andresen C, Redfield MM, Butt E, dos Remedios CG, Linke WA. (2009) Protein kinase G modulates human myocardial passive stiffness by phosphorylation of the titin springs. *Circ Res.* 104(1):87-94.
- Kurokawa M, Zhao C, Reya T, Kornbluth S. (2008) Inhibition of apoptosome formation by suppression of Hsp90 β phosphorylation in tyrosine kinase-induced leukemias. *Mol Cell Biol.* 28(17):5494-506.
- Kwan HY, Huang Y, Yao X. (2006) Protein kinase C can inhibit TRPC3 channels indirectly via stimulating protein kinase G. *J Cell Physiol.* 207(2):315-21.
- Lampe PD, Cooper CD, King TJ, Burt JM (2006) Analysis of Connexin43 phosphorylated at S325, S328 and S330 in normoxic and ischemic heart. *J Cell Sci* 119, 3435-42
- Larsen MR, Thingholm TE, Jensen ON, Roepstorff P, Jørgensen TJ. (2005) Highly selective enrichment of phosphorylated peptides from peptide mixtures using titanium dioxide microcolumns. *Mol Cell Proteomics* 4, 873-86.
- Lee IH, You JO, Ha KS, Bae DS, Suh PG, Rhee SG, Bae YS. (2004) AHNAK-mediated activation of phospholipase C- γ 1 through protein kinase C. *J Biol Chem.* 279(25):26645-53.
- Lee IH, Lim HJ, Yoon S, Seong JK, Bae DS, Rhee SG, Bae YS. (2008) Ahnak protein activates protein kinase C (PKC) through dissociation of the PKC-protein phosphatase 2A complex. *J Biol Chem.* 283(10):6312-20.
- Lees-Miller SP, Anderson CW (1989) Two human 90-kDa heat shock proteins are phosphorylated in vivo at conserved serines that are phosphorylated in vitro by casein kinase II. *J Biol Chem* 264, 2431-7
- Lim G, Venetucci L, Eisner DA, Casadei B. (2008) Does nitric oxide modulate cardiac ryanodine receptor function? Implications for excitation-contraction coupling. *Cardiovasc Res.* 77 (2):256-64.

- Little GH, Bai Y, Williams T, Poizat C. (2007) Nuclear calcium/calmodulin-dependent protein kinase II δ preferentially transmits signals to histone deacetylase 4 in cardiac cells. *J Biol Chem.* 282(10):7219-31.
- Liu W, Zi M, Jin J, Prehar S, Oceandy D, Kimura TE, Lei M, Neyses L, Weston AH, Cartwright EJ, Wang X. (2009) Cardiac-specific deletion of mkk4 reveals its role in pathological hypertrophic remodeling but not in physiological cardiac growth. *Circ Res.* 104(7): 905-14.
- Lohan J, Ohlendieck K. (2004) Drastic reduction in the luminal Ca²⁺-binding proteins calsequestrin and sarcoplumenin in dystrophin-deficient cardiac muscle. *Biochim Biophys Acta.* 1689(3):252-8.
- Lorenzen-Schmidt I, Stuyvers BD, ter Keurs HE, Date MO, Hoshijima M, Chien KR, McCulloch AD, Omens JH. (2005) Young MLP deficient mice show diastolic dysfunction before the onset of dilated cardiomyopathy. *J Mol Cell Cardiol.* 39(2):241-50.
- Lu H, Zong C, Wang Y, Young GW, Deng N, Souda P, Li X, Whitelegge J, Drews O, Yang PY, Ping P. (2008) Revealing the dynamics of the 20 S proteasome phosphoproteome: a combined CID and electron transfer dissociation approach. *Mol Cell Proteomics.* 7(11):2073-89.
- Lucas KA, Pitari GM, Kazerounian S, Ruiz-Stewart I, Park J, Schulz S, Chepenik KP, Waldman SA. (2000) Guanylyl cyclases and signaling by cyclic GMP. *Pharmacol Rev.* 52(3):375-414.
- MacDonald JA, Walker LA, Nakamoto RK, Gorenne I, Somlyo AV, Somlyo AP, Haystead TA. (2000) Phosphorylation of telokin by cyclic nucleotide kinases and the identification of in vivo phosphorylation sites in smooth muscle. *FEBS Lett.* 479(3):83-8.
- MacKenzie A, Wadsworth RM. (2003) Extracellular L-arginine is required for optimal NO synthesis by eNOS and iNOS in the rat mesenteric artery wall. *British Journal of Pharmacology* (2003) 139, 1487–1497.
- Maier LS. (2009) Role of CaMKII for signaling and regulation in the heart. *Front Biosci.* 14:486-96.
- Maile LA, Clemmons DR. (2002) Regulation of insulin-like growth factor I receptor dephosphorylation by SHPS-1 and the tyrosine phosphatase SHP-2. *J Biol Chem.* 277, 8955-60.
- Maiolica A, Borsotti D, Rappsilber J. (2005) Self-made frits for nanoscale columns in proteomics. *Proteomics.* 5, 3847-50.
- Marx SO, Reiken S, Hisamatsu Y, Jayaraman T, Burkhoff D, Rosemblyt N, Marks AR. (2000) PKA phosphorylation dissociates FKBP12.6 from the calcium release channel (ryanodine receptor): defective regulation in failing hearts. *Cell.* 101(4):365-76.
- Matitau AE, Scheid MP. (2008) Phosphorylation of MEKK3 at threonine 294 promotes 14-3-3 association to inhibit nuclear factor kappaB activation. *J Biol Chem.* 283(19):13261-8.

- Macek B, Mijakovic I, Olsen JV, Gnad F, Kumar C, Jensen PR, Mann M. (2007) The serine/threonine/tyrosine phosphoproteome of the model bacterium *Bacillus subtilis*. *Mol Cell Proteomics*. 6(4):697-707.
- Mayer EJ, Huckle W, Johnson RG Jr, McKenna E. (2000) Characterisation and Quantitation of Phospholamban and Its Phosphorylation State Using Antibodies. *Biochem Biophys Res Commun*. 267, 40-8.
- McDonald BJ, Moss SJ (1994) Differential phosphorylation of intracellular domains of gamma-aminobutyric acid type A receptor subunits by calcium/calmodulin type 2-dependent protein kinase and cGMP-dependent protein kinase. *J Biol Chem* 269, 18111-7.
- Mills GD, Kubo H, Harris DM, Berretta RM, Piacentino V 3rd, Houser SR. (2006) Phosphorylation of phospholamban at threonine-17 reduces cardiac adrenergic contractile responsiveness in chronic pressure overload-induced hypertrophy. *Am J Physiol Heart Circ Physiol*. 291 (1):H61-70.
- Miura Y, Kaibuchi K, Itoh T, Corbin JD, Francis SH, Takai Y. (1992) Phosphorylation of smg p21B/rap1B p21 by cyclic GMP-dependent protein kinase. *FEBS Lett* 297, 171-4.
- Moncada S, Erusalimsky JD. (2002) Does nitric oxide modulate mitochondrial energy generation and apoptosis? *Nat Rev Mol Cell Biol*. 3(3):214-20.
- Motoyama A, Xu T, Ruse CI, Wohlschlegel JA, Yates JR 3rd. (2007) Anion and cation mixed-bed ion exchange for enhanced multidimensional separations of peptides and phosphopeptides. *Anal Chem*. 79, 3623-34.
- Mudd JO, Kass DA. (2008) Tackling heart failure in the twenty-first century. *Nature*, 451, 919-928.
- Murray JT, Campbell DG, Morrice N, Auld GC, Shpiro N, Marquez R, Pegg M, Bain J, Bloomberg GB, Grahammer F, Lang F, Wulff P, Kuhl D, Cohen P. (2004) Exploitation of KESTREL to identify NDRG family members as physiological substrates for SGK1 and GSK3. *Biochem J*. 384(Pt 3):477-88.
- Münch G, Böck B, Brixius K, Reuter H, Mehlhorn U, Bloch W, Schwinger, RHG. (2000) SERCA2a activity correlates with the force-frequency relationship in human myocardium *Am J Physiol Heart Circ Physiol* 278: H1924-H1932.
- Murad F, Arnold WP, Mittal CK, Braugher JM. (1979) Properties and regulation of guanylate cyclase and some proposed functions of cyclic GMP. *Adv. Cyclic Nucleotide Res.* 11, 175-204
- Navarro A, Boveris A. (2008) Mitochondrial nitric oxide synthase, mitochondrial brain dysfunction in aging, and mitochondria-targeted antioxidants. *Adv Drug Deliv Rev*. 60, 1534-44.
- Nett IR, Martin DM, Miranda-Saavedra D, Lamont D, Barber JD, Mehlert A, Ferguson MA. (2009) The phosphoproteome of bloodstream form *Trypanosoma brucei*, causative agent of African sleeping sickness. *Mol Cell Proteomics*. 2009 Apr 4. [Epub ahead of print]

- Nicolaou P, Knöll R, Haghighi K, Fan GC, Dorn GW 2nd, Hasenfub G, Kranias EG. (2008) Human mutation in the anti-apoptotic heat shock protein 20 abrogates its cardioprotective effects. *J Biol Chem.* 283(48):33465-71.
- O'Brien PJ, O'Grady M, McCutcheon LJ, Shen H, Nowack L, Horne RD, Mirsalimi SM, Julian RJ, Grima EA, Moe GW, et al. (1992) Myocardial myoglobin deficiency in various animal models of congestive heart failure. *J Mol Cell Cardiol.* 24, 721-30.
- O'Brien PJ, Gwathmey JK. (1995) Myocardial Ca(2+)- and ATP-cycling imbalances in end-stage dilated and ischemic cardiomyopathies. *Cardiovasc Res.* 30, 394-404.
- Oda, Y., Huang, K., Cross, F. R., Cowburn, D., Chait BT. (1999) Accurate quantitation of protein expression and site-specific phosphorylation. *Proc. Natl. Acad. Sci.* 96, 6591–6596.
- O'Farrell PH. (1975) High resolution two-dimensional electrophoresis of proteins. *J Biol Chem.* 250, 4007-21.
- Ogut O, Brozovich FV. (2008) The potential role of MLC phosphatase and MAPK signalling in the pathogenesis of vascular dysfunction in heart failure. *J Cell Mol Med.* 12(6A):2158-64. Review.
- Ohtani T, Mano T, Hikoso S, Sakata Y, Nishio M, Takeda Y, Otsu K, Miwa T, Masuyama T, Hori M, Yamamoto K. (2009) Cardiac steroidogenesis and glucocorticoid in the development of cardiac hypertrophy during the progression to heart failure. *J Hypertens.* 2009 Apr 3. [Epub ahead of print]
- Olsen JV, Blagoev B, Gnäd F, Macek B, Kumar C, Mortensen P, Mann M. (2006) Global, in vivo, and site-specific phosphorylation dynamics in signaling networks. *Cell.* 127, 635-48.
- Ong SE, Blagoev B, Kratchmarova I, Kristensen DB, Steen H, Pandey A, Mann M. (2002) Stable isotope labeling by amino acids in cell culture, SILAC, as a simple and accurate approach to expression proteomics. *Mol Cell Proteomics.* 1(5):376-86.
- Perkins D N, Pappin D J C, Creasy D M, Cottrell J S. (1999) Probability-based protein identification by searching sequence databases using mass spectrometry data. *Electrophoresis*, 20, 3551-67
- Pacher P, Beckman JS, Liaudet L. (2007) Nitric oxide and peroxynitrite in health and disease. *Physiol Rev.* 87, 315-424.
- Palmer BM, Noguchi T, Wang Y, Heim JR, Alpert NR, Burgon PG, Seidman CE, Seidman JG, Maughan DW, LeWinter MM. (2004) Effect of cardiac myosin binding protein-C on mechanoenergetics in mouse myocardium. *Circ Res.* 94(12):1615-22.
- Palmisano G, Sardanelli AM, Signorile A, Papa S, Larsen MR. (2007) The phosphorylation pattern of bovine heart complex I subunits. *Proteomics.* 7(10):1575-83.

- Palomer X, Alvarez-Guardia D, Rodríguez-Calvo R, Coll T, Laguna JC, Davidson MM, Chan TO, Feldman AM, Vázquez-Carrera M. (2009) TNF- α reduces PGC-1 α expression through NF- κ B and p38 MAPK leading to increased glucose oxidation in a human cardiac cell model. *Cardiovasc Res*. 81(4):703-12.
- Papa S, De Rasmio D, Scacco S, Signorile A, Technikova-Dobrova Z, Palmisano G, Sardanelli AM, Papa F, Panelli D, Scaringi R, Santeramo A. (2008) Mammalian complex I: a regulable and vulnerable pacemaker in mitochondrial respiratory function. *Biochim Biophys Acta*. (7-8): 719-28.
- Park JM, Intine RV, Maraia RJ. (2007) Mouse and human La proteins differ in kinase substrate activity and activation mechanism for tRNA processing. *Gene Expr*. 14(2):71-81.
- Pierce MW, Palmer JL, Keutmann HT, Hall TA, Avruch J. (1982) The insulin-directed phosphorylation site on ATP-citrate lyase is identical with the site phosphorylated by the cAMP-dependent protein kinase in vitro. *J Biol Chem*. 257(18):10681-6.
- Peshenko IV, Olshevskaya EV, Dizhoor AM (2004) Ca(2+)-dependent conformational changes in guanylyl cyclase-activating protein 2 (GCAP-2) revealed by site-specific phosphorylation and partial proteolysis. *J Biol Chem* 279, 50342-9
- Picciotto MR, Cohn JA, Bertuzzi G, Greengard P, Nairn AC. (1992) Phosphorylation of the cystic fibrosis transmembrane conductance regulator. *J Biol Chem* 267, 12742-52
- Piccoli C, Scacco S, Bellomo F, Signorile A, Iuso A, Boffoli D, Scrima R, Capitanio N, Papa S. (2006) cAMP controls oxygen metabolism in mammalian cells. *FEBS Lett*. 580(18):4539-43.
- PhosphoSitePlus at www.phosphosite.org.
- Potapova IA, El-Maghrabi MR, Doronin SV, Benjamin WB. (2000) Phosphorylation of recombinant human ATP:citrate lyase by cAMP-dependent protein kinase abolishes homotropic allosteric regulation of the enzyme by citrate and increases the enzyme activity. Allosteric activation of ATP:citrate lyase by phosphorylated sugars. *Biochemistry*. 39(5): 1169-79.
- Raha S, Myint AT, Johnstone L, Robinson BH (2002) Control of oxygen free radical formation from mitochondrial complex I: roles for protein kinase A and pyruvate dehydrogenase kinase. *Free Radic Biol Med*. 32(5):421-30.
- Ramamoorthy S, Samuvel DJ, Buck ER, Rudnick G, Jayanthi LD. (2007) Phosphorylation of threonine residue 276 is required for acute regulation of serotonin transporter by cyclic GMP. *J Biol Chem*. 282(16):11639-47.
- Ramirez-Correa GA, Jin W, Wang Z, Zhong X, Gao WD, Dias WB, Vecoli C, Hart GW, Murphy AM. (2008) O-linked GlcNAc modification of cardiac myofilament proteins: a novel regulator of myocardial contractile function. *Circ Res* 103, 1354-8.

- Rastaldo R, Pagliaro P, Cappello S, Penna C, Mancardi D, Westerhof N, Losano G. (2007) Nitric oxide and cardiac function. *Life Sci.* 81, 779-93.
- Rettori V, Fernandez-Solari J, Mohn C, Zorrilla Zubilete MA, de la Cal C, Prestifilippo JP, De Laurentiis A. (2009) Nitric oxide at the crossroad of immunoneuroendocrine interactions. *Ann NY Acad Sci.* 1153:35-47. Review.
- Roell W, Lewalter T, Sasse P, Tallini YN, Choi BR, Breitbach M, Doran R, Becher UM, Hwang SM, Bostani T, von Maltzahn J, Hofmann A, Reining S, Eiberger B, Gabris B, Pfeifer A, Welz A, Willecke K, Salama G, Schrickel JW, Kotlikoff MI, Fleischmann BK. (2007) Engraftment of connexin 43-expressing cells prevents post-infarct arrhythmia. *Nature.* 450(7171): 819-24.
- Ross PL, Huang YN, Marchese JN, Williamson B, Parker K, Hattan S, Khainovski N, Pillai S, Dey S, Daniels S, Purkayastha S, Juhasz P, Martin S, Bartlet-Jones M, He F, Jacobson A, Pappin DJ. (2004) Multiplexed protein quantitation in *Saccharomyces cerevisiae* using amine-reactive isobaric tagging reagents. *Mol Cell Proteomics.* 3(12):1154-69.
- Ruse CI, Tan FL, Kinter M, Bond M. (2004) Integrated analysis of the human cardiac transcriptome, proteome and phosphoproteome. *Proteomics.* 4(5):1505-16.
- Rybalkin SD, Rybalkina IG, Feil R, Hofmann F, Beavo JA. (2002) Regulation of cGMP-specific phosphodiesterase (PDE5) phosphorylation in smooth muscle cells. *J Biol Chem* 277, 3310-7
- Sadayappan S, Gulick J, Osinska H, Martin LA, Hahn HS, Dorn GW 2nd, Klevitsky R, Seidman CE, Seidman JG, Robbins J. (2005) Cardiac myosin-binding protein-C phosphorylation and cardiac function. *Circ Res.* 97(11):1156-63.
- Sadayappan S, Osinska H, Klevitsky R, Lorenz JN, Sargent M, Molkentin JD, Seidman CE, Seidman JG, Robbins J. (2006) Cardiac myosin binding protein C phosphorylation is cardioprotective. *Proc Natl Acad Sci.* 103(45):16918-23.
- Said M, Vittone L, Mundina-Weilenmann C, Ferrero P, Kranias EG, Mattiazzi A. (2003) Role of dual-site phospholamban phosphorylation in the stunned heart: insights from phospholamban site-specific mutants. *Am J Physiol Heart Circ Physiol.* 285(3):H1198-205.
- Sambandam N, Lopaschuk GD, Brownsey RW, Allard MF. (2002) Energy metabolism in the hypertrophied heart. *Heart Fail Rev.* 7, 161-73.
- Sandner P, Neuser D, Bischoff E. (2009) Erectile dysfunction and lower urinary tract. *Handb Exp Pharmacol.* 2009;(191):507-31. Review.
- Sawada N, Itoh H, Yamashita J, Doi K, Inoue M, Masatsugu K, Fukunaga Y, Sakaguchi S, Sone M, Yamahara K, Yurugi T, Nakao K. (2001) cGMP-dependent protein kinase phosphorylates and inactivates RhoA. *Biochem Biophys Res Commun* 280, 798-805

- Scheid MP, Marignani PA, Woodgett JR. (2002) Multiple phosphoinositide 3-kinase-dependent steps in activation of protein kinase B. *Mol Cell Biol.* 22(17):6247-60.
- Scherer-Oppliger T, Leimbacher W, Blau N, Thöny B (1999) Serine 19 of human 6-pyruvoyltetrahydropterin synthase is phosphorylated by cGMP protein kinase II. *J Biol Chem* 274, 31341-8
- Schlossmann J, Ammendola A, Ashman K, Zong X, Huber A, Neubauer G, Wang GX, Allescher HD, Korth M, Wilm M, Hofmann F, Ruth P. (2000) Regulation of intracellular calcium by a signalling complex of IRAG, IP3 receptor and cGMP kinase I β . *Nature.* 404(6774): 197-201.
- Schröder F, Handrock R, Beuckelmann DJ, Hirt S, Hullin R, Priebe L, Schwinger RHG, Weil J, Herzig S. (1998) Increased Availability and Open Probability of Single L-Type Calcium Channels From Failing Compared With Nonfailing Human Ventricle. *Circulation.* 98:969-976.
- Schultess J, Danielewski O, Smolenski AP (2005) Rap1GAP2 is a new GTPase-activating protein of Rap1 expressed in human platelets. *Blood* 105, 3185-92
- Seymour AM, Chatham JC. (1997) The effects of hypertrophy and diabetes on cardiac pyruvate dehydrogenase activity. *J Mol Cell Cardiol.* 29(10):2771-8.
- Shevchenko A, Wilm M, Vorm O, Mann M. (1996) Mass spectrometric sequencing of proteins silver-stained polyacrylamide gels. *Anal Chem.* 68, 850-8.
- Shimura M, Minamisawa S, Takeshima H, Jiao Q, Bai Y, Umemura S, Ishikawa Y. (2008) Sarcalumenin alleviates stress-induced cardiac dysfunction by improving Ca²⁺ handling of the sarcoplasmic reticulum. *Cardiovasc Res.* 77(2):362-70.
- Shoshan-Barmatz V, Orr I, Weil S, Meyer H, Varsanyi M, Heilmeyer LM. (1996) The identification of the phosphorylated 150/160-kDa proteins of sarcoplasmic reticulum, their kinase and their association with the ryanodine receptor. *Biochim Biophys Acta.* 1283(1):89-100.
- Spirito P, Seidman CE, McKenna WJ et al. (1997) The management of hypertrophic cardiomyopathy. *N Engl J Med* 336:775–85.
- Solan JL, Lampe PD (2007) Key connexin 43 phosphorylation events regulate the gap junction life cycle. *J Membr Biol* 217, 35-41
- Sonveaux P, Jordan BF, Gallez B, Feron O. (2009) Nitric oxide delivery to cancer: why and how? *Eur J Cancer.* 2009 May;45(8):1352-69. Epub 2009 Jan 17. Review.
- Sorensen SD, Macek TA, Cai Z, Saugstad JA, Conn PJ. (2002) Dissociation of protein kinase-mediated regulation of metabotropic glutamate receptor 7 (mGluR7) interactions with calmodulin and regulation of mGluR7 function. *Mol Pharmacol* 61, 1303-12
- Suk JY, Kim YS, Park WJ. (1999) HRC (Histidine-Rich Ca²⁺ Binding Protein) Resides in the Lumen of Sarcoplasmic Reticulum as a Multimer. *Biochem Biophys Res Commun.* 263(3) 667-671.

- Suko J, Maurer-Fogy I, Plank B, Bertel O, Wyskovsky W, Hohenegger M, Hellmann G. (1993) Phosphorylation of serine 2843 in ryanodine receptor-calcium release channel of skeletal muscle by cAMP-, cGMP- and CaM-dependent protein kinase. *Biochim Biophys Acta* 1175, 193-206
- Stelzer JE, Patel JR, Walker JW, Moss RL. (2007) Differential roles of cardiac myosin-binding protein C and cardiac troponin I in the myofibrillar force responses to protein kinase A phosphorylation. *Circ Res.* 101(5):503-11
- Steppan J, Ryoo S, Schuleri KH, Gregg C, Hasan RK, White AR, Bugaj LJ, Khan M, Santhanam L, Nyhan D, Shoukas AA, Hare JM, Berkowitz DE. (2006) Arginase modulates myocardial contractility by a nitric oxide synthase I-dependent mechanism. *Proc Natl Acad Sci U S A* 103:4759–4764
- Swiderek K, Jaquet K, Meyer HE, Schächtele C, Hofmann F, Heilmeyer LM Jr.(1990) Sites phosphorylated in bovine cardiac troponin T and I. Characterization by 31P-NMR spectroscopy and phosphorylation by protein kinases. *Eur J Biochem* 190, 575-82
- Taimor G, Rakow A, Piper HM. (2001) Transcription activator protein 1 (AP-1) mediates NO-induced apoptosis of adult cardiomyocytes. *FASEB J.* 15, 2518-20.
- Takahashi S, Lin H, Geshi N, Mori Y, Kawarabayashi Y, Takami N, Mori MX, Honda A, Inoue R. (2008) Nitric oxide-cGMP-protein kinase G pathway negatively regulates vascular transient receptor potential channel TRPC6. *J Physiol.* 586(Pt 17):4209-23.
- Takai Y, Kishimoto A, Inoue M, Nishizuka Y (1977) Studies on a cyclic nucleotide-independent protein kinase and its proenzyme in mammalian tissues. I. Purification and characterization of an active enzyme from bovine cerebellum. *J Biol Chem* 252, 7603-9
- Takasago T, Imagawa T, Furukawa K, Ogurusu T, Shigekawa M.(1991) Regulation of the cardiac ryanodine receptor by protein kinase-dependent phosphorylation. *J Biochem.* 109(1): 163-70.
- Takeya R, Taniguchi K, Narumiya S, Sumimoto H (2008) The mammalian formin FHOD1 is activated through phosphorylation by ROCK and mediates thrombin-induced stress fibre formation in endothelial cells. *EMBO J* 27, 618-28
- Tanaka, K.; Waki, H.; Ido, Y.; Akita, S.; Yoshida, Y.; Yoshida, T. (1988). Protein and Polymer Analyses up to m/z 100 000 by Laser Ionization Time-of flight Mass Spectrometry. *Rapid Commun Mass Spectrom* 2 (20): 151–3.
- Taniike M, Yamaguchi O, Tsujimoto I, Hikoso S, Takeda T, Nakai A, Omiya S, Mizote I, Nakano Y, Higuchi Y, Matsumura Y, Nishida K, Ichijo H, Hori M, Otsu K. (2008) Apoptosis signal-regulating kinase 1/p38 signaling pathway negatively regulates physiological hypertrophy. *Circulation.* 117(4):545-52.

- Towbin JA, Bowles KR, Bowles NE. (1999) Etiologies of cardiomyopathy and heart failure. *Nature Medicine*, 5, 266 - 267.
- Towbin JA, Bowles NE. (2006) Dilated cardiomyopathy: a tale of cytoskeletal proteins and beyond. *J Cardiovasc Electrophysiol*. 17(8):919-26
- Xiao B, Zhong G, Obayashi M, Yang D, Chen K, Walsh MP, Shimoni Y, Cheng H, Ter Keurs H, Chen SR. (2006) Ser-2030, but not Ser-2808, is the major phosphorylation site in cardiac ryanodine receptors responding to protein kinase A activation upon beta-adrenergic stimulation in normal and failing hearts. *Biochem J*. 396(1):7-16.
- Xue J, Milburn PJ, Hanna BT, Graham ME, Rostas JA, Robinson PJ. (2004) Phosphorylation of septin 3 on Ser-91 by cGMP-dependent protein kinase-I in nerve terminals. *Biochem J*. 381(Pt 3):753-60.
- Yan M, Dai T, Deak JC, Kyriakis JM, Zon LI, Woodgett JR, Templeton DJ. (1994) Activation of stress-activated protein kinase by MEKK1 phosphorylation of its activator SEK1. *Nature*. 372 (6508):798-800.
- Yang L, Liu G, Zakharov SI, Bellinger AM, Mongillo M, Marx SO. (2007) Protein kinase G phosphorylates Cav1.2 alpha1c and beta2 subunits. *Circ Res*. 101(5):465-74.
- Yang XJ, Seto E. (2008) The Rpd3/Hda1 family of lysine deacetylases: from bacteria and yeast to mice and men. *Nature Reviews Molecular Cell Biology* 9, 206-218
- Yong-Ling P. Ow, Douglas R. Green, Zhenyue Hao & Tak W. Mak (2008) Cytochrome c: functions beyond respiration *Nature Reviews Molecular Cell Biology* 9, 532-542
- Yoshida M, Minamisawa S, Shimura M, Komazaki S, Kume H, Zhang M, Matsumura K, Nishi M, Saito M, Saeki Y, Ishikawa Y, Yanagisawa T, Takeshima H. (2005) Impaired Ca²⁺ store functions in skeletal and cardiac muscle cells from sarcalumenin-deficient mice. *J Biol Chem*. 280 (5):3500-6.
- Zanivan S, Gnad F, Wickström SA, Geiger T, Macek B, Cox J, Fässler R, Mann M. (2008) Solid Tumor Proteome and Phosphoproteome Analysis by High Resolution Mass Spectrometry. *J Proteome Res*. 7 (12), 5314–5326
- Zhang X, Ye J, Jensen ON, Roepstorff P. (2007) Highly Efficient Phosphopeptide Enrichment by Calcium Phosphate Precipitation Combined with Subsequent IMAC Enrichment. *Mol Cell Proteomics* 6, 2032-2042.
- Zhao W, Uehara Y, Chu G, Song Q, Qian J, Young K, Kranias EG. (2004) Threonine-17 phosphorylation of phospholamban: a key determinant of frequency-dependent increase of cardiac contractility. *J Mol Cell Cardiol*. 37(2):607-12.
- Zhao X, Zhuang S, Chen Y, Boss GR, Pilz RB. (2005) Cyclic GMP-dependent protein kinase regulates CCAAT enhancer-binding protein beta functions through inhibition of glycogen synthase kinase-3. *J Biol Chem* 280, 32683-92

- Zhou X, Fan GC, Ren X, Waggoner JR, Gregory KN, Chen G, Jones WK, Kranias EG. (2007) Overexpression of histidine-rich Ca-binding protein protects against ischemia/reperfusion-induced cardiac injury. *Cardiovasc Res.* 75(3):487-97.
- Zhou Z, Sayed N, Pyriochou A, Roussos C, Fulton D, Beuve A, Papapetropoulos A. (2008) Protein kinase G phosphorylates soluble guanylyl cyclase on serine 64 and inhibits its activity. *Arterioscler Thromb Vasc Biol.* (10):1803-10.
- Vallance P. & Leiper J. (2002) Blocking NO synthesis: how, where and why? *Nature Reviews Drug Discovery* 1, 939-950
- Walter U, Gambaryan S. (2009) cGMP and cGMP-dependent protein kinase in platelets and blood cells. *Handb Exp Pharmacol.* (191):533-48. Review.
- Wang Y, El-Zaru MR, Surks HK, Mendelsohn ME (2004) Formin homology domain protein (FHOD1) is a cyclic GMP-dependent protein kinase I-binding protein and substrate in vascular smooth muscle cells. *J Biol Chem* 279, 24420-6
- Wang L, Liu N, Yao L, Li F, Zhang J, Deng Y, Liu J, Ji S, Yang A, Han H, Zhang Y, Zhang J, Han W, Liu X. (2008) NDRG2 is a new HIF-1 target gene necessary for hypoxia-induced apoptosis in A549 cells. *Cell Physiol Biochem.* 21(1-3):239-50.
- Washburn MP, Wolters D, Yates JR 3rd. (2001) Large-scale analysis of the yeast proteome by multidimensional protein identification technology. *Nat Biotechnol.* 19, 242-7.
- Wehrens XH, Lehnart SE, Reiken S, Vest JA, Wronska A, Marks AR. (2006) Ryanodine receptor/calcium release channel PKA phosphorylation: a critical mediator of heart failure progression. *Proc Natl Acad Sci U S A.* 103(3):511-8.
- Wessel D, Flügge UI. (1984) A method for the quantitative recovery of protein in dilute solution in the presence of detergents and lipids. *Anal. Biochem.* 138, 141-143.
- Wunderlich C, Flögel U, Gödecke A, Heger J, Schrader J. (2003) Acute inhibition of myoglobin impairs contractility and energy state of iNOS-overexpressing hearts. *Circ Res.* 92(12): 1352-8.



Annamária Simon

PLACE AND DATE OF BIRTH

Keszthely (Hungary), 9 Dec 1979

ADDRESS

Krahestr. 23.
40233 Düsseldorf, Germany

PHONE

+49 211 976 2545
+49 157 7878 6727

EMAIL

annamaria.simon@uni-duesseldorf.de

Curriculum Vitae

Education

- 2005-2009 PhD studies in the Institute of Cardiovascular Physiology (Prof. Schrader) Heinrich-Heine-University, Düsseldorf, Germany
PhD thesis title: Global cardiac phosphoproteome analysis in nitric oxide-induced heart failure
- 1998-2003 M. Sc. Bioengineer, Faculty of Chemical Engineering, Budapest University of Technology and Economics, Budapest, Hungary
Master thesis title: Cloning and expressing the gene of human antithrombin III from human liver cDNA library to Pichia pastoris
- 1994-1998 University entrance diploma, Bibó István Alternative Secondary School of Economics, Hévíz, Hungary

Scholarship

- 2005-2008 PhD Scholarship of the Graduate College 1089

Internship

- 2004-2005 Biomolecular Analytics, Proteincenter, Ruhr-University-Bochum (Dr. Wolters), Topic: Membrane protein purification and analysis using multidimensional chromatography and mass spectrometry (nanoHPLC-ESI-MS/MS)

Membership

- Since 2005 Member of the German Society for Proteome Research (DGPF)
- Since 2008 Member of the Human Proteome Organisation (HUPO)

Skills

Language skills:

- 2004 Intermediate written and oral language exam in English
- 2002 Intermediate written and oral language exam in German

Computer skills: MS Office, MSQuant, MASCOT, Chromeleon, XCalibur, Bioworks, Proteome Discoverer, Unicorn,

Driving license: 1998 Type B

Hobby

literature, inline skating, sailing

Düsseldorf, June 7. 2009

Annamária Simon

EIDESSTATTLICHE ERKLÄRUNG

Ich versichere an Eides statt, daß ich die vorliegende Arbeit selbstständig verfaßt und keine anderen als die angegebenen Hilfsmittel verwendet habe.

Düsseldorf, Juni 2009

Annamária Simon